Luminescence of Fluorinated β-Diketonate Complexes of Lanthanides

Thesis submitted to
The University of Kerala
for the award of the degree of

Doctor of Philosophy
in Chemistry
Under The Faculty of Science

BY
AMBILI RAJ D. B

NATIONAL INSTITUTE FOR INTERDISCIPLINARY SCIENCE AND TECHNOLOGY
COUNCIL OF SCIENTIFIC AND INDUSTRIAL RESEARCH
THIRUVANANTHAPURAM-695 019
KERALA, INDIA

2011

..... *Dedicated to my Parents, Brother, Sister & Jai* .....

DECLARATION

I hereby declare that Ph.D thesis entitled "**Luminescence of Fluorinated *β*-Diketonate Complexes of Lanthanides**" is an independent work carried out by me at the Chemical Sciences and Technology Division, National Institute for Interdisciplinary Science and Technology (NIIST), CSIR, Thiruvananthapuram, under the supervision of Dr. M. L. P. Reddy and it has not been submitted anywhere else for any other degree, diploma or title.

Ambili Raj D. B.

Thiruvanathapuram
January, 2011

NATIONAL INSTITUTE FOR INTERDISCIPLINARY SCIENCE AND TECHNOLOGY (NIIST)

Council of Scientific & Industrial Research (CSIR)
(Formerly Regional Research Laboratory)
Industrial Estate P.O., Trivandrum - 695 019
Kerala, INDIA

ISO 9001 REGISTERED
DNV Certification B.V., The Netherlands

Dr. M. L. P. Reddy
Scientist F
Inorganic and Polymer Materials Section
Chemical Sciences and Technology Division

Tel: 91-471-2515 360
Fax: +91-471-2491 712
E-mail: mlpreddy55@gmail.com

CERTIFICATE

This is to certify that the work embodied in the thesis entitled "**Luminescence of Fluorinated *β*-Diketonate Complexes of Lanthanides**" has been carried out by **Ms. Ambili Raj D. B** under my supervision and guidance at the Chemical Sciences and Technology Division of National Institute for Interdisciplinary Science and Technology (Formerly Regional Research Laboratory), Council of Scientific and Industrial Research, Thiruvanathapuram and the same has not been submitted elsewhere for any other degree.

Dr. M. L. P. Reddy
(Thesis Supervisor)

Thiruvanathapuram

January, 2011

Acknowledgements

It is with great pleasure that I extend my deep sense of respect, regard and gratitude to Dr. M. L. P. Reddy, my thesis supervisor for suggesting the research problem and for his valuable and patience guidance, support and encouragement, leading to the successful completion of this work.

I am grateful to Dr. Suresh Das, Director, NIIST, and former directors Prof. T. K. Chandrasekhar and Dr. B. C. Pai for providing me the necessary facilities and infrastructure of the Institute for carrying out this work.

I sincerely thank Prof. Alan H. Cowley (University of Texas) and Dr. Babu Varghese (SAIF, IIT Madras) for their valuable help in single crystal XRD measurements.

I have great pleasure in thanking Dr. A. Srinivasan, Dr. M. Jayakannan and Dr. S. K. Asha and Scientists of the Chemical Sciences and Technology Division for their help and valuable suggestions at different stages of my work.

More than a heartfelt gratitude is not enough to express my feeling for Dr. Biju S., Mr. Biju Francis, Dr. Remya P.N., Mr. Vishnu V.S. and Mr. Praveen L. for their timely help and co-operation.

My Sincere thanks are due to:

- *Ms. Rachel R. Butorac and Mr. Vincent M. Lynch (University of Texas) for the help rendered towards single crystal XRD measurements.*
- *Ms. Soumini Mathew, Ms. Viji, Mr. B. Adarsh and Mr. Preethanuj for the help rendered in recording, ^{1}H NMR, ^{13}C NMR and FAB-MS analysis.*
- *All former and present colleagues in my division for the help and support.*
- *Library and other supporting staff of NIIST for the help rendered.*
- *All my friends at NIIST for their support and all individuals who came in my life and encouraged me in my career.*

I acknowledge the University Grant Commission, New Delhi for the award of Research Fellowship.

Ambili Raj D. B.

CONTENTS

List of Tables **Page**

List of Figures **Page**

List of Abbreviations

1)	UV	Ultra Violet
2)	DSC	Differential Scanning Calorimeter
3)	XRD	X-Ray Diffraction
4)	DLS	Dynamic Light Scattering
5)	$CHCl_3$	Chloroform
6)	$CDCl_3$	Chloroform-d
7)	SEM	Scanning Electron Microscopy
8)	FT-IR	Fourier Transform Infra-Red
9)	IR	Infrared
10)	NIR	Near-Infrared
11)	FAB-MS	Fast Atom Bombardment Mass Spectrometer
12)	NMR	Nuclear Magnetic Resonance
13)	TEM	Transmission Electron Microscopy
14)	THF	Tetrahydrofuran
15)	ILCT	Intraligand Charge Transfer
16)	MLCT	Metal-to-Lignad Charge Transfer
17)	LMCT	Ligand-to-Metal Charge Transfer
18)	EL	Electroluminescence
19)	PL	Photoluminescence
20)	OLED	Organic Light Emitting Diode
21)	Ln^{3+}	Lanthanide
22)	Energy Transfer	ET
23)	S_1	Singlet
24)	T_1	Triplet
25)	Hfa	hexafluoroacetylacetonate
26)	acbz	1,4-diacetylbenzene
27)	acetbz	1,4-diacetoxybenzene
28)	dmtph	dimethyltherephtalate
29)	tta	thenoyl trifluoroacetonate

30)	APO	aryl phosphineoxide
31)	DPEPO	bis(2-(diphenylphosphino)phenyl) ether oxide
32)	TMOADPO	2-(diphenylphosphoryl)-*N*-(2-(diphenylphosphoryl)-4-ethoxyphenyl)-4-methoxy-*N*-(4-methoxyphenyl)aniline
33)	EtCzDPO	3,6-bis(diphenylphosphoryl)-9-ethyl-9*H*-carbazole
34)	PhCzDPO	3,6-bis(diphenylphosphoryl)-9-phenyl-9*H*-carbazole
35)	TPPO	triphenylphosphine oxide
36)	TAPO	4-diphenylaminophenyl) diphenylphosphine oxide
37)	NaDAPO	(4-naphthalen-1-yl-phenylaminophenyl)diphenylphosphine oxide
38)	CPPO	9-[4-(diphenylphosphinoyl) phenyl]-9H-carbazole
39)	2-TFDBC	2-(4´4´4´-trifluoro-1´3´-dioxobutyl)-carbazole
40)	2,7-BTFDBC	2,7-bis(4´4´4´-trifluoro-1´3´-dioxobutyl)-carbazole
41)	Phen	1,10-phenanthroline
42)	DPPPO	bis[*o*-(diphenylphosphoryl)phenyl] phenylphosphaneoxide
43)	DPPYPO	bis[*o*-(diphenylphosphoryl)pyridyl]-phenylphosphane oxide
44)	DPBTPO	bis[*o*-(diphenylphosphoryl)benzothienyl]phenylphosphane oxide
45)	Dfppy	2-(4′,6′-difluorophenyl)-pyridinato-N,$C^{2'}$
46)	phen5f	4,4,5,5,5-pentafluoro-1-(1′,10′-phenanthrolin-2′-yl)-pentane-1,3-dionate
47)	TFA	trifluoroacetylacetonate
48)	Fc_2phen	bis(ferrocenyl-ethynyl)-1,10-phenanthroline
49)	Hfta	ferrocenoyltrifluoroacetone
50)	HFNH	4,4,5,5,6,6,6-heptafluoro-1-(2-naphthyl)hexane-1,3-dione
51)	NTA	1-(2-naphthoyl)-3,3,3-trifluoroacetonate
52)	PMMA	poly(methyl methacrylate)
53)	PS	polystyrene
54)	PVP	poly(vinylpyrrolidine)
55)	PHB	poly-β-hydroxybutyrate
56)	Hpffpd	4,4,5,5,5-pentafluoro-1-(9H-fluoren-2-yl)-1,3-pentanedione

57)	DDXPO	4,5-bis(diphenylphosphino)-9,9-dimethylxanthene oxide
58)	CPFHP	1-(9H-carbazol-2-yl)-4,4,5,5,5-pentafluoro-3-hydroxypent-2-en-1-one
59)	HPFNP	4,4,5,5,5-pentafluoro-1-(naphthalen-2-yl)pentane-1,3-dione
60)	bpy	2,2′- bipyridine
61)	bath	4,7-diphenyl-1,10-phenanthroline

PREFACE

The versatile photophysical properties of lanthanide ions (Ln^{3+}) have inspired vigorous research activities because of the wide range of photonic applications, such as tunable lasers, amplifiers for optical communications, luminescent probes for analytes and components of the emitting materials in multilayer organic light emitting diodes. Unfortunately, due to the Laporte forbidden character and intraconfigurational nature of the 4f transitions, the molar absorption coefficients of lanthanide transitions are typically very small (less than 10 L M^{-1} cm^{-1}). To obviate this problem, organic ligands with large molar absorption coefficients can be coordinated to the lanthanide ion, resulting in sensitized emission by means of the so-called ‘‘antenna effect’’. The β-diketone ligand class is emerging as one of the important ‘‘antennas’’ in terms of high harvest emissions due to the effectiveness of the energy transfer from this ligand type to the Ln^{3+} cation. However, the use of fluorinated β-diketones as a sensitizer for Ln^{3+} cation luminescence is very scarce. Earlier reports demonstrated that the replacement of C-H bonds in a β-diketone with low-energy oscillators (C-F) is able to lower the vibrational energy of the ligand, which minimizes the energy loss caused by ligand vibration and enhances the luminescent intensity of the Ln^{3+} ion. Further, because of the heavy-atom effect, which facilitates intersystem crossing, the lanthanide-centered luminescent properties are enhanced. Thus, the primary objective of the present work is to design and develop a novel class of fluorinated β-diketonate molecules with conjugated motifs for the sensitization of Eu^{3+} ions. The thesis comprises of five chapters.

The introductory chapter highlights the need for the development of new class of antenna molecules for the sensitization of Eu^{3+} ions based on fluorinated β-diketonates. Further, a detailed literature review on the recent developments in the photophysical properties of Eu^{3+}-β-diketonates has been brought out towards the end of this chapter.

The second chapter describes the results on the synthesis, characterization and photophysical properties of Eu^{3+}- 4,4,5,5,5-pentafluoro-1-(9H-fluoren-2-yl)-1,3-pentanedione (Hpffpd) complex in the presence of 4,5-bis(diphenylphosphino)-9,9-dimethylxanthene oxide (DDXPO) as an ancilliary ligand [$Eu(pffpd)_3$(DDXPO)] **2**. For comparison, the [$Eu(pffpd)_3$(DPEPO)] **3** complex was also synthesized involving a known chelate phosphine oxide, bis(2-(diphenylphosphino)phenyl) ether oxide (DPEPO).The single-crystal X-ray diffraction analyses of **2** and **3** revealed that these complexes are mononuclear, and that the central Eu^{3+} ion is surrounded by eight oxygen atoms, six of which are from the three bidentate fluorinated *β*-diketonates, and the other two oxygen atoms from the chelate phosphine oxide. Compound **2** has a solid-state photoluminescence quantum yield of 48%, which is about two times higher than that of compound **3** (28%). This may be due to the fact that DDXPO in **2** has the mezzo first triplet excited state energy level (T_1) between the first singlet excited energy level (S_1) and T_1 of Hpffpd, which may support one more additional energy transfer from the T_1 energy level of DDXPO to that of Hpffpd, and consequently improves the energy transfer in the Eu^{3+} complex. (These results were published in ***Dalton Trans.*, 2009, 7519-7528**).

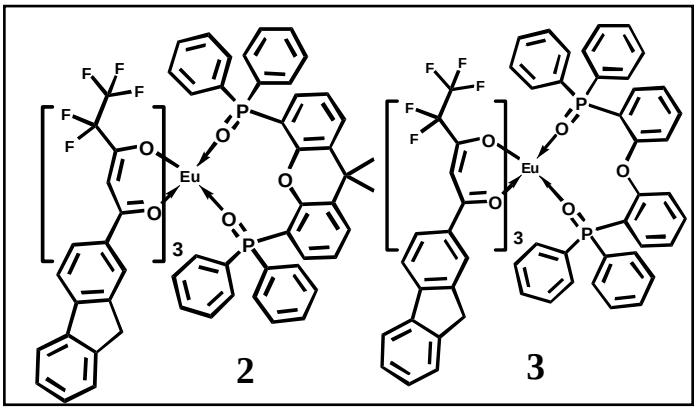

A novel efficient antenna complex of Eu^{3+} [$Eu(CPFHP)_3$(DDXPO)] supported by a highly fluorinated carbazole-substituted *β*-diketonate ligand, namely, 1-(9H-carbazol-2-yl)-4,4,5,5,5-pentafluoro-3-hydroxypent-2-en-1-one (CPFHP) and the 4,5-bis(diphenylphosphino)-9,9-dimethylxanthene oxide (DDXPO) ancillary ligand, has been synthesized, structurally characterized, and its photoluminescent behaviour examined. These results have been incorporated in chapter 3. The photophysical properties of $Eu(CPFHP)_3$(DDXPO) benefit from adequate protection of the metal by the ligands with respect to non-radiative deactivation as

well as an efficient ligand-to-metal energy transfer process which exceeds 66% in chloroform solution with a quantum yield of 47%. As an integral part of this work, the synthesis, characterization, and luminescent properties of poly(methyl methacrylate) (PMMA) polymer films doped with $Eu(CPFHP)_3(DDXPO)$ are also reported. The luminescent efficiencies of the doped films (photoluminescence quantum yields 79−84%) are dramatically enhanced in comparison with that of the precursor complex. The new luminescent PMMA-doped complex therefore shows considerable promise for polymer light-emitting diode and active polymer optical fiber applications. (These results were published in ***Inorg. Chem.,* 2010*, 49,* 9055-9063**.)

The fourth chapter deals with the results on the role of ancilliary ligands, various bidentate nitrogen donors on the sensitization of Eu^{3+} in the presence of a new *β*-diketone, 4,4,5,5,5-pentafluoro-1-(naphthalen-2-yl)pentane-1,3-dione (HPFNP), which contains polyfluorinated alkyl group, as well as the long conjugated naphthyl group. The single-crystal X-ray diffraction analysis of $Eu(PFNP)_3(bpy)$ revealed that the complex is mononuclear, the central Eu^{3+} ion is coordinated by six oxygen atoms furnished by three *β*-diketonate ligands, and two nitrogen atoms from a bidentate bipyridyl ligand, in an overall distorted square prismatic geometry. Further, analysis of the X-ray crystal data of the above complex also revealed interesting 1D, 2D, and 3D networks based on intra- and intermolecular hydrogen bonds. The results demonstrate that the substitution of solvent molecules by bidentate nitrogen ligands in $Eu(PFNP)_3(H_2O)(EtOH)$ greatly enhances the quantum yields and lifetime values. (These results were published in ***Inorg. Chem.,* 2008*, 47,* 8091-8100)**.

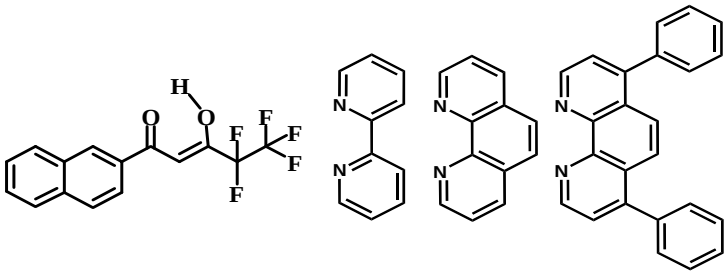

The fifth chapter describes the results of a highly luminescent Eu^{3+} ternary complex which has been covalently immobilized in the ordered MCM-41 mesoporous host through modification of a novel polyfluorinated β-diketone with 3-(triethoxysilyl)propylisocyanate by a co-condensation route. X-Ray diffraction confirms that this luminescent material has ordered hexagonal mesoporosity. Dynamic light scattering and SEM studies indicate that the newly designed mesoporous luminescent material has particle size in the range 250–300 nm. The photoluminescent properties of $Eu(PFNP\text{-}Si)_3(bath)$/MCM-41 mesoporous material indicates that the present hybrid material exhibits higher $^5D_0$ quantum efficiency (Φ_{Ln} = 81%) and longer lifetime (1.05 ms) values. Moreover, the MCM-based material provides several additional advantages, such as being able to be processed as silica based templates for optical centers (compatible with the silicon devices technology), opening up the possibility of designing new luminescent displays with highly oriented MCM-41 films impregnated with emitting centers showing enhanced antenna effects (These results were published in ***J. Mater. Chem.*****, 2009*****, 19,*** **7976–7983**).

The contributions to the new knowledge arising out of this thesis have been highlighted in the concluding chapter. The relevant references have been cited towards the end of the thesis

Chapter 1

Introduction

1.1 Photoluminescence of trivalent lanthanides

The intricate optical properties of the trivalent lanthanide ions, hereafter Ln^{3+}, are fascinating and originate in the special features of the electronic $[Xe]4f^n$ configurations (n = 0-14). These configurations generate a rich variety of electronic levels, the number of which is given by [14!/n!(14- n)!] [Bünzli 2010]. The energies of these levels are well-defined due to the shielding of the 4f orbitals by the filled $5s^25p^6$ subshells, and they are a little sensitive to the chemical environments in which the lanthanide ions are inserted. As a corollary, inner-shell 4f-4f transitions which span both the visible and near-infrared (NIR) ranges are sharp and easily recognizable (Figure 1.1, Table 1.1). In addition, because these transitions are formally parity forbidden, the lifetimes of the excited states are long.

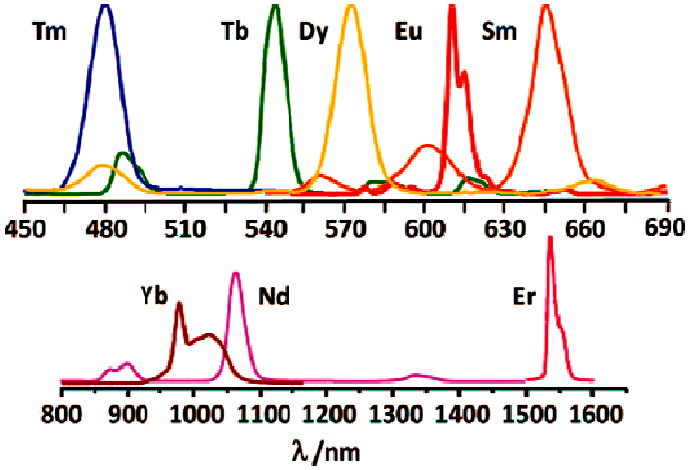

Figure 1.1. Luminescence spectra of some lanthanide tris(*β*-diketonates).

The long excited-state lifetimes and the high chromaticity of lanthanides are also interesting for applications in solid-state materials technologies. For instance, Tb^{3+}, Eu^{3+} and Tm^{3+} are used as green, red, and blue emitters in, respectively, trichromatic fluorescent tubes, multicolor displays, [Justel *et al.* 1998; Hao *et al.* 2001] and organic light-emitting diodes (OLEDs) [Kido and Okamota 2002; de Bettencourt-Dias 2007]. Dy^{3+} is found in persistent-luminescence phosphors as these materials do not need radioactive ions such as ^3H or ^{147}Pm to sustain their

phosphorescence [Matsuzawa *et al.* 1996]. The near-IR emitters Nd^{3+}, Yb^{3+}, and Er^{3+} are of special interest in photonics, being used as laser-active dopants in a variety of host materials, including both crystals and glasses [Geusic *et al.* 1964; Guyot *et al.* 2005]. Er^{3+} is of interest for use as a planar-waveguide optical amplifier, as it emits at 1.5 μm, one of the standard telecommunication wavelengths [Kuriki *et al*. 2002; Polman and van Veggel 2004; Righini *et al.* 2005]. A schematic representation of the type of emission and some major areas of application of lanthanides [Armelao *et al*. 2009] is evidenced in Figure 1.2.

Table 1.1. Selected luminescent properties of Ln^{3+} ions[a]

Ln	G	I	F	λ/μm or nm[b]	gap/cm^{-1}[b]	τ^{rad}/ms[b]
Ce	$^2F_{5/2}$	5d	$^2F_{5/2}$	tunable, 300–450		
Pr	$^3H_4$	$^1D_2$	$^3F_4$, $^1G_4$, $^3H_4$, $^3H_5$	1.0, 1.44, 600, 690	6940	(0.05[c]–0.35)
		$^3P_0$	^3H_J (J = 4–6)	490, 545, 615	3910	(0.003[c]–0.02)
		$^3P_0$	^3F_J (J = 2–4)	640, 700, 725		
Nd	$^4I_{9/2}$	$^4F_{3/2}$	^4I_J (J = 9/2–13/2)	900, 1.06, 1.35	5400	0.42 (0.2–0.5)
Sm	$^6H_{5/2}$	$^4G_{5/2}$	^6H_J (J = 5/2–13/2)	560, 595, 640, 700, 775	7400	6.26
		$^4G_{5/2}$	^6F_J (J = 1/2–9/2)	870, 887, 926, 1.01, 1.15		
		$^4G_{5/2}$	$^6H_{13/2}$	877		
Eu[d]	$^7F_0$	$^5D_0$	^7F_J (J = 0–6)	580, 590, 615, 650, 720, 750, 820	12300	9.7 (1–11)
Gd	$^8S_{7/2}$	$^6P_{7/2}$	$^8S_{7/2}$	315	32100	10.9
Tb	$^7F_6$	$^5D_4$	^7F_J (J = 6–0)	490, 540, 580, 620	14800	9.0 (1–9)
				650, 660, 675		
Dy	$^6H_{15/2}$	$^4F_{9/2}$	^6H_J (J = 15/2–9/2)	475, 570, 660, 750	7850	1.85 (0.15–1.9)
		$^4F_{15/2}$	^6H_J (J = 15/2–9/2)	455, 540, 615, 695	1000	3.22[b]
Ho	$^5I_8$	$^5S_2$	^5I_J (J = 8,7)	545, 750	3000	0.37 (0.51[c])
		$^5F_5$	$^5I_8$	650	2200	0.8[c]
		$^5F_5$	$^5I_7$	965		
Er[e]	$^4I_{15/2}$	$^4S_{3/2}$	^4I_J (J = 15/2, 13/2)	545, 850	3100	0.7[c]
		$^4F_{9/2}$	$^4I_{15/2}$	660	2850	0.6[c]
		$^4I_{9/2}$	$^4I_{15/2}$	810	2150	4.5[c]
		$^4I_{13/2}$	$^4I_{15/2}$	1.54	6500	0.66 (0.7–12)
Tm	$^3H_6$	$^1D_2$	$^3F_4$, $^3H_4$, $^3F_3$, $^3F_2$	450, 650, 740, 775	6650	0.09
		$^1G_4$	$^3H_6$, $^3F_4$, $^3H_5$	470, 650, 770	6250	1.29
		$^3H_4$	$^3H_6$	800	4300	3.6[c]
Yb	$^2F_{7/2}$	$^2F_{5/2}$	$^2F_{7/2}$	980	10 250	2.0 (0.5–2.0)[f]

[a] G = ground state; I = main emissive state; F = final state; gap = energy difference between I and the highest SO level of F. [b] Values for the aqua ions [Carnall, 1979] otherwise stated, and ranges of observed lifetimes in all media, if available, between parentheses. [c] Doped in Y_2O_3 or in $YLiF_4$ (Ho), or in $YAl_3(BO_3)_4$ (Dy). [d] Luminescence from $^5D_1$, $^5D_2$, and $^5D_3$ is sometimes observed as well. [e] Luminescence from four other states has also been observed: $^4D_{5/2}$, $^2P_{3/2}$, $^4G_{11/2}$, $^2H_{9/2}$. [f] Complexes with organic ligands: 0.5-1.3 ms [Aebischer *et al.* 2009 Shavaleev *et al.* 2009]; solid-state inorganic compounds: ≈2 ms.

The only drawback of f-f transitions, their faint oscillator strengths, may in fact be turned into advantages. Indeed, Weissman demonstrated in 1942 that excitation of lanthanide complexes into the ligand states results in metal-centered luminescence [Weissman 1942]. Part of the energy absorbed by the organic receptor(s) is transferred onto Ln^{3+} excited states, and

sharp emission bands originating from the metal ion are detected after rapid internal conversion to the emitting level (Figure 1.3). The phenomenon is termed sensitization of the metal-centered luminescence (also referred to as "antenna effect") and is quite complex (Figure 1.4).

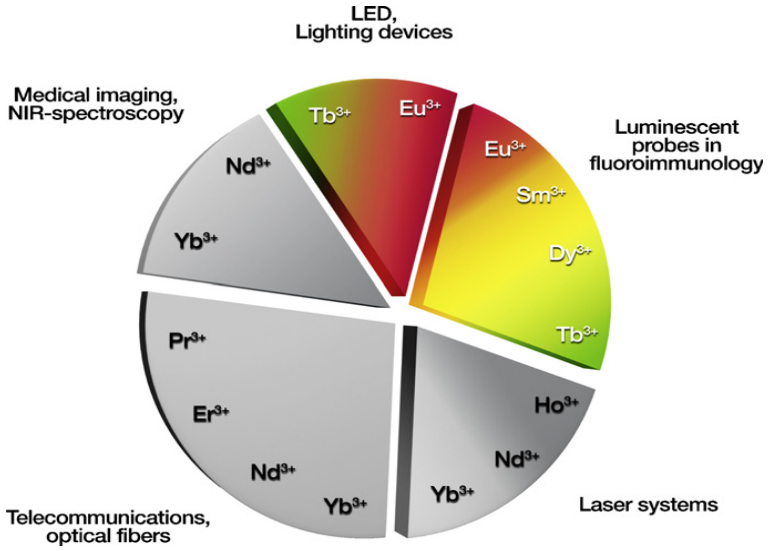

Figure 1.2. Type of emission and related applications of lanthanides.

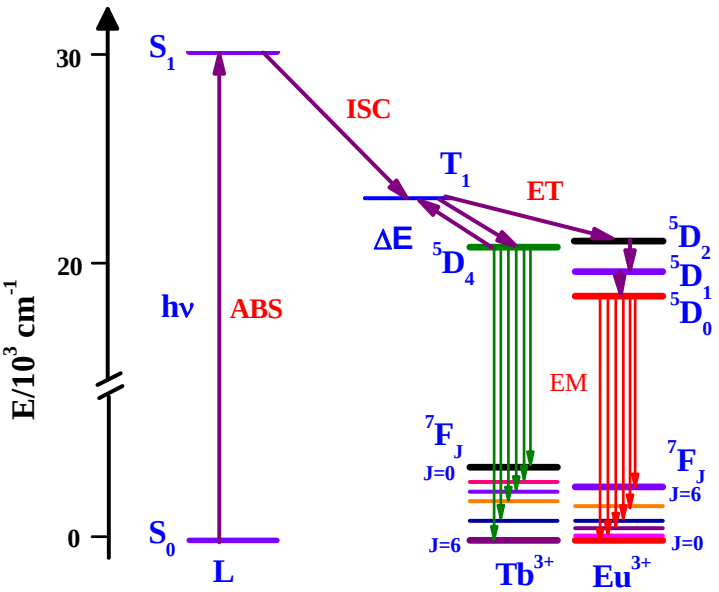

Figure 1.3. Modified Jablonski diagram for the sensitization pathway in luminescent Ln^{3+} complexes.

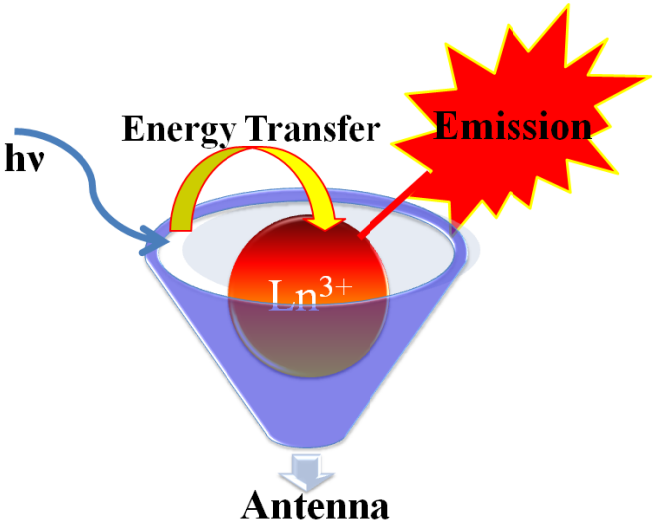

Figure 1.4. Pictorial representation of antenna effect.

Several energy migration paths may be involved, e.g., exchange or superexchange (Dexter), dipole-dipole, or dipole-multipole (Förster) mechanisms [de Sa *et al.* 2000], which entail the participation of several ligand levels, singlet, triplet, and/or intraligand charge transfer (ILCT) states. A commonly observed energy migration path though goes through the long-lived triplet state(s) of the ligand(s) [Eliseeva and Bünzli 2010]. Alternatively, other states may funnel energy onto the metal ion such as intracomplex ligand-to-metal (LMCT) charge transfer states [Blasse, 1976], 4f5d states [Zolin *et al.* 2004], or metal-to-ligand (^{1}MLCT, ^{3}MLCT) charge transfer states from chromophores containing d-transition metal ions [Faulkner *et al.* 2009], such as Cr^{3+} [Imbert *et al.* 2003], Re^{+} [Pope *et al.* 2004], Ru^{2+} [Lazarides *et al.* 2008; Torelli *et al.* 2004], Os^{2+} [Lazarides *et al.* 2009; Riis-Johannessen *et al.* 2008], Co^{3+} [Lazarides *et al.* 2007], Ir^{3+} [Mehlstäubl *et al.* 2008], or Pt^{2+} [Xu *et al.* 2009; Ziessel *et al.* 2007; Shavaleev *et al.* 2003]. These d-ions are essentially used for the sensitization of NIR luminescence [Comby and Bünzli, 2007]. The sensitization process generates two advantages. First, while Ln^{3+} ions display a negligible Stokes' shift upon direct excitation, owing to the inner nature of the 4f-orbitals, ligand excitation results in pseudo Stokes' shifts which are often far larger than those of organic fluorophores, henceforth allowing easy spectral discrimination of the emitted light.

Second, Ln^{3+} ions are usually good quenchers of triplet states so that photobleaching is substantially reduced.

The overall quantum yield ($\Phi_{overall}$) for a sensitized Ln^{3+} complex is given by the equation:

$$\Phi_{overall} = \Phi_{ISC}\Phi_{ET}\Phi_{Ln} \qquad (1)$$

where Φ_{ISC} and Φ_{ET} are the respective efficiencies of intersystem crossing (ISC) and ligand-to-Ln^{3+} energy transfer (ET), and Φ_{Ln} is the intrinsic quantum yield of the Ln^{3+} ion. In terms of ligand design, this means that the antenna chromophore should

(i) be efficient at absorbing light (i.e., have large ε values),

(ii) have an ISC quantum yield near unity,

(iii) have a triplet state that is close enough in energy to the Ln^{3+} emitting state to allow for effective ligand-to-Ln^{3+} energy transfer (but not so close that thermal back transfer competes effectively with Ln^{3+} emission), and

(iv) protect the Ln^{3+} from the quenching effects of bound water molecules.

A wide array of antenna chromophores that yield emissive Ln^{3+} complexes have been studied extensively, including bipyridines [[a]Alpha *et al.* 1987; [b]Alpha *et al.* 1987; Mukkala and Kankare 1992; Sabbatini *et al*. 1993], calixarenes [Bünzli *et al*. 1993; Bünzli and Ihringer 1996; Charbonniere *et al*. 1998], dipicolinic acids [Lamture *et al.* 1995; George *et al.* 2006] and β-diketonates [de Sa *et al*. 2000; Binnemans 2005; Binnemans 2009], to highlight a few. The β-diketone ligand class is emerging as one of the important "antennas" in terms of high harvest emissions due to the effectiveness of the energy transfer from this ligand type to the Ln^{3+} cation [de Sa *et al*. 2000; Binnemans 2005; Binnemans 2009]. In part, this is due to the fact that the π–π* transition for β-diketones is intense and occurs over a significant range of wavelengths that is appropriate for sensitization of Ln^{3+} cation luminescence. An additional and practical advantage of the use of β-diketone ligands is that they form stable complexes with Ln^{3+} cations [de Sa *et al*. 2000; Binnemans 2005; Eliseeva *et al*. 2006; Sun *et al.* 2006; Binnemans 2009].

1.2. Overview on the visible emitting luminescent lanthanide fluorinated *β*-diketonates

The luminescent properties of of Ln^{3+}-*β*-diketonate complexes have been extensively investigated and these data are well documented in many review articles [de Sa *et al.* 2000; Binnemans 2009; Swavey and Swavey 2009]. As a matter of fact, one of the largest quantum yields reported to date for Eu^{3+} complexes with organic ligands, 85%, was found for the adduct of tris(thenoyltrifluoroacetylacetonate) with dibenzyl sulfoxide [Malta *et al.* 1998].

Highly luminescent and triboluminescent coordination polymers $[Ln(hfa)_3(Q)]_\infty$ (where, Ln = Eu, Gd, Tb and Lu, hfa = hexafluoroacetylacetonate and Q = 1,4-diacetylbenzene (acbz), 1,4-diacetoxybenzene (acetbz), or 1,4-dimethyltherephtalate (dmtph) shown in Figure 1.5) assembled from lanthanide *β*-diketonates and aromatic bidentate O-donor ligands have been recently disclosed [Eliseeva *et al.* 2010]. The triplet state energies of the ancillary ligands, 21,600 (acetbz), 22,840 (acbz), and 24,500 (dmtph) cm^{-1}, were found to be lie in an ideal range for sensitizing the luminescence of both Eu^{3+} and Tb^{3+}. As a result, all of the $[Ln(hfa)_3(Q)]_\infty$ polymers display bright red or green luminescence due to the characteristic $^5D_0 \rightarrow {}^7F_J$ (J = 0-4) or $^5D_4 \rightarrow {}^7F_J$ (J = 6-0) transitions, respectively. Absolute quantum yields reach 51 (Eu) and 56 (Tb) % for the frameworks built from dmtph. Finally, the crystalline samples exhibit strong triboluminescence, which could be useful in the design of pressure and/or damage detection probes.

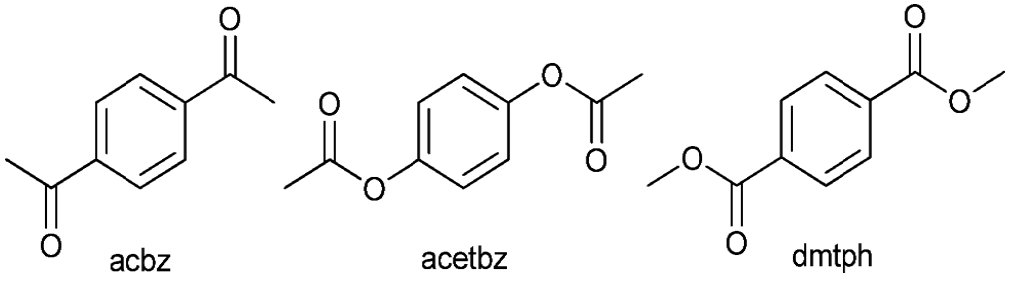

Figure 1.5. Structural formulae of ancilliary ligands used by Eliseeva *et al.* 2010.

A new class of highly luminescent lanthanide complexes that utilize a 2,6-bis(pyrazol-1-yl)-pyridine ligand functionalized with 3,4-ethylenedioxythiophene (L) in conjunction with various

β-diketones (Figure 1.6) has been reported to indirectly excite the europium metal center (Stanley *et al.* 2010). The solid-state structure of complex **1** has been determined by single-crystal X-ray crystallography and shows the geometry of the local coordination environment around the Eu^{3+} ion to be a slightly distorted tricapped trigonal prism. Luminescence lifetimes were found to be 581, 473, and 576 μs and absolute quantum yields were measured as 16.4 ± 1.4%, 27.5 ± 1.2%, and 22.2% ± 0.3%, for complexes **1**-**3**, respectively.

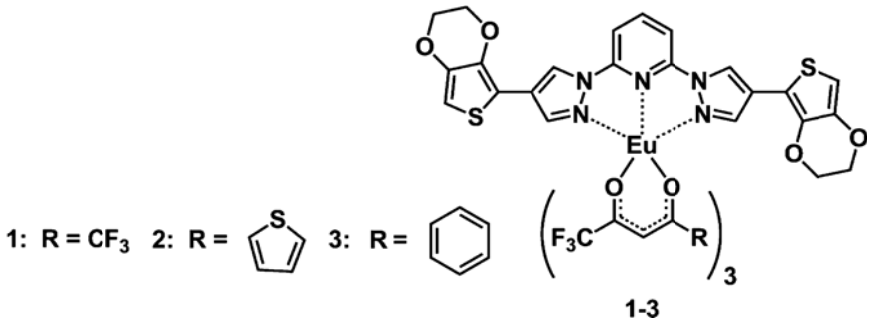

Figure 1.6. Structure of the Eu^{3+} complexes Eu(*β*-diketonate)$_3$(L).

The role of lignad-to-metal energy transfer state in nontriplet photosensitization of luminescent Eu^{3+} complex [Eu(tta)$_3$(dpbt), where tta = thenoyl trifluoroacetonate and Dbpt = 2-(*N*,*N*-diethylanilin-4-yl)-4,6-bis(3,5-dimethylpyrazol-1-yl)-1,3,5-triazine)] (Figure 1.7), has been investigated by means of steady-state and time-resolved optical spectroscopies [Fu *et al.* 2010]. In the Eu(tta)$_3$(dpbt) complex, the ligand dpbt exhibited biphasic fluorescence decay kinetics; the faster component (decay time constant, 8.5 ps) is ascribed to the rapid conversion of the lowest-lying singlet excited state of dpbt (S_1 or ^{1}dpbt*) to a ligand-to-metal charge transfer singlet state of the complex (^{1}LMCT*), whereas the slower one (1.8 ns) is shown by temperature-dependent luminescence spectroscopy to be delayed fluorescence due to the LMCT-to-dpbt backward energy transfer and represents the time scale of efficient excitation energy flow from the ^{1}LMCT* state to the $^5D_1$ state of Eu^{3+}. In conclusion, this work established a non-triplet photosensitization pathway for the Eu^{3+} complex, which may shed

light on the development of highly efficient and long-wavelength sensitized organic luminescent lanthanide complexes.

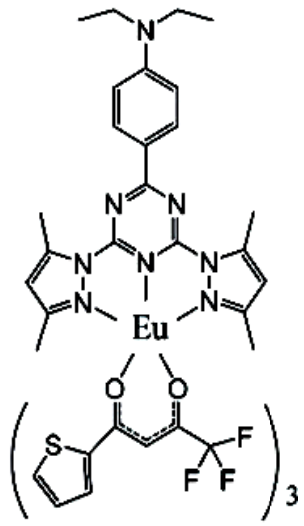

Figure 1.7. Structure of $Ln(tta)_3(dpbt)$ complex (where Ln = Eu, Gd, Tb).

Aryl phosphine oxide (APO) derivatives seem to be attractive as neutral ligands for light emitting lanthanide complexes with much stronger coordination to the metal ions, adaptability of functionalization and with tunable excited energy levels. In view of these, recently a series of bidentate aryl phosphine oxide derivatives charecterized by two diphenylphosphine oxide moieties [2-(diphenylphosphoryl)-*N*-(2-(diphenylphosphoryl)-4-methoxyphenyl)-4-methoxy-*N*-(4-methoxyphenyl)aniline (TMOADPO), 3,6-bis(diphenylphosphoryl)-9-ethyl-9*H*-carbazole (EtCzDPO), and 3,6-bis(diphenylphosphoryl)-9-phenyl-9*H*-carbazole (PhCzDPO)] bridged with a hole-transporting arylamine, as well as their tertiary complexes $[Eu(TTA)_3(TMOADPO)_2$, $Eu(TTA)_3(EtCzDPO)_2$, and $Eu(TTA)_3(PhCzDPO)_2$ (TTA = 2-thenoyltrifluoroacetonate)] (Figure 1.8), were designed and reported their photophysical properties [Xu *et al.* 2010]. The strong absorption antennae effect of the functional APO ligands was proved. It is shown that their more rigid structure and chelate coordinate mode impart a decreased degree of freedom and form much more compact complex structures, which not only reduces the energy loss caused by the structure relaxation but also restrains the solvent

quenching and facilitates the energy transfer from the APO ligands to Eu^{3+}. All of the complexes exhibited excellent electroluminescent (EL) performance, such as maximum brightness around 1000 cd m^{-2}, an external quantum efficiency (EQE) around 3%, and stable monochromic red emission at 614 nm.

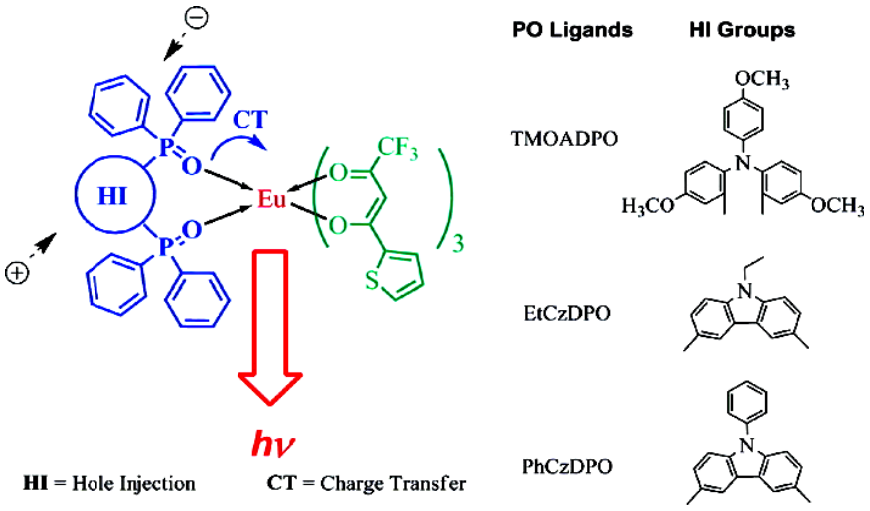

Figure 1.8. Structure of complexes 1-3 reported by Xu *et al.* 2010.

In thier former works, these authors reported an efficient electroluminescent bidentate APO Eu^{3+} complex $Eu(TTA)_3(DPEPO)$ (DPEPO = bis(2-(diphenylphosphino)phenyl) ether oxide) [Xu *et al.* 2006]. The improved structural stability, intermediate excited energy levels, and efficient photoluminescence (PL) and EL were demonstrated. The complex $Eu(TTA)_3(DPEPO)$ exhibited a photoluminescence (PL) quantum yield of 55.3% in dichloromethane, which is more than twice of the PL quantum yield of $Eu(TTA)_3(TPPO)_2$ (TPPO = triphenylphosphine oxide) [Fu *et al.* 2003]. Further, the multilayered electroluminescent (EL) device of $Eu(TTA)_3(DPEPO)$ used as the red dopant exhibited an impressive brightness of 632 cd m^{-2} at 25 V. In the subsequent studies, these authors also demonstrated highly improved electroluminescence from a series of novel Eu^{3+} complexes [$(Eu(TTA)_3(L)_2$ where L= (4-diphenylaminophenyl) diphenylphosphine oxide (TAPO), (4-naphthalen-1-yl-phenylaminophenyl) diphenylphosphine oxide (NaDAPO), and 9-[4-(diphenylphosphinoyl) phenyl]-9H-carbazole (CPPO) (Figure 1.9)] with functional single-coordinated phosphine oxide

ligands [Xu *et al.* 2007; Xu *et al.* 2008]. The investigation indicated that by taking advantage of the modification inertia of the phosphine oxide ligands, the direct introduction of the hole-transport groups as chromophore made TAPO, NaDAPO, and CPPO to obtain the most compact structure and mezzo S_1 and T_1 energy levels, which improved the intramolecular energy transfer in these Eu^{3+} complexes.

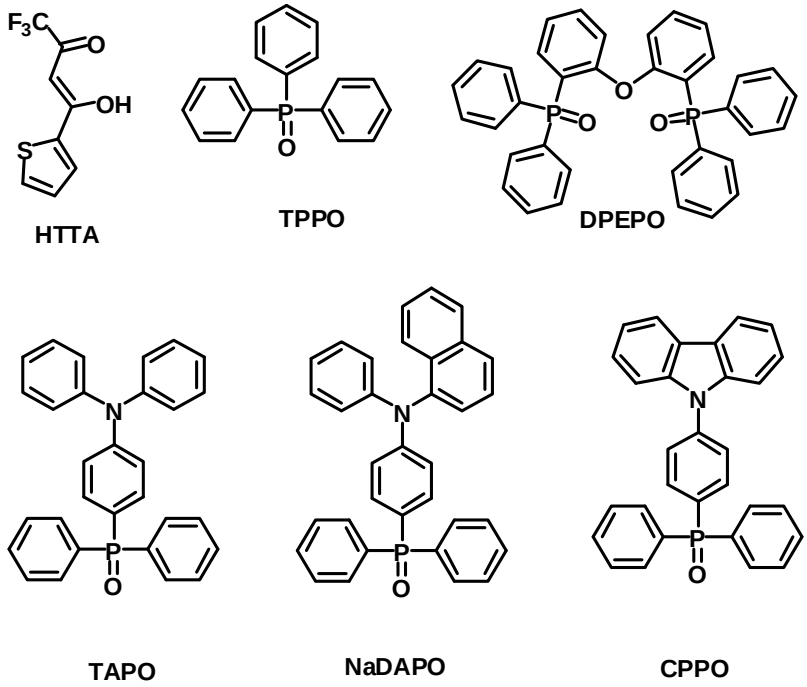

Figure 1.9. Molecular structures of the ligands used by Xu *et al*.

Carbazole-based compounds are excellent optical and electronic materials and their metal complexes show interesting and unique chemical and physical properties. Hence, carbazole-containing *β*-diketones and their Eu^{3+} complexes have been investigated intensively [Robinson *et al.* 2000; Li *et al.* 2006]. Two novel carbazole-based *β*-diketones with 2- or 2,7-substituted groups in the carbazole ring, 2-(4´4´4´-trifluoro-1´3´-dioxobutyl)-carbazole (2-TFDBC) and 2,7-bis(4´4´4´-trifluoro-1´3´-dioxobutyl)-carbazole (2,7-BTFDBC), and their Eu^{3+} ternary complexes $Eu(2\text{-TFDBC})_3phen$ and $Eu_2(2,7\text{-BTFDBC})_3(phen)_2$ (Figure 1.10) were synthesized via a dexterously designed routine, charectarized and investigated their photophysical properties [[a]He *et al.* 2009]. PL measurement results indicated that suitably expanded π-conjugation in the complex molecules makes the excitation band redshifted to the visible

region, and both the Eu^{3+} complexes exhibit intense red emission under blue-light excitation. The triplet state energy levels of 2-TFDBC and 2,7-BTFDBC in the complexes are found to be higher than that of the lowest excited level of Eu^{3+} ion, $^5D_0$, so the photoluminescence mechanism of the Eu^{3+} complexes was proposed as a ligand-sensitized luminescence process. All of the results indicate that $Eu(2\text{-}TFDBC)_3phen$ and $Eu_2(2,7\text{-}BTFDBC)_3(phen)_2$ are promising candidates as visible-light excitable red phosphor for luminescence applications.

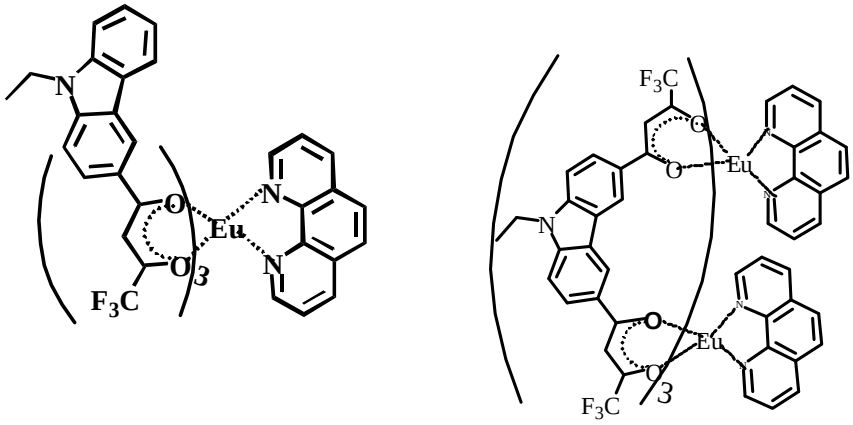

Figure 1.10. Molecular structures of the complexes by [a]He *et al.* 2009.

In their subsequent studies, these authors have investigated the effect of different alkyl group at the N-position on the luminescence of carbazole based *β*-diketonate Eu^{3+} complexes [[b]He *et al.* 2009] and fabricated bright red LEDs. There exists a competition between the absorption capacity and the energy transfer efficiency as the alkyl substituent at the N-position in the carbazole ring of the complexes (Figure 1.11) changes, and as a consequence, the total sequence of the emission intensity is $Eu(N\text{-}C2)_3(phen)$ > $Eu(N\text{-}C3)_3(phen)$ > $Eu(N\text{-}C5)_3(phen)$ > $Eu(N\text{-}C1)_3(phen)$.

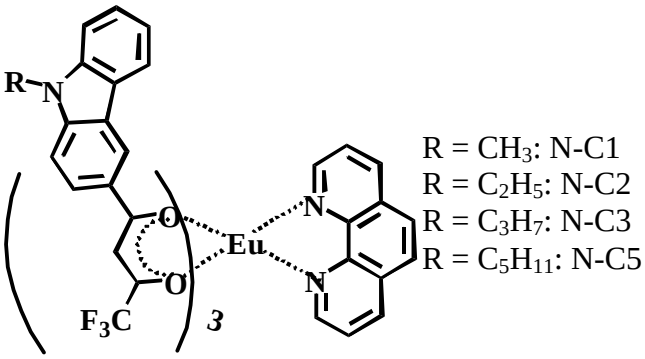

Figure 1.11. Structure of Eu(*β*-diketonate)$_3$(phen) complex.

A new Eu^{3+} complex acting as a single component white light-emitting fluorophore with tunable emission colors has been reported [[c]He *et al*. 2009]. By tailoring the excitation energies, the synthetic dye exhibited three individual primary colors (blue, green, and red) as well as white emission as can seen from Figure 1.12. The new fluorophore exhibits characteristic blue emission of the coumarin fluorophore centered at 460 nm, green rhodamine emission centered at 550 nm, and typical red emission of the Eu^{3+} ion with dominant peak at 612 nm when its solution in acetonitrile (50 μM) is excited at 415, 525, and 360 nm, respectively.

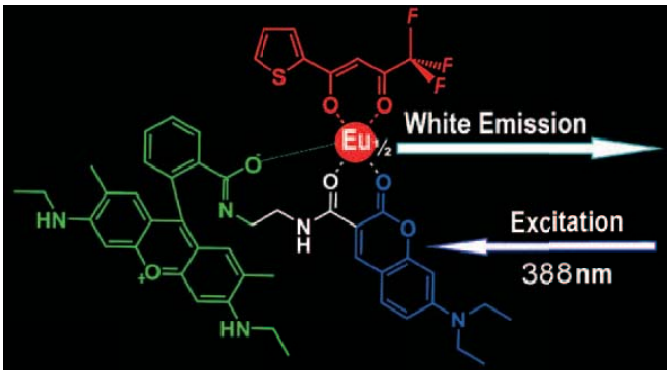

Figure 1.12. The structure of the white-emitting dye showing the fragments of the coumarin (blue), rhodamine 6G (green), and Eu^{3+} based (red) primary-color-emitting fluorophores.

A new direction for white organic light emitting devices is disclosed by employing a novel Eu^{3+} complex shown in Figure 1.13 [Law *et al.* 2009]. This single component contains a double emission center of bluish-green and red combine to give a pure white emission with CIE colour coordinates x = 0.34 and y = 0.35.

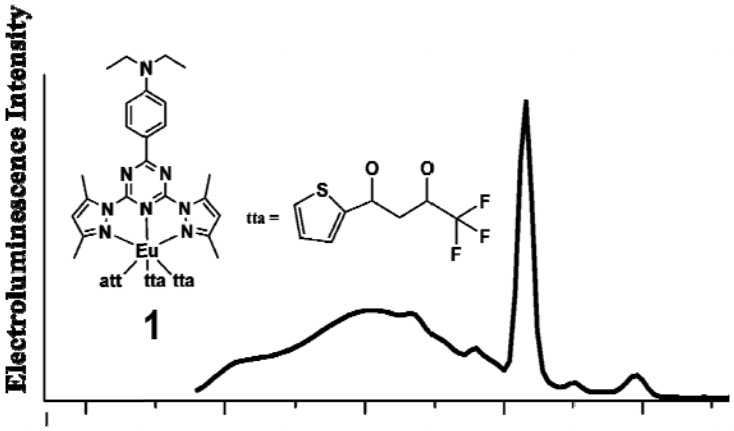

Figure 1.13. EL spectra of the complex reported by Law *et al.* 2009.

Novel nine coordinate Eu^{3+} complexes {[$Eu(hfa)_3$(DPPPO)], [$Eu(hfa)_3$(DPPYPO)] and [$Eu(hfa)_3$(DPBTPO)], where hfa = hexafluoroacetylacetonate; DPPPO = bis[*o*-(diphenylphosphoryl)phenyl] phenylphosphaneoxide; DPPYPO = bis[*o*-(diphenylphosphoryl)pyridyl]-phenylphosphane oxide and DPBTPO = bis[*o*-(diphenylphosphoryl) benzothienyl]phenylphosphane oxide} (Figure 1.14) with tandem-connected tridentate phosphane oxide ligands with high emission quantum yields (>60%) have been reported [Miyata *et al.* 2009]. These Eu^{3+} complexes showed characteristic emission properties depending on their moiety between phosphane oxides.

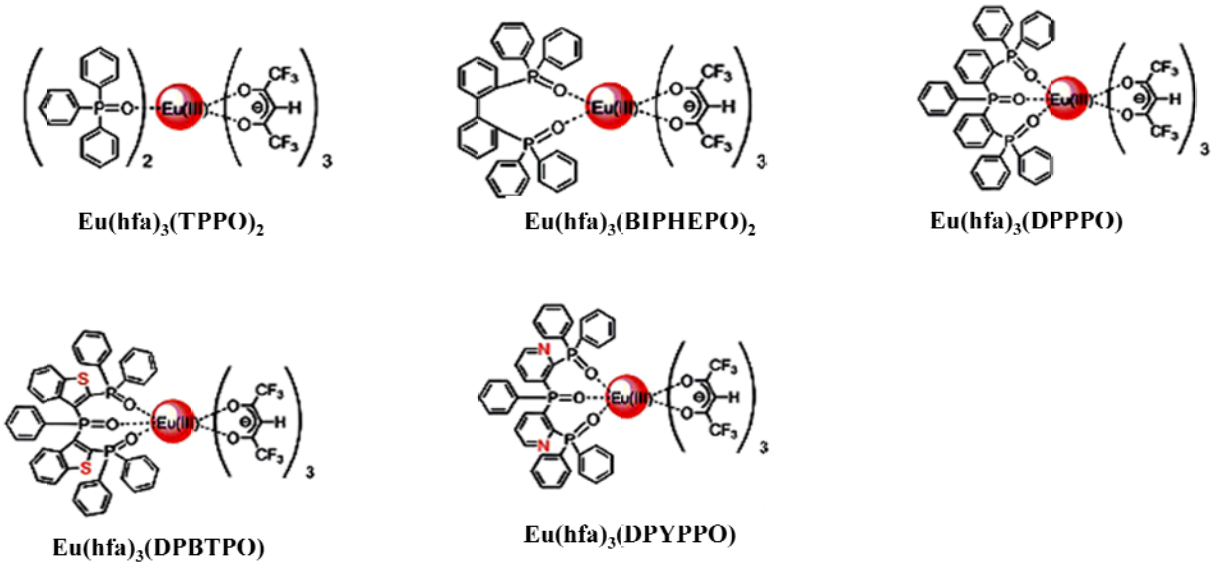

Figure 1.14. Chemical structures of Eu^{3+} complexes with phosphane oxides.

The role of ancilliary ligand *N*,*N*-dimethylaminoethanol in the sensitization of Eu^{3+} and Tb^{3+} luminescence in dimeric β-diketonate complex [$Ln_2(HFA)_6(\mu_2$-$O(CH_2)_2NHMe_2)_2$] (Ln = Eu^{3+} and Tb^{3+}) has been investigated [Eliseeva *et al.* 2008]. The dimeric β-diketonate complex shown in Figure 1.15 was obtained by reacting [$Ln(HFA)_3(H_2O)_2$] with *N*,*N*-dimethylaminoethanol in toluene and fully charecterized. X-Ray single crystal analysis performed for the Tb^{3+}compound confirms its dimeric structure. In [$Tb_2(HFA)_6(\mu_2$-$O(CH_2)_2NHMe_2)_2$], eight-coordinate Tb^{3+} ions adopt distorted square-antiprismatic coordination environments and are O-bridged by two zwitterionic *N*,*N*-dimethylaminoethanol ligands with a

Tb1···Tb2 separation of 3.684 Å. The Eu^{3+} and Tb^{3+} dimers display metal-centered luminescence with quantum yields of 58% for $[Eu_2(HFA)_6(O(CH_2)_2NHMe_2)_2]$ and 0.04% for $[Tb_2(HFA)_6(O(CH_2)_2NHMe_2)_2]$, respectively. Consideration of energy migration paths within the dimers, based on the study of both pure and Eu^{3+}- or Tb^{3+}-doped (0.01-0.1 mol %) Lu^{3+} analogues, leads to the conclusion that the β-diketone and *N*,*N*-dimethylaminoethanol ligands contribute significantly to the sensitization process of the Eu^{3+} luminescence. The ancillary ligand increases considerably the luminescence of $[Eu_2(HFA)_6(O(CH_2)_2NHMe_2)_2]$, compared to $[Eu(HFA)_3(H_2O)_2]$, through the formation of intra-ligand states while it is detrimental to Tb^{3+} luminescence.

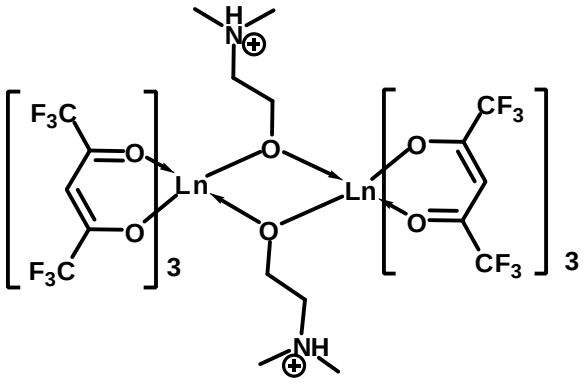

Figure 1.15. Structural formulas of the Ln^{3+} complexes $[Ln_2(HFA)_6(\mu_2\text{-}O(CH_2)_2NHMe_2)_2]$; (Ln = Eu^{3+}, Tb^{3+}).

A novel ligand, 4,4,5,5,5-pentafluoro-1-(1′,10′-phenanthrolin-2′-yl)-pentane-1,3-dionate having four coordination sites was designed as a bridge to link the Ir^{3+} center and the Eu^{3+} center and iridium-europium bimetallic complexes, $\{[(dfppy)_2Ir(\mu\text{-phen5f})]_3EuCl\}Cl_2$ and $(dfppy)_2Ir(\mu\text{-phen5f})Eu(TFAcA)_3$ [dfppy represents 2-(4′,6′-difluorophenyl)-pyridinato-N,$C^{2'}$, phen5f stands for 4,4,5,5,5-pentafluoro-1-(1′,10′-phenanthrolin-2′-yl)-pentane-1,3-dionate and TFA represents trifluoroacetylacetonate] shown in Figure 1.16, were successfully synthesized and evaluated their luminescent properties [Chen *et al.* 2008]. Photophysical studies implied that the high efficient red luminescence from the Eu^{3+} was sensitized by the ^{3}MLCT (metal-to-

ligand charge transfer) energy based on an Ir^{3+} complex-ligand in a *d-f* bimetallic assembly. The excitation window for the new bimetallic complex extends up to 530 nm (1×10^{-3} M in ethanol), indicating that this bimetallic complex can emit red light under the irradiation of sunlight.

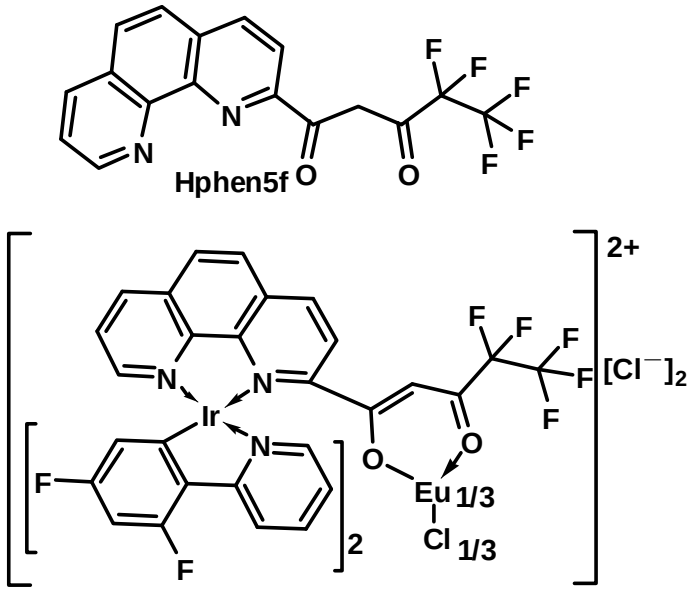

Figure 1.16. Structural formulas of the ligand 4,4,5,5,5-pentafluoro-1-(1′,10′-phenanthrolin-2′-yl)-pentane-1,3-dione (Hphen5f) and bimetallic complex.

In order to shift the excitation wavelength of lanthanide *β*-diketonate complexes to longer wavelengths, the ferrocene-derivatives bis(ferrocenyl-ethynyl)-1,10-phenanthroline (Fc_2phen) and ferrocenoyltrifluoroacetone (Hfta) have been synthesized and used for the design of two ferrocene containing lanthanide *β*-diketonate complexes [Yuan *et al.* 2007]. The complexes $[Ln(TTA)_3(Fc_2phen)]$ and $[Ln(fta)_3(phen)]$ (where Ln = La, Nd, Eu and Yb) depicted in Figure 1.17 showed structural similarities to the parent $[Ln(TTA)_3(phen)]$ complexes. The presence of the ferrocene moiety improves the solubility of the complexes in organic solvents like dichloromethane, chloroform, and toluene. The best luminescence properties were found for the $[Ln(TTA)_3(Fc_2phen)]$ complexes of the ferrocene-substituted 1,10-phenanthroline ligand. Here, visible light with a wavelength up to 420 nm (blue light) could be used for excitation of Eu^{3+} (red emission) and of Nd^{3+} and Yb^{3+} (both near-infrared emission).

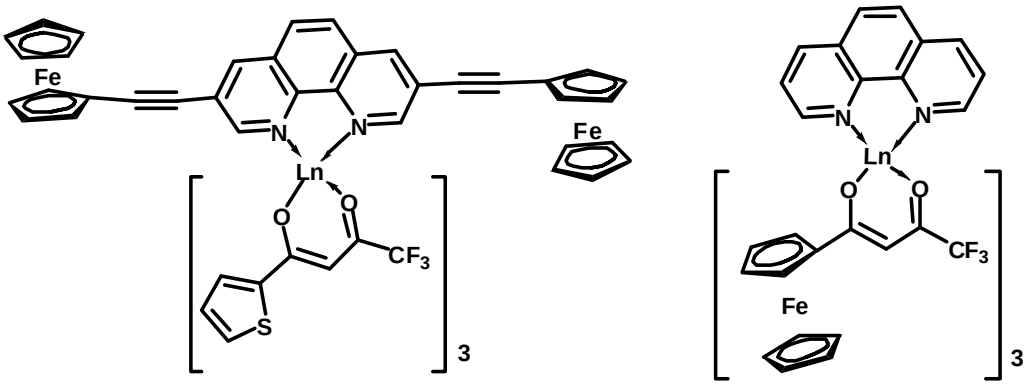

Figure 1.17. Structural formulas of the complexes $[Ln(tta)_3(Fc_2phen)]$ and $[Ln(fta)_3(phen)]$, with Ln = La, Nd, Eu and Yb.

The reaction of lanthanide hexafluoroacetylacetonates $[Ln(HFA)_3(H_2O)_2]$ (Ln = Sm^{3+}–Ho^{3+} and Tm^{3+}) with 4-cyanopyridine *N*-oxide (4-cpyNO) in a 1:1 ratio results in the formation of $[Ln(HFA)_3(4\text{-cpyNO})]_2$ dimers as shown in Figure 1.18, in which the two metal ions are separated by about 3.99-4.13 Å [Eliseeva *et al.* 2006]. The substitution of water molecules in the parent hydrated complexes $Ln(HFA)_3(H_2O)_2]$ by 4-cpyNO has a large effect on the luminescence properties. Such a combination of organic ligands is able to sensitize the metal-centered luminescence of Sm^{3+}, Eu^{3+}, Tb^{3+}, Dy^{3+} and Tm^{3+} ions that emit pink, red, green, yellow and blue light, respectively, i.e. within the entire spectral visible range. The introduction of the ancillary ligand leads to substantial and varying changes in the luminescence quantum yields. The greatest effect occurs for $[Eu(HFA)_3(4\text{-cpyNO})]_2$, with a ten-fold increase in the absolute quantum yield (from 2.6 to 25.7%) with respect to the hydrated complex. In the case of corresponding terbium dimer increases only a factor of 2. On the other hand, a decrease in the quantum yield is observed for Sm^{3+}, Dy^{3+} and Tm^{3+} dimers with respect to the hydrated chelates.

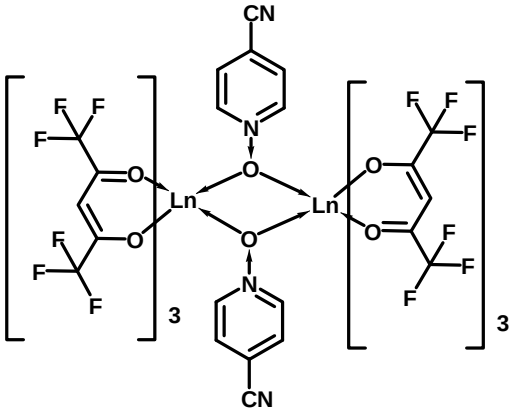

Figure 1.18. Molecular structures of the Ln^{3+} complexes $[Ln(hfa)_3(4\text{-}cpyNO)]_2$. (Ln = Sm^{3+}–Ho^{3+} and Tm^{3+})

Bright photoluminescence as well as efficient electroluminescence has been reported with lanthanide complexes $Ln(HFNH)_3(phen)$ [HFNH = 4,4,5,5,6,6,6-heptafluoro-1-(2-naphthyl)hexane-1,3-dione; phen = 1,10-phenanthroline; Ln = Eu^{3+}, Sm^{3+}] depicted in Figure 1.19 [Yu *et al.* 2005]. By the comparison of the electroluminescent properties of devices based on $Eu(TTA)_3(phen)$ (TTA = 2-thenoyltrifluoroacteonate) and $Eu(HFNH)_3(phen)$, it has been concluded that the polyfluorination on the alkyl group of the ligand and the introduction of the long conjugate naphthyl group into the ligand improve the efficiency of $Eu(HFNH)_3(phen)$ doped devices, especially at high current densities.

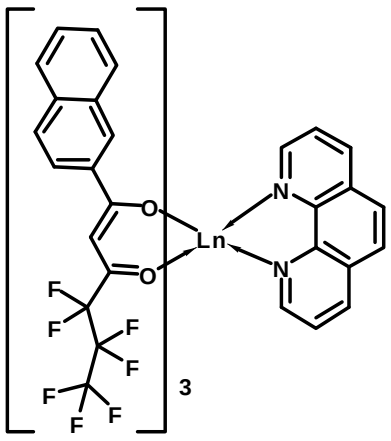

Figure 1.19. Structure of the Ln^{3+} complexes $Ln(HFNH)_3(phen)$; (Ln = Eu^{3+}, Sm^{3+}).

Adducts of the type $Ln(NTA)_3 \cdot L$ [Ln = Eu, Gd; NTA = 1-(2-naphthoyl)-3,3,3-trifluoroacetonate; L = 1,4-diaza-1,3-butadiene RN=CHCH=NR (R = *p*-tolyl, *o*-tolyl)] displayed in Figure 1.20 were prepared by treatment of $Ln(NTA)_3(2H_2O)$ with one equivalent of the chelating N−N ligand and the designed complexes were charecterized by various spectroscopic techniques [Fernandes *et al.* 2004]. The room-temperature PL spectra of the Eu^{3+} complexes are composed of the typical Eu^{3+} red emission, assigned to transitions between the first excited state ($^5D_0$) and the ground multiplet ($^7F_{0-4}$). Based on the room-temperature emission spectra and lifetime measurements, the quantum efficiencies of the $^5D_0$ Eu^{3+} excited state were estimated and found to be quite low (e.g. 2−3%). The low efficiencies are attributed to the presence of thermally activated nonradiative channels involving ligand-to-metal charge-transfer (LMCT) states. Indeed, a low-lying LMCT band was detected for the Eu^{3+} complex containing the ligand *p*-tolyl-DAB by comparison of the room-temperature diffuse reflectance spectrum for this complex with that of the corresponding Gd^{3+} analogue.

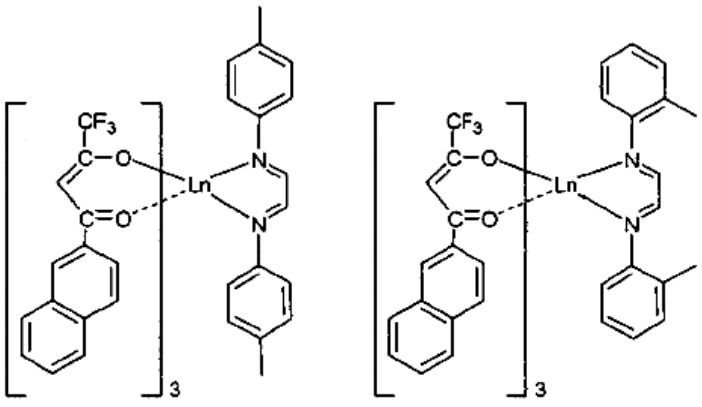

Ln = Eu (1), Gd (3) Ln = Eu (2), Gd (4)

Figure 1.20. Structure of the Ln^{3+} complexes $Ln(NTA)_3(DAB)$; (Ln = Eu^{3+}, Gd^{3+}).

Photoluminescent properties of polymer systems doped with Eu^{3+} fluorinated *β*-diketonates: Recent developments

The incorporation of lanthanide complexes in a polymer matrix has been found to be of enormous interest, because such a composite material possesses advantages of the luminescence characteristics of lanthanide ions with excellent mechanical properties, lightweight, good transparency, low temperature processability, etc [Liang *et al.* 2005; Luo *et al.* 2007]. PMMA is one of the best studied polymer matrixes for the above purpose, as it has a low optical absorbance, has a low cost, is easily synthesized, and its refractive index can be tailored with molecular weight. A series of Eu^{3+} luminescent complexes based on fluorinated *β*-diketonates and bis(2-(diphenylphosphino)phenyl)ether oxide as an ancilliary ligand (summarized in Figure 1.21) have been synthesized, incorporated in to a PMMA matrix and investigated their photophysical properties [Moudam *et al.* 2009]. These authors have demonstrated exceptionally high values of photoluminescent quantum yield of Eu^{3+} complexes ($\Phi_{overall}$ = 80%) in solution and in common optical polymer PMMA. This may arise from enhanced encapsulation of the Eu^{3+} center that reduces the detrimental effect of C-H oscillators in the PMMA matrix and provides non-radiative pathways for the Eu^{3+} excited state.

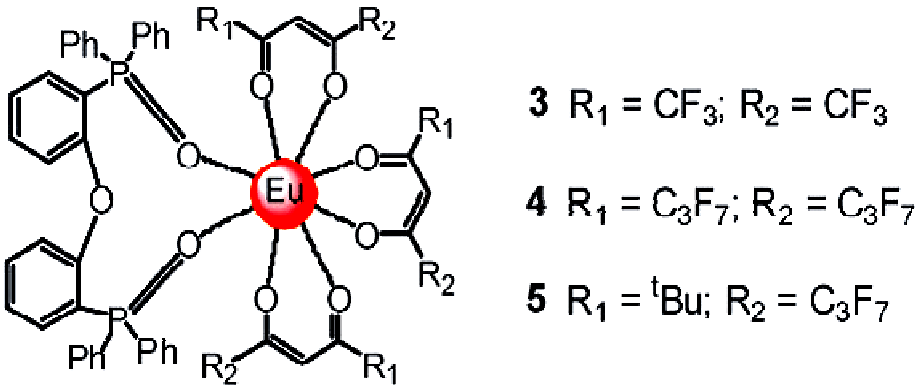

Figure. 1.21. Molecular structure of complexes **3** [$Eu(hfac)_3(DPEPO)$], **4** [$Eu(tfn)_3(DPEPO)$] and **5** [$Eu(dho)_3(DPEPO)$].

Luminescent PMMA containing $Eu(hfa\text{-}D)_3(DPFBPO)_2$ complex exhibiting high quantum yield and fast radiation rate (quantum yield = 78 ± 6%, radiation rate = 1.2×10^3 s^{-1}) has been disclosed elsewhere [Hasegawa *et al.* 2003]. The synthesized luminescent polymers showed promising results for applications to novel organic Eu^{3+} devices, such as organic liquid lasers, plastic lasers, and optical fibers.

Optical properties of highly transparent blends formed by bisphenol A polycarbonate (PC) and poly(methylmethacrylate) (PMMA) and doped with Eu^{3+} thenoyltrifluoroacetone hydrate [$Eu(TTA)_3$-hydrate] were studied and found the interaction between PC/PMMA blend with the complex leads to the quenching of luminescence in these polymer blends [Velasco *et al.* 2010].

The Eu^{3+} complex $Eu(TTA)_3(TPPO)_2$ (TTA = thenoyl trifluoroacetone, TPPO = triphenyl phosphine oxide) was incorporated into poly(methyl methacrylate) (PMMA), polystyrene (PS) poly(vinylpyrrolidine) (PVP) matrixes (Figure 1.22) and electrospun into various composite fibres and investigated their photophysical properties [Zhang *et al.* 2008].

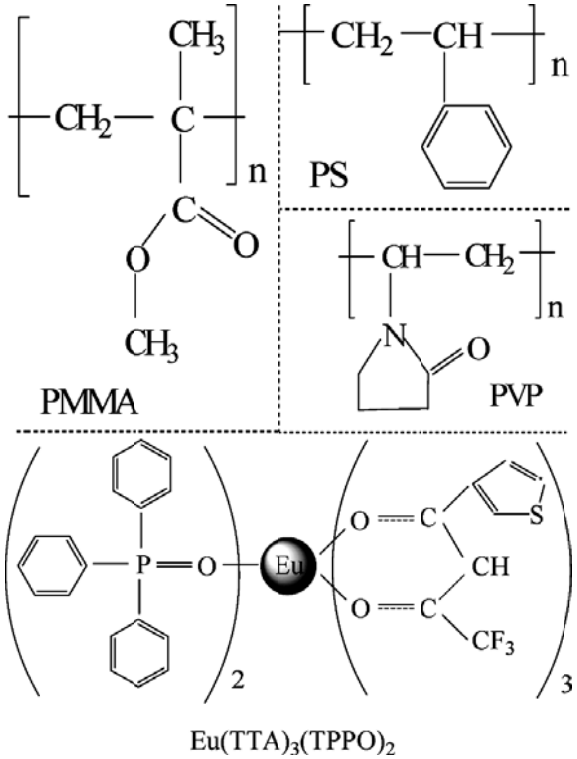

Figure 1.22. Molecular structures of polymers PMMA, PS, and PVP and of the $Eu(TTA)_3(TPPO)_2$ complex.

The results indicate that, in all of the composite fibres, the excitation bands of the ligands split into different components because of the distorted crystal field, which reduces the degree to which the $^5D_0$-$^7F_0$ transition is parity forbidden. In addition, the thermal stability of the photoluminescence of Eu^{3+} in the composite fibres is considerably improved over that of the pure complex. Also, the $Eu(TTA)_3(TPPO)_2$/PS composite fibres exhibit better photostability upon exposure to ultraviolet light. In the $Eu(TTA)_3(TPPO)_2$/PS composite, blue and green band emissions caused by fluorescent impurities appear and together with red emissions of Eu^{3+}, produce white light which might have a potential application in white-light emitting diodes.

The sensitization effect by polymer matrices on the photoluminescence properties of diaquatris(thenoyltrifluoroacetonate)europium(III), $[Eu(tta)_{3(}H_2O)_2]$, doped into poly-β-hydroxybutyrate (PHB) with doping percentage at 1, 3, 5, 7 and 10% (mass) in film form (Figure 1.23) has been investigated [Kai *et al.* 2008].

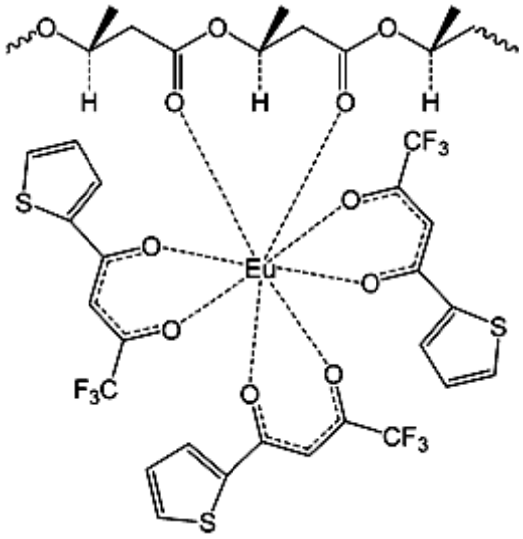

Figure 1.23. A schematic illustration of the structure of $Eu(tta)_3$ complex doped in polymer.

The emission spectra of the Eu^{3+} complex doped PHB films recorded at 298 K exhibited the five characteristic bands arising from the $^5D_0 \rightarrow {}^7F_J$ intraconfigurational transitions (J = 0–4). The fact that the quantum efficiencies of the doped film increased significantly revealed that the polymer matrix acts as an efficient co-sensitizer for Eu^{3+} luminescent centres and therefore

enhances the quantum efficiency of the emitter $^5D_0$ level. The luminescence intensity decreases, however, with increasing precursor concentration in the doped polymer to greater than 5% where a saturation effect is observed at this specific doping percentage, indicating that changes in the polymeric matrix improve the absorption property of the film, consequently quenching the luminescent effect.

Photoluminescent properties of Eu^{3+} fluorinated *β*-diketonate complexes covalently grafted on to the mesoporous hybrid materials: Recent developments

Inorganic-organic hybrid materials have attracted considerable attention with the expansion of soft inorganic chemistry processes and provided a wealth of opportunities for combination of organic and inorganic networks to exhibit their extraordinary properties such as luminescent systems in lighting displays, optical amplifiers, and lasers [Molina *et al.* 2001; Suratwala *et al* 1998]. According to the interaction between the organic and inorganic components or phases, these hybrid materials can be divided into two major classes. One is so-called physically mixed by weak interactions (hydrogen bonding, van der Waals force, or weak static effects) between the organic and inorganic phases; the other is chemically bonded by powerful covalent bonds [Harreld *et al.* 2003; Minoofar *et al.* 2002]. In the first class, although the metal complex, especially lanthanide organic complexes that have been doped into a silica matrix, have shown superior emission intensities and organic components are considered to be efficient sensitizers for the lanthanide ions, this kind of material cannot solve the problems of the quenching effect of luminescent centers, inhomogeneous dispersion of two phases, or leaching of the photoactive molecules with a low concentration of the complex. Moreover, because the latter class hybrid material belongs to the molecular-based composite material with excellent chemical stability and a monophasic appearance even with a high concentration of lanthanide complexes [[a]Li *et al.* 2001; Li *et al.* 2002], we can tailor the multifunctional advanced materials for different

demands in physiology, biochemistry, and photochemistry areas through the combination of the different components with chemical bonds.

A novel kind of luminescent ternary organic inorganic hybrid Eu(TTA-Si-SBA-15)$_3$(phen) (TTA = thenoyltrifluoroacetone, phen = 1,10-phenanthroline) (Figure 1.24) has been assembled by the Eu^{3+} complex covalently attached to the TTA directly functionalised by ordered mesoporous SBA-15, which is charecterized to have high surface area, uniformity in the mesostructure and crystallinity [Yan and Li, 2010]. Investigations into the luminescence of Eu(TTA-Si-SBA-15)$_3$(phen) mesoporous material shows that the charecteristic luminescence of the corresponding Eu^{3+} occurs via intramolecular energy transfer from the modified ligand to the central Eu^{3+} ions. The good luminescent properties of these materials, together with the highly ordered hexagonal channel structures and uniform pore sizes of the organic group functionalized SBA-15 mesoporous material will expand their applications in optical or electronic areas.

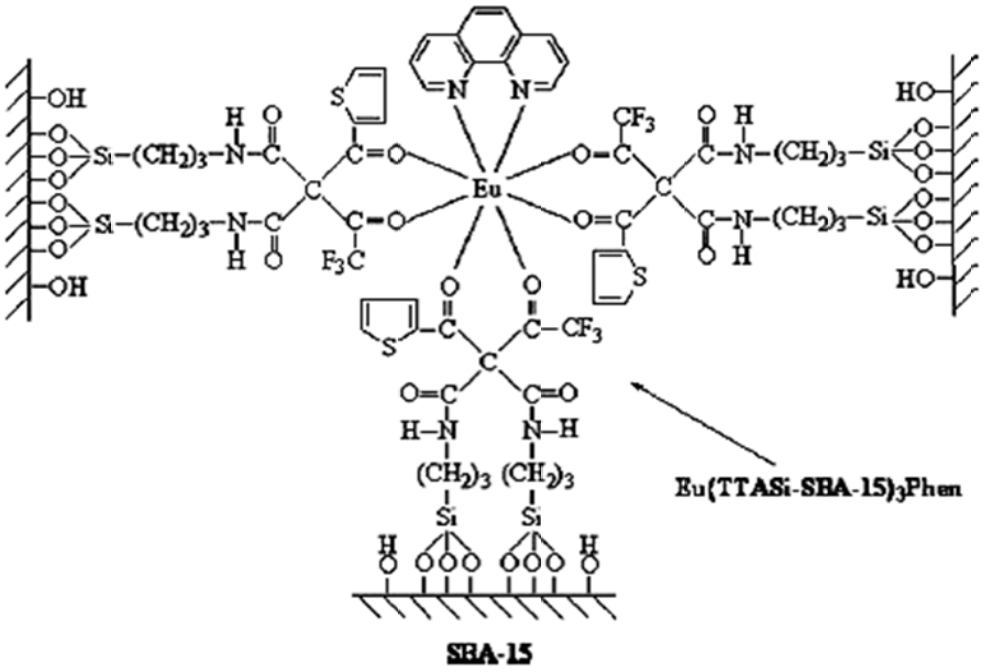

Figure 1.24. Predicted structure of the ternary hybrid mesoporous material Eu(TTA-Si-SBA 15)$_3$(phen).

The Eu^{3+} complexes have been covalently immobilized in the ordered SBA-15 mesoporous host through modification of 1-(2-naphthoyl)-3,3,3-trifluoroacetonate (NTA) with 3-(triethoxysilyl)propyl isocyanate (TEPIC) using a cocondensation method [Li *et al.* 2008]. Synthesis of NTA-SBA-15 provides a convenient approach for tailoring the surface properties of mesoporous silicates by organic functionalization, and the resulting materials all retain the ordered mesoporous structures. Further investigation on the luminescence properties of Eu-(NTA-SBA-15)$_3$(bpy) (Figure 1.25) mesoporous materials shows that the characteristic luminescence of the corresponding Eu^{3+} through the intramolecular energy transfers from the modified ligand (NTA-Si) to the central Eu^{3+} ions.

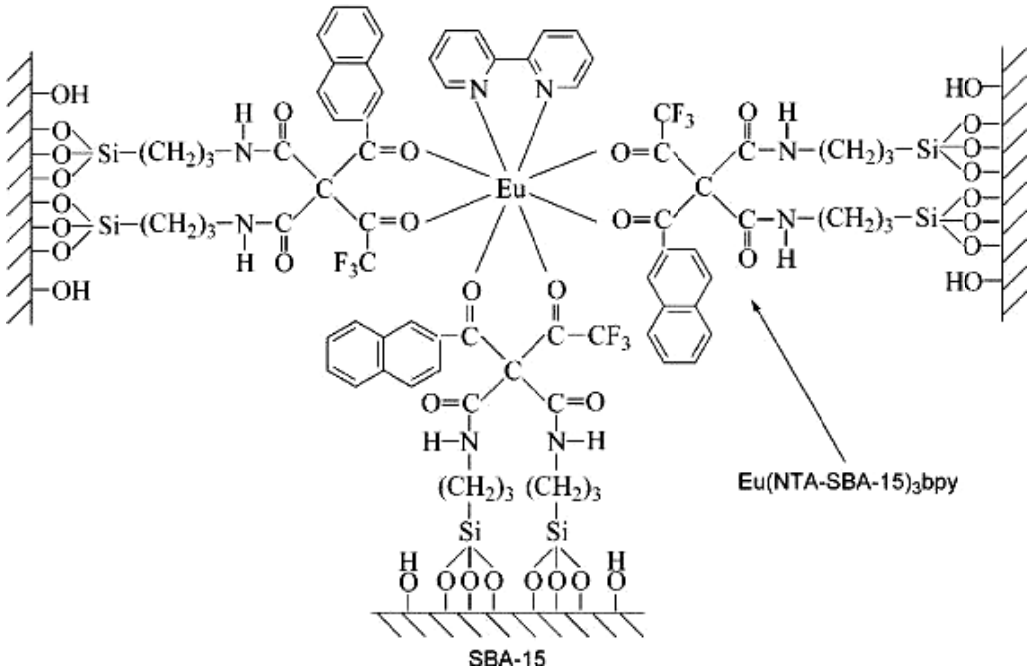

Figure 1.25. Predicted structure of hybrid mesoporous material Eu(NTA-SBA-15)$_3$bpy.

1.3. Objectives of the present investigation

The fascinating optical properties of europium(III) ions have promoted the use of their complexes in an increasing number of technological applications ranging from biomedical analysis to materials science. An exciting physicochemical feature of Eu^{3+} β-diketonates is their bright luminescence [Filipescu and Mushrush 1966], which motivated Weissman to propose the concept of population of the emitting 4f levels through energy transfer from the ligand (sensitization process) [Weissman 1942]. In part, this is due to the fact that the π–π^* transition for β-diketones is intense and occurs over a significant range of wavelengths that is appropriate for sensitization of Eu^{3+} cation luminescence. Eu^{3+} β-diketonate compounds usually crystallize with solvent molecules, which are detrimental to their photophysical properties. To overcome the solvent-quenching problem, neutral chromophoric ligands may be used as ancillary ligands to saturate the inner coordination sphere of the metal ion. As a consequence, the sensitization of Eu^{3+} luminescence can be additionaly improved when the ancilliary ligands possesses suitable energy levels to provide an effective intra-molecular energy transfer from the ligand to the central Eu^{3+} ion.

It is well documented that the replacement of the C-H bonds of a β-diketone ligand with lower-energy C-F oscillators is capable of lowering the vibrational energy of the ligand. In turn, this decreases the energy loss because of ligand vibration and therefore enhances the emission intensity of the Eu^{3+} ion. Furthermore, because of the heavy-atom effect, which facilitates intersystem crossing, the lanthanide-centered luminescent properties are also improved. Therefore, the primary objective of the present work is to design and develop a novel class of fluorinated β-diketonate molecules with conjugated motifs for the sensitization of Eu^{3+} ions.

Another objective of the present work is to design and develop a novel chelating phosphine oxide and to investigate its role as an ancilliary ligand on the photosensitization of Eu^{3+} fluorinated β-diketonate complexes. Yet another objective of the present investigation is the

structural authentification of the designed Eu^{3+} antenna complexes by X-ray single crystal analysis. The structure property correlations of the designed complexes with that of the photophysical properties will also be evaluated.

It has always been a challenging task to synthesize Eu^{3+} complexes with high quantum yields that will also be thermodynamically stable and compatible with advanced microelectronic technologies for thin film production [Kuriki *et al.* 2002]. Upon inheriting the advantages of both the luminescence characteristics of Eu^{3+} ions and the material properties of plastics, Eu^{3+} metal-containing polymers have also attracted attention in the past decade. In comparison with small molecular weight Eu^{3+} complexes, besides the advantage of the desired mechanical flexibility, polymer-based Eu^{3+} luminescent materials can be solution or fused processable, this is more attractive for optical and electronic applications. Furthermore, the dissociation may be minimal in the solid polymer complexes, where Eu^{3+} complex units should be, to a certain extent, locked into a specific configuration due to the synergistic effects of metal complexes with polymers. Therefore, in the present study an attempt has also been made to incorporate the designed highly luminescent Eu^{3+}complexes into poly-(methyl methacrylate) (PMMA) and investigated their photophysical properties.

Lanthanide-containing hybrid materials have stimulated great research interest for their excellent luminescent properties and the special functions make them widely applied in various fields such as photonic crystal, optical glasses and fluorescent or laser systems [Carlos *et al.* 2009]. Hence, in the present study an effort also has been made to synthesize a highly luminescent novel organic-inorganic hybrid material by covalently anchoring the newly designed Eu^{3+} fluorinted antenna complex to the functionalized ordered mesoporous silica host MCM-41 and investigated its photophysical properties.

Chapter 2

4,4,5,5,5-Pentafluoro-1-(9H-fluoren-2-yl)-1,3-pentanedione complex of Eu^{3+} with 4,5-bis(diphenylphosphino)-9,9-dimethylxanthene oxide as a promising light-conversion molecular device

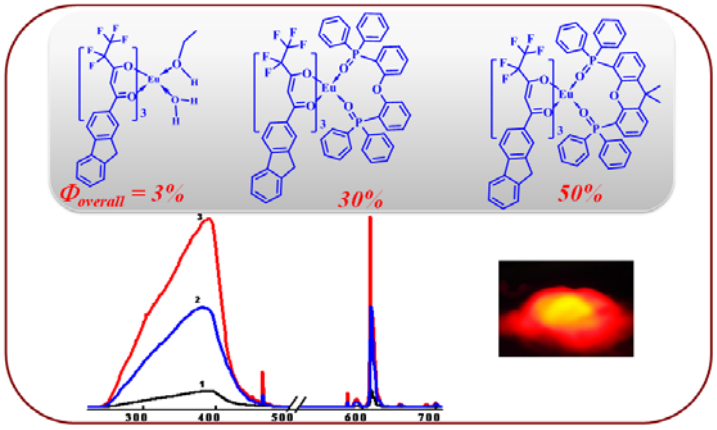

2.1. Summary. A novel *β*-diketone ligand, 4,4,5,5,5-pentafluoro-1-(9H-fluoren-2-yl)-1,3-pentanedione (Hpffpd), which contains a polyfluorinated alkyl group, as well as a long conjugated fluorene unit, and a chelate phosphine oxide ligand, 4,5-bis(diphenylphosphino)-9,9-dimethylxanthene oxide (DDXPO) were synthesized and utilized for the synthesis of two new europium complexes $[Eu(pffpd)_3(C_2H_5OH)(H_2O)]$ **1** and $[Eu(pffpd)_3(DDXPO)]$ **2**. For comparison, the $[Eu(pffpd)_3(DPEPO)]$ **3** complex was also synthesized involving a known chelate phosphine oxide, bis(2-(diphenylphosphino)phenyl)ether oxide (DPEPO). The synthesized complexes have been characterized by various spectroscopic techniques and their solid-state photophysical properties were investigated. The single-crystal X-ray diffraction analyses of **2** and **3** revealed that these complexes are mononuclear, and that the central Eu^{3+} ion is surrounded by eight oxygen atoms, six of which are from the three bidentate fluorinated *β*-diketonates, and the other two oxygen atoms from the chelate phosphine oxide. The coordination polyhedra can be described as distorted square antiprism. Compound **2** has a solid-state photoluminescence quantum yield of 50%, which is about two times higher than that of compound **3** (28%). This may be due to the fact that DDXPO in **2** has the mezzo first triplet excited state energy level (T_1) between the first singlet excited energy level (S_1) and T_1 of Hpffpd, which may support one more additional energy transfer from the T_1 energy level of DDXPO to that of Hpffpd, and consequently improves the energy transfer in the Eu^{3+} complex. Furthermore, DDXPO (average Eu–O = 2.34 Å) in complex **2** coordinates more strongly with the central Eu^{3+} as compared to DPEPO in complex **3** (average Eu–O = 2.38 Å) which can improve the energy transfer between the ligands and central metal ion, and consequently enhances the photoluminescence efficiency of the corresponding Eu^{3+} complex.

D.B. Ambili Raj *et al.*, *Dalton Trans.*, **2009**, 7519-7528.

2.2.Introduction

Due to the Laporte forbidden character and intra-configurational nature of the 4f transitions, luminescence from lanthanide cations is typically highly monochromatic, exhibits long-lived excited-state lifetimes when compared to organic compounds, and is usually insensitive to quenching by molecular oxygen, making these metal ions ideal for many applications in multidisciplinary fields such as materials for telecommunications, lighting devices, and luminescent probes for bio-analyses and live cell imaging and sensing [Kido and Okamoto 2002; Kuriki *et al*. 2002; Brunet *et al*. 2007; de Bettencourt-Dias 2007; Eliseeva and Bünzli 2010]. However, because they are forbidden, these transitions exhibit low extinction coefficients (ε < 10 L M^{-1} cm^{-1}) [Carnall *et al.* 1962; Carnall 1963; Carnall *et al.* 1965]. The weak absorbance can be overcome by coordinating chromophore-containing ligands to the metal ion, which upon irradiation, transfers energy to the metal center, typically *via* the ligand triplet excited state, populating the Ln^{3+} emitting levels in a process known as the "antenna effect" [Lehn 1990]. For this process to be efficient, it is important that the triplet level of the ligand is situated slightly above the accepting energy levels of the lanthanide ion (ideally about 1500 cm^{-1}). Because the accepting energy levels of the visible lanthanide emitters are all situated at relatively high energy positions (typically between 17 000 and 23 000 cm^{-1}), it is obvious that the absorption bands of the antenna molecules are likely to be located in the UV region [Deun *et al.* 2006].

The β-diketone ligand class is emerging as one of the important "antennas" in terms of high harvest emissions due to the effectiveness of the energy transfer from this ligand type to the Ln^{3+} cation [Binnemans 2009; de Sa *et al.* 2000]. In part, this is due to the fact that the π–π^* transition for β-diketones is intense and occurs over a significant range of wavelengths that is appropriate for sensitization of Ln^{3+} cation luminescence. An additional and practical advantage of the use of β-diketone ligands is that they form stable complexes with Ln^{3+} cations [de Sa *et al.* 2000; Biju *et al.* 2006; Pavithran *et al.* 2006; Binnemans 2009]. It is well documented that

the replacement of C–H bonds in a *β*-diketone ligand with lower-energy C–F oscillators is able to lower the vibration energy of the ligand, which minimizes the energy loss caused by ligand vibrations and consequently enhances the emission intensity of the lanthanide ion [Yu *et al*. 2005; Eliseeva *et al*. 2006; Sun *et al*. 2006; Fratini *et al*. 2008]. Further, due to the heavy-atom effect, which facilitates intersystem crossing, the lanthanide-centered luminescent properties are enhanced [Grushin *et al*. 2001; Omary *et al*. 2003]. Fluorene and its derivatives have been widely studied as building blocks for photoluminescent and electroluminescent materials [Wang *et al.* 2004; Ostrowski *et al.* 2002] because of their rigid conjugated structures and excellent thermal and photochemical stabilities [Werts *et al*. 2004; Day *et al.* 2005]. The above factors prompted to design a new *β*-diketone ligand, Hpffpd 4,4,5,5,5-pentafluoro-1-(9H-fluoren-2-yl)-1,3-pentanedione, which has the polyfluorinated alkyl group, as well as larger conjugated fluorene unit. In this work, the new *β*-diketone ligand Hpffpd is used as the main sensitizer for developing new luminescent Eu^{3+} complexes.

In general, lanthanide *β*-diketonate chelates are usually isolated as hydrates in which one or two water molecules are included in the first coordination sphere of the central metal ion, quenching the emission from the activation of non-radiative decay paths [Gao *et al.* 1999; Robinson *et al.* 2000]. A way to circumvent these difficulties is to use ancillary ligands bearing suitable chromophores that are capable of forming thermodynamically stable complexes with lanthanide ions. These ancilliary ligands would also play the antenna role, absorbing light and transferring excitation energy to the emitting ion. Additionally, when the Ln^{3+} cation is coordinatively unsaturated by the original ligands, an additional neutral ligand coordinates to the lanthanide center to form a highly coordinated complex, thereby excluding the coordination of solvent molecules. In this way, not only the volatility and thermal stability can be improved, but also the film forming properties and the carrier-transport ability [Robinson *et al.* 2000; Reyes *et al.* 2002]. As a consequence, a significant number of lanthanide tris(*β*-diketonates) that also feature coordinated nitrogen [Försberg 1973; Fukuda *et al.* 2002; Bellusci *et al.* 2005;

Chen *et al.* 2007] and phosphine oxide [Xu *et al.* 2006; Xu *et al.* 2007; Xu *et al.* 2008; Xu *et al.* 2010] ligands has been reported to serve as efficient light conversion molecular devices. Compared with N-heterocyclic ligands, the aryl phosphine oxide (APO) derivatives seem attractive as neutral ligands for light-emitting lanthanide complexes with much stronger coordination to lanthanide ions, adaptability of functionalization, and tunable excited energy levels.

Herein, we have designed and synthesized a new chelate phosphine oxide, 4,5-bis(diphenylphosphino)-9,9-dimethylxanthene oxide (DDXPO). The corresponding highly luminescent tertiary complex [$Eu(pffpd)_3$(DDXPO)] was isolated and structurally characterized by single-crystal X-ray analysis. The choice of DDXPO is based on its strong ability to coordinate lanthanide ions, its structure rigidity, and its good electron transporting ability. The chelate phosphine oxide ligand has the rigid structure, which not only can enforce the rigidity and form the more compact complexes so as to improve the triplet energy transporting from ligands to the center Ln^{3+} ion, but also can improve energy transfer between the two diphenyl phosphine oxide moieties through the bridge moieties to eliminate the formation of the exciplex.

2.3. Experimental Section

Materials and Instrumentation. The following chemicals were procured commercially and used without subsequent purification: europium(III) nitrate hexahydrate, 99.9% (Treibacher); gadolinium(III) nitrate hexahydrate 99.9% (Aldrich); 2-acetylfluoren 98% (Aldrich); methyl pentafluoropropionate 99% (Aldrich); sodium hydride 60% dispersion in mineral oil (Aldrich); bis(2-(diphenylphosphino)phenyl) ether, 97% (Aldrich); 4,5-bis(diphenylphosphino)-9,9-dimethylxanthene 97% (Aldrich). All the other chemicals used were of analytical reagent grade.

Elemental analyses were performed with a Perkin-Elmer Series 2 Elemental Analyzer 2400. A Perkin-Elmer Spectrum One FT-IR spectrometer using KBr (neat) was used to obtain the IR spectral data. A Bruker 500 MHz NMR spectrometer was used to record the ^1H NMR (500

MHz), ^{13}C NMR (125.7 MHz), and ^{31}P NMR (202.4 MHz) spectra of the new compounds in chloroform-d or acetone-d_6 solution. The chemical shifts are reported in parts per million relative to tetramethylsilane, $SiMe_4$ for ^{1}H NMR and ^{13}C NMR spectra and with respect to 85% phosphoric acid for ^{31}P NMR spectra. The mass spectra were recorded on a JEOL JSM 600 fast atom bombardment (FAB) high resolution mass spectrometer (FAB-MS), and the thermogravimetric analyses were performed on a TG/DTA-6200 instrument (SII Nano Technology Inc., Japan). UV-absorption spectra were recorded with a Shimadzu, UV-2450 UV−vis spectrophotometer. All spectra were corrected for the background spectrum of the solvent. The absorbances of the ligands and complexes were measured in CH_3CN solution. The PL spectra were recorded on a Spex-Fluorolog FL22 spectrofluorimeter equipped with a double grating 0.22 m Spex 1680 monochromator and a 450W Xe lamp as the excitation source operating in the front face mode. The lifetime measurements were carried out at room temperature using a Spex 1040 D phosphorimeter.

The overall quantum yields ($\Phi_{overall}$) were measured at room temperature using the technique for powdered samples described elsewhere [Bril and De Jager-Veenis 1976], through the following expression:

$$\Phi_{overall} = \frac{1-r_{st}}{1-r_X} \times \frac{A_x}{A_{st}} \times \Phi_{st}$$

where r_x and r_{st} represent the diffuse reflectance (with respect to a fixed wavelength) of the complexes and of the standard phosphor, respectively, and Φ_{st} is the quantum yield of the standard phosphor. The terms A_x and A_{st} represent the areas under the complex and the standard emission spectra, respectively. To have absolute intensity values, $BaSO_4$ was used as the reflecting standard. For measuring $\Phi_{overall}$ for Eu^{3+} complexes, Pyrene was employed as a standard, whose emission spectrum comprises an intense broad band peaking around 475 nm, with a constant Φ value (61%) for an excitation wavelength of 313 nm [Melhuish 1964]. Three measurements were carried out for each sample, and each reported $\Phi_{overall}$ value corresponds to

the arithmetic mean of the three values. The errors in the quantum yield values associated with this technique were estimated to lie within ±10% [Carlos *et al.* 2003]. The overall quantum yields for the Eu^{3+} complexes were also measured using an integrating sphere in a SPEX Fluorolog spectrofluorimeter. The photoluminescence quantum yields in thin films ($\Phi_{overall}$) were determined using a calibrated integrated sphere system. The Xe-arc lamp was used to excite the thin-film samples placed in the sphere with 320-370 nm as the excitation wavelength. Samples were prepared by drop casting the material placed between two quartz cover slips, the quantum yield was determined by comparing the spectral intensities of the lamp and the sample emission as reported in the literature [de Mello *et al.* 1997; Palsson and Monkman 2002; Shah *et al.* 2006]. Using this experimental setup and the integrating sphere system, the solid-state fluorescence quantum yield of thin film of the standard green OLED material tris-8-hydroxyquinolinolato aluminum (Alq_3) was determined to be 19%, which is consistent with previously reported values [Colle *et al.* 2003; Saleesh Kumar *et al.* 2008]. Each sample was measured several times under slightly different experimental conditions. The estimated error for quantum yields is ±10% [Eliseeva *et al.* 2008].

Crystallographic Characterization. Single-crystal X-ray diffraction data were recorded at 257 K on a Bruker AXS (Kappa Apex II) diffractometer equipped with an Oxford Cryostream low-temperature device and a graphite-monochromated Mo Kα radiation source (λ = 0.71073 Å). Data were processed using SAINTPLUS (SAINTPLUS, program suite for data processing, Bruker AXS, Inc., Madison, WI). Structures were solved and refined using SHELXTL. Corrections were applied for Lorentz and polarization effects. All of the structures were solved by direct methods and refined by full-matrix least-squares cycles on F^2. All of the non-hydrogen atoms were allowed anisotropic thermal motion, and the hydrogen atoms were placed in fixed, calculated positions using a riding model (C–H, 0.96 Å). The thermal vibrations of the lattice solvents ($CHCl_3$) in **2** were quiet high. Here the C–Cl distances of the three $CHCl_3$ molecules were restrained to be 1.74(1) Å. This restrain was performed to avoid bad bond

distances. The Cl–Cl distances in the $CHCl_3$ molecule (C96, H96, Cl8, Cl9, Cl10) were restrained to be 2.89(1) Å. This restrain was applied to maintain the tetrahedral geometry of $CHCl_3$ molecule. The $CHCl_3$ molecule (C95, H95, C4, C5, C6) showed one disordered position in the Fourier difference map. The four peak positions were assigned as chlorine atoms and were refined with sum of their occupancies restrained to be three.

Crystals of **3** was poorly diffracting at higher values of Bragg angles. Situation did not improve even after re-crystallizing and collecting data on fresh crystals. There were no reflection with $I > 3\sigma(I)$ for theta > 21°. The structure has several disorders, which lead to the application of 124 restrains during the refinement. Minor disorders are left uncorrected. One of the pentafluoroethane groups (C1–C3, F1–F5) suffers two fold disorders. The C–F distances were restrained as 1.36(1) Å. At one place the F–F distance is restrained (2.22(1) Å) to preserve the tetrahedral geometry of the CF_3 group. One of the fluorine ring (C24–C36) had distortion from planarity for its phenyl rings. Hence the phenyl rings were idealized as hexagons with sides 3.90 Å. All the H atoms were geometrically fixed at chemically meaningful positions and were allowed to ride on the parent atom during refinement. The CCDC numbers 722364 for **2** and 722365 for **3**. For crystallographic data in CIF or other electronic format see DOI:10.1039/b907031a (*Dalton Trans.*, **2009**, 7519-7528).

Synthesis of 1-(9H-fluoren-2-yl)-4,4,5,5,5-pentafluoropentane-1,3-dione (Hpffpd). A modified method of typical Claisen condensation procedure was used for the synthesis of Hpffpd as shown in Scheme 2.1. Acetylfluorene (0.002 mmol) and methyl pentafluoropropionate (0.002 mmol) was added into 20 mL dry THF and stirred for 10 min at 0 °C. To this mixture, sodium hydride was added in inert atmosphere and stirred for 12 h. The resulting solution was quenched with water, added 2 M HCl (50 mL), and the solution was extracted twice with chloroform (70 mL). The organic layer was dried over Na_2SO_4, and the solvent was evaporated. The reaction mixture was then purified by chromatography on a silica

gel column with mixture of chloroform and hexane as the eluent to get the yellow solid as the product (yield: 80%).

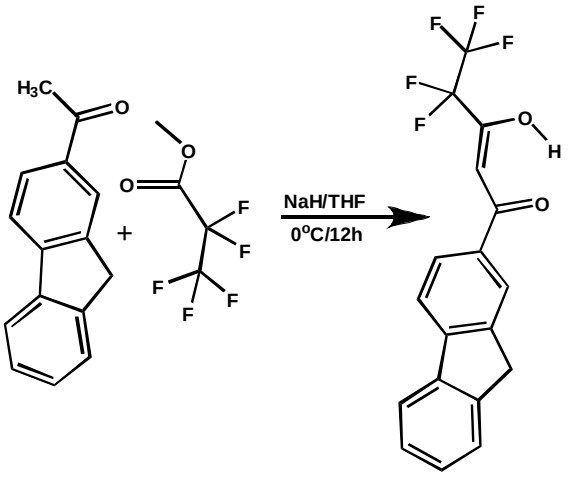

Scheme 2.1. Synthesis of the ligand Hpffpd.

Elemental analysis (%): calcd for $C_{18}H_{10}F_5O_2$ (354.06): C 61.02, H 3.13. Found: C 61.28, H 3.43. ^{1}H NMR (500 MHz, $CDCl_3$) δ (ppm): 15.53 (broad, enol–OH), 8.09 (s, 1H), 7.97–7.96 (d, 1H), 7.84–7.82 (t, 2H), 7.58–7.56 (d, 1H), 7.43–7.38 (m, 2H), 6.68 (s, 1H) 3.93 (s, 2H). ^{13}C NMR (125.7 MHz, $CDCl_3$) δ (ppm): 186.13, 178.42–178.00, 147.86, 144.54, 143.68, 140.09, 130.77, 128.57, 127.21–127.07, 125.30, 124.29, 121.07, 120.10, 93.43, 37.43–33.44. FT-IR (KBr) ν_{max}: 2924, 1599, 1494, 1454, 1399, 1225, 1167, 1011, 796 cm^{-1}. *m*/*z* = 355.22 $(M + H)^+$.

Synthesis of 4,5-bis(diphenylphosphino)-9,9-dimethylxanthene oxide (DDXPO). 4,5-Bis(diphenylphosphino)-9,9-dimethylxanthene (5 mmol) was dissolved in 10 mL of 1,4-dioxane solution, to which 1 mL of 30% H_2O_2 (10.5 mmol) was added drop wise with vigorous stirring (Scheme 2.2). The resultant mixture was then stirred for 2 h and then 10 mL of water was added to the reaction mixture to arrest the reaction. The mixture was extracted with 3 × 30 mL of dichloromethane. The oily phase was then washed with 2 × 30 mL of water to remove 1,4-dioxane. The dichloromethane layer was dried with Na_2SO_4. The solvent was removed *in vacuo*. A white powder was obtained with a yield of 99%. The product was recrystallized from dichloromethane. DDXPO: elemental analysis (%): calcd for $C_{39}H_{32}O_3P_2$ (610.18): C 76.71, H

5.28. Found: C 76.52, H 5.40. ^{1}H NMR ($CDCl_3$, 500 MHz) δ (ppm): 7.62–7.61 (d, 2H), 7.43–7.39 (q, 12H), 7.32–7.28 (q, 8H), 7.00–6.97 (m, 2H), 6.80–6.76 (q, 2H), 1.70 (s, 6H). ^{31}P NMR ($CDCl_3$, 202.4 MHz) δ (ppm): 30.97. FT-IR (KBr) ν_{max}: 1727, 1670, 1436, 1401, 1229, 1180, 1114, 875, 785, 746, 719, 694 cm^{-1}. m/z = 611.31 $(M + H)^+$.

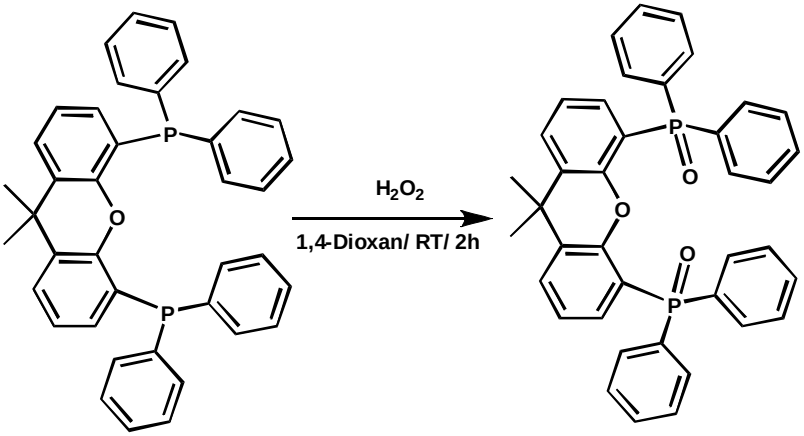

Scheme 2.2. Synthesis of the ligand DDXPO.

Synthesis of bis(2-(diphenylphosphino)phenyl)ether oxide (DPEPO). DPEPO was synthesized according to the method reported elsewhere [Xu *et al.* 2006] (Scheme 2.3). DPEPO: elemental analysis (%): calcd for $C_{36}H_{28}O_3P_2$ (570.55): C 75.78, H 4.95. Found: C 75.52, H 4.85.^{1}H NMR ($CDC1_3$, 500 MHz) δ (ppm): 7.71–7.62 (m, 9H), 7.49–7.27 (m, 13H), 7.17–7.14 (t, 2H), 7.08 (t, 2H), 7.10 (q, 2H). ^{31}P NMR ($CDCl_3$, 202.4 MHz) δ (ppm): 26.20. FT-IR (KBr) ν_{max}: 1590, 1566, 1461, 1435, 1221, 1197, 1120, 1074, 877, 804, 748, 707, 549 cm^{-1}. m/z = 571.60 $(M + H)^+$.

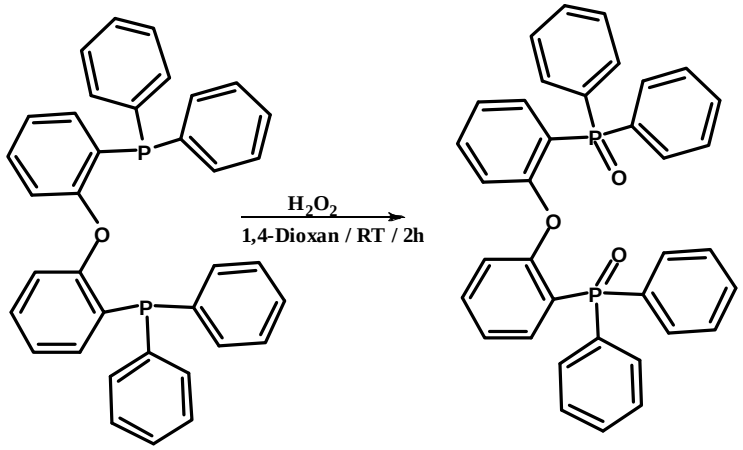

Scheme 2.3. Synthesis of the DPEPO ligand.

Synthesis of Ln(pffpd)$_3$(C_2H_5OH)(H_2O) [Ln = Eu^{3+} (1), Gd^{3+}(4)]. To an ethanolic solution of Hpffpd (0.6 mmol), NaOH (0.6 mmol) is added and stirred for 5 min. To this, a saturated ethanolic solution of $Ln(NO_3)_3 \cdot 6H_2O$ (0.2 mmol) is added drop wise and stirred for 10 h. Water is then added to this mixture and the precipitate thus formed is filtered, washed with water, dried and purified the product by recrystallization from acetone–water mixture (Scheme 2.4). Unfortunately, efforts to grow the single crystals of complexes were not fruitful.

Elemental analysis (%): calcd for $C_{56}H_{38}F_{15}O_8Eu$ (**1**) (1276.15): C 52.72, H 3.00. Found: C 52.62, H 3.21. FT-IR (KBr) ν_{max}: 3421, 2925, 1609, 1528, 1463, 1328, 1277, 1199, 1015, 796 cm^{-1}. *m*/*z* = 1235.97 [($M^+ - H_2O$, C_2H_5OH) + Na].

Elemental analysis (%): calcd for $C_{56}H_{38}F_{15}O_8Gd$ (**4**) (1281.72): C 52.50, H 2.99. Found: C 52.42, H 3.31. FT-IR (KBr) ν_{max}: 3423, 2925, 1609, 1528, 1464, 1328, 1277, 1197, 1015, 798 cm^{-1}. *m*/*z* = 1239.21 [($M^+ - H_2O$, C_2H_5OH) + Na].

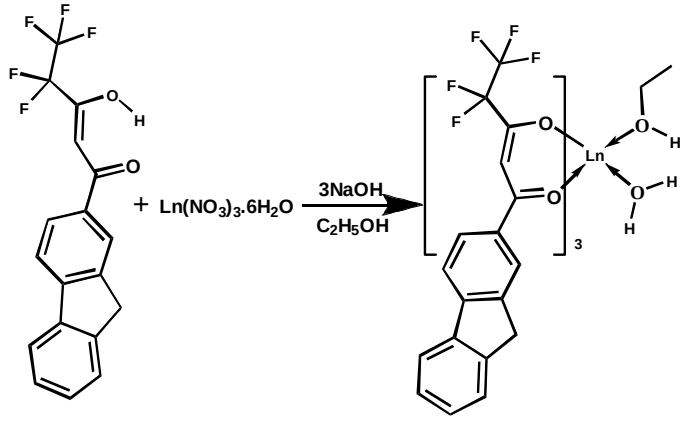

Scheme 2.4. Synthesis of Ln(pffpd)$_3$(H_2O)(C_2H_5OH), Ln = Eu (**1**), Gd (**4**).

Synthesis of Complexes Eu(pffpd)$_3$(DDXPO) (2) and Eu(pffpd)$_3$(DPEPO) (3). The complexes **2–3** were prepared by stirring equimolar solutions of Ln(pffpd)$_3$(H_2O)(C_2H_5OH) and phosphine oxide in $CHCl_3$ for 24 h at room temperature (Scheme 2.5). The products were obtained after solvent evaporation and are purified by recrystallization from chloroform–hexane

mixture. Crystals of complex **2** suitable for single-crystal X-ray diffraction experiments were obtained from a saturated solution of the complex from $CHCl_3$–hexane mixture. Crystals of complex **3** suitable for analysis were obtained from a 2-methoxy ethanol–$CHCl_3$ medium.

Eu(pffpd)$_3$(DDXPO) (2). Elemental analysis (%): calcd for $C_{93}H_{62}EuF_{15}O_9P_2$ (1822.37): C 61.29, H 3.43. Found: C 60.92, H 3.44. FT-IR (KBr) ν_{max}: 2923, 1618, 1522, 1403, 1270, 1173, 1152, 1122, 1075, 1007, 747, 693, 539 cm^{-1}. *m*/*z* = 1822.37 [Eu(pffpd)$_3$(DDXPO)]. ^{31}P NMR ($CDCl_3$, 202.4 MHz) δ (ppm): −85.38.

Eu(pffpd)$_3$(DPEPO) (3). Elemental analysis (%): calcd for $C_{90}H_{58}EuF_{15}O_9P_2$ (1782.32): C 60.65, H 3.28. Found: C 61.00, H 3.88. FT-IR (KBr) ν_{max}: 2924, 1619, 1506, 1402, 1270, 1191, 1004, 693, 545 cm^{-1}. *m*/*z* = 1782.34 [Eu(pffpd)$_3$(DPEPO)]$^+$. ^{31}P NMR ($CDCl_3$, 202.4 MHz): δ (ppm): −103.84.

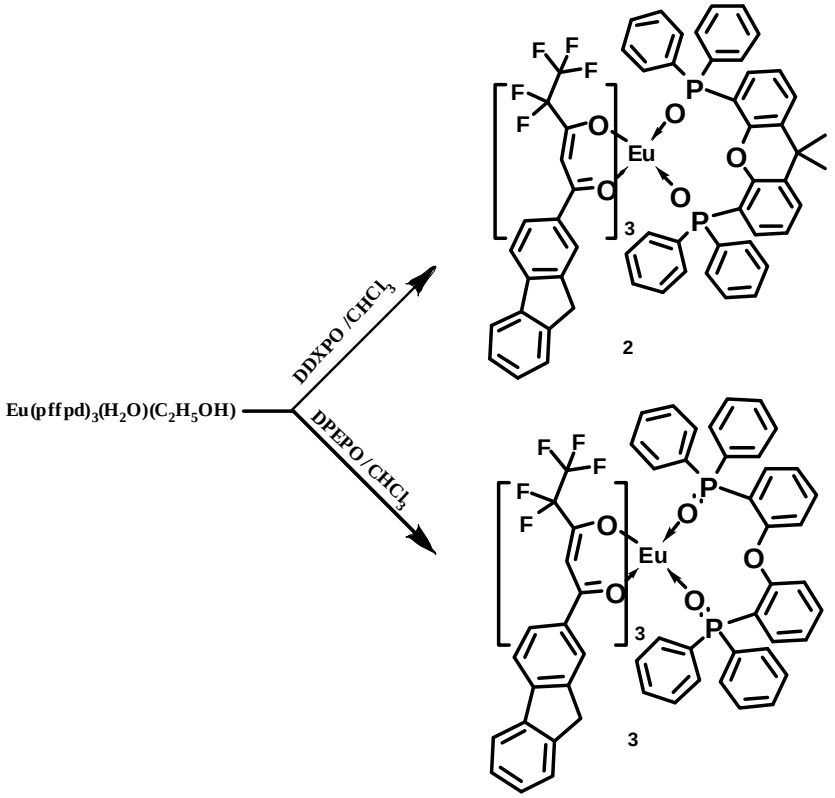

Scheme 2.5. Synthesis of complexes **2-3**.

Synthesis of Gd(NO$_3$)$_3$(DDXPO) and Gd(NO$_3$)$_3$(DPEPO). 1.0 mmol of $Gd(NO_3)_3(H_2O)_6$ (dissolved in 0.1 mL of water) was added drop wise to the ethanolic solution of corresponding phosphine oxide (1 mmol) under stirring and the mixture was refluxed for 2 h in an oil bath at

70 °C. The white precipitate formed from the above reaction mixture was filtered and recrystallized from chloroform–hexane mixture.

$Gd(NO_3)_3$(DDXPO). Elemental analysis (%): calcd for $C_{39}H_{32}GdN_3O_{12}P_2$ (953.88): C 49.10, H 3.38, N 4.40. Found: C 49.44, H 3.46, N 4.29. FT-IR (KBr) ν_{max}: 1607, 1473, 1437, 1404, 1358, 1295, 1235, 1159, 1119, 1100, 875, 789, 723, 693, 556, 540 cm^{-1}. *m*/*z* = 894.40 [$Gd(NO_3)_2$ (DDXPO)] + 1.

$Gd(NO_3)_3$(DPEPO). Elemental analysis (%): calcd for $C_{36}H_{28}GdN_3O_{12}P_2$ (913.82): C 47.32, H 3.09, N 4.60. Found: C 47.44, H 3.16, N 4.69. FT-IR (KBr) ν_{max}: 1588, 1565, 1461, 1436, 1386, 1308, 1234, 1155, 1135, 1111, 879, 722, 717, 693, 550, 514 cm^{-1} cm^{-1}. *m*/*z* = 852.90 [$Gd(NO_3)_2$(DPEPO)] + 1.

2.4. Results and Discussion

Structural Characterization of Ln^{3+} Complexes. The synthesis procedures for the Ln^{3+} complexes **1–4** are shown in Schemes 2.4 and 2.5. The microanalyses and HRMS studies of the complexes **1–4** shows that Ln^{3+} ion has reacted with Hpffpd in a metal-to-ligand molar ratio of 1 : 3 and in complexes **2** and **3** one molecule of phosphine oxide is also involved. The IR spectrum of the complexes **1** and **4** shows a broad absorption in the region 3000–3500 cm^{-1}, indicating the presence of solvent molecules in the complex. On the other hand, the absence of the broad band in the region 3000–3500 cm^{-1} for complexes **2–3**, suggests that solvent molecules have been successfully displaced by the bidentate neutral donors. In addition, the carbonyl stretching frequency of the ligand Hpffpd (1599 cm^{-1}) is shifted to higher wave numbers in **1–4** (1609 cm^{-1} in **1**; 1618 cm^{-1} in **2**; 1619 cm^{-1} in **3** and 1609 in **4**), thus indicating the coordination of the carbonyl oxygen to the Ln^{3+} cation. The P=O stretching frequency of DDXPO, 1180 cm^{-1} has been shifted to 1173 cm^{-1} in complex **2** and the value of 1197 cm^{-1} for DPEPO is red shifted to 1191 cm^{-1} in complex **3**, indicating the involvement of P=O in the complex formation with Eu^{3+} ion. Further, as can be noted from the ^{31}P NMR spectra of the complexes **2** and **3** the P=O resonances are upfield shifted from the position of this group in the

free ligand indicating the involvement of phophoryl oxygen in coordination with the metal ion. The thermal behaviour of the new Eu^{3+} complexes was examined by means of thermogravimetric analysis (TGA) under a nitrogen atmosphere and the results are depicted in the Figure 2.1. It is clear from the thermogravimetric analysis data that complex **1** undergoes a mass loss of about 6% (calcd: 5.5%) in the first step (160 to 220 °C), which corresponds to the elimination of the coordinated solvent molecules. On the other hand, complexes **2–3** are more stable than the precursor sample **1** and they undergo single step decomposition at 220 °C.

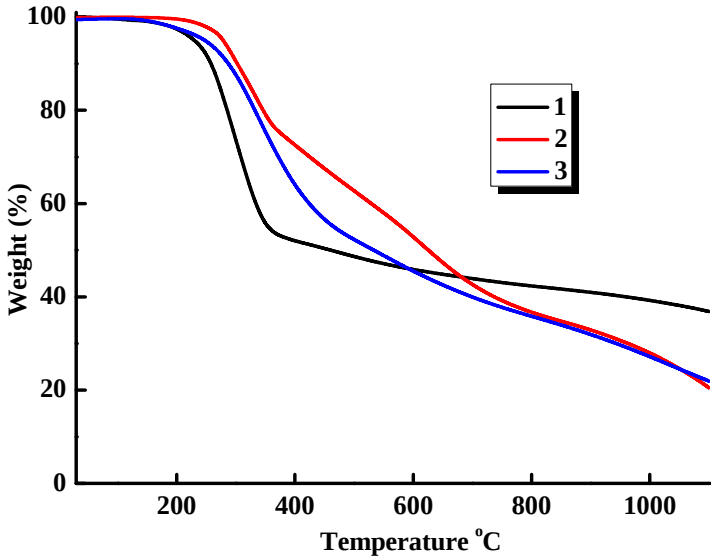

Figure 2.1. Thermogravimetric curve for complexes **1-3.**

Crystal Structures of [Eu(pffpd)$_3$(DDXPO)] 2 and [Eu(pffpd)$_3$(DPEPO)] 3 complexes. The crystal structures of Eu^{3+} complexes **2** and **3** were determined by single-crystal X-ray crystallography and the obtained asymmetric structures are depicted in Figure 2.2 and 2.3. The crystal data and the data collection parameters are given in Table 2.1, and the selected bond lengths and bond angles are presented in Table 2.2. These compounds crystallize in the triclinic space group *P*$\bar{1}$. The single-crystal X-ray data indicates that complexes **2** and **3** have no centre of inversion in the crystal field, resulting in an increase in electron transitions in the 4f orbitals due to odd parity [Hasegawa *et al.* 2003].

Table 2.1. Crystal data, collection, and structure refinement parameters for the complexes **2·2.5CHCl$_3$** and **3· CH$_3$COCH$_3$**.

Parameters	**2**	**3**
Empirical formula	$C_{95.5}$ $H_{64.5}$ $Cl_{7.5}$ Eu F_{15} O_9 P_2	C_{93} H_{64} Eu F_{15} O_{10} P_2
fw	2120.75	1840.34
Crystal system	Triclinic	Triclinic
Space group	*P*$\bar{1}$	*P*$\bar{1}$
Cryst size (mm^3)	0.3 x 0.2 x 0.2	0.15 x 0.10 x 0.10
Temperature (K)	257 (2)	257 (2)
a/Å	14.3330(3)	15.1515(4)
b/Å	15.3440(3)	16.0282(4)
c/Å	23.9480(5)	17.9664(5)
α (deg)	86.1900(10)	82.9260(10)
β (deg)	76.4390(10)	74.1250(10)
γ (deg)?	66.5010(10)	83.8700(10)
V / Å^3	4693.17(17)	4152.58(19)
Z	2	2
ρ_{calcd}/Mg m^{-3}	1.501	1.472
μ/mm^{-1}	1.002	0.887
F(000)	2130	1860
R1 [$I > 2\sigma(I)$]	0.0586	0.0679
wR2 [$I > 2\sigma(I)$]	0.1673	0.1844
R1 (all data)	0.0729	0.0848
wR2 (all data)	0.1795	0.2131
Number of reflections	87492	52601
Number of independent reflections	18809	8841
$R_{(int)}$	0.0364	0.0351
GOF	1.058	1.102

Table 2.2. Selected bond lengths [Å] and angles [°] for complexes **2** and **3**.

2		**3**	
Eu(1)-O(1)	2.376(4)	Eu(1)-O(1)	2.463(7)
Eu (1)-O(2)	2.325(3)	Eu(1)-O(2)	2.346(8)
Eu (1)-O(3)	2.406(4)	Eu(1)-O(3)	2.343(8)
Eu (1)-O(4)	2.397(3)	Eu(1)-O(4)	2.440(7)
Eu (1)-O(5)	2.448(4)	Eu(1)-O(5)	2.375(6)
Eu (1)-O(6)	2.383(4)	Eu(1)-O(6)	2.378(7)
Eu (1)-O(7)	2.362(3)	Eu(1)-O(7)	2.377(6)
Eu (1)-O(8)	2.325(3)	Eu(1)-O(8)	2.381(6)
O(1)- Eu (1)-O(2)	71.42(13)	O(1)-Eu(1)-O(2)	68.6(3)
O(3)- Eu (1)-O(4)	71.54(12)	O(3)-Eu(1)-O(4)	70.2(3)
O(5)- Eu (1)-O(6)	70.06(12)	O(5)-Eu(1)-O(6)	70.0(2)
O(7)- Eu (1)-O(8)	73.69(12)	O(7)-Eu(1)-O(8)	76.7(2)

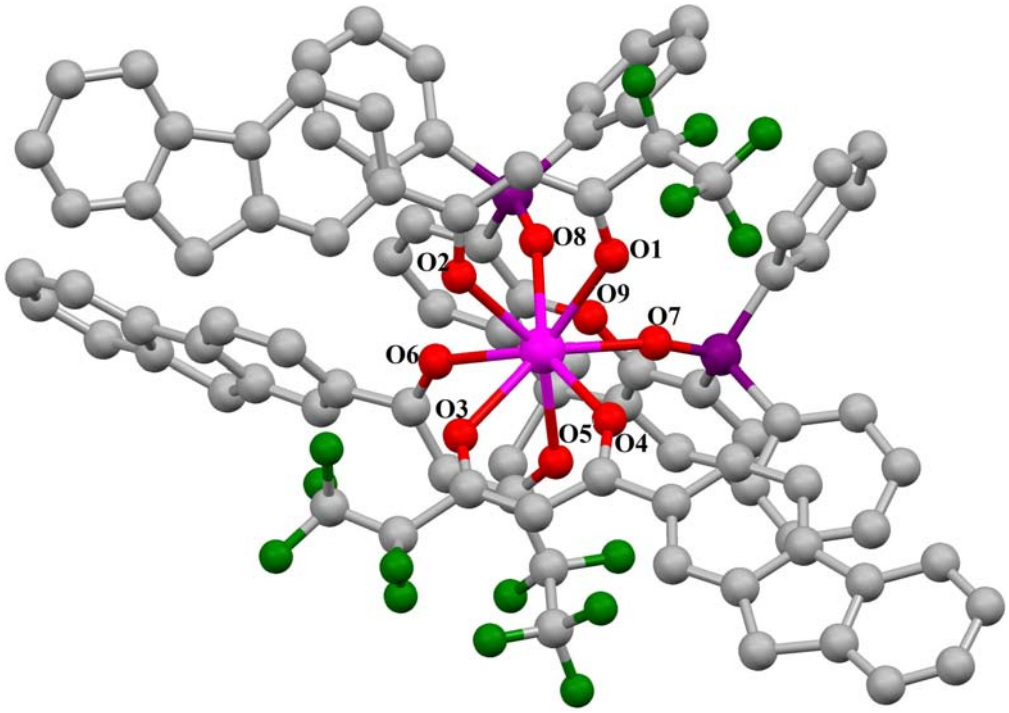

Figure 2.2. Asymmetric unit of complex **2**: Thermal ellipsoids drawn with 30% probability, H atoms and non-coordinated solvent molecules omitted for clarity.

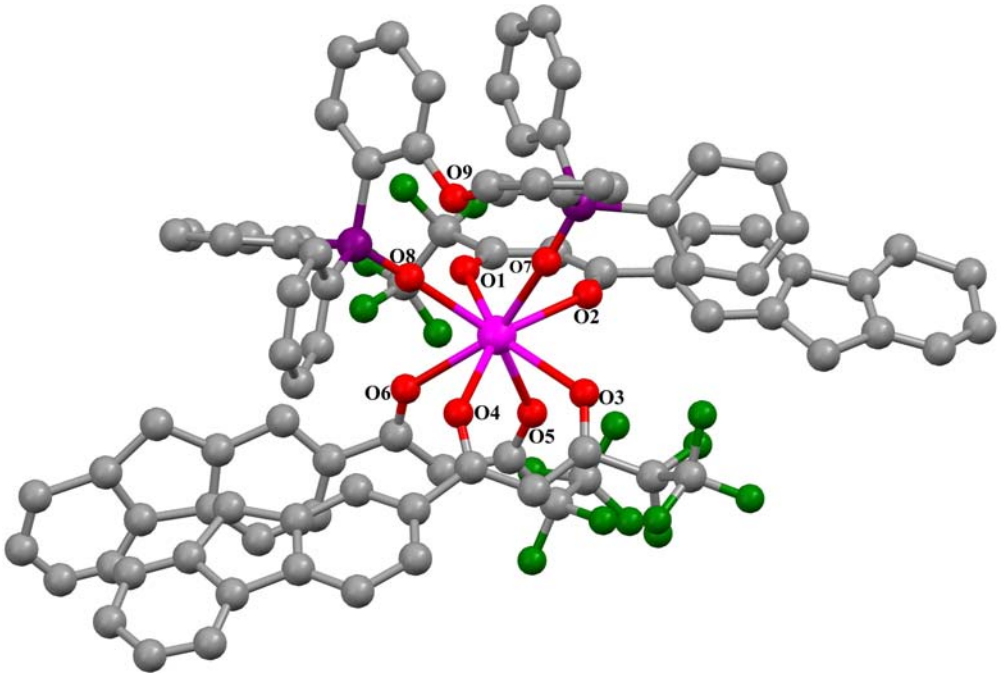

Figure 2.3. Asymmetric unit of complex **3**: Thermal ellipsoids drawn with 30% probability, H atoms and non-coordinated solvent molecules omitted for clarity.

The central Eu^{3+} ion is surrounded by eight oxygen atoms, six of which are from the three bidentate fluorinated *β*-diketonates, and the other two oxygen atoms from the chelate phosphine oxide. The coordination polyhedra can be described as distorted square antiprism. The bridging oxygen atom connecting the two triphenyl phosphine oxide units of the chelate phosphine oxide is not coordinating to the central Eu^{3+} ion in either of the complexes. In complex **2**, the Eu–O bonds adjacent to the fluorene ring are slightly shorter than the others, which may be due to the inductive effect of the fluorine atoms present in the Hpffpd. In the *β*-diketone rings of the Eu^{3+} complexes, the average distances for the C–C and C–O bonds are shorter than a single bond but longer than a double bond. This can be explained by the fact that there exists a strong conjugation between the fluorene ring and the coordinated *β*-diketone, which leads to the delocalization of electron density of the coordinated *β*-diketonate chelate ring [Yu *et al.* 2003; Sun *et al.* 2006]. The two Eu–O bonds with the chelate phosphine oxide ligand (2.36 Å and 2.33 Å for **2**; 2.38 Å and 2.38 Å for **3**) were shorter than the six Eu–O bonds with Hpffpd ligands (2.33 Å−2.45 Å for **2**; 2.34–2.46 for **3**), as observed in the in the single-crystal X-ray data of the complex, Eu^{3+}-hexafluroacetylacetonato-1,1′-biphenyl-2,2′-diylbis(diphenylphosphine oxide) [Nakamura *et al.* 2007] (Eu–O bonds 2.32–2.33 Å in BIPHEPO and Eu–O bonds 2.40–2.44 Å in *β*-diketone). Further, it can also be noted that the Eu–O bonds of DDXPO in **2** are shorter than that of Eu–O bonds of DPEPO in **3**. Thus the chelate phosphine oxide DDXPO strongly coordinates with Eu^{3+} ion than DPEPO. In DDXPO, the two diphenylphosphine oxide units are linked by the xanthene moiety increases the conjugated area of the neutral ligand, which can improve carrier injunction and transport in **2**. Furthermore, the introduction of more conjugated DDXPO ligand makes the complex more rigid, which reduces the structure relaxation in the excited state.

UV-vis Spectra. The UV-vis absorption spectra of the free ligands (Hpffpd, DDXPO and DPEPO) and the corresponding Eu^{3+} complexes were measured in CH_3CN solution ($c = 2 \times 10^{-6}$ M) are displayed in Figure 2.4 and 2.5.

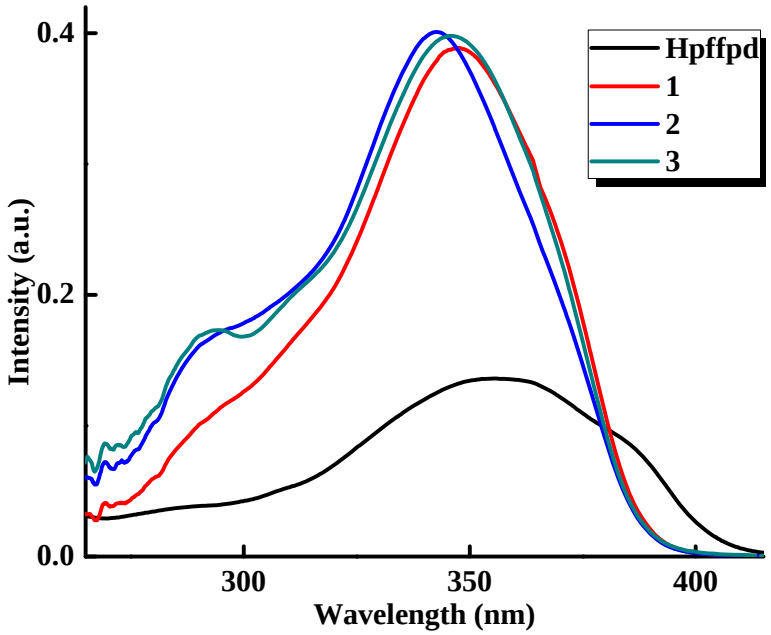

Figure 2.4. UV-visible absorption spectra of Hpffpd and complexes **1-3** in CH_3CN (c = 2 × 10^{-6} M).

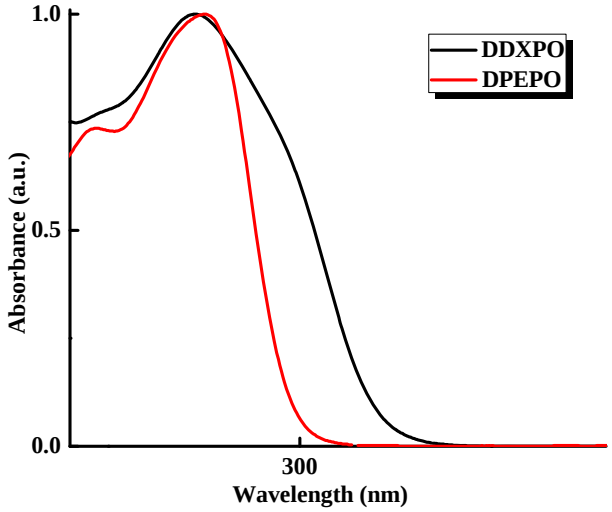

Figure 2.5. UV-visible absorption spectra of the neutral ligands in CH_3CN.

The spectral shapes of the complexes in CH_3CN are similar to that of the free ligands, suggesting that the coordination of Eu^{3+} ion does not have a significant influence on the $^1\pi$-π* state energy. However, a small blue shift observed in the absorption maximum of all the complexes is caused by the perturbation induced by the metal coordination. The ligand Hpffpd

exhibits a broad band in the UV corresponding to singlet – singlet π-π* enolic transition [Sun *et al*. 2006] assigned to the β-diketonate ligand, with a lowest energy maximum at 300-425 nm (λ_{max} = 356 nm) and a molar absorption coefficient of 6.75×10^4 L mol^{-1} cm^{-1}. The presence of the ancillary ligand (DDXPO or DPEPO) not only enhances the absorption intensity but also satisfies the high coordination number of the central Eu^{3+} ion and thus improves the coordination and thermal stabilities of complexes **2** and **3**. The molar absorption coefficient values for the complexes 1-3 were calculated at the respective λ_{max} value and were found to be 1.94×10^5, 2×10^5 and 2×10^5 L mol^{-1} cm^{-1}, respectively. The magnitude of these values are about three times higher than that of the Hpffpd (6.75×10^4 at 356 nm), indicating the presence of three β-diketonate ligands in the corresponding complexes. Further the higher molar absorption coefficient of Hpffpd reveals that the β-diketonate ligand has a strong ability of absorbing light.

Photophysical properties of Eu^{3+} complexes. The room temperature excitation and emission spectra of Eu^{3+} complexes **1–3** in the solid state have been studied and the results are depicted in Figure 2.6. The excitation spectra of these complexes were all obtained by monitoring the strongest emission wavelength of the Eu^{3+} at 612 nm. The excitation spectra of all the complexes exhibit a broad band between 250 and 450 nm, which is attributed to singlet-singlet π–π* enol absorption of the β-diketonate ligand [de Sa *et al.* 2000; Biju *et al.* 2006; Pavithran *et al.* 2006; [b]Biju *et al.* 2009]. In all cases, the excitation spectra recorded by monitoring the f–f transitions matched with the absorption spectra, evidencing that the emission arose from energy transfer from the ligand to the metal excited states as a result of the antenna effect [Kawa and Frechet 1998; Li *et al.* 2002]. A series of sharp lines assigned to transition between the $^7F_{0,1}$ and $^5D_{2\text{-}1}$ are also seen in the solid state excitation spectra of these complexes. However, these transitions are weaker than the absorption of the organic ligands and are overlapped by broad excitation band, which proves that luminescence sensitization *via* excitation of the ligand, is much more efficient than the direct excitation of Eu^{3+} absorption level.

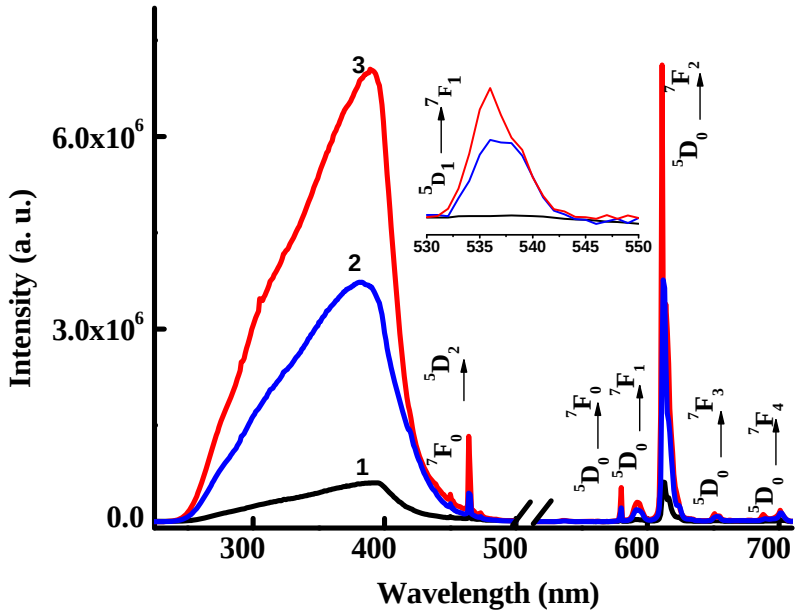

Figure 2.6. Solid state excitation and emission spectra for complexes **1** (λ_{ex} 390 nm), **2** (λ_{ex} 383 nm) and **3** (λ_{ex} 393 nm) at 298 K, emission monitored around 612 nm.

The emission spectra of complexes **1–3** in solid state (Figure 2.6) exhibited the characteristic narrow bands arising from the intra-configurational $^5D_0 \rightarrow {}^7F_J$ (J = 0–4) transitions of the Eu^{3+} ion [Pavithran *et al.* 2006; [b]Biju *et al.* 2009]. Furthermore, a weak green emission band at 535 nm occurs, corresponding to the high energy transition of $^5D_1 \rightarrow {}^7F_1$ [Dejneka *et al* 1995; Kadjane *et al.* 2008]. No ligand-based emission is observed, indicating an efficient ligand-to-metal energy transfer process. The five narrow emission peaks centered at 579, 590, 612, 649 and 699 nm, assigned to $^5D_0 \rightarrow {}^7F_0$, $^5D_0 \rightarrow {}^7F_1$, $^5D_0 \rightarrow {}^7F_2$, $^5D_0 \rightarrow {}^7F_3$, and $^5D_0 \rightarrow {}^7F_4$ transitions, respectively [Försberg 1973]. Among the peaks, the emission at 612 nm from the $^5D_0 \rightarrow {}^7F_2$ induced electronic dipole transition is the strongest, suggesting the chemical environment around Eu^{3+} ions does not have an inversion center [Lenaerts *et al.* 2005]. Moreover, the presence of only one sharp peak in the region of the $^5D_0 \rightarrow {}^7F_0$ transition at 579 nm suggests the existence of a single chemical environment around the Eu^{3+} ion of point group symmetry C_1 [Kai *et al.* 2008; Liu *et al.* 2008] which is in good agreement with the X-ray crystal structure of complexes **2–3**. The experimental data on the Ln^{3+} complexes indicated that the magnetic dipole

transition $^5D_0 \rightarrow {}^7F_1$ of Eu^{3+} is largely independent of the ligand field and therefore can be used as an internal standard to account for the ligand differences [Bunzli 1989]. The electric dipole transition $^5D_0 \rightarrow {}^7F_2$, so-called hypersensitive [Dossing 2005; Beeby *et al.* 1999] transition, is sensitive to the symmetry of the coordination sphere. The intensity ratio of the electric dipole transition to the magnetic dipole transition in the lanthanide complex measures the symmetry of the coordination sphere [Forsberg 1973]. For the Eu^{3+} complex **1**, in the absence of chelate phosphine oxides, the intensity ratio of the transitions of $^5D_0 \rightarrow {}^7F_2/{}^5D_0 \rightarrow {}^7F_1$ (R_{21}) is 10.82 (Table 2.3). It increases to 13.35 in complex **2** and 13.04 in **3**. In short, the presence of chelate phosphine oxides increases the luminescent intensity of the hypersensitive transitions of the Eu^{3+} ion. One can easily understand from the Figure 2.6 that the displacement of the solvent molecules from the complex $Eu(pffpd)_3(C_2H_5OH)(H_2O)$ by the chelating phosphine oxides significantly enhances the luminescent intensity.

The luminescence decay curves of Eu^{3+} complexes **1–3** were obtained by monitoring the emission at the hypersensitive $^5D_0 \rightarrow {}^7F_2$ transition (612 nm) and excitation at wavelengths that maximizes the Eu^{3+} emission intensity. These data were adjusted with a first-order exponential decay function and the lifetime values (τ) of the emitter $^5D_0$ level of the Eu^{3+} complexes were determined and are listed in Table 2.3. Typical decay profiles of complexes **1–3** are shown in Figure 2.7. Decay curves fit to a monoexponential indicating only one species exists in the excited state [Biju *et al.* 2006; Pavithran *et al.* 2006]. The relatively shorter lifetime observed for complex **1** may be due to the dominant non-radiative decay channels associated with vibronic coupling induced by the presence of solvent molecules, as well documented in many of the hydrated europium β-diketonate complexes [de Sa *et al*. 2000; Yu *et al.* 2005; Eliseeva *et al*. 2006; Sun *et al*. 2006; Fratini *et al*. 2008]. For Eu^{3+} the energy gap between the luminescent state and the ground state manifold is approximately 12,000 cm^{-1} [Dossing 2005; Beeby *et al*. 1999]. Thus, relatively efficient coupling of the Eu^{3+} excited states occurs to the third vibrational overtone of proximate OH oscillators (ν_{OH}~3300–3500 cm^{-1}) consistent with the

observed efficient quenching of Eu^{3+} luminescence. On the other hand, longer lifetime values have been observed for complexes **2–3** due to the absence of non-radiative decay pathways.

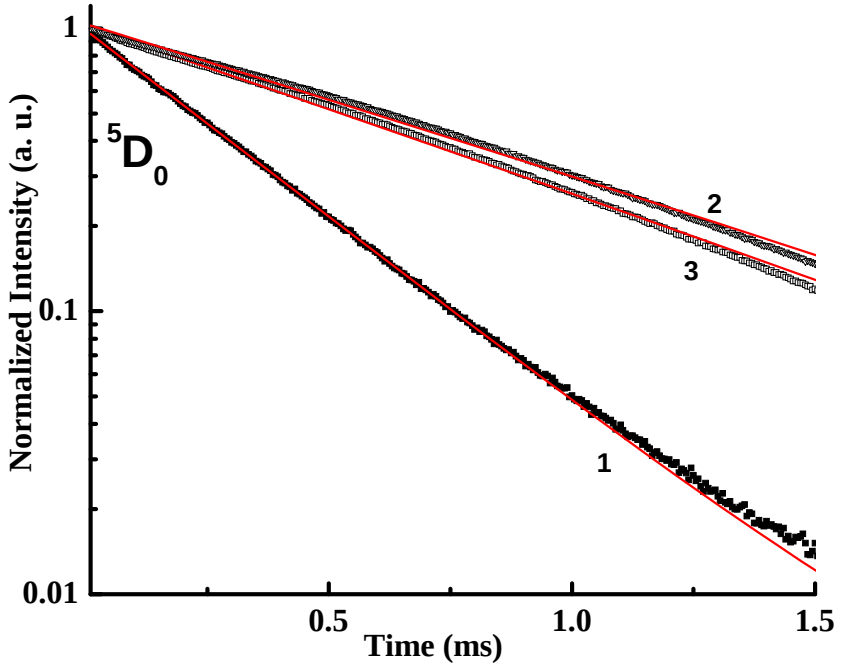

Figure 2.7. Experimental solid state luminescence decay profiles of complexes monitored around 612 nm and excited at their maximum emission wavelengths.

Table 2.3. Radiative (A_{RAD}) and nonradiative (A_{NR}) decay rates, $^5D_0$ lifetime (τ_{obs}), intrinsic quantum yield (Φ_{Ln},%), energy transfer efficiency (Φ_{sens},%), and overall quantum yield ($\Phi_{overall}$,%) for complexes **1-3** in solid state.

Complex	R_{21}	τ_{obs} (μs)	A_{RAD} (s^{-1})	A_{NR} (s^{-1})	Φ_{Ln}(%)	Φ_{sens} (%)	$\Phi_{overall}$ (%)
1	10.823	328 ± 3	783	2265	26	13	3 ± 0.3
2	13.351	820±2	821	398	67	74	48 ± 5
3	13.036	742± 1	796	552	59	48	28 ± 3

The overall quantum yield ($\Phi_{overall}$) of a Eu^{3+} coordination compound is the product of the intrinsic quantum yield Φ_{Ln} (measured upon f–f excitation), which reflects the extent of non-radiative deactivation processes taking place within the luminescent edifice, and the sensitization efficiency of the ligand (Φ_{sens}), which reflects the efficacy with which the latter transfers its excitation energy onto the metal ion [Xiao and Selvin 2001; Comby *et al.* 2004].

$$\Phi_{overall} = \Phi_{sens} \times \Phi_{Ln} \quad (1)$$

In the case of Eu^{3+}, simple equations allow one to determine the otherwise difficult-to-measure Φ_{Ln} from spectral parameters and lifetimes:

$$\Phi_{Ln} = \left(\frac{A_{RAD}}{A_{RAD} + A_{NR}} \right) = \frac{\tau_{obs}}{\tau_{RAD}} \quad (2)$$

The radiative lifetime (τ_{RAD}) can be calculated using eqn (3) [Viswanathan and de Bettenacourt-Dias 2006; Kim *et al*. 2006], which relates the shape of the emission spectrum of Eu^{3+} to its radiative lifetime and assuming that the energy of the $^5D_0 \rightarrow {}^7F_1$ transition (MD) and its oscillator strength are constant:

$$A_{RAD} = \frac{1}{\tau_{RAD}} = A_{MD,0}\, n^3 \left(\frac{I_{TOT}}{I_{MD}} \right) \quad (3)$$

In this formula, *n* is the refractive index of the medium, $A_{MD,0}$ is the spontaneous emission probability for the $^5D_0 \rightarrow {}^7F_1$ transition *in vacuo*, and I_{TOT}/I_{MD} is the ratio of the total area of the corrected Eu^{3+} emission spectrum to the area of the $^5D_0 \rightarrow {}^7F_1$ band. From the theoretically calculated dipole strength it is found that $A_{MD,0}$ has a value of 14.65 s^{-1}[Kim *et al*. 2006; Viswanathan and de Bettenacourt-Dias 2006]. An average index of refraction equal to 1.5 was considered [Biju *et al.* 2006; Pavithran *et al*. 2006].

The overall quantum yield ($\Phi_{overall}$), radiative (A_{RAD}) and non-radiative (A_{NR}) decay rates, intrinsic quantum yield (Φ_{Ln}) and energy transfer efficiency (Φ_{sens}) of complexes **1–3** were presented in Table 2.3. At room temperature, the substitution of solvent molecules in $Eu(pffpd)_3(C_2H_5OH)(H_2O)$ complex by a chelating phosphine oxide, DDXPO leads to a 2.5-fold increase in observed luminescence lifetime (τ_{obs}) values and to an approximately 16-fold enhancement in absolute overall quantum yield as determined upon ligand excitation. Similarly, a 2.26-fold enhancement in luminescence lifetime and 9-fold enhancement in the absolute overall quantum yield has been noted by replacing solvent molecules in the $Eu(pffpd)_3(C_2H_5OH)(H_2O)$ by DPEPO. According to energy gap theory, radiation less

transitions is prompted by ligands and solvents with high frequency vibrational modes. A creation of Eu^{3+} complex with higher quantum yields is directly linked to suppression of radiation less transitions caused by vibrational excitations in surrounding media [Wada *et al.* 2000; Hasegawa *et al*. 2003; Peng *et al*. 2005]. It is clear from the Table 2.3 that complex **1**, having solvent molecules in the coordination sphere exhibits lower overall quantum yield and life time values. This is due to the presence of O–H oscillators in this system, which effectively quenches the luminescence of the Eu^{3+} ion. On the other hand, complexes **2** and **3** exhibit high overall quantum yield and lifetime values due to the displacement of solvent molecules from the coordination sphere by the bidentate phosphine oxides. Among complexes **2** and **3**, **2** exhibits better quantum yields than **3** due to the extended conjugation and strong coordination with the central Eu^{3+}, which might enable efficient energy transfer. Thus the substantial contribution of the chelating phosphine oxide to the overall sensitization of the Eu^{3+}-centered luminescence in complexes **2** and **3** is confirmed by (i) an increase of the intrinsic quantum yield by a factor of 2.58 in **2** and 2.26 in **3**, which results from removal of the quenching effect of the O–H vibrations, and (ii) the significant enhancement of Φ_{sens} from 13 to 74% in **2** (5.69-fold) and 48% in **3** (3.69-fold). The much larger increase in Φ_{sens}, compared with intrinsic quantum yield is reflecting the contribution of the ancillary ligand to the energy transfer process.

Intramolecular Energy Transfer in the Eu^{3+} Complexes. It is well documented that in the lanthanide *β*-diketonate complexes, ancillary ligand often play a role in absorbing and transporting energy to the primary ligand *β*-diketone or to the central Ln^{3+} ion [Xu *et al.* 2006]. For effective energy transfer to occur, the overlap between the emission spectrum of the donor and the absorption spectrum of the acceptor is essential [Berlman 1973]. It is evident from Figure 2.8 that the room temperature emission spectrum of chelating ligand (DDXPO) is overlapped by the absorption spectrum of the Hpffpd in the region 375–425 nm, and hence it means that nearly all the radiation from the singlet state of DDXPO can be absorbed by the

Hpffpd ligand. The large area overlap of room temperature emission spectrum of Hpffpd with that of low-temperature phosphorescence spectrum of $Gd(NO_3)_3$(DDXPO) in the region 450–600 nm, indicates that energy transfer from singlet state (S_1) of Hffpd to the triplet state (T_1) of DDXPO is effective (Figure 2.8).

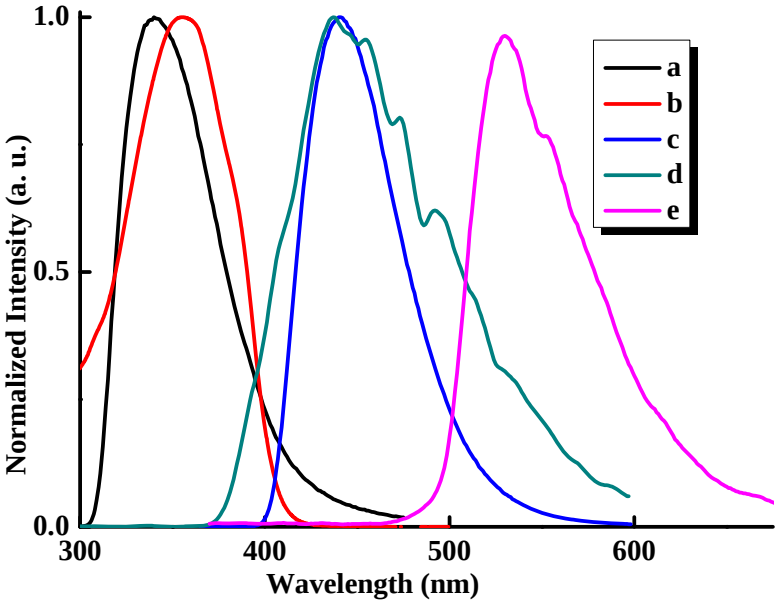

Figure 2.8. (a) Room-temperature emission spectrum of DDXPO, (b) UV-vis absorption spectra of Hpffpd (2×10^{-5} M in CH_3CN), (c) Room-temperature emission spectrum of Hpffpd, **(**d**)** 77K phosphorescence spectra of Gd $(NO_3)_3$(DDXPO), (e) 77K phosphorescence spectra of $Gd(pffpd)_3(H_2O)(C_2H_5OH)$,.All spectra are normalized to a constant intensity at the maximum.

The overlap of low-temperature phosphorescence spectra of $Gd(NO_3)_3$(DDXPO) and $Gd(pffpd)_3(H_2O)(C_2H_5OH)$ (Figure 2.8) again highlights that the T_1 of ancillary ligand can transfers energy to the T_1 of Hpffpd, which in turn transfers energy to the $^5D_0$ state of the Eu^{3+} ion. Finally, the Eu^{3+} ion emits when transition to the ground state occurs [Biju *et al.* 2006; Pavithran *et al*. 2006]. Apart from the above energy transfer pathways, the overlap of room-temperature emission and low-temperature phosphorescence spectra of DDXPO and Hpffpd, indicates that effective intersystem crossing process between S_1 and T_1 of the ligands (Figure 2.8).

To demonstrate the energy transfer process of the Eu^{3+} complexes, the energy levels of relevant electronic states of the ligands have been determined. The S_1 and T_1 energy levels of Hpffpd and chelating phosphine oxides were estimated by referring to their wavelengths of UV-vis absorption edges and the lower wavelength emission edges of the corresponding phosphorescence spectra of the complexes $Gd(pffpd)_3(H_2O)(C_2H_5OH)$, $Gd(NO_3)_3$(DDXPO) and $Gd(NO_3)_3$(DPEPO) (Figure 2.9).

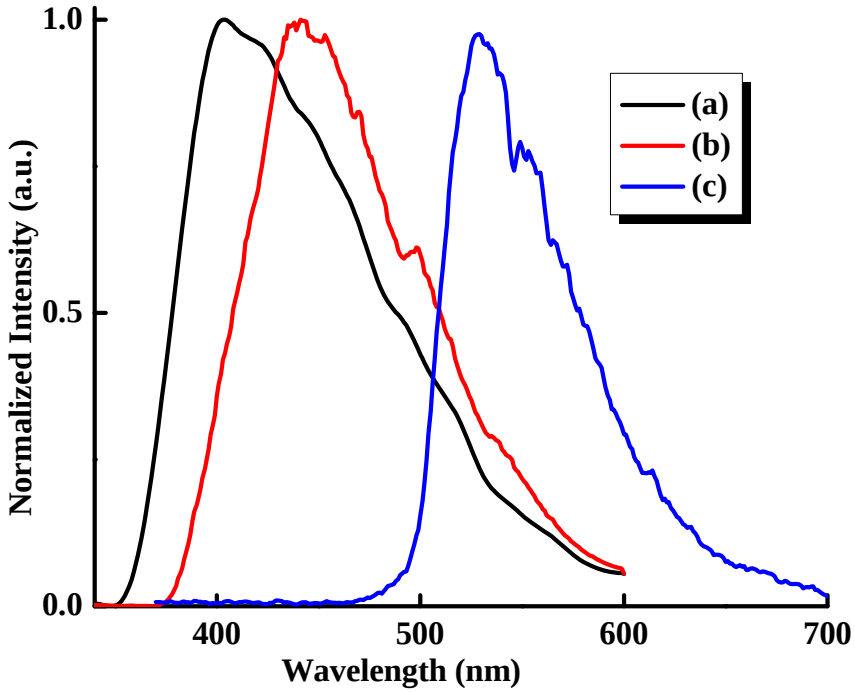

Figure 2.9. Phosphorescence spectra of (a) $Gd(NO_3)_3$(DPEPO), (b) $Gd(NO_3)_3$(DDXPO) and (c) $Gd(pffpd)_3(H_2O)(C_2H_5OH)$ at 77K.

The T_1 of Hpffpd, DDXPO and DPEPO are found to be 19,450, 23,470, and 25,640 cm^{-1}, respectively. The S_1 levels of Hpffpd, DDXPO and DPEPO are found to be 23,920, 31,850 and 32,900 cm^{-1}, respectively. Thus, the energy gap between the Eu^{3+} core ($^5D_0 \approx$ 17,250 cm^{-1}) and the donor ligands T_1 levels turns out to be 2200, 6220 and 8390 cm^{-1} for Hpffpd, DDXPO and DPEPO, respectively. This suggests that although the triplet states of the ancillary ligands are

energetically compatible with an efficient energy transfer process, the lower lying Hpffpd level may undergo thermal back-energy transfer from the central core [Armaroli *et al.* 1999]. Furthermore, the $^5D_1$ Eu^{3+} emitting state, located at approximately 18,800 cm^{-1}, is critically close to the triplet energy level of Hpffpd (19 450 cm^{-1}). On the other hand, in complexes **2** and **3**, the T_1 of DDXPO and DPEPO lie well above the higher excited states of Eu^{3+}, such as $^5D_2$ (21,200 cm^{-1}), and $^5D_1$ (18,800 cm^{-1}). The corresponding energy gaps $\Delta E(T_1–^5D_1)$ = 4670 cm^{-1} (DDXPO), 6840 cm^{-1} (DPEPO) and $\Delta E(T_1–^5D_2)$ = 2470 cm^{-1} (DDXPO), 4640 cm^{-1} (DPEPO) are too high to allow thermal back-energy transfer from the central Eu^{3+} ion [Latva *et al.* 1997]. The T_1 of ancillary ligand DDXPO can also transfer energy to the central Eu^{3+} ion directly or through the T_1 of Hpffpd (low temperature emission spectra of DDXPO and Hpffpd are overlapped; (Figure 2.8). The room-temperature emission spectrum of **2** and **3** exhibits transitions from excited $^5D_1$ state to $^7F_0$ at 535 nm (inset as shown in Figure 2.6), which is absent in complex **1** indicating the transfer of energy from the T_1 of neutral ligand to the higher excited states of Eu^{3+}.

Investigations indicated that DDXPO in complex $Eu(pffpd)_3(DDXPO)$ has the mezzo first triplet excited energy level (T_1) between the first singlet excited energy level (S_1) and T_1 of Hpffpd, which support one more additional energy transfer routines from the T_1 level of DDXPO to that of Hpffpd, and consequently results in improvement of energy transfer in the Eu^{3+} complex **2** (Φ_{sens}= 74%) as compared to $Eu(pffpd)_3(H_2O)(C_2H_5OH)$ (Φ_{sens}= 13%). On the other hand, DPEPO in $Eu(pffpd)_3(DPEPO)$ does not show any mezzo state. Here, both the S_1 and T_1 of DPEPO lies above the S_1 level of the primary ligand. Hence in the present study, complex **2** shows higher quantum yield than complex **3** even though the ancillary ligands do not differ much in their electronic structure and coordination modes. Based on the preceding observations, the schematic representation of energy level diagram showing the possible energy transfer pathways for complexes **2** and **3** are depicted in Figures 2.10 and 2.11, respectively.

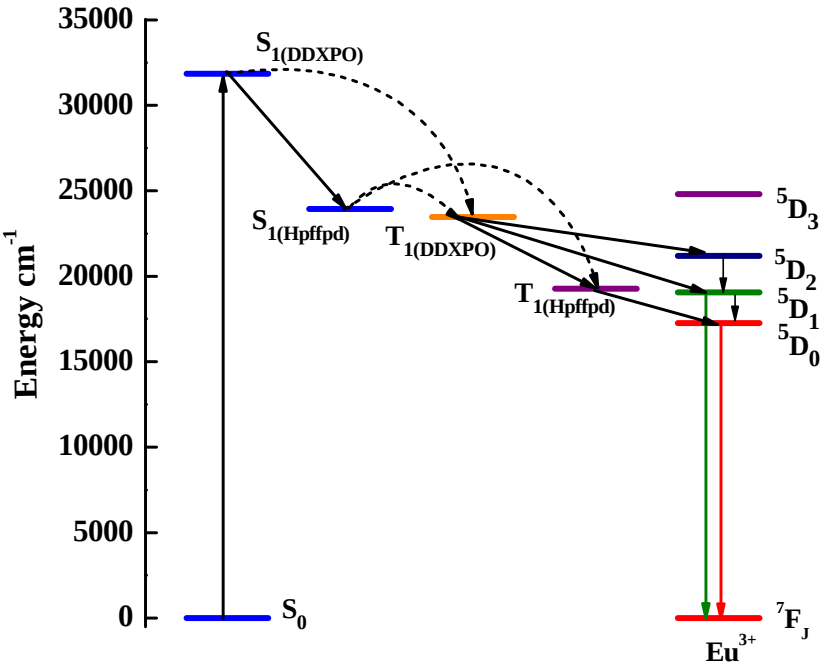

Figure 2.10. Schematic energy level diagram and energy transfer processes for complex **2**. S_1 represents the first excited singlet state and T_1 represents the first excited triplet state.

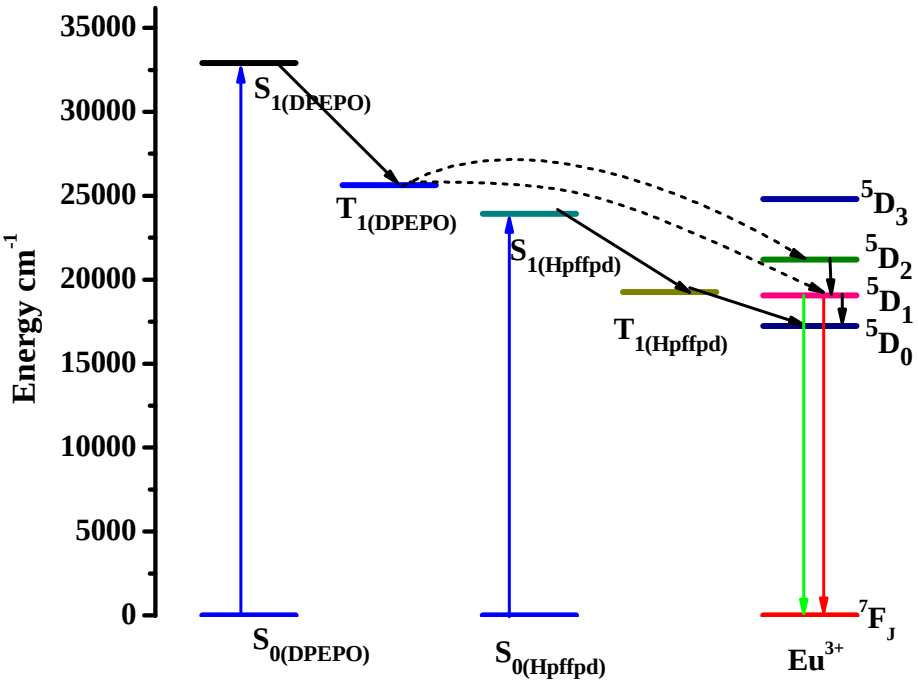

Figure 2.11. Schematic energy level diagram and energy transfer processes for complex **3.** S_1 represents the first excited singlet state and T_1 represents the first excited triplet state.

2.5. Conclusions

Based on the designed fluorinated *β*-diketone (Hpffpd) and highly rigid chelate phosphine oxide (DDXPO) ligands, two new europium complexes $[Eu(pffpd)_3(C_2H_5OH)(H_2O)]$ **1** and $[Eu(pffpd)_3(DDXPO)]$ **2** have been successfully synthesized and fully characterized. For comparison, $[Eu(pffpd)_3(DPEPO)]$ **3** complex was also designed. The structures of the complexes **2** and **3** have been determined by single-crystal X-ray diffraction. The luminescent study demonstrated that the replacement of solvent molecules in $[Eu(pffpd)_3(C_2H_5OH)(H_2O)]$ by DDXPO leads to a huge enhancement in overall quantum yield (from 3 to 48%) and $^5D_0$ lifetime (from 328 to 820 μs). Further, the substantial contribution of ancillary ligand for overall sensitization process of Eu^{3+}-centered luminescence in $[Eu(pffpd)_3(DDXPO)]$ is confirmed by increase of intrinsic quantum yield from 26 to 67% and the substantial enhancement of Φ_{sens} from 13 to 74%. Investigations indicated that DDXPO has the mezzo first triplet excited state energy level (T_1) between the first singlet excited energy level (S_1) and T_1 of Hpffpd. This may support one more additional energy transfer from the T_1 energy level of DDXPO to that of Hpffpd, and consequently improves the energy transfer in the Eu^{3+} complex **2**. These effects makes the $[Eu(pffpd)_3(DDXPO)]$ **2** complex has the promising PL efficiency of 48%. On the other hand, in $[Eu(pffpd)_3(DPEPO)]$ **3**, both the S_1 and T_1 levels of DPEPO lies above the S_1 of Hpffpd and hence no mezzo state exists, and consequently exhibits lower quantum yield (28%) than that of **2**. Most importantly, the DDXPO could serve an effective ancillary ligand to afford high luminescence performance in Eu^{3+}-tris-*β*-diketonate complexes, which may find certainly an outstanding candidate for the design of red-emitting electroluminescent materials.

Chapter 3

Highly luminescent poly(methyl methacrylate)-incorporated europium complex supported by a carbazole-based fluorinated *β*-diketonate ligand and a 4,5-bis(diphenylphosphino)-9,9-dimethylxanthene oxide co-ligand

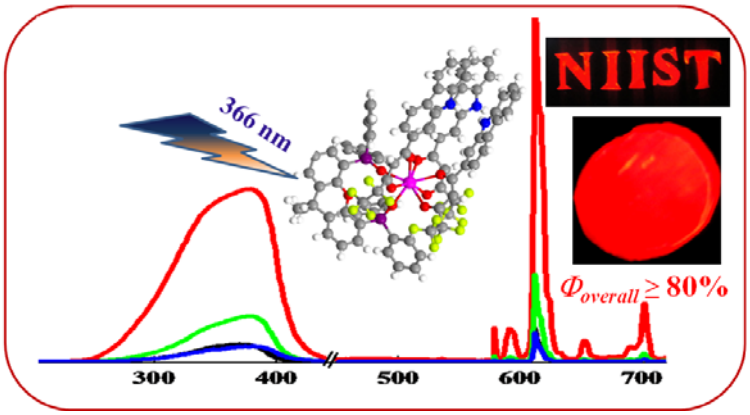

3.1. Summary. A novel efficient antenna complex of Eu^{3+} [$Eu(CPFHP)_3(DDXPO)$] supported by a highly fluorinated carbazole-substituted *β*-diketonate ligand, namely, 1-(9H-carbazol-2-yl)-4,4,5,5,5-pentafluoro-3-hydroxypent-2-en-1-one (CPFHP) and the 4,5-bis(diphenylphosphino)-9,9-dimethylxanthene oxide (DDXPO) ancillary ligand, has been synthesized, structurally characterized, and its photoluminescent behaviour examined. The single-crystal X-ray diffraction analysis of $Eu(CPFHP)_3(DDXPO)$ revealed that this complex is mononuclear, and that the central Eu^{3+} ion is surrounded by eight oxygen atoms, six of which are provided by the three bidentate *β*-diketonate ligands. The remaining two oxygen atoms are furnished by the chelating phosphine oxide ligand. The coordination polyhedron is best described as that of a distorted square antiprism. The photophysical properties of $Eu(CPFHP)_3(DDXPO)$ benefit from adequate protection of the metal by the ligands with respect to non-radiative deactivation as well as an efficient ligand-to-metal energy transfer process which exceeds 66% in chloroform solution with a quantum yield of 47%. As an integral part of this work, the synthesis, characterization, and luminescent properties of poly(methyl methacrylate) (PMMA) polymer films doped with $Eu(CPFHP)_3(DDXPO)$ are also reported. The luminescent efficiencies of the doped films (photoluminescence quantum yields 79−84%) are dramatically enhanced in comparison with that of the precursor complex. The new luminescent PMMA-doped $Eu(CPFHP)_3(DDXPO)$ complex therefore shows considerable promise for polymer light-emitting diode and active polymer optical fiber applications.

D.B. Ambili Raj *et al.*, *Inorg. Chem.* **2010**, *49*, 9055-9063.

3.2 Introduction

The unique photoluminescent properties of europium complexes render them appropriate for a host of applications, such as display devices, solid state lighting (including OLEDS), and sensors [Kido and Okamoto 2002; Kuriki *et al*. 2002; Polman and van Veggel 2004; Bünzli and Piguet 2005; de Bettencourt-Dias 2007; Bünzli 2010]. The shielding of the f orbitals by the $5s^2$ and $5p^6$ closed shells results in narrow line-like emissions of optically pure colors with long radiative lifetimes. However, the f-f transitions that result in light emission from the lanthanides are both spin- and parity-forbidden which, in turn, mandates the use of antenna molecules for indirect excitation of the metal center. This indirect excitation, also known as the antenna effect, takes advantage of the coordinated ligands in the sense that energy transfer from the ligand-centered excited states to the metal center results in lanthanide ion luminescence [Lehn 1990; Sabbatini *et al*. 1993; Piguet and Bünzli 1999]. In 1942, Weissman observed that the use of organic ligands in europium complexes increased the luminescence intensity from the lanthanide ion when such complexes were irradiated with ultraviolet (UV) light [Weissman 1942]. The *β*-diketone ligand class represents one of the important ‘‘antennas’’ for facilitating efficient ligand to lanthanide ion energy transfers, thus generating high harvest emissions [Binnemans 2009; Xu *et al.* 2006; Remya *et al.* 2008].

It is well known that the replacement of the C−H bonds of a *β*-diketone ligand with lower-energy C−F oscillators is capable of lowering the vibrational energy of the ligand [Hasegawa *et al.* 2000; Glover *et al*. 2007]. In turn, this decreases the energy loss because of ligand vibration and therefore enhances the emission intensity of the lanthanide ion [Chauvin *et al.* 2006; Sun *et al.* 2006]. In recent years, the carbazole functional group has been incorporated into *β*-diketonate ligands to improve the hole transport mobility of lanthanide complexes [Nie *et al.* 2007; Zheng *et al.* 2008; ^{a}He *et al.* 2009; Baek *et al.* 2010]. Carbazoles possess a number of other desirable properties which include good chemical and environmental stability, modest cost, and the ability to tune the optical and electrical properties by substitution with a wide

variety of functional groups [Grazulevicius *et al.* 2003; Morin *et al.* 2005]. It was consideration of these factors that prompted us to design and synthesize the new *β*-diketonate ligand, 1-(9*H*-carbazol-2-yl)-4,4,5,5,5-pentafluoro-3-hydroxypent-2-en-1-one, which features both a polyfluorinated alkyl group and a carbazole unit.

Chelated lanthanide *β*-diketonate complexes typically are isolated with two water molecules incorporated in the first coordination sphere of the central metal ion. Unfortunately, the presence of such water molecules quenches the lanthanide emission by activation of non-radiative decay pathways [de Sa *et al.* 2000]. One way to overcome this problem is to replace the water molecules with ancillary ligands bearing chromophores that are capable of playing the antenna role. An additional requirement in this regard is that the antenna ligand should bind sufficiently strongly to the lanthanide center that the coordination of water molecules is precluded. In selecting the ancillary ligand, attention needs to be paid to enhancing the volatility and thermal stability as well as to the film forming properties and the carrier transport behavior. Given the foregoing considerations, a significant number of lanthanide tris(*β*-diketonates) have been prepared that also feature coordinated bidentate nitrogen [Bellusci *et al.* 2005; Biju *et al.* 2006; Chen *et al.* 2007] and phosphine oxide [Xu *et al.* 2006; Xu *et al.* 2007; Xu *et al.* 2008; Xu *et al.* 2010] ligands. Such complexes have been reported to serve as efficient light conversion molecular devices. Consideration of the foregoing results motivated us to design the new europium antenna complex, $Eu(CPFHP)_3(DDXPO)$, which contains a highly fluorinated carbazole-substituted *β*-diketonate, namely, 1-(9*H*-carbazol-2-yl)-4,4,5,5,5-pentafluoro-3-hydroxypent-2-en-1-one (CPFHP). The coordination sphere also contains 4,5-bis(diphenylphosphino)-9,9-dimethylxanthene oxide (DDXPO) as an ancillary ligand. The newly synthesized Eu^{3+} complex was characterized on the basis of elemental analysis, ^{1}H and ^{13}C NMR, and mass spectroscopy.

Recent years have witnessed a growing interest in lanthanide−polymer complexes because of the combination of the good luminescent properties of lanthanide complexes and the

excellent mechanical processing properties of polymers [McGehee *et al.* 1999; Kai *et al.* 2008; Balamurugan *et al.* 2009; Boyer *et al.* 2009]. Typical applications for such polymer films are as organic light emitting diodes [Liang *et al.* 2003; Yu *et al.* 2005; Shunmugam and Tew, 2005; Chen *et al.* 2008] (OLEDs) or as active optical polymer fibers for data transmission [McGehee *et al.* 1999; Klink *et al.* 2000]. A popular polymer matrix for use as a host for luminescent lanthanide complexes is poly(methyl methacrylate) (PMMA) which is a low-cost, simply prepared polymer of excellent optical quality. This material is transparent at wavelengths longer than 250 nm [Hasegawa *et al.* 2003*;* Fan *et al.* 2010; Lunstroot *et al.* 2010]. In the present work, we report the synthesis and photophysical properties of the new Eu^{3+} complex, $[Eu(CPFHP)_3(DDXPO)]$ which exhibits excellent quantum yield values (79−84%) in PMMA. The overall aim of this work was to develop a simple and feasible method for the production of a luminescent material with the objective of obtaining information about the photoluminescence (PL) behavior of the optical material incorporated into the polymer film. The sensitization effect of the polymer matrixes on the Eu^{3+} luminescent center is discussed in detail based on excitation and emission spectra, luminescence decay curves, experimental intensity parameters, and quantum yields.

3.3. Experimental section

Materials and instrumentation. Europium(III) nitrate hexahydrate of 99.9% purity and 4,5-bis(diphenylphosphino)-9,9-dimethylxanthene of 97% purity were purchased from Treibacher and Alfa-Aesar, respectively. Gadolinium(III) nitrate hexahydrate, 2-acetylcarbazole (98% purity), methyl pentafluoropropionate (99% purity), 4,5-bis(diphenylphosphino)-9,9-dimethylxanthene 97% (Aldrich). and sodium hydride (60% dispersion in mineral oil) were procured from Sigma-Aldrich. The bidentate phosphine oxide, DDXPO was synthesized according to the method described in the earlier chapter. All the other chemicals used were of analytical reagent grade.

The overall quantum yields of the sensitized Eu^{3+} emissions of the complexes were measured in $CHCl_3$ solution at room temperature and are cited relative to a reference solution of quinine sulfate in 1 N H_2SO_4 (Φ = 54.6%). Corrections were made for the refractive index of the solvent. All solvents were of spectroscopic grade. The overall luminescent quantum yields of the complexes were calculated according to the well-known equation [Eaton 1988; Demasa and Crosby 1971; Werts *et al* 2002]

$$\Phi_{overall} = \frac{n^2 A_{ref} I}{n_{ref}^2 A I_{ref}} \Phi_{ref} \qquad (1)$$

where *n*, *A*, and *I* denote the refractive index of solvent, the area of the emission spectrum, and the absorbance at the excitation wavelength, respectively, and Φ_{ref} represents the quantum yield of the standard quinine sulfate solution. The subscript *ref* denotes the reference, and the absence of a subscript implies an unknown sample. The refractive index is assumed to be equivalent to that of the pure solvent: 1.45 for chloroform and 1.33 for water at room temperature. The overall quantum yields for the Eu^{3+} doped films were determined under ligand excitation (330−420 nm) and are based on the absolute method using a calibrated integrating sphere in a SPEX Fluorolog spectrofluorimeter. A Xe-arc lamp was used to excite the thin-film samples placed in the sphere. The quantum yield was determined by comparing the spectral intensities of the lamp and the sample emission as reported in the literature [Wrighton *et* al. 1974; de Mello *et al.* 1997; Palsson and Monkman 2002]. Using this experimental setup and the integrating sphere system, the solid-state fluorescence quantum yield of a thin film of the standard green OLED material tris-8-hydroxyquinolinolato aluminum (Alq_3) was determined to be 0.19, which is consistent with previously reported values [Colle *et al.* 2003; Saleesh Kumar *et al.* 2008]. Each sample was measured several times under slightly different experimental conditions. The estimated error for the quantum yields is (±10%) [Eliseeva *et al.* 2008].

Crystallographic characterization. The X-ray diffraction data were collected on a Rigaku AFC-12 Saturn 724+ CCD diffractometer equipped with a graphite-monochromated Mo Kα

radiation source (λ = 0.71073 Å) and a Rigaku XStream low temperature device cooled to 100 K. Corrections were applied for Lorentz and polarization effects. The structure was solved by direct methods and refined by full-matrix least-squares cycles on F^2 using the Siemens SHELXTL PLUS 5.0 (PC) software package [Sheldrick 1994] and PLATON [Sluis and Spek, 1990]. All non-hydrogen atoms were refined anisotropically, and the hydrogen atoms were placed in fixed, calculated positions using a riding model. Selected crystal data and data collection and refinement parameters are listed in Table 1. Two of the C_2F_5 groups in complex $Eu(CPFHP)_3(DDXPO)$ display a typical disorder, which has been modeled and refined successfully. X-ray crystallographic information files can be obtained free of charge via www.ccdc.cam.ac.uk/consts/retrieving.html (or from CCDC, 12 Union Road, Cambridge CB2 1EZ, U.K.; fax, +44 1223 336033; e-mail, deposit@ccdc.cam.ac.uk). The CCDC number for the $Eu(CPFHP)_3(DDXPO)$ complex is CCDC 771380.

Other instrumental techniques employed for the characterization of the ligands and complexes are the same as that described in the previous chapter.

Synthesis of 1-(9*H*-Carbazol-2-yl)-4,4,5,5,5-pentafluoro-3-hydroxypent-2-en-1-one (CPFHP). A modification of the typical Claisen condensation procedure was used for the synthesis of CPFHP as shown in Scheme 3.1. 2-Acetylcarbazole (0.002 mmol) and methyl pentafluoropropionate (0.002 mmol) were dissolved in 20 mL of anhydrous tetrahydrofuran (THF) under a N_2 atmosphere, and the temperature was maintained at 0 °C. Sodium hydride was added, and the reaction mixture was stirred for 12 h, following which it was quenched with water. Hydrochloric acid (2.0 M) was then added, and the resulting mixture was extracted with CH_2Cl_2 and dried over anhydrous Na_2SO_4. The residue was purified by column chromatography (chloroform/hexane =1:4) to give the final product as a yellowish solid (yield 65%). Elemental analysis (%): Calcd for $C_{17}H_{10}F_5NO_2$ (355.26): C, 57.47; H, 2.84; N, 3.94. Found: C, 57.73; H, 3.17; N, 3.98. ^{1}H NMR (500 MHz, CDCl3): δ (ppm) 15.57 (broad, enol −OH), 8.36 (s, 1H), 8.17−8.13 (m, 3H), 7.83−7.81 (dd, 1H, J = 1.5 Hz, J = 1.5 Hz), 7.55−7.50

(m, 2H), 7.32−7.29 (m, 1H), 6.77 (s, 1H). ^{13}C NMR (125 MHz, acetone-d_6): δ (ppm) 186.72, 178.06−177.64, 142.95−142.81,140.51−140.37, 140.09, 130.12, 129.22−128.71, 122.96, 122.92, 122.31−121.97, 121.57−121.23, 120.62−120.15, 119.49−119.29, 118.15, 112.42−112.09, 109.01, 94.62. FT-IR (KBr) ν_{max}: 3346, 2923, 2853, 1630, 1580, 1203, 1173, 1118, 1018, 804 cm^{-1}. m /*z* = 356.76 $(M+H)^+$.

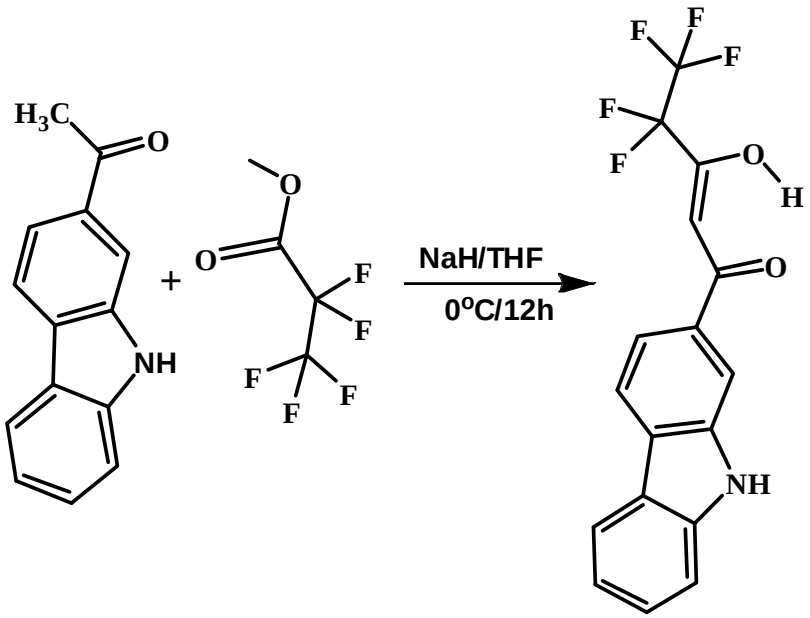

Scheme 3.1. Synthesis of the CPFHP Ligand.

Synthesis of Ln(CPFHP)$_3$(C$_2$H$_5$OH)(H$_2$O) [Ln = Eu^{3+} (1), Gd^{3+}(3)]. A mixture of the *β*-diketonate ligand CPFHP (0.6 mmol) and NaOH (0.6 mmol) in an acetone-ethanol solvent mixture was stirred for 10 min at room temperature, following which a saturated ethanolic solution of Ln$(NO_3)_3\cdot 6H_2O$ (0.2 mmol) was added dropwise, and the reaction mixture was stirred subsequently for 10 h. Water was then added, and the precipitate that had formed was filtered off, washed with water, dried and purified by recrystallization from an acetone-water mixture (Scheme 3.2).

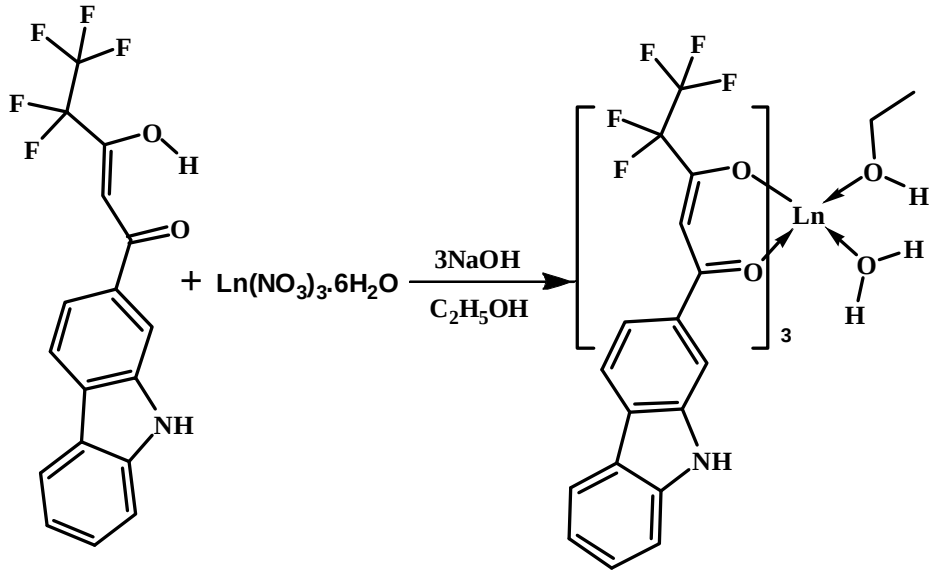

Scheme 3.2. Synthesis of $Ln(CPFHP)_3(H_2O)(C_2H_5OH)$.[Ln = Eu^{3+} (**1**), and Gd^{3+} (**3**)].

Elemental analysis (%): Calcd for $C_{53}H_{35}F_{15}O_8N_3Eu$ (**1**) (1278.81): C, 49.78; H, 2.76; N, 3.29. Found: C, 49.97; H, 2.54; N, 3.07. FT- IR (KBr) ν_{max}: 3418, 2924, 1603, 1529, 1469, 1327, 1259, 1166, 1013, 750 cm^{-1}. *m*/*z* = 1233.65 [(M^+ − C_2H_5OH) + H]. Elemental analysis (%): $C_{53}H_{35}F_{15}O_8N_3Gd$ (**3**) (1284.76): C, 49.78; H, 2.76; N, 3.29. Found: C, 50.02; H, 2.61; N, 3.17. FT-IR (KBr) ν_{max}: 3423, 2925, 1602, 1528, 1464, 1328, 1277, 1197, 1015, 798 cm^{-1}. *m*/*z* = 1222.89 [(M^+ − H_2O, C_2H_5OH) + H].

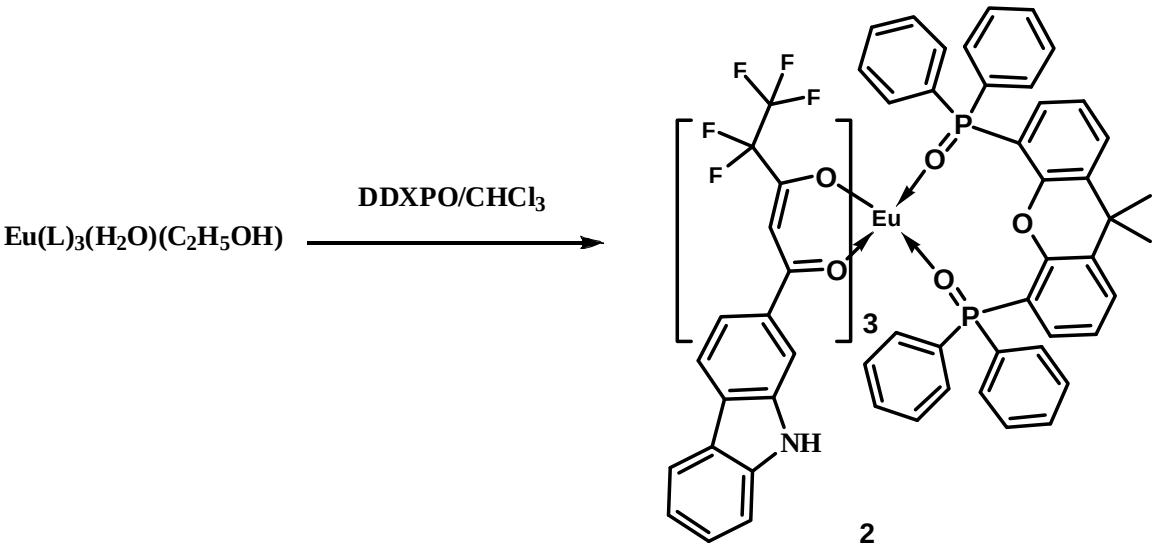

Scheme 3.3. Synthesis of $Eu(CPFHP)_3(DDXPO)$.

Synthesis of Eu(CPFHP)$_3$(DDXPO) (2). Complex **2** was prepared by stirring equimolar quantities of Eu(CPFHP)$_3$(H_2O)(C_2H_5OH) and the phosphine oxide DDXPO in $CHCl_3$ solution for 24 h at room temperature (Scheme 3.3). The product was isolated by solvent evaporation and purified by recrystallization from a chloroform-hexane mixture. Crystals of complex **2** suitable for single-crystal X-ray diffraction study were obtained upon storage of a saturated solution of the complex in a $CHCl_3$/2-methoxy-ethanol solvent mixture. Elemental analysis (%): Calcd for $C_{90}H_{59}EuF_{15}N_3O_9P_2$ (1825.35): C, 59.22; H, 3.26; N, 2.30. Found: C, 59.47; H, 3.24; N, 2.38. FT-IR (KBr) ν_{max}: 2924, 1611, 1520, 1404, 1212, 1195, 1173, 1146, 1125, 1070, 1007, 748, 689, 539 cm^{-1}; *m*/*z* = 1470.21 [Eu(CPFHP)$_2$(DDXPO) + H].

Synthesis of Eu^{3+} Complex-Doped PMMA Polymer Films. The PMMA polymer was doped with the Eu^{3+} complex **2** in the proportions 2.5 (**4**), 7.5 (**5**), 10 (**6**), and 15% (**7**) (w/w). The PMMA powder was dissolved in chloroform, followed by addition of the required amount of complex **2** in chloroform solution, and the resulting mixture was heated at 40 °C for 30 min. The polymer film was obtained after evaporation of excess solvent at 60 °C [Moudam *et al.* 2009].

2.4. Results and Discussion

Synthesis and Characterization of the CPFHP Ligand and Ln^{3+} Complexes 1−3. The ligand 1-(9*H*-carbazol-2-yl)-4,4,5,5,5-pentafluoro-3-hydroxypent-2-en-1-one (CPFHP) was synthesized in 65% yield from the corresponding ketone and ester by a modified Claisen condensation reaction. The overall procedure is summarized in Scheme 3.1. The ligand, CPFHP was characterized by ^{1}H NMR, ^{13}C NMR, FT-IR, and mass spectroscopic (FAB-MS) methods, as well as by elemental analysis. The lanthanide complexes were prepared as shown in Schemes 3.2 and 3.3. The complexes were characterized by FT-IR, mass spectroscopy (FAB-MS), and elemental analyses. The elemental analyses and FAB-MS studies revealed that the central Ln^{3+} ion is coordinated to three *β*-diketonate ligands. In the case of complex **2**, one molecule of the

bidentate phosphine oxide, DDXPO, is also present in the coordination sphere. The FT-IR spectra of complexes **1** and **3** exhibit a broad absorption in the 3000−3500 cm^{-1} region, thereby indicating the presence of solvent molecules in the coordination sphere of the Ln^{3+} ion. On the other hand, the absence of this broad band in the 3000−3500 cm^{-1} region in the case of complex **2** implied that the solvent molecules had been replaced successfully by the bidentate phosphine oxide ligand. The carbonyl stretching frequency for the CPFHP ligand (1630 cm^{-1}) shifted to lower wave numbers in compounds **1**−**3** (1603 cm^{-1} for **1**; 1611 cm^{-1} for **2**; 1602 cm^{-1} for **3**), thus confirming coordination of the carbonyl oxygen to the Ln^{3+} cation in each case. The fact that the P=O stretching frequency of DDXPO at 1180 cm^{-1} shifted to 1173 cm^{-1} in complex **2** confirms the involvement of the P═O bond of DDXPO in complex formation.

The thermal behavior of the Eu^{3+} complexes under a nitrogen atmosphere was examined by means of thermogravimetric analysis (TGA). The general profiles of the weight losses for complexes **1** and **2** are displayed in Figure 3.1. It is clear from the TGA data that complex **1** undergoes a mass loss of approximately 5% (Calcd: 5.01%) in the first step (120 to 180 °C), which corresponds to the elimination of the coordinated water and solvent molecules. On the other hand, complex **2** is stable up to 180 °C, above which it decomposes. The final residue for complex **1** is approximately 20% of the initial mass while that for complex **2** is approximately 15%. These residual masses correspond to formation of the non-volatile europium(III) oxyfluoride.

The PMMA polymer was doped with $Eu(CPFHP)_3(DDXPO)$ (**2**) in the proportions of 2.5, 7.5, 10, and 15% (w/w) and characterized by FT-IR spectroscopy. The band at 1726 cm^{-1} for PMMA corresponds to the C═O vibration [Liu *et al.* 2004], whereas for the Eu/PMMA films, this vibration shifts to 1731 cm^{-1}. In turn, this implies that the Eu^{3+} complex is stabilized by means of interactions with the oxygen atoms of the carbonyl group of PMMA. Such interactions might stem from the donation of a pair of electrons from the carbonyl oxygen to the lanthanide ions. The broad absorption band assigned to the H_2O vibrational modes in the FT-IR

spectrum of Eu^{3+} complex **1**, which appears in the 3000−3500 cm^{-1} region, is absent in the doped PMMA polymer films thereby confirming that the polymer films are anhydrous. Such a conclusion is in good agreement with the TG analyses of the doped polymer film, for which no mass loss was observed in the temperature region 50−200 °C (Figure 3.2). Both the doped and the undoped films decompose at approximately 150 °C.

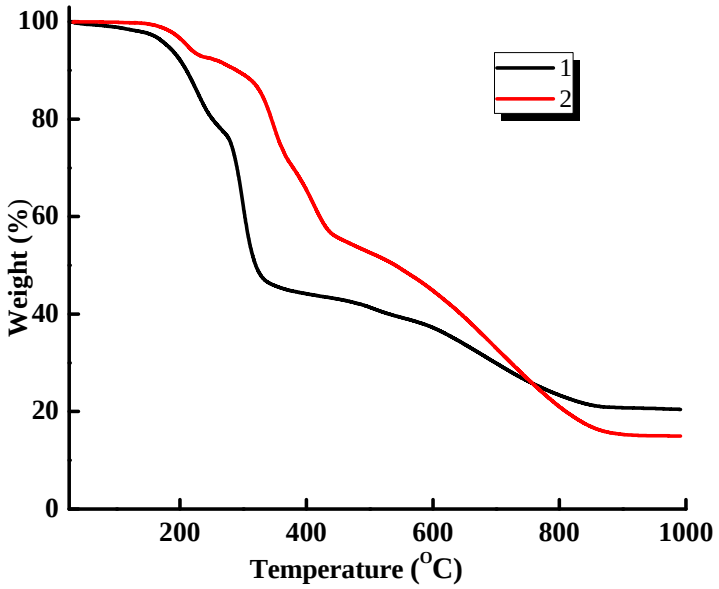

Figure 3.1. Thermogravimetric curves for the complexes **1**and **2.**

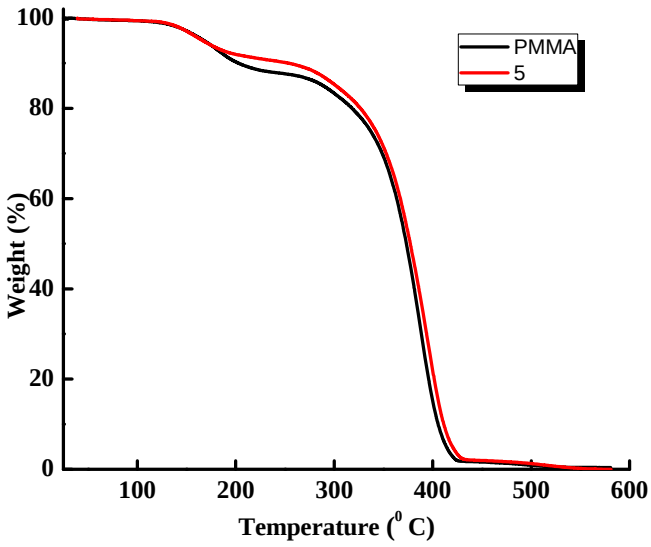

Figure 3.2. Thermogravimetric curves for PMMA and 7.5% Eu^{3+} doped polymer film.

X-ray Crystal Structure of [Eu(CPFHP)$_3$(DDXPO)] 2. Single crystals of complex **2** suitable for X-ray analysis were grown from a $CHCl_3$/2-methoxy ethanol solution. The crystal structure of **2** was determined by single-crystal X-ray diffraction, and the asymmetric unit is depicted in Figure 3.3. The crystal data and data collection parameters are presented in Table 3.1, and selected bond distances and bond angles are summarized in Table 3.2. The single crystal X-ray analysis reveals that the complex **2** crystallizes in the monoclinic space group *P*21/*n*. The absence of a center of symmetry in **2** results in an increase in the number of electronic transitions of the 4f orbitals because of the odd parity [Hasegawa *et al*. 2003].

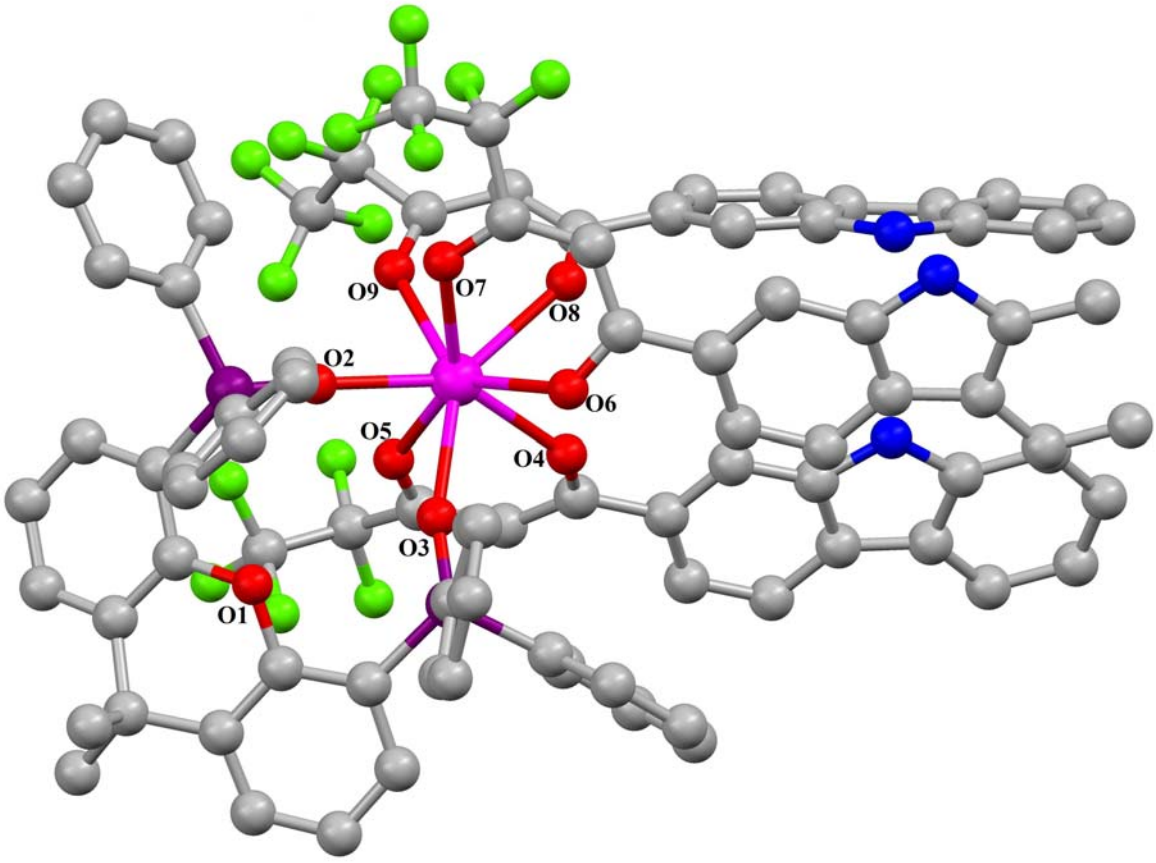

Figure 3.3. Asymmetric unit of complex **2** displayed as a ball and stick model at 25% probability level. All hydrogen atoms have been omitted for clarity.

An Oak Ridge thermal ellipsoid plot (ORTEP) view of **2** reveals an eight-coordinate Eu^{3+} cation environment comprising one chelated phosphine oxide (DDXPO) and three bidentate fluorinated *β*-diketonate ligands. The coordination polyhedron can best be described as that of a distorted square antiprism. The central Eu^{3+} ion is surrounded by bulky carbazole-substituted fluorinated *β*-diketonates and bidentate chelating phosphine oxide ligands. This encapsulated structure therefore meets the structural requirements for an efficient lanthanide luminescent material since the Eu^{3+} ion is protected from vibrational coupling thereby increasing the light absorption cross-section by the so-called "antenna effect". It is interesting to note that the bridging oxygen atom that connects the two triphenylphosphine oxide units of the chelated phosphine oxide is not coordinated to the central Eu^{3+} ion. The two Eu−O bonds of the chelated phosphine oxide ligand (2.30 Å and 2.37 Å) are shorter than the six Eu−O bonds of the fluorinated *β*-diketonate ligands (2.34 Å−2.41 Å). A similar trend is evident in the single-crystal X-ray data for the complex Eu^{3+}-hexafluoroacetylacetonato-1,1′-biphenyl-2,2′-diylbis(diphenylphosphine oxide) [Eu−O bond distances 2.32−2.33 Å in BIPHEPO and 2.40−2.44 Å in the *β*-diketone] [Nakamura *et al.* 2007]. Thus the chelating phosphine oxide DDXPO coordinates more strongly to the Eu^{3+} ion than the *β*-diketonate ligands. Furthermore, in the case of DDXPO, the two diphenylphosphine oxide units are linked by a xanthene moiety that increases the extent of conjugation in the chelating ligand. In turn, this serves to improve the carrier injection and transport properties of **2**. Moreover, the introduction of a more conjugated DDXPO ligand renders the complex more rigid, which in turn reduces the structural relaxation in the excited state.

Table 3.1. Crystallographic and refinement data for **2.**

Parameters	**2**
formula	$C_{96}H_{75}EuF_{15}N_3O_{13}P_2$
fw	1977.49
cryst syst	monoclinic
space group	P21/n
cryst size	0.1× 0.1 × 0.09 mm^3
temp/K	100(2) K
a (A°)	11.4888(11)
b (A°)	33.356(3)
c (A°)	22.684(2)
α (deg)	90
β (deg)	96.751(3)
γ (deg)	90
V/A° ^{3}	8632.6(14)
Z	4
D_{calcd}	1.522 Mg/m^3
μ(Mo,Kα), mm^{-1}	0.863
F(000)	4016.0
R1 [I > 2σ(I)]	0.0823
wR2 [I > 2σ(I)]	0.1580
R1 (all data)	0.1609
wR2 (all data)	0.1810
GOF	1.054

Table 3.2. Selected bond lengths (Å) and angles (deg) for complex 2**.**

2	
Eu (1)-O(2)	2.300(9)
Eu (1)-O(3)	2.372(10)
Eu (1)-O(4)	2.345(7)
Eu (1)-O(5)	2.414(7)
Eu (1)-O(6)	2.400(9)
Eu (1)-O(7)	2.411(10)
Eu (1)-O(8)	2.399(11)
Eu (1)-O(9)	2.358(12)
O(2)- Eu (1)-O(3)	73.0(3)
O(4)- Eu (1)-O(5)	70.75(19)
O(6)- Eu (1)-O(7)	69.6(3)
O(8)- Eu (1)-O(9)	69.9(4)

Electronic States of the Ligands. The UV−visible absorption spectra of the free ligands (CPFHP and DDXPO) and their corresponding Eu^{3+} complexes (**1** and **2**) in $CHCl_3$ solution (c = 2 × 10^{-6} mol dm^{-3}) are displayed in Figure 3.4.

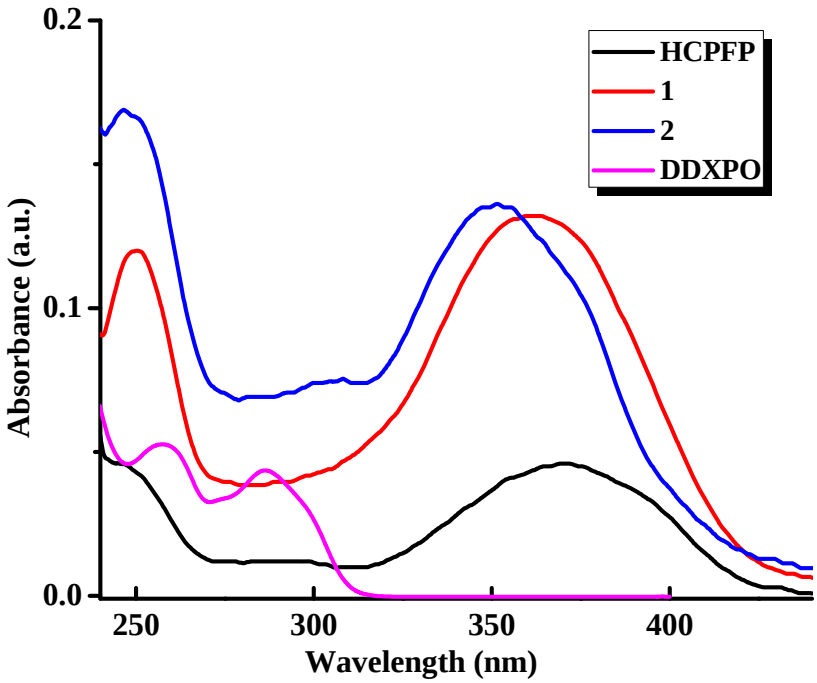

Figure 3.4. UV−vis absorption spectra of the ligands CPFHP and DDXPO and complexes **1** and **2** in $CHCl_3$ solution (c = 2 × 10^{-6} mol dm^{-3}).

The trends in the absorption spectra of these complexes are identical to the ones observed for the free ligands, indicating that the singlet excited states of the ligands are not significantly affected by the complexation to the Eu^{3+} ion. However, a small blue shift that is discernible in the absorption maximum of complex **2** is attributable to the perturbation induced by metal coordination. The ligand CPFHP displays a composite broad band in the UV corresponding to a singlet−singlet π−π* enolic transition assigned to the *β*-diketonate moiety [Remya *et al*. 2008; [b]Biju *et al*. 2009], with a lowest energy maximum at 315−440 nm (λ_{max} = 370 nm) and a molar absorption coefficient of 2.3 × 10^4 L M^{-1} cm^{-1}. The higher energy absorption bands detected in the range 240−270 nm are attributable to the π−π* transition of the locally excited state of the carbazole moiety of the *β*-diketonate ligand [Nie *et al.* 2007]. The electronic transitions of the

β-diketonate (peak at ca. 240−270 nm) and the chelated phosphine oxide (peak at ca. 248−270 nm) units are overlapped by the carbazole features [Zheng *et al.* 2008]. The presence of the ancillary ligand DDXPO not only enhances the absorption intensity but also satisfies the high coordination number of the central Eu^{3+} ion and thus improves the coordination and thermal stabilities of complex **2**. The molar absorption coefficient values for **1** and **2** were calculated at the respective λ_{max} value and were found to be 6.68×10^4 and 6.75×10^4 L mol^{-1} cm^{-1}, respectively. The magnitudes of these values are approximately three times higher than that of the *β*-diketonate ligand, and this trend is consistent with the presence of three *β*-diketonate ligands in each complex. Note also that the large molar absorption coefficient obtained for the newly designed *β*-diketonate ligand indicates that it has a strong ability to absorb light.

Solution-State PL. The excitation and emission spectra of **1** and **2** in $CHCl_3$ solution ($c = 1.5 \times 10^{-6}$ mol dm^{-3}) are displayed in Figure 3.5. The excitation profile of each complex closely mimics that of its corresponding absorption spectrum in the 250−400 nm region, thus demonstrating that energy transfer occurs from the *β*-diketonate ligands to the Eu^{3+} ion. The excitation spectra of **1** and **2** exhibit a broad band between 250 and 400 nm which is attributable to the π−π* transition of the coordinated ligands. The absence of any absorption bands due to the f-f transitions of the Eu^{3+} ion proves that luminescence sensitization *via* excitation of the ligand is effective. The ambient-temperature emission spectra of Eu^{3+} complexes **1** and **2** show characteristics of the metal ion emissions in the 550−725 nm region, and exhibit well resolved peaks that are due to the transitions from the metal-centered $^5D_0$ excited state to the ^7F_J ground state multiplet. Maximum peak intensities at 580, 592, 612, 652, and 702 nm were observed for the J = 0, 1, 2, 3, and 4 transitions, respectively, and the J = 2 so-called "hypersensitive" transition is intense [Pavithran *et al.* 2006; Biju *et al.* 2006]. The intensity of the $^5D_0 \rightarrow {}^7F_2$ transition (electric dipole) is greater than that of the $^5D_0 \rightarrow {}^7F_1$ transition (magnetic dipole), which indicates that the coordination environment of the Eu^{3+} ion is devoid of an inversion center.

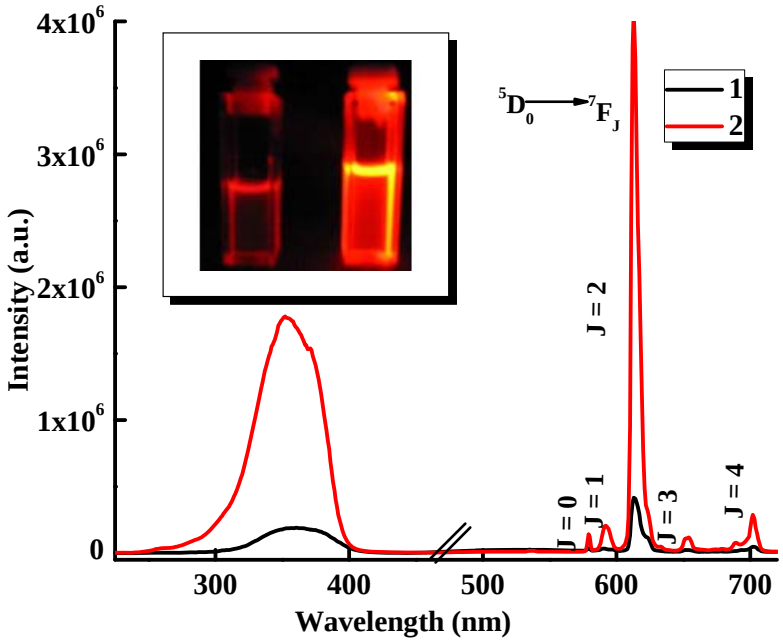

Figure 3.5. Room temperature (303 K) excitation and emission spectra of complexes **1** and **2** in $CHCl_3$ solution (c = 1.5 × 10^{-6} mol dm^{-3}).

To estimate the relative transition probability of the electric-dipole transition, the relative integrated intensity of the $^5D_0 \rightarrow {}^7F_2$ transition with respect to that of the $^5D_0 \rightarrow {}^7F_1$ transition band was evaluated [Harada *et al.* 2009] ($A_{21} = A_{ED}/A_{MD}$; A_{ED}, integrated intensity at the electric-dipole transition; A_{MD}, integrated intensity at the magnetic-dipole transition). The A_{21} values for the Eu^{3+} complexes are listed in Table 3.3. The A_{21} value for complex **2** in the presence of ancillary ligand was considerably larger than that of complex **1** with the carbazole-substituted fluorinated *β*-diketonate ligand. No broad emission band resulting from organic ligand molecules in the blue region can be observed, which indicates that the ligand transfers the absorbed energy effectively to the emitting level of the metal ion. The introduction of a highly rigid chelating phosphine oxide into the coordination sphere of the Eu^{3+}-tris-*β*-diketonate complex would lead to an effective reduction of the symmetry around the Eu^{3+} ion. Briefly, the presence of the chelating phosphine oxide increases the luminescent intensity of the hypersensitive transition of the Eu^{3+} ion. It is easy to understand from Figure 3.5 that the

displacement of the solvent molecules from the complex Eu**(**CPFHP)$_3$(C_2H_5OH)(H_2O) by the chelating phosphine oxide significantly enhances the luminescent intensity.

The observed luminescence decays (τ_{obs}) are single exponential functions for chloroform solutions of complexes **1** and **2** at 303 K, thus indicating the presence of only one emissive Eu^{3+} center. Typical decay profiles for complexes **1** and **2** are displayed in Figure 3.6.

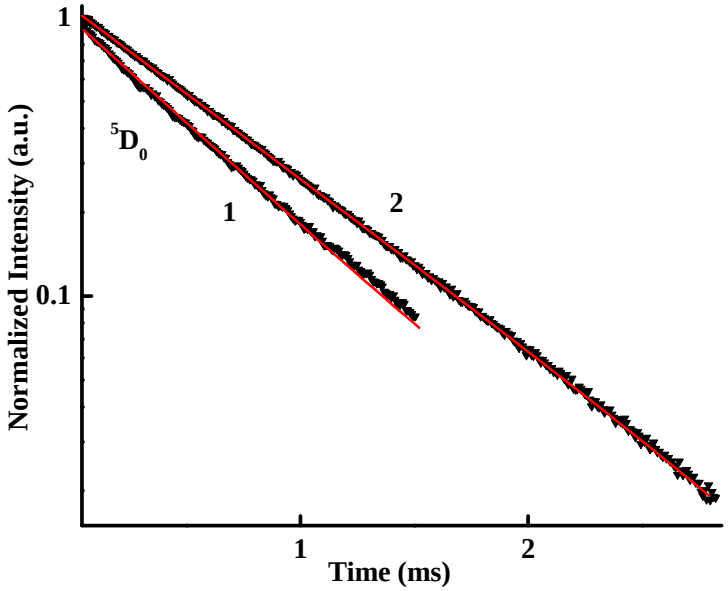

Figure 3.6. Experimental luminescence decay profiles for complexes **1** and **2** in $CHCl_3$ solution (c = 1.5 × 10^{-6} mol dm^{-3}) monitored at approximately 612 nm and excited at the maximum emission wavelengths.

The somewhat shorter lifetime observed for complex **1** may be due to the dominant non-radiative decay channels associated with vibronic coupling induced by the presence of solvent molecules, as has been well documented for several hydrated europium β-diketonate complexes [de Sa *et al.* 2000; Binnemans 2009]. In the case of Eu^{3+}, the energy gap between the luminescent state and the ground state manifold is approximately 12,000 cm^{-1}. Thus, relatively efficient coupling of the Eu^{3+} excited states occurs to the third vibrational overtone of the proximate OH oscillators (ν_{OH}~3300−3500 cm^{-1}) which is consistent with the observed quenching of Eu^{3+} luminescence [Werts 2005; Ramya *et al.* 2010]. On the other hand, because of the absence of non-radiative decay pathways, longer lifetime values have been observed for complex **2** in which the solvent molecules have been replaced by the chelating phosphine oxide.

The overall quantum yields ($\Phi_{overall}$), radiative (A_{RAD}) and non-radiative (A_{NR}) decay rates, and energy transfer efficiencies (Φ_{sens}) for **1** and **2** are presented in Table 3.3.

Table 3.3. Radiative (A_{RAD}) and nonradiative (A_{NR}) decay rates, $^5D_0$ lifetime (τ_{obs}), intrinsic quantum yield (Φ_{Ln}, %), energy transfer efficiency (Φ_{sens}, %), and overall quantum yield ($\Phi_{overall}$, %) for complexes **1**-**2** in $CHCl_3$ solution and as PMMA films (**4**-**7**).

Complex	A_{21}	τ_{obs} (μs)	A_{RAD} (s^{-1})	A_{NR} (s^{-1})	Φ_{Ln} (%)	$\Phi_{overall}$ (%)	Φ_{sens} (%)
1	7.903	585 ± 2	603	1104	35	8	22
2	16.13	714 ± 1	986	413	70	47	66
4	14.53	764 ± 1	934	375	73	79	100
5	15.23	751 ± 1	986	345	74	84	100
6	15.56	732 ± 1	977	390	72	80	100
7	15.01	762 ± 1	960	352	73	83	100

The overall quantum yields of ligand-sensitized europium luminescence for complexes **1** and **2** in $CHCl_3$ solution have been calculated by a relative method using quinine sulfate as the standard [Demasa and Crosby 1971; Eaton 1988; Werts *et al* 2002]. At room temperature, the substitution of solvent molecules in the Eu^{3+}-tris-*β*-diketonate complex by the chelating phosphine oxide, DDXPO, results in an increase in the $^5D_0$ luminescence lifetime from 585 ± 2 to 714 ± 1 μs and an approximately 6-fold enhancement in the absolute quantum yield (8 to 47%) in chloroform solution. To achieve bright luminescence, the ligands must protect the Eu^{3+} ion from non-radiative deactivation (term Φ_{Ln}), and provide efficient light harvesting and energy transfer (term Φ_{sens}). The substantial contribution of the chelating phosphine oxide to the overall sensitization of the Eu^{3+}-centered luminescence in **2** is confirmed by (i) an increase of the intrinsic quantum yield by a factor of 2.3 which results from removal of the quenching effect of the O−H vibrations, and (ii) the significant enhancement of Φ_{sens} from 22 to 66%.

To investigate the PL mechanism of the Eu^{3+} complexes, it was desirable to determine the energy levels of relevant electronic states of the ligands. The singlet (S_1) energy levels of CPFHP and the chelating phosphine oxide, DDXPO, were estimated by referring to the upper

wavelengths of the UV−vis absorption edges of the $Gd(CPFHP)_3(H_2O)(C_2H_5OH)$ and $Gd(NO_3)_3(DDXPO)$ complexes. The triplet (T_1) energy levels were calculated by referring to the lower wavelength emission edges of the corresponding phosphorescence spectra of complexes $Gd(CPFHP)_3(H_2O)(C_2H_5OH)$ (Figure 3.7) and $Gd(NO_3)_3(DDXPO)$. Thus, the S_1 and T_1 values for CPFHP were found to be 24,630 cm^{-1} and 20,750 cm^{-1}, respectively. The S_1 (31,850 cm^{-1}) and T_1 (23,470 cm^{-1}) levels for DDXPO were taken from chapter 2.

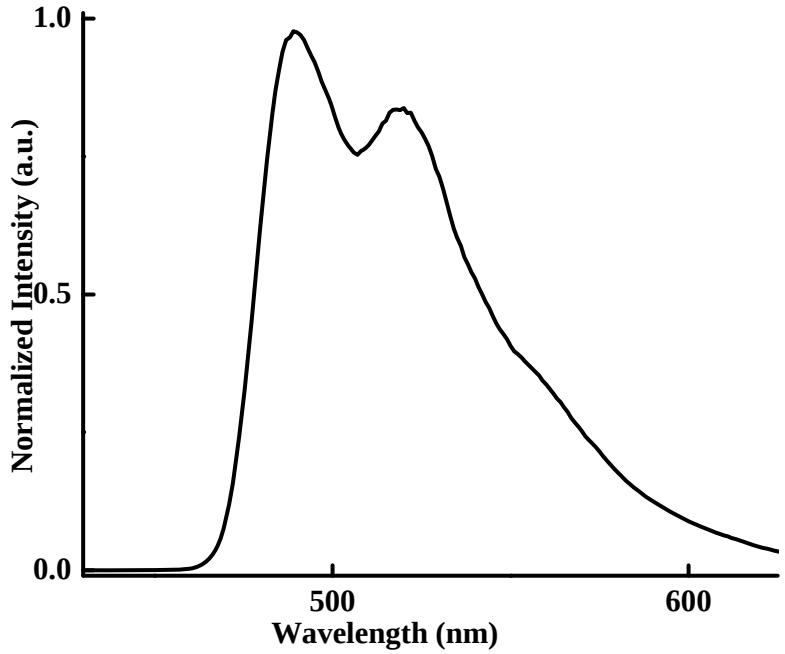

Figure 3.7. Phosphorescence spectrum of $Gd(CPFHP)_3(H_2O)(C_2H_5OH)$ at 77K.

The triplet energy level of the CPFHP ligand appears at appreciably higher energy than that of the $^5D_0$ state of Eu^{3+}, thus indicating that the newly designed *β*-diketonate ligand can act as an antenna for the photosensitization of the Eu^{3+} ion. On the other hand, the $^5D_1$ emitting state of Eu^{3+} (18,800 cm^{-1}) is found to be critically close to the triplet state of the CPFHP ligand, which can lead to the thermally assisted back-energy transfer from the central core [Armaroli *et al*. 1999; Accorsi *et al* 2009]. However, the triplet energy level of the chelating phosphine oxide, DDXPO (23,470 cm^{-1}), is appropriate for efficient energy transfer with all the $^5D_2$, $^5D_1$, and $^5D_0$ energy levels of Eu^{3+}. Therefore, the PL mechanism for the Eu^{3+} complexes is proposed to

involve a ligand-sensitized luminescence process (antenna effect) [Lehn 1990; Sabbatini *et al*. 1993; Piguet and Bunzli 1999].

Photophysical Properties of Eu^{3+} Complexes Doped in PMMA Polymer Films. Lanthanide complexes incorporated into polymer matrixes represent a new class of materials that offer the characteristics of both complexes and polymers, thus making them ideal candidates for use in wide range of new technologies [McGehee *et al.* 1999; Kai *et al.* 2008; Balamurugan *et al.* 2009; Boyer *et al.* 2009]. In the present manuscript, we describe the incorporation of a newly designed, highly luminescent complex into PMMA, a well-known, low-cost, easily prepared polymer of excellent optical quality. Figure 3.8 shows the excitation spectra of the PMMA polymer films doped with $Eu(CPFHP)_3(DDXPO)$ at different concentrations [2.5 (**4**), 7.5 (**5**), 10 (**6**), and 15% (**7**) (w/w)] and recorded at 303 K in the spectral range of 250 to 480 nm, by monitoring the emission at 612 nm.

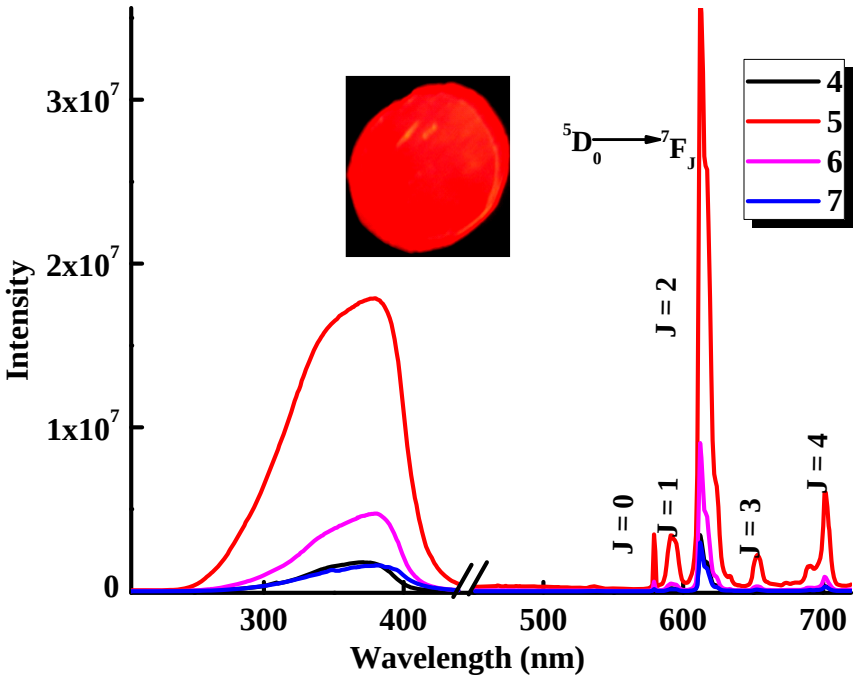

Figure 3.8. Excitation and emission spectra of PMMA films doped with 2.5 to 15% (w/w) $Eu(CPFHP)_3(DDXPO)$ systems recorded at 303 K.

The excitation spectra are dominated by an intense broad band in the 250 to 400 nm region, which can be assigned to absorptions of both the PMMA polymer and the organic chromophore. Of particular note is the observation that the excitation maximum of the spectra is red-shifted as compared to the solution phase spectra. This can be attributed to the considerable interaction of the ligands with PMMA matrix. The emission spectra of PMMA doped with $Eu(CPFHP)_3(DDXPO)$ at a variety of concentrations [2.5 (**4**), 7.5 (**5**), 10 (**6**), and 15% (**7**) (w/w)] and excited at 370 nm exhibit five emission bands that are assigned to the characteristic $^5D_0 \rightarrow {}^7F_J$ (J = 0−4) transitions of the Eu^{3+} ion. As displayed in Figure 3.8, the luminescent intensity of the Eu^{3+} emission at 612 nm increases with increasing Eu^{3+} content and reaches a maximum at a Eu^{3+} content of 7.5%. A further increase in the Eu^{3+} content decreases the luminescent intensity. The energy transfer between the lanthanide ions themselves is a non-radiative process, which accounts for the decrease in the Eu^{3+} emission, especially at high Eu^{3+} content (**6** and **7**) [[b]Li *et al* 2001; Parra *et al.* 2004; [a]Biju *et al.* 2009]. The transition of highest intensity is dominated by the hypersensitive $^5D_0 \rightarrow {}^7F_2$ transition at approximately 612 nm, which implies that the Eu^{3+} ion does not occupy a site with inversion symmetry. Moreover, the presence of only one sharp peak in the region of the $^5D_0 \rightarrow {}^7F_0$ transition at 580 nm suggests the occurrence of a unique chemical environment around the Eu^{3+} ion of symmetry type C_s, C_n, or C_{nv}. It is well-known that the magnetic-dipole transition $^5D_0 \rightarrow {}^7F_1$ is nearly independent of the ligand field and therefore can be used as an internal standard to account for ligand differences. The electric-dipole transition $^5D_0 \rightarrow {}^7F_2$, the so-called hypersensitive transitions, is sensitive to the symmetry of the coordination sphere. The intensity ratio of the magnetic-dipole transition to the electric-dipole transition in the lanthanide complex measures the symmetry of the coordination sphere [Zhang *et al.* 2008]. The intensity ratios (A_{21}) of the $^5D_0 \rightarrow {}^7F_2$ transition to the $^5D_0 \rightarrow {}^7F_1$ transition in the Eu/PMMA were shown in Table 3.3. The intensity ratio of the transitions of $^5D_0 \rightarrow {}^7F_2$ to $^5D_0 \rightarrow {}^7F_1$ is 15.23 for the complex **2** when incorporated into the

PMMA matrix (7.5%). These results suggest that, when the Eu complex is incorporated into the microcavities of the polymer matrix, the Eu^{3+} ions exhibit different local environments because of the influence of the surrounding polymer. The symmetry of the coordination sphere for the Eu^{3+} ions changes moderately in the Eu/PMMA as compared to the pure precursor complex. When incorporated into the microcavities of the PMMA matrix, however, the complexes exhibit disorder of a certain magnitude. Under the influences of the electric field of the surrounding ligands, the distortion of the symmetry around the Eu^{3+} ion by the capping PMMA results in the polarization of the Eu^{3+}, which increases the probability for electric-dipole, allowed transition. The influences of PMMA on the coordinative environment of the Eu^{3+} ions changes the energy-transfer probabilities of the electric-dipole transitions, accounting for the increases in luminescent intensity of the 612 peak.

The luminescence decay curves of the doped films were obtained by monitoring the emission at the hypersensitive $^5D_0 \rightarrow {}^7F_2$ transition (612 nm) and excitation at 370 nm (Figure 3.9). These data were adjusted with a first-order exponential decay function, and the lifetime values (τ) of the emitter $^5D_0$ level of the doped systems were determined and are listed in Table 3.3. All τ values for the doped polymer systems are higher than that of the hydrated Eu^{3+}complex, thus indicating that radiative processes are operative in all the doped polymer films because of the absence of multiphonon relaxation by coupling with the OH oscillators from the $Eu(CPFHP)_3(C_2H_5OH)(H_2O)$ complex. On the other hand, the $^5D_0$ lifetime of the doped films was not obviously influenced by the embedded PMMA.

The overall quantum yields ($\Phi_{overall}$) determined by the absolute method, radiative (A_{RAD}) and non-radiative (A_{NR}) decay rates, intrinsic quantum yields (Φ_{Ln}), and energy transfer efficiencies (Φ_{sens}) of the PMMA films doped with $Eu(CPFHP)_3$(DDXPO) at different doping concentrations are presented in Table 3.3. All the PMMA doped films exhibit excellent overall quantum yield values, ranging from 79 to 84%. This range is comparable to that reported recently for luminescent europium β-diketonate complexes doped in PMMA matrixes

[Hasegawa *et al.* 2003; Hasegawa *et al.* 2006; Moudam *et al.* 2009]. Furthermore, the substantial increase in Φ_{sens} (from 66% in complex **2** to 100% in luminescent PMMA films) on going from $CHCl_3$ to PMMA is consistent with the elimination of collisional quenching of the ligand triplet state in the polymer matrix.

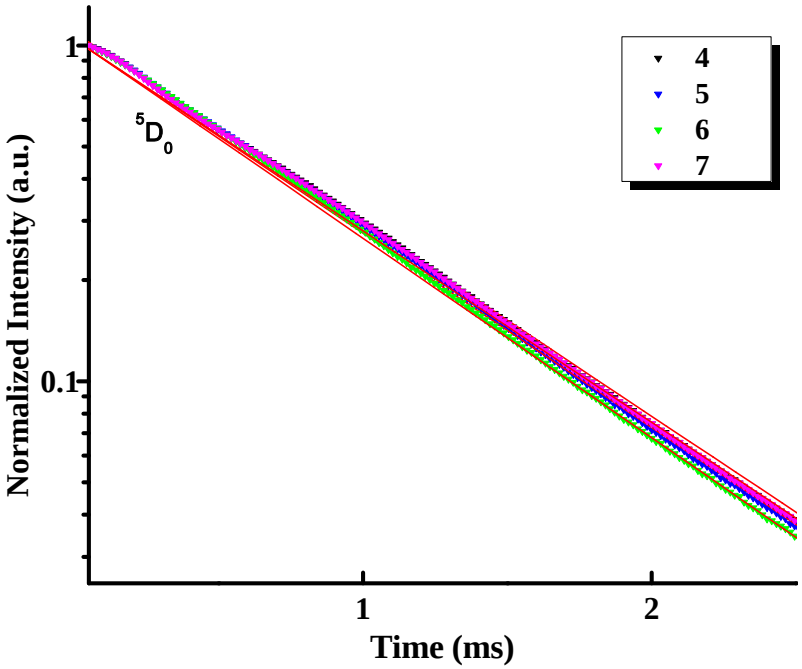

Figure 3.9. Experimental luminescence decay profiles of Eu^{3+} complex 2 doped into PMMA polymer.

It is well-known that the efficiency of the intermolecular energy transfer is strongly dependent on the distance between the donor and acceptor. According to this point of view, it is suggested that for the present system, the PMMA molecule, because of its long chain, has the capability to enwrap the $Eu(CPFHP)_3(DDXPO)$ complex and keeps the acceptor and donor close. In such a case, energy can be transferred efficiently from ligand to Eu^{3+}, resulting in the enhancement of intrinsic Eu^{3+} emission of a $Eu(CPFHP)_3(DDXPO)$. Thus the preserved rigidity in the complex structure in PMMA could be the origin of the enhanced overall quantum yield. Strikingly, the present work shows the role of DDXPO is much more significant in PMMA than in chloroform, with europium complex **2** doped in a PMMA polymer matrix (**4**−**7**) displaying markedly higher Φ_{Ln} values (72 to 74%) than **1** and **2**. Again, this may arise from the enhanced encapsulation of

Eu^{3+} center minimizing the detrimental effect of the C−H oscillators in the PMMA matrix that potentially provide non-radiative decay pathways for the Eu^{3+} excited state.

3.5. Conclusions

In summary, we have designed, synthesized, and characterized a novel eight-coordinate, highly luminescent lanthanide complex that utilizes a fluorinated carbazole-substituted *β*-diketonate in conjunction with the ancilliary ligand, 4,5-bis(diphenylphosphino)-9,9-dimethylxanthene oxide, for indirect excitation of the europium metal center. The new complex displays efficient sensitized luminescence in chloroform solution (Φ_{sens} = 66%) with a quantum yield of 47%. Additionally, the newly designed europium complex was incorporated into PMMA polymer films, which were shown to exhibit exceptionally high PL quantum yields (79−84%). This implies that the PMMA with high molecular weight enwraps the Eu^{3+} complex and keeps the donor and acceptor close, which results in the effective intermolecular energy transfer and, consequently, the high sensitization efficiency. In conclusion, the PMMA films doped with the Eu^{3+}-*β*-diketonate complex show promising PL efficiency and therefore have potential applications as polymer light-emitting diodes and active polymer optical fibers.

Chapter 4

Luminescent properties of novel Eu^{3+}-4,4,5,5,5-pentafluoro-1-(naphthalen-2-yl)pentane-1,3-dione complexes in the prescence of N-heterocyclic ligands

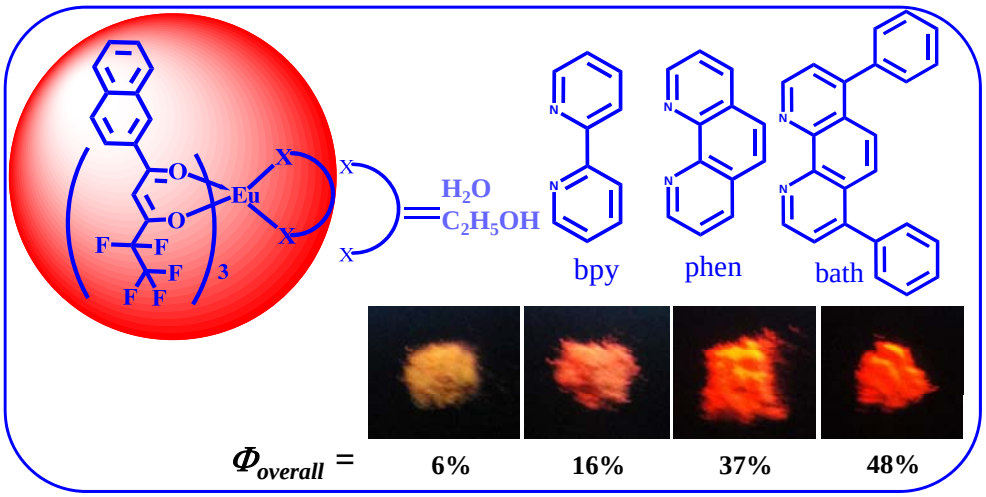

4.1. Summary. A novel *β*-diketone, 4,4,5,5,5-pentafluoro-1-(naphthalen-2-yl)pentane-1,3-dione (HPFNP), which contains polyfluorinated alkyl group, as well as the long conjugated naphthyl group, has been used for the synthesis of a series of new tris(*β*-diketonate)europium(III) complexes of the general formula $Eu(PFNP)_3(L)$ [where L = H_2O, 2,2′- bipyridine (bpy), 1,10-phenanthroline (phen), 4,7-diphenyl-1,10-phenanthroline (bath)] and characterized by various spectroscopic techniques. The single-crystal X-ray diffraction analysis of $Eu(PFNP)_3(bpy)$ revealed that the complex is mononuclear, the central Eu^{3+} ion is coordinated by six oxygen atoms furnished by three *β*-diketonate ligands, and two nitrogen atoms from a bidentate bipyridyl ligand, in an overall distorted square prismatic geometry. Further, analysis of the X-ray crystal data of the above complex also revealed interesting 1D, 2D, and 3D networks based on intra- and intermolecular hydrogen bonds. The room-temperature PL spectra of the complexes are composed of typical Eu^{3+} red emissions, assigned to transitions between the first excited state ($^5D_0$) and the multiplet ($^7F_{0\text{-}4}$). The results demonstrate that the substitution of solvent molecules by bidentate nitrogen ligands in $Eu(PFNP)_3(H_2O)(EtOH)$ greatly enhances the quantum yields and lifetime values.

D.B. Ambili Raj *et al.*, *Inorg. Chem.*, **2008**, *47*, 8091-8100.

4.2. Introduction

The versatile photophysical properties of lanthanide ions have inspired vigorous research activities owing to wide range of photonic applications such as tunable lasers, amplifiers for optical communications, luminescent probes for analytes, components of the emitting materials in multilayer organic light emitting diodes and efficient light conversion molecular devices [Kido and Okamoto 2002; Bunzli and Piguet 2005; de Bettencourt-Dias 2007; Brunet *et al*. 2007]. The Eu^{3+} and Tb^{3+} ions are of particular interest because of their long luminescence lifetime and narrow emission bands in the visible region [Yang *et al*. 2004; Xin *et al*. 2003]. Because the Laporte-forbidden 4f-4f transition prevents direct excitation of lanthanide luminescence, Ln^{3+} ions always require sensitization by suitable organic chromophores. Furthermore, for practical applications, Ln^{3+} ion must be incorporated into highly stable coordinated complexes. The efficiency of ligand-to-metal energy transfer, which requires compatibility between the energy levels of the ligand excited states and accepting levels of Ln^{3+} ions, is crucial in the design of high performance luminescent molecular devices. Moreover, ligands containing high-energy oscillators, such as C−H and O−H bonds, are able to quench the metal excited states nonradiatively, thereby leading to lower luminescence intensities and shorter excited-state lifetimes. Thus the replacement of C−H bonds with C−F bonds is important in the design of new lanthanide luminescent complexes with efficient emission properties.

Recently, a large number of highly coordinated complexes of lanthanide tris(*β*-diketonates) containing several nitrogen ligands such as 1,10-phenanthroline, 2,2′-bipyridine, 4,4′-disubstituted-2,2′-bipyridines, and 2,2′:6′,6″-terpyridine have been reported [Försberg 1973; McGehee *et al.* 1999; Fukuda *et al.* 2002; Fu *et al.* 2005; Bellusci *et al.* 2005; Chen *et al.* 2007]. However, the photoluminescence efficiency of these reported Eu^{3+} coordination complexes are not very attractive. These factors have motivated us to synthesize a new *β*-diketone ligand, 4,4,5,5,5-pentafluoro-1-(naphthalen-2-yl)pentane-1,3-dione, which has the

polyfluorinated alkyl group, as well as the long conjugated naphthyl group. The synthesized ligand has been utilized for the synthesis of various Eu^{3+} complexes with various bidentate nitrogen donors (Figure 4.1) and investigated their photophysical properties for possible use in OLEDs as emitting materials.

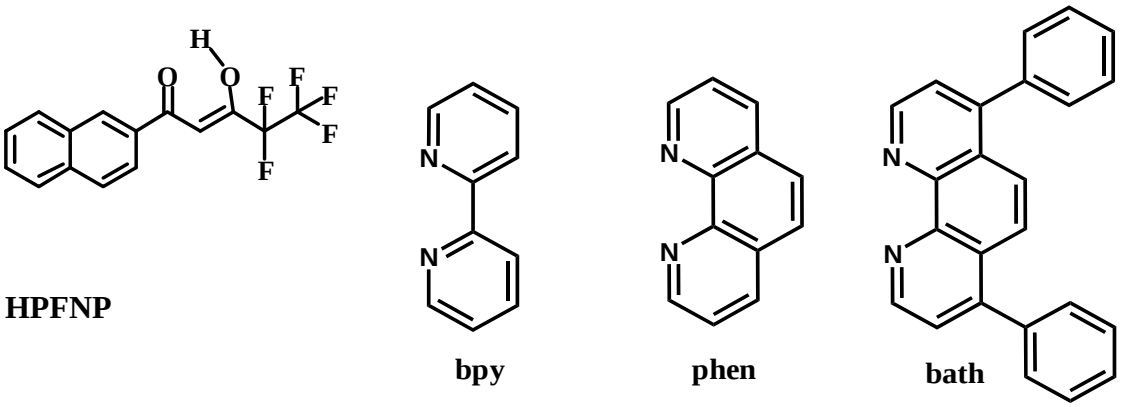

Figure 4.1. Structural formulae of the lignads HPFNP, 2,2′-bipyridine (bpy), 1,10-phenanthroline (phen) and 4,7-diphenyl-1,10-phenanthroline (bath).

4.3. Experimental Section

Materials and Instrumentation. The following chemicals were procured commercially and used without subsequent purification:europium(III) nitrate hexahydrate, 99.9% (Treibacher); gadolinium(III) nitrate hexahydrate (Aldrich); 2-acetonaphthone, 98% (Aldrich); methyl pentafluoropropionate 99% (Aldrich); sodium hydride 60% dispersion in mineral oil (Aldrich); 2,2′-dipyridyl, 99%, (Aldrich), 4,7-diphenyl-1,10-phenanthroline, 97%, (Aldrich), 1,10-phenanthroline monohydrate (Merck)] are used without further purification. All the other chemicals used were of analytical reagent grade.

DSC measurements were performed on a DSC-Perkin-Elmer Pyris 6 DSC instrument at a heating rate of 10 °C/min under nitrogen atmosphere. X-ray powder diffraction (XRD) analyses were performed with a Philips X'Pert Pro diffractometer. The XRD patterns were recorded in the 5-70° 2θ range using Ni-filtered Cu Kα radiation. Other instrumental techniques employed

for the characterization of the ligands and complexes are the same as that described in the second chapter.

Synthesis of 4,4,5,5,5-Pentafluoro-1-(naphthalen-2-yl)pentane-1,3-dione (HPFNP). A modified method of typical Claisen condensation procedure is used as shown in Scheme 4.1. 2-Acetonaphthone (0.34 g, 0.002 mmol) and methyl pentafluoropropionate (0.356 g, 0.002 mmol) were added into 20 mL dry THF, and the mixture was stirred for 10 min. To this sodium hydride was added in inert atmosphere and stirred at room temperature for 12 h. The resulting solution was quenched with water; 2 M HCl (50 mL) was added, and the solution was extracted twice with chloroform (70 mL). The organic layer was dried over Na_2SO_4, and the solvent was evaporated to obtain a maroon oily liquid, which was purified by chromatography on a silica gel column with chloroform and hexane as the eluent to get the maroon liquid as the product (0.51 g, 80% yield). ^{1}H NMR (300 MHz, $CDCl_3$): δ (ppm) 7.57-7.46 (m, 2H), 7.89-7.78 (m, 4H), 8.42 (s, 1H), 6.68 (s, 1H), 15.38 (broad, 1H). FT-IR (KBr) ν_{max}: 3063, 1602, 1328, 1202, 1010, 795 cm^{-1}. *m*/*z* = 317 $(M + 1)^+$.

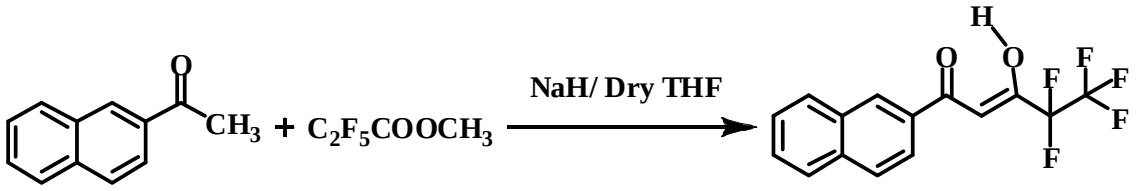

Scheme 4.1. Synthesis of the Ligand HPFNP.

Synthesis of Ln(PFNP)$_3$(C_2H_5OH)(H_2O) [Ln = Eu^{3+} (1), Gd^{3+}(5)]. To an ethanolic solution of HPFNP (0.6 mmol), NaOH (0.6 mmol) is added, and the mixture was stirred for 5 min. To this a saturated ethanolic solution of $Ln(NO_3)_3 \cdot 6H_2O$ (0.2 mmol) is added dropwise and stirred for 10 h. Water is then added to this mixture, and the precipitate thus formed is filtered, washed with water, dried, and purified by recrystallization from diethyl ether-hexane mixture (Scheme 4.2). The efforts to grow single crystals of complexes **1** and **5** were unsuccessful.

Elemental analysis (%) Calcd for $C_{47}H_{32}F_{15}O_8Eu$ (**1**) (1161.70): C, 48.59; H, 2.78. Found: C, 48.92; H, 2.51. IR (KBr) ν_{max}: 3435, 1610, 1527, 1457, 1326, 1197, 1013, 792 cm^{-1}. *m/z* = 1120.12 [(M^+ - H_2O, C_2H_5OH) + Na].

Elemental analysis (%) Calcd for $C_{47}H_{32}F_{15}O_8Gd$ (**5**) (1166.98): C, 48.37; H, 2.76. Found: C, 48.52; H, 2.80. IR (KBr) ν_{max}: 3421, 1613, 1574, 1470, 1327, 1196, 1013, 790 cm^{-1}. *m/z* = 1125.05 [(M^+ - H_2O, C_2H_5OH) + Na].

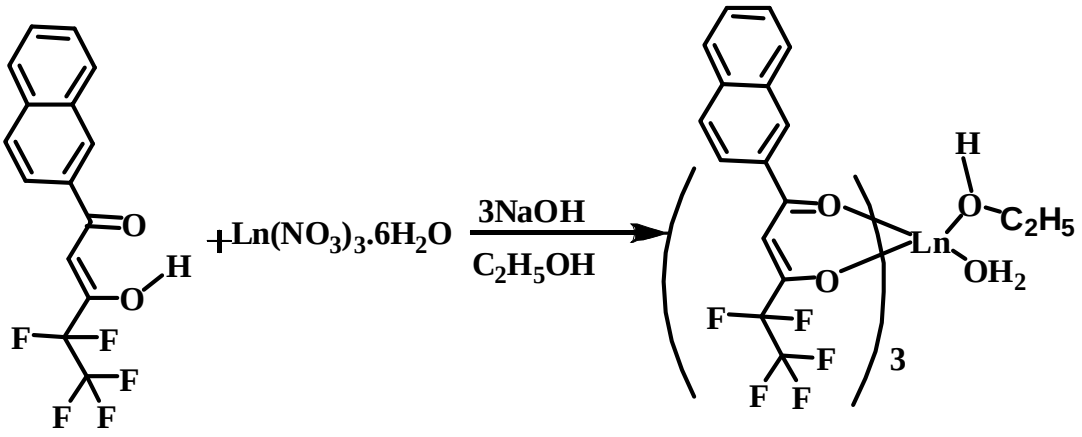

Ln = Eu (**1**), Gd (**5**)

Scheme 4.2. Synthesis of Ln $(PFNP)_3(H_2O)(C_2H_5OH)$.

Syntheses of Complexes 2-4. Synthesis routes of the complexes **2-4** are shown in Scheme 4.3. All these complexes were prepared by stirring equimolar solutions of $Eu(PFNP)_3$ $(C_2H_5OH)(H_2O)$ and the nitrogen donor in $CHCl_3$ for 24 h at room-temperature. The products were obtained after solvent evaporation and are purified by recrystallization from a chloroform-hexane mixture. A crop of crystals of complex **2** were formed after ~2 weeks. However, our efforts to grow single crystals of complexes **3** and **4** were unsuccessful.

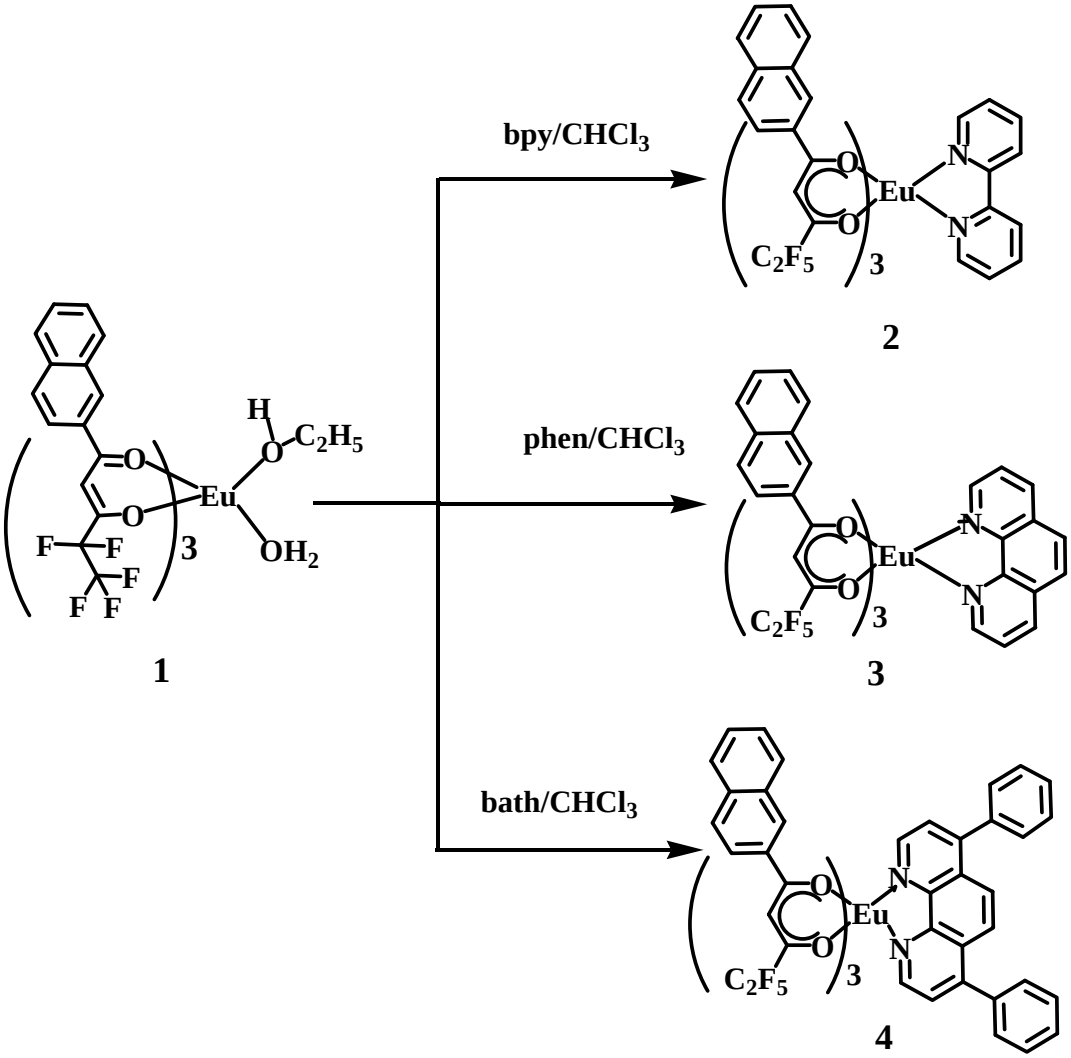

Scheme 4.3. Synthetic procedures for the Complexes **2-4.**

Eu(PFNP)$_3$(bpy) (2). Elemental analysis (%) Calcd for $C_{55}H_{32}F_{15}N_2O_6Eu$ (1253.80): C, 52.69; H, 2.57; N, 2.23. Found: C, 52.77; H, 2.53; N, 2.37. FT-IR (KBr) ν_{max}: 3058, 1637, 1610, 1594, 1507, 1473, 1328, 1281, 1197, 1162, 1013, 790 cm^{-1}. *m*/*z* = 1255.10 [(M^+) + 1]. mp: 200 °C.

Eu(PFNP)$_3$(phen) (3). Elemental analysis (%) Calcd for $C_{57}H_{32}F_{15}N_2O_6Eu$ (1277.82): C, 53.58; H, 2.52; N, 2.19. Found: C, 53.62; H, 2.49; N, 2.36. FT-IR (KBr) ν_{max}: 3056, 1610, 1592, 1568, 1506, 1327, 1279, 1197, 1153, 1009, 791 cm^{-1}. *m*/*z* = 1278.21 (M^+). mp: 185 °C.

Eu(PFNP)$_3$(bath) (4). Elemental analysis (%) Calcd for $C_{69}H_{40}F_{15}N_2O_6Eu$ (1430.03): C, 57.95; H, 2.82; N, 1.96. Found: C, 57.92; H, 2.87; N, 1.96. FT-IR (KBr): ν_{max}: 1610, 1598, 1524, 1384, 1329, 1285, 1214, 1195, 791 cm^{-1}. *m*/*z* = 1431.12 (M^+). mp: 200 °C.

Synthesis of $Gd(bath)_2(NO_3)_3$. To a 50 mL ethanol solution containing 2.0 mmol of 4,7-diphenyl-1,10-phenanthroline, 1.0 mmol of $Gd(NO_3)_3(H_2O)_6$ was added dropwise under constant stirring, and then the solution was refluxed for 6 h at 80 °C. The resulting solution was filtered to obtain a white powder. Elemental analysis (%) Calcd for $C_{48}H_{32}N_7O_9Gd$ (1008.08): C, 57.19; H, 3.20; N, 9.72. Found: C, 57.50; H, 3.45; N, 9.72. FT-IR (KBr) ν_{max}: 1492, 1384, 1307, 1029, 835, 766, 740, 702 cm^{-1}. *m*/*z* = 946.11 (M^+ - NO_3).

4.4. Results and Discussion

Structural Characterization of Europium(III) Complexes. The synthesis procedures for the europium complexes **1**-**5** are shown in Schemes 4.2 and 4.3. The microanalyses and HRMS studies of the complexes **1**-**5** shows that Ln^{3+} ion has reacted with HPFNP in a metal-to-ligand mole ratio of 1:3 and in **2**-**4,** one molecule of bidentate nitrogen ligand is involved. The IR spectrum of the complexes **1** and **5** shows a broad absorption in the region 3000-3500 cm^{-1}, indicating the presence of solvent molecules in the complex. On the other hand, the absence of the broadband in the region 3000-3500 cm^{-1} for complexes **2**-**4**, suggests that solvent molecules have been displaced by the bidentate neutral donors. The carbonyl stretching frequency of HPFNP (1602 cm^{-1}) has been shifted to longer wave numbers in complexes **1**-**5** (1610 cm^{-1} in **1**; 1613 cm^{-1} in **5**; 1610 cm^{-1} in **2**-**4**) indicating the involvement of carbonyl oxygen in the complex formation with Ln^{3+} ion. Further, the red shifts observed in the C=N stretching frequencies of nitrogen donors (1615 cm^{-1}) in complexes **2**-**4** (1594 cm^{-1} in **2**; 1592 cm^{-1} in **3**; 1598 cm^{-1} in **4**) show the involvement of nitrogen atoms in the complex formation with Eu^{3+} ion. The X-ray powder diffraction patterns of complexes **1** and **5** are similar, indicating they are isostructural and amorphous (Figure 4.2a). Similarly, from the XRD patterns of complexes **2**-**4** (Figure 4.2b), one can conclude that they are isostructural and crystalline.

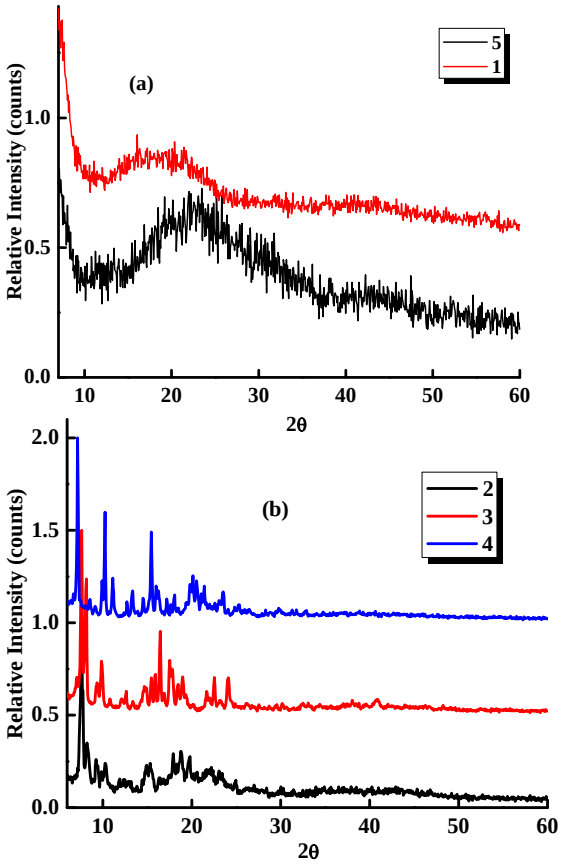

Figure 4.2. XRD patterns for the complexes (a) **1** and **5**, (b) **2**-**4**.

It is clear from the thermogravimetric analysis data that complex **1** (Figure 4.3) undergoes a mass loss of about 6% (calcd 5.5%) in the first step (120-230 °C), which corresponds to the elimination of the coordinated solvent molecules. Complex **1** is stable up to 230 °C, and then it under goes a single step decomposition. On the other hand, complexes **2**-**4** are more stable than the precursor sample **1**, and they undergo singlestep decomposition at 275 °C. The total weight loss occurred in the TGA of all these complexes are much higher than that calculated for the thermal decomposition of these complexes into nonvolatile europium(III) oxide, indicating the partial sublimation of these complexes under atmospheric pressure, which is common in poly fluorinated *β*-diketonate complexes.

The DSC curve of the precursor sample (**1**) shows a shallow broad endothermic peak in the temperature range from 90-150 °C relative to the release of solvent molecules, as observed in

the first event of the TG curve. Further, the absence of sharp endothermic peak in **1**, indicates the amorphous nature of the complex or at least it is difficult for it to crystallize. On the other hand, DSC curve of complexes **2-4** shows sharp endothermic peaks at 200, 185, and 200 °C, respectively, corresponding to their melting points.

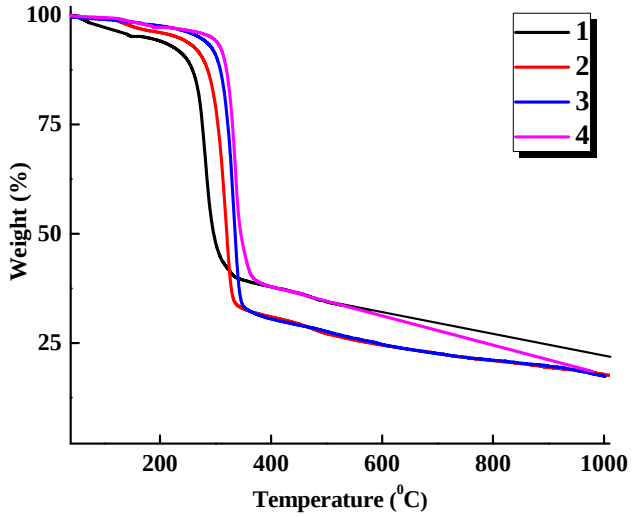

Figure 4.3. Thermogravimetric curves for the complexes **1-4.**

X-Ray Structural Characterization. The structure of complex **2** was characterized by single-crystal X-ray crystallography. The asymmetric unit is shown in Figure 4.4, and the structure of complex **2**, with the numbering scheme is displayed in Figure 4.5. The details of crystal data and data collection parameters for complex **2** are given in Table 4.1. The selected bond lengths and bond angles for **2** are listed in Table 4.2. The structure with the intramolecular H-bonding interactions is shown in Figure 4.6. As predicted from the mass spectral and elemental analyses, the central Eu^{3+} ion is coordinated with six oxygen atoms from the three β-diketonate ligands and two nitrogen atoms from a bidentate bipyridyl ligand. The coordination geometry of the metal center is best described as a distorted square antiprism. The central Eu^{3+} ion is thus completely surrounded by the bulky aromatic anionic ligand PFNP and the ancilliary bpy ligand, and this encapsulated structure therefore meets the structural requirements of an efficient lanthanide luminescent material by protecting the Eu^{3+} ion from vibrational coupling and increasing the light absorption cross-section by the so-called “antenna effect”.

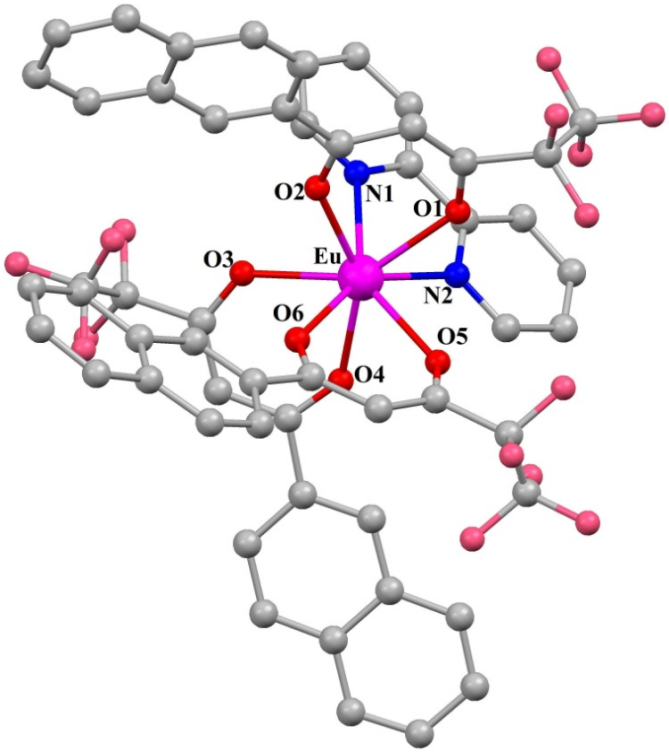

Figure 4.4. Asymmetric unit of complex **2**.

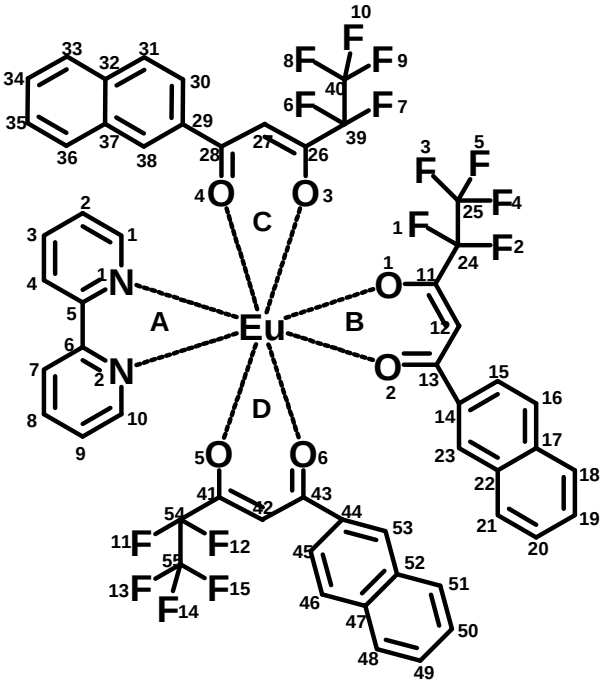

Figure 4.5. The structure of complex **2**, with the numbering scheme.

Table 4.1. Crystal Data, Collection, and Structure Refinement Parameters for complex **2**

Parameters	**2**
empirical formula	C_{57} H_{36} Cl_3 Eu F_{15} N_2 $O_{6.50}$
fw	1396.19
crystal system	Triclinic,
space group	P-1
cryst size (mm^3)	0.20 x 0.15 x 0.15 mm
temperature (K)	293(2) K
a/Å	10.338(4)
b/Å	14.784(6)
c/Å	19.431(7)
α (deg)	96.238(19)
β (deg)	93.336(18)
γ (deg)	90 96.523(19)
V / $Å^3$	2925.7(18)
Z	2
ρ_{calcd}/g cm^{-3}	1.585
μ/mm^{-1}	1.308
F(000)	1386
R1 [$I > 2\sigma(I)$]	0.0436
wR2 [$I > 2\sigma(I)$]	0.1252
R1 (all data)	0.0520
wR2 (all data)	0.1400
GOF	1.111

Table 4.2. Selected bond lengths (Å) and angles (˚) for complex **2**.

2	Lengths (Å)
Eu1-N1	2.554(4)
Eu1-N2	2.570(4)
Eu1-O1	2.367(4)
Eu1-O2	2.352(3)
Eu1-O3	2.374(3)
Eu1-O4	2.336(3)
Eu1-O5	2.359(4)
Eu1-O6	2.343(3)
	Angles (˚)
N1-Eu1-N2	63.03(10)
O1-Eu1-O2	71.32(18)
O3-Eu1-O4	71.92(19)
O5-Eu1-O6	71.24(18)

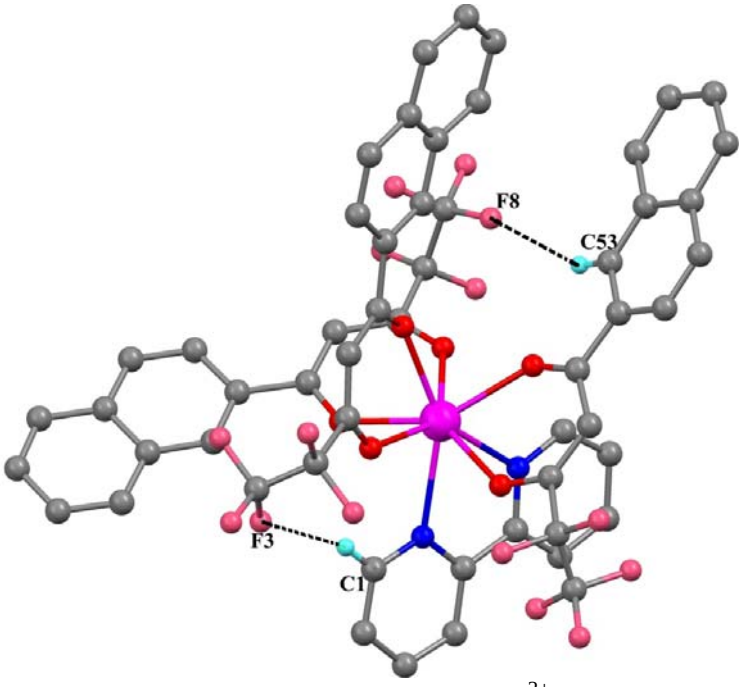

Figure 4.6. Coordination environment of the Eu^{3+} ion in complex **2**. The intramolecular H-bonding interactions are shown in broken lines.

The average Eu-N bond distance (2.56 Å) is longer than the Eu-O bonds of HPFNP ligands (2.34-2.37 Å), as observed in the X-ray single crystal data of the complexes, tris(4,4,4,-trifluoro-1-(2-naphthyl)-1,3-butanedionato)europium(III)-dipyridyl (Eu-O bonds 2.34- 2.39 Å NTA; Eu-N, 2.58 Å in bpy) [Thompson *et al.* 1998] and tris(4,4,4,- trifluoro-1-phenyl 2,4-butanedionato) europium(III)-dipyridyl (Eu-O bonds 2.32-2.40 Å in btfa; Eu-N, 2.58 Å in bpy) [Batista *et.al* 1998]. Further, in this complex, the Eu-O bonds adjacent to the naphthyl ring are slightly shorter than the others, which may be caused by the inductive effect of the fluorine atoms present in the HPFNP. In the *β*-diketone rings of the Eu^{3+} complex, the average distances for the C-C and C-O bonds are shorter than a single bond but longer than a double bond. This can be explained by the fact that there exists a strong conjugation between the naphthyl ring and the coordinated *β*-diketone, which leads to the delocalization of electron density of the coordinated *β*-diketonate chelate ring [Yu *et.al*. 2003; Sun *et.al*. 2006].

Two types of intramolecular interactions are observed between C1-H1· · · F3 and C53-H53 · · · F8 with the distances of 2.63 and 2.83 Å, and the angles are 161.49 and 155.84°,

respectively (Figure 4.6). Apart from the strong intramolecular hydrogen bonding interactions, three different intermolecular hydrogen bonding interactions are also observed in **2**. Two of them form the self-assembled dimer (dimer **a** and **b**), while the third one adopts 1D structure (**c**) in the solid state. All the three interactions are shown in Figures 4.7 and 4.8. The bipyridyl ring in **A** and the naphthyl ring in **D** interact with the -CF_3 groups of another molecule to form the self-assembled dimer and the observed interactions in C3-H3 · · · F14 (dimer **a**) and C50-H50 · · · F7 (dimer **b**) with the distances of 2.68 and 2.60 Å and the angles of 145.9° and 168°. On the other hand, the bridging CH group and the naphthyl group in ring **B** interact with the -CF_3 group of another molecule to form the rodlike 1D network. The distances and angles in 1D network are: 2.70 Å and 168° (C15-H15 · · · F15) and 2.84 Å and 176° (C12-H12 · · · F15). The distance between the two Eu centers is from 10.34 to 14.83 Å which is considerably longer than the Eu-Eu single bond distance.

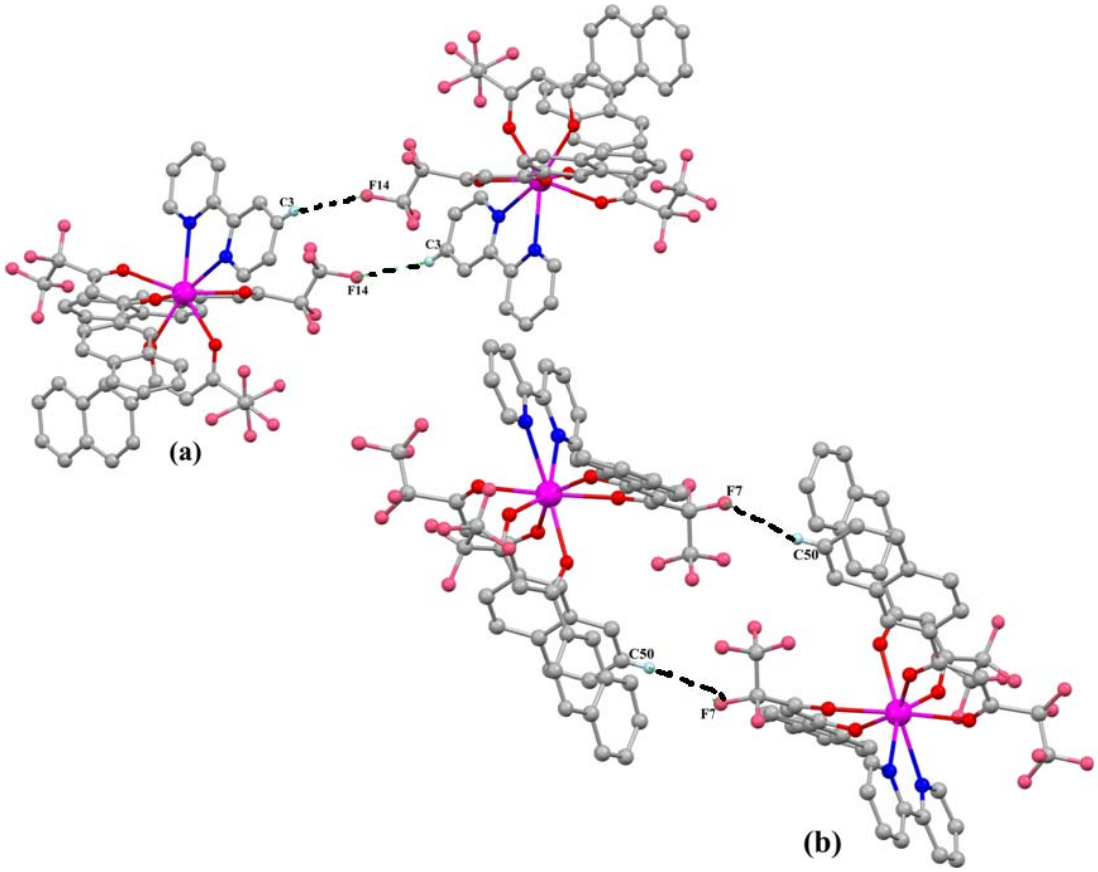

Figure 4.7. Self-assembled dimers a and b of **2**. In (a) and (b) except for the intermolecular H-bonding interactions, all the other H groups are omitted for clarity.

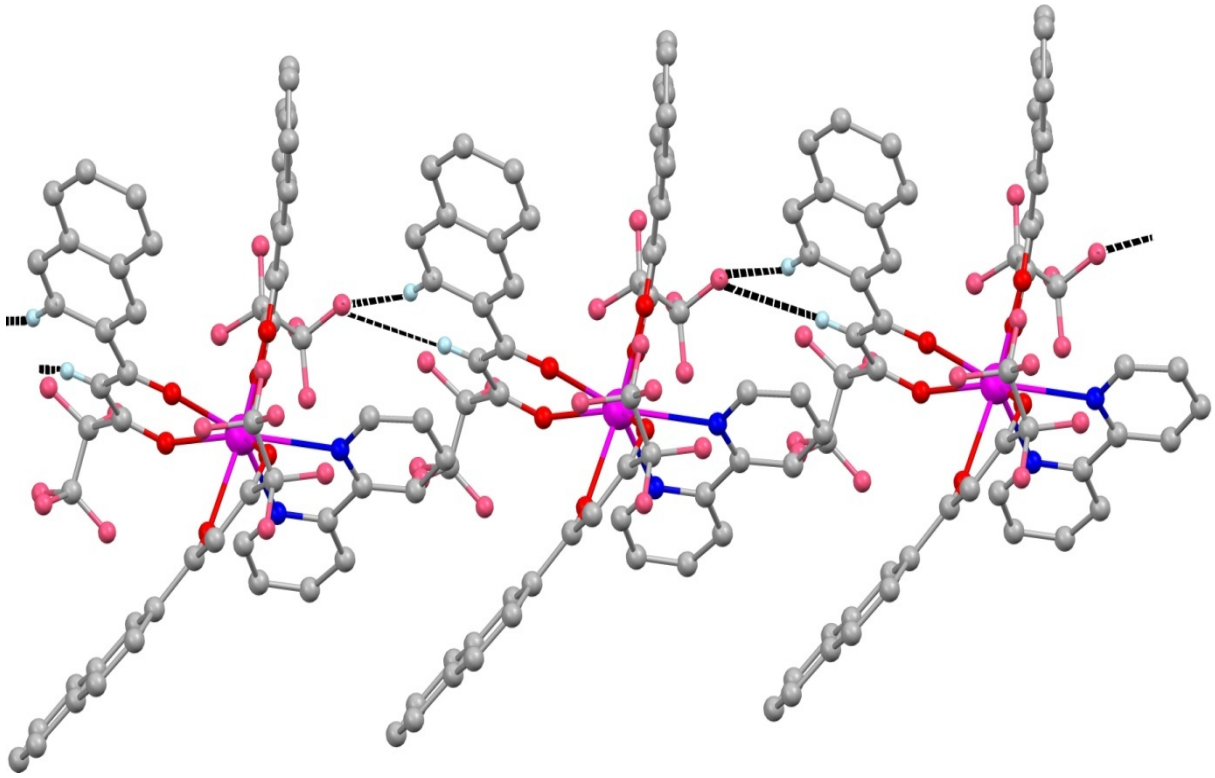

Figure 4.8. Self-assembled 1D network of **2**. All the other H groups, except those for the intermolecular H-bonding interactions, are omitted for clarity.

Apart from the self-assembled dimer and 1D network, a series of 2D networks are seen in **2**. Three different 2D networks are observed: (i) the two self-assembled dimers interact with each other to form the first one (Figure 4.9 a) Further, each of the self-assembled dimer interacts with 1D network to form the (Figure 4.9 b and Figure 4.9 c) 2D networks. Finally, all the dimers, 1D and 2D networks combine each other to form the hitherto unknown three-dimensional networks in the solid state. The observed supramolecular assembly is shown in Figure 4.10. To the best of our knowledge, this is the first example of Eu-β-diketonate complex which shows all the 1D, 2D, and 3D networks.

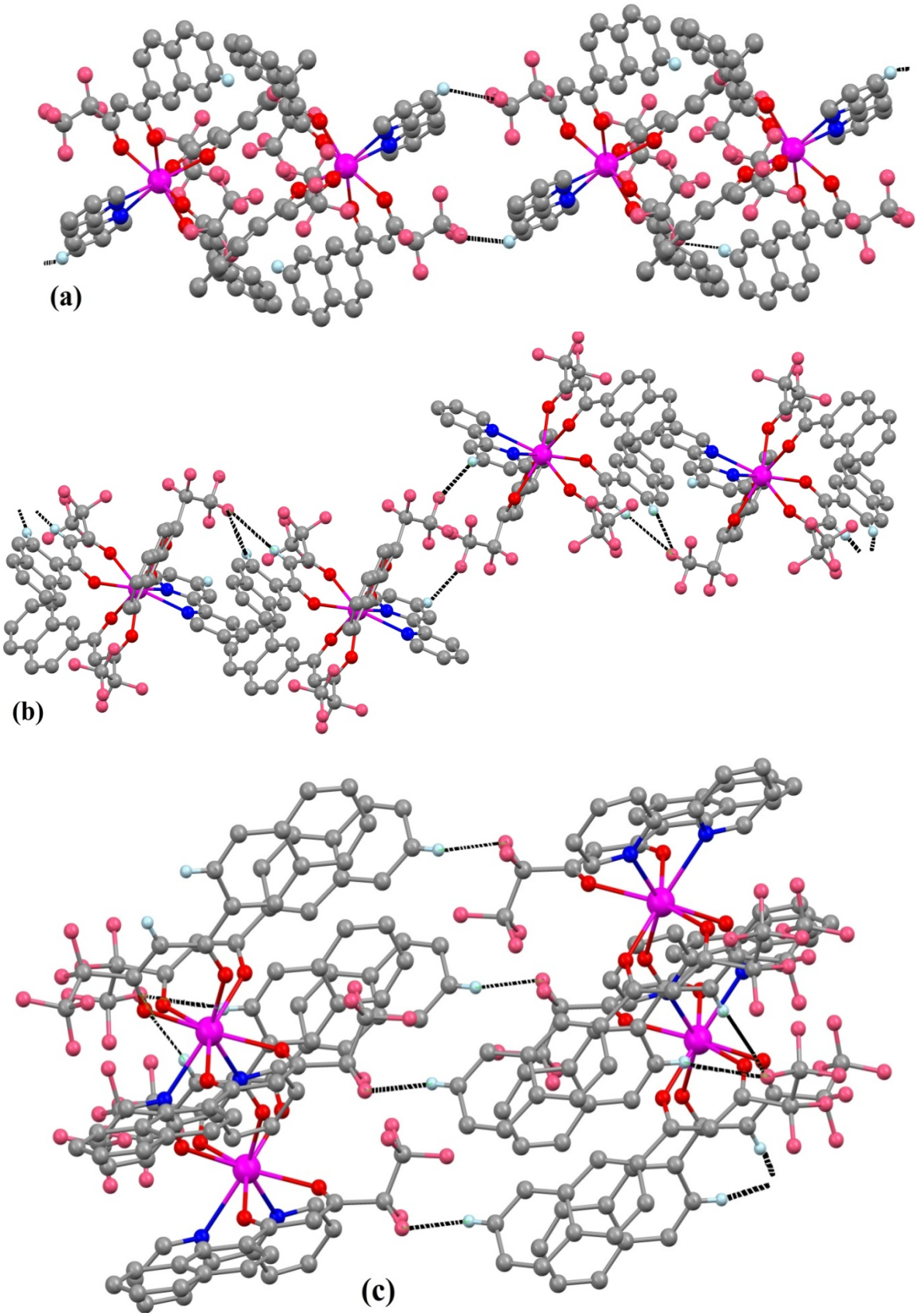

Figure 4.9. 2D network of **2.** All the other H groups, except those for the intermolecular H-bonding interactions, are omitted for clarity.

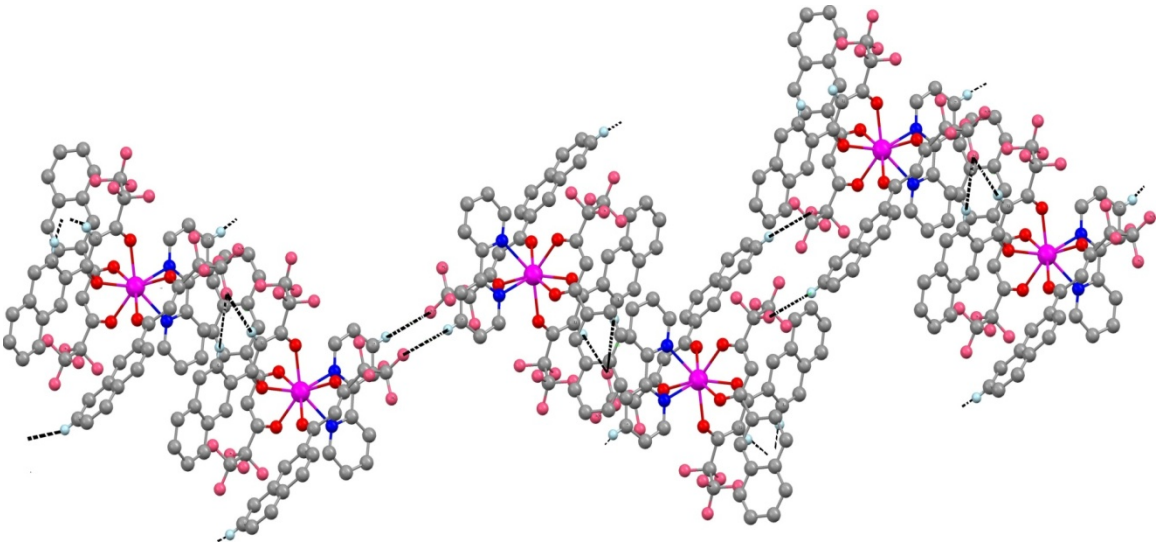

Figure 4.10. Supramolecular assembly of **2**.

UV-vis Spectra. The UV-vis absorption spectra of the free ligand HPFNP and the corresponding Eu^{3+} complexes were measured in CH_3CN solution (c = 1 × 10^{-5} M), and are displayed in Figure 4.11. UV-vis absorption spectra of the neutral donors (bpy, phen, bath) are shown in Figure 4.12. The maximum absorption bands at 345 nm and 333 nm noted for HPFNP and in complexes **1-4,** respectively, are attributed to singlet-singlet π-π* enol absorption of β-diketonate ligand [Remya *et al*. 2008; Shi *et al*. 2005]. Compared with the ligand HPFNP (λ_{max} = 345 nm), the absorption maxima are blue-shifted to 333 nm in all the complexes. The absorption maxima at 290, 289, and 287 nm in complexes **2**-**4**, respectively, are the result of the $^1\pi$-π* absorption of the aromatic rings of bidentate nitrogen donors. These values also shows a blue shift of 7, 4, and 13 nm, respectively, in complexes than in free nitrogen donors (297, 293, and 300 nm). The spectral shapes of the complexes in CH_3CN are similar to that of the free ligands, suggesting that the coordination of Eu^{3+} ion does not have a significant influence on the $^1\pi$-π* state energy. However, a small blue shift observed in the absorption maximum of all the complexes is caused by the perturbation induced by the metal coordination. The determined molar absorption coefficient values of the complexes **1**-**4** at 333 nm, 5.67 × 10^4, 5.7 × 10^4, 5.2 × 10^4, and 5.3 × 10^4 L mol^{-1} cm^{-1}, respectively, are about three times higher than that of the

HPFNP (1.8 × 10^4 at 345 nm), indicating the presence of three β-diketonate ligands in the corresponding complexes. Further the higher molar absorption coefficient of HPFNP reveals that the β-diketonate ligand has a strong ability of absorbing light.

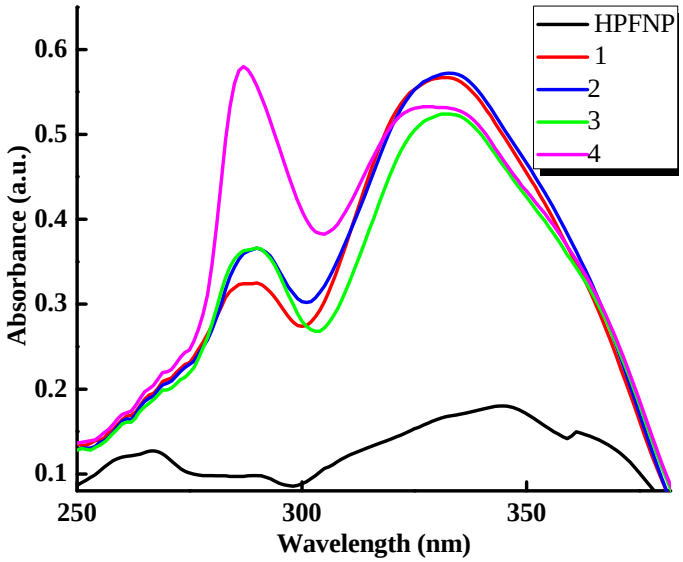

Figure 4.11. UV-visible absorption spectra of HPFNP and complexes **1-4** in acetonitrile (c = 1 × 10^{-5} M).

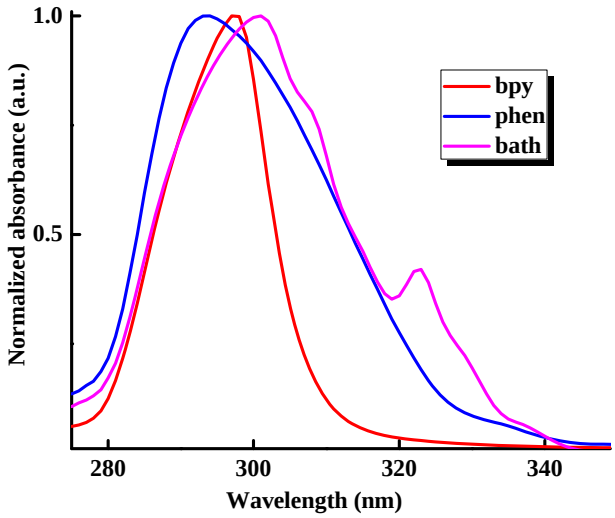

Figure 4.12. UV-visible absorption spectra of the neutral ligands in acetonitrile (c = 2×10^{-5}M).

PL Properties of Complexes 1-4. The excitation spectra of the Eu^{3+} complexes **1-4** recorded at 303 K and monitored around the intense $^5D_0 \rightarrow {}^7F_2$ transition of the Eu^{3+} ion, are shown in Figure 4.13. The excitation spectra of all the complexes exhibit a broad band between 250 and 450 nm and it is completely overlapped by the absorption spectra of the ligands employed in the

corresponding complexes. Thus it is clear that, the central europium(III) is effectively sensitized by the coordinated ligands. A series of sharp lines assigned to transitions between the $^7F_{0,1}$ and the $^5L_6$, $^5D_{3,2,1}$ levels are also observed in the excitation spectra of all these complexes. These transitions are weaker than the absorption of the organic ligands and are overlapped by broad excitation band, which proves that luminescence sensitization *via* excitation of the ligand is much more efficient than the direct excitation of the europium(III) ion absorption level.

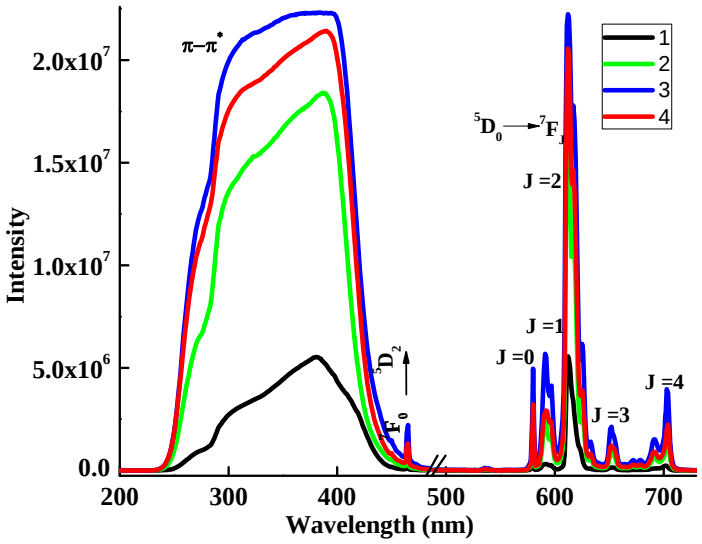

Figure 4.13. Solid state excitation and emission for complexes 1-4 at 298 K, emission monitored at around 613 nm.

Upon excitation under the wavelengths that maximizes the europium(III) emission intensity, complexes **1-4** showed characteristic narrow band emissions of Eu^{3+} corresponding to the $^5D_0 \rightarrow {}^7F_J$ (J = 0-4) transitions (Figure 4.13). The five expected peaks for the $^5D_0 \rightarrow {}^7F_{0\text{-}4}$ transitions are well resolved, and the emission bands at 580 and 650 nm are very weak since their corresponding transitions $^5D_0 \rightarrow {}^7F_{0,3}$ are forbidden both in magnetic and electric dipole schemes [Werts *et al*. 2002]. The intensity of the emission band at 593 nm is relatively strong and independent of the coordination environment because the corresponding transition $^5D_0 \rightarrow {}^7F_1$ is a magnetic transition; on the contrary, the $^5D_0 \rightarrow {}^7F_2$ transition is an induced electric dipole transition and its corresponding intense emission at λ = 613 nm is very sensitive to the

coordination environment [Werts *et al*. 2002]. This very intense $^5D_0 \rightarrow {}^7F_2$ peak, pointing to a highly polarizable chemical environment around the Eu^{3+} ion and is responsible for the brilliant red emission of these complexes. A relevant feature may be noted for the complexes **1-4** is the very high intensity of $^5D_0 \rightarrow {}^7F_2$ transition, relative to the $^5D_0 \rightarrow {}^7F_1$ lines, indicating that the Eu^{3+} ion coordinated in a local site without an inversion center. Further, the emission spectra of the complexes show only one peak for $^5D_0 \rightarrow {}^7F_0$ transition and three stark components for $^5D_0 \rightarrow {}^7F_1$ transition indicating the presence of a single chemical environment around the Eu^{3+} ion.

The $^5D_0$ lifetime values (τ_{obs}) were determined from the luminescent decay profiles for the complexes **1-4** at room temperature by fitting with a monoexponential curve, indicating the presence of single chemical environment around the emitting Eu^{3+} ion and the values are depicted in Table 4.3. Typical decay profiles of complexes **1-4** are shown in Figure 4.14.

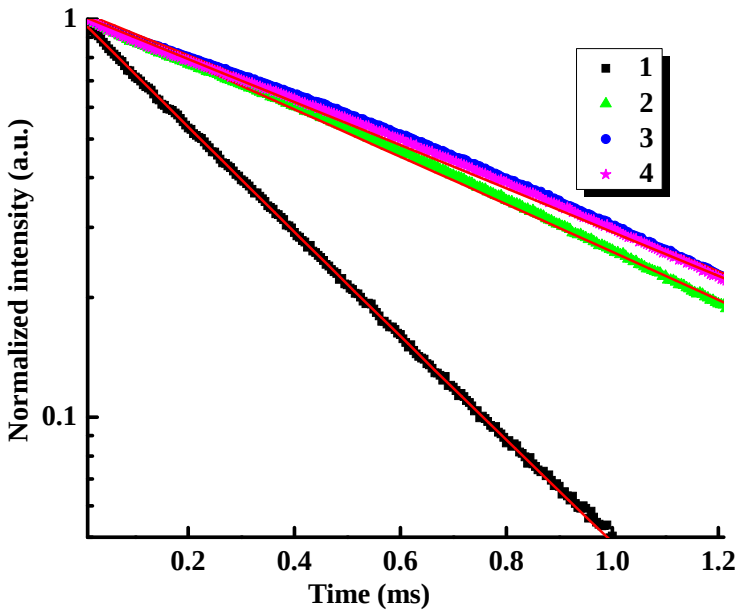

Figure 4.14. Experimental luminescence decay profiles of complexes **1** and **4** monitored around 612 nm and excited at their maximum emission wave lengths.

The relatively shorter lifetime observed for complex **1** may be caused by dominant nonradiative decay channels associated with vibronic coupling because of the presence of solvent molecules, as well documented in many of the hydrated europium β-diketonate

complexes [Yu *et al*. 2005; Fratini *et al*. 2008; Hasegawa *et al*. 2003; Binnemans. 2005]. On the other hand, longer lifetime values have been observed for complexes **2-4** because of the absence of nonradiative decay pathways.

Table 4.3 gives the radiative (A_{RAD}) and nonradiative (A_{NR}) decay rates, $^5D_0$ lifetime (τ_{obs}), intrinsic quantum yield (Φ_{Ln}), energy transfer efficiency (Φ_{sens}), and overall quantum yield ($\Phi_{overall}$) for complexes **1**-**4** at 303 K. According to energy gap theory, radiation less transitions is prompted by ligands and solvents with high frequency vibrational modes. Creation of Eu^{3+} complexes with higher quantum yields is directly linked to suppression of radiation less transitions caused by vibrational excitations in surrounding media [Wada *et al.* 2000; Fu *et al*. 2005; Peng *et al*. 2005]. It is clear from the Table 4.3 that complex **1,** having solvent molecules in the coordination sphere exhibits lower overall quantum yield and lifetime values. This is caused by the presence of O-H oscillators in this system, which effectively quenches the luminescence of the Eu^{3+} ion. On the other hand, complexes **2-4** exhibit high overall quantum yield and lifetime values because of the displacement of solvent molecules from the coordination sphere by the bidentate nitrogen donors. Among complexes **2-4**, **3** and **4** exhibits better quantum yields than **2** because of the presence of additional aromatic chromophore moieties in the bidentate nitrogen donors. Considerable enhancement in the luminescent intensity noticed, especially in complex **4** can be explained on the basis of extended conjugation induced by the introduction of two phenyl groups in the 4,7-positions of the phenanthroline ligand. It is notable from the present investigations that the intrinsic quantum yield and $^5D_0$ lifetime values obtained for Eu^{3+} complexes **2-4** are significantly higher than that of Eu^{3+}-naphthoyltrifluoroacetone-phenanthroline (Φ_{Ln} = 40%; τ_{obs} = 662 μs) [Fernandes *et al.* 2005] or Eu^{3+}-naphthoyltrifluoroacetone-bipyridyl complexes (Φ_{Ln} = 51%; τ_{obs} = 620 μs) [Fu *et al*. 2005].

Table 4.3. Radiative (A_{RAD}) and nonradiative (A_{NR}) decay rates, $^5D_0$ lifetime (τ_{obs}), intrinsic quantum yield (Φ_{Ln},%), energy transfer efficiency ($\Phi_{sens,}$%), and overall quantum yield ($\Phi_{overall}$,%) for Complexes **1-4** at 303 K.

Complex	A_{RAD} (s^{-1})	A_{NR} (s^{-1})	τ_{obs} (μs)	Φ_{Ln} (%)	Φ_{sens} (%)	$\Phi_{overall}$ (%)
1	899	557	687 ± 4	62	10	6
2	560	248	1238 ± 8	69	23	16
3	591	255	1183 ± 8	70	53	37
4	661	160	1218 ± 8	81	59	48

Energy Transfer Processes between Ligands and Eu^{3+}. In general, the sensitization pathway in luminescent Eu^{3+} complexes consists of excitation of the ligands into their excited singlet states, subsequent intersystem crossing of the ligands to their triplet states, and the energy transfer from the triplet state to the ^5D_J manifold of the Eu^{3+} ions, followed by internal conversion to the emitting $^5D_0$ state. Finally, the Eu^{3+} ion emits when transition to the ground-state occurs [Bünzli 1989; Huang 1997]. Moreover, the electron transition from the higher excited states, such as $^5D_3$ (24,800 cm^{-1}), $^5D_2$ (21,200 cm^{-1}), and $^5D_1$ (19,000 cm^{-1}) to $^5D_0$ (17, 500 cm^{-1}) becomes feasible by internal conversion, and most of the photophysical processes take place in this orbital. Consequently, most Eu^{3+} complexes give rise to typical emission bands at ~581, 593, 614, 654, and 702 nm corresponding to the deactivation of the excited state $^5D_0$ to the ground states ^7F_J (J = 0-4). Thus, matching the energy levels of the triplet state of the ligands to $^5D_0$ of Eu^{3+} is one of the key factors that affect the luminescent properties of the europium complexes.

It is well-known that in organolanthanide complexes neutral ligands often play a role in absorbing and transporting energy to other ligands or to the central metal ion [[b]Biju *et al*. 2009]. For energy transfer to occur efficiently, the overlap between the emission spectrum of the donor and the absorption spectrum of the acceptor is essential [Berlman 1973]. Considering complex **2** as a typical example, the possible energy transfer channels are explained from the absorption

and emission spectra of the ligands. According to absorption and photoluminescence spectra of HPFNP and bidentate nitrogen donors (Figure 4.15) it is clear that there is an overlap between the room-temperature emission spectrum of bidentate nitrogen donors and the absorption spectrum of the HPFNP (from 315-395 nm for bpy; 340-395 nm for phen; 350-395 nm for bath).

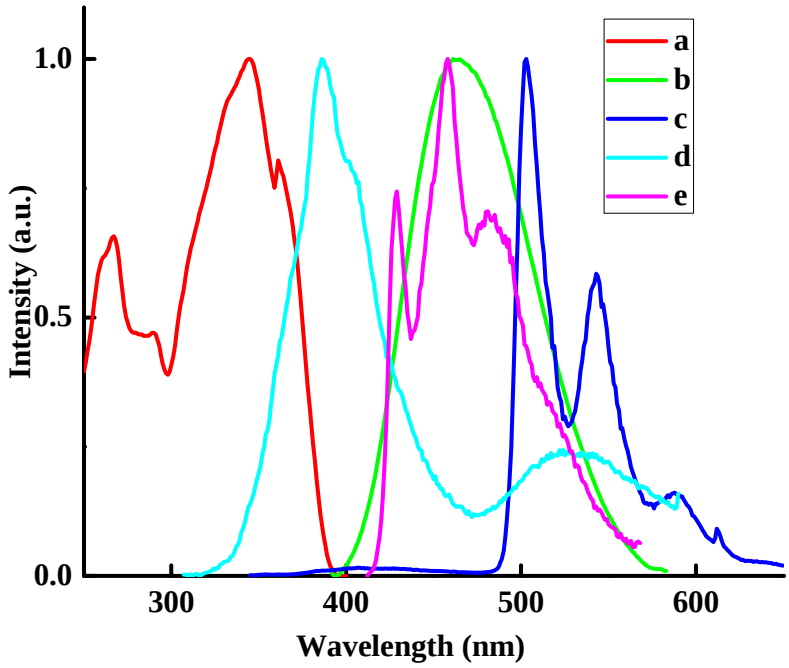

Figure 4.15. Absorption spectrum of HPFNP at 303K (a), emission spectra of HPFNP in CH_3CN solution [303 K (b); 77K (c)], and emission spectra of bpy [303K (solid state, d); 77K (CH_3CN solution, e)].

It means that the radiations from the singlet state of bidentate nitrogen donor can be absorbed by the β-diketonate ligand. The singlet state of nitrogen donor can also transfer energy to the triplet level of HPFNP or to its own triplet level (overlap between the room-temperature emission of bpy with the low-temperature emission spectra of HPFNP). The singlet level of HPFNP can transfer energy to the emitting level of metal ion through its own triplet energy level (overlap between the roomtemperature and low-temperature emission of HPFNP). The triplet level of neutral ligand, bpy can also transfer energy to the central Eu^{3+} ion directly or through the triplet state of HPFNP (low-temperature emission spectra of bpy and HPFNP are

overlapped). Thus the energy transfer process can be summarized in four steps. Absorbed energy is transferred from the singlet state of bpy to that of the singlet state of HPFNP, then from singlet excited-state to triplet state of the HPFNP or from singlet excited-state of HPFNP to the triplet state of bpy. The triplet state of bpy can transfer energy to the emitting level of Eu^{3+} ion directly or through the triplet level of HPFNP. Finally, energy transfers from triplet excited-state of HPFNP to the emitting level of Eu^{3+}.

To elucidate the energy transfer process of the Eu^{3+} complexes, the energy levels of the relevant electronic states of the ligands have been determined. The singlet and triplet energy levels of HPFNP and bidentate nitrogen donors were estimated by referring to their wavelengths of UV-vis absorbance edges and the lower wavelength emission edges of the corresponding phosphorescence spectra. The triplet energy level of the ligand was not affected significantly by the Ln^{3+} ion, and the lowest-lying excited level ($^6P_{7/2} \rightarrow {}^8S_{7/2}$) of Gd^{3+} is located at 32,150 cm^{-1} [Dieke 1968]. On this basis, the phosphorescence spectra of $Gd(PFNP)_3(C_2H_5OH)(H_2O)$ (Figure 4.16) and $Gd(bath)_2(NO_3)_3$ (Figure 4.16) allow one to evaluate the triplet energy levels ($^3\pi\pi^*$) corresponding ligand anions for all the lanthanide chelates.

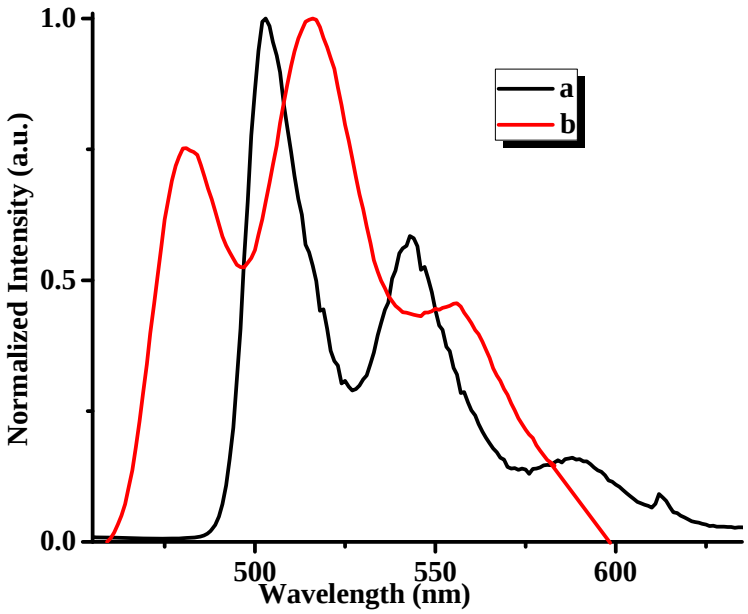

Figure 4.16. Phosphorescence spectra of $Gd(PFNP)_3(H_2O)(C_2H_5OH)$ (a) and $Gd(bath)_2\cdot(NO_3)_3$ (b) at 77K.

From the phosphorescence spectra, the triplet energy levels of $Gd(PFNP)_3(C_2H_5OH)(H_2O)$ and $Gd(bath)_2(NO_3)$, which correspond to their lower emission edge wavelengths, are 20,000 (500 nm) and 21,000 cm^{-1} (476 nm), respectively. The singlet energy levels ($^1\pi\pi^*$) of HPFNP and 4,7-diphenyl- 1,10-phenanthroline are estimated by referencing their higher absorption edges, which are 25,900 (386 nm) and 29,000 cm^{-1} (344 nm), respectively. The singlet and triplet energy levels of bpy (29,900 and 22,900 cm^{-1}) and phen (31,000 and 22,100 cm^{-1}) were taken from the literature [Yu and Su 2003]. According to Reinhoudt's empirical rule [Steemers *et al.* 1995], the intersystem crossing process becomes effective when $\Delta E(^1\pi\pi^* - {}^3\pi\pi^*)$ is at least 5000 cm^{-1} . The energy gap $\Delta E(^1\pi\pi^* - {}^3\pi\pi^*)$ for HPFNP, bpy, phen, bath are 5900, 7000, 8900, and 8000 cm^{-1}, respectively. Thus, the intersystem crossing is effective in all the ligands. According to the empirical rule proposed by Latva, for an optimal ligand-to-metal energy transfer process $2500 < \Delta E(^3\pi\pi^* - {}^5D0) > 3500$ cm^{-1} for Eu^{3+} [Latva *et al.* 1997]. It is also noted that the energy gaps, $\Delta E(^3\pi\pi^* - {}^5D_0)$ of the HPFNP, bpy, phen, and bath are 2500, 5400, 4600, and 3500 cm^{-1}, respectively. The triplet energy levels of HPFNP (20,000 cm^{-1}), bpy (22,900 cm^{-1}), phen (22,100 cm^{-1}), and bath (21,000 cm^{-1}) are higher than the $^5D_0$ level of Eu^{3+} (17,500 cm^{-1}), and also their energy gaps are too high to allow an effective back energy transfer. The schematic energy level diagrams for the complexes **1**-**4** are shown in Figure 4.17. Luminescence studies demonstrated that the 4,4,5,5,5-pentafluoro-1-(naphthalen-2-yl)pentane-1,3-dione ligand exhibits a good antennae effect with respect to the Eu^{3+} ion because of efficient intersystem crossing and ligand to- metal energy transfer. Moreover, the triplet state of the 4,4,5,5,5-pentafluoro-1-(naphthalen-2-yl)pentane-1,3-dione ligand is located at 20,000 cm^{-1}, which results in a sizable sensitization of the Eu^{3+}-centered luminescence.

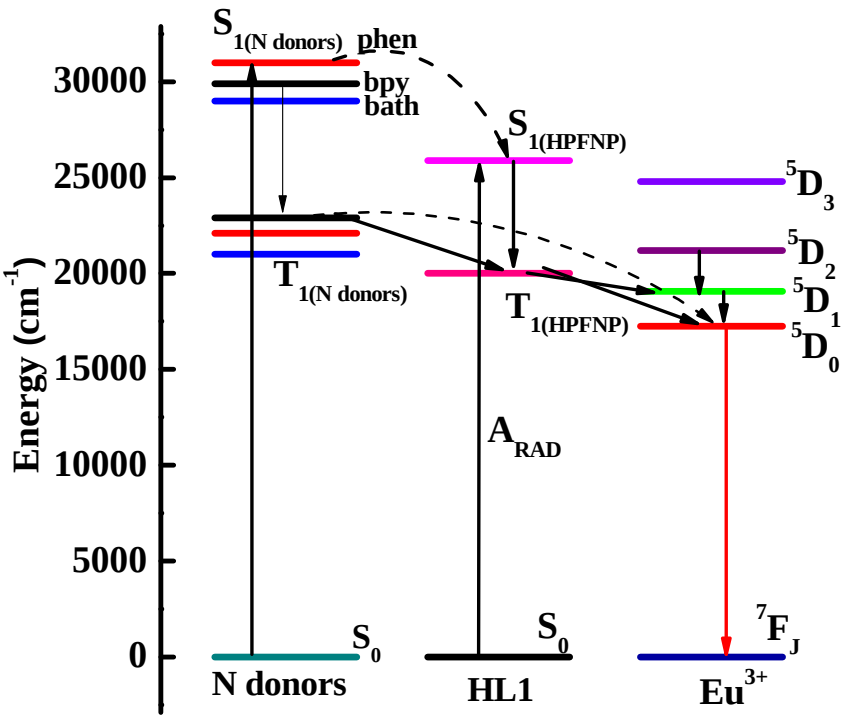

Figure 4.17. Schematic energy level diagrams and energy transfer processes for complex **1-4**. S_1 represents the first excited singlet state and T_1 represents the first excited triplet state.

4.6. Conclusions

Based on the novel *β*-diketone, HPFNP, four new Eu^{3+} complexes **1**−**4** have been synthesized, one of which has been structurally characterized by single crystal X-ray crystallography. The X-ray crystal structure of $Eu(PFNP)_3(bpy)$ reveals a distorted square antiprismatic around the Eu^{3+} atom. Further, analysis of the X-ray crystal data reveals interesting one-, two-, and three-dimensional arrays of Eu^{3+}-4,4,5,5,5-pentafluoro-1-(naphthalen-2-yl)pentane-1,3-dione-2,2′-bipyridine complex through intra- and intermolecular hydrogen bonds. The luminescent studies demonstrate that the displacement of solvent molecules by bidentate nitrogen donors in $Eu(PFNP)_3(C_2H_5OH)(H_2O)$ greatly enhances the metal-centered luminescence quantum yields and lifetime values. The introduction of polyfluorinated alkyl group, as well as long conjugated naphthyl group in *β*-diketonate ligand, significantly improves the intrinsic luminescent quantum yields of Eu^{3+} ion in complexes **1**−**4** (62−81%) as compared to existing Eu^{3+}-naphthoyltrifluoroacetone-nitrogen donor complexes (40−50%). Thus the present results clearly

highlights that Eu^{3+}-4,4,5,5,5-pentafluoro-1-(naphthalen-2-yl)pentane-1,3-dione complexes involving bidentate nitrogen donors may find potential applications as light conversion molecular devices in many photonic applications.

Chapter 5

Highly luminescent europium(III) complexes containing organosilyl 4,4,5,5,5-pentafluoro-1-(naphthalen-2-yl)pentane-1,3-dionate ligands grafted on silica nanoparticles

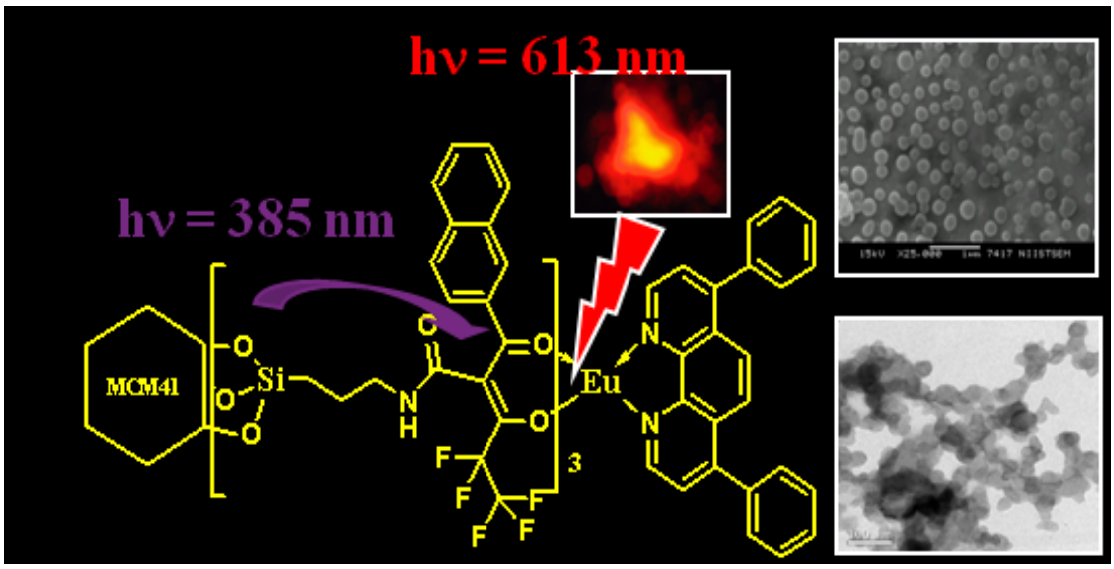

5.1. Summary. A novel organic–inorganic mesoporous luminescent hybrid material was designed by linking a ternary Eu^{3+} complex to the functionalized hexagonal mesoporous MCM-41 with the modified *β*-diketone, 4,4,5,5,5-pentafluoro-1-(naphthalen-2-yl)pentane-1,3-dione (HPFNP), which contains a polyfluorinated alkyl group as well as the long conjugated naphthyl group. *β*-Diketone grafted to the coupling agent 3-(triethoxysilyl)propylisocyanate was used as the precursor for the preparation of mesoporous materials. MCM-41, consisting of ternary complex, $Eu(PFNP\text{-}Si)_3(bath)$ covalently bonded to the silica-based network, which was designated as $Eu(PFNP\text{-}Si)_3(bath)$/MCM-41, was obtained by interacting europium nitrate, SiPFNP-Na and 4,7-diphenyl-1,10-phenanthroline (bath) into the mesoporous material *via* a ligand-exchange reaction. The synthesized luminescent hybrid material was fully characterized by various spectroscopic techniques, and its photophysical properties were investigated. $Eu(PFNP\text{-}Si)_3(bath)$/MCM-41 exhibits an efficient intramolecular energy transfer process from the silylated *β*-diketone to the central Eu^{3+}, namely, the "antenna effect", which favoured highly luminescent behaviour in the modified hexagonal mesoporus silica.

D.B. Ambili Raj *et al., J. Mater. Chem.*, **2009**, *19*, 7976-7983.

5.2. Introduction

Recently, lanthanide-containing inorganic–organic hybrid materials has attracted considerable attention due to their unique photophysical properties [Carlos *et al.* 2009; Bünzli and Piguet 2005; de Bettencourt-Dias 2007] and specific functions make them useful in a wide range of photonic applications that includes tunable lasers [Taniguchi *et al.* 1995], amplifiers for optical communications [Kuriki *et al.* 2002; Polman and van Veggel 2004] and components of emitting materials in multilayer organic light-emitting diodes [Kido and Okamoto 2002; Capecchi *et al.* 2000]. It is well documented that organolanthanide complexes, especially with ligands *β*-diketones [de Sá *et al.* 2000], aromatic carboxylic acids [Shiny *et al.* 2007, Shiny *et al.* 2008] and heterocyclic ligands [Watson *et al.* 1972; Bellusci *et al.* 2005; Chen *et al.* 2007] have characteristic luminescence properties and give sharp, intense emission lines upon ultraviolet light irradiation, because of the effective intramolecular energy transfer from the coordinated ligands to the central Ln^{3+} ions (the "antenna effect") [Lehn 1990; Bekiari and Lianos. 1998; Chen *et al.* 2007]. However, the poor stabilities and low mechanical strength of the lanthanide complexes always hinders their use in practical applications such as tunable solid-state lasers or phosphor devices. In order to overcome these shortcomings, many research efforts are focused on preparing lanthanide organic–inorganic hybrids through functionalization of the exterior and/or interior surfaces, prompting the utilization of mesoporous materials such as MCM-41 [Bruno *et al.* 2008; Xu *et al.* 2002; Yan and Zhou 2008] and SBA-15 [Li *et al.* 2008; Corriu *et al.* 2004]. Conventional methods of doping lanthanide complexes into silica matrices seem unable to solve the problem of the quenching effect of luminescent centers because only weak interactions such as hydrogen bonding, van der Waals forces, or weak static effects [Koslova *et al.* 1993; Tanner *et al.* 2000] exist between organic and inorganic moieties. Furthermore, inhomogeneous dispersion of two phases and leaching of the photoactive molecules frequently occur in such designed hybrid materials for which the concentration of complexes is also greatly reduced. Due to the above reasons, another novel approach concerning the complexation

of lanthanide ions using antenna chromophore ligands that are covalently bonded to the inorganic networks has emerged.

Several reports are available on the covalent grafting of lanthanide *β*-diketone chelates to silica hosts [Xu *et al.* 2002; Binnemans *et al.* 2004; Tan *et al.* 2004; Gago *et al.* 2005; DeOliveira *et al.* 2007; Bruno *et al.* 2008; Cousinié *et al* 2008; Li *et al.* 2008; Liu and Yan 2008; Qiao and Yan 2008; Yan and Wang 2008; Yan and Lu 2008; Yan and Zhou 2008; Carlos *et al.* 2009; Qiao and Yan 2009]. However, in most cases the co-ligands 1,10-phenanthroline [Binnemans *et al.*2004; Liu and Yan 2008] or 2,2′-bipyridyl [Cousinié *et al* 2008] bridged covalently bonded hybrids and the *β*-diketones simply behave as second ligand to the Ln^{3+} ion. On the other hand, recently a few investigations have described the modification of *β*-diketones and lanthanide chelates directly covalently bonded to the silica host, in which bidentate nitrogen donors bind to the central Ln^{3+} ions to saturate the coordination sphere [Li *et al.* 2008; Qiao and Yan 2008; Qiao and Yan 2009]. Novel organic–inorganic mesoporous luminescent hybrid materials were designed by linking the ternary Eu^{3+} complexes to the functionalized ordered mesoporous SBA-15 with the modified 1-(2-naphthoyl)-3,3,3-trifluoroacetonate (NTA) [Li *et al.* 2008]. Further investigations on the luminescence properties of Eu-(NTA-SBA-15)$_3$bpy mesoporous materials show that they exhibit characteristic luminescence of the corresponding Eu^{3+}, through intramolecular energy transfer from the modified ligand (NTA-Si) to the central Eu^{3+} ion, and higher $^5D_0$ luminescence quantum efficiencies and longer lifetime than the pure Eu(NTA)$_3$bpy complex. However, the synthesis and luminescence properties of MCM-41 mesoporous materials covalently bonded with lanthanide complexes by the modified highly fluorinated *β*-diketonates have not been explored to date.

Here, we report on the synthesis and characterization of 4,4,5,5,5-pentafluoro-1-(naphthalen-2-yl)pentane-1,3-dionate (HPFNP) functionalized MCM-41 mesoporous hybrid material (PFNP-MCM41) in which HPFNP was covalently bonded to the framework of MCM-41. The highly luminescent ternary complex Eu(PFNP)$_3$(bath)-functionalized MCM-41, denoted as

Eu(PFNP-Si)$_3$(bath)/MCM-41, was obtained by introducing Eu(NO$_3$)$_3$6H$_2$O, SiPFNP-Na and bathophenanthroline (bath) into the mesoporous material *via* a ligand-exchange reaction. The synthesized mesoporous materials were characterized by powder X-ray diffraction, N_2 adsorption–desorption, thermogravimetric analysis, FT-IR, Raman spectroscopy and photoluminescence spectroscopy.

5.3. Experimental Section

Materials. Commercially available chemicals: europium(III) nitrate hexahydrate, 99.9% (Arcos Organics); gadolinium(III) nitrate hexahydrate, 99.9% (Aldrich), 2-acetonaphthone 98% (Aldrich), methyl pentafluoropropionate 99% (Aldrich), sodium hydride 60% dispersion in mineral oil, (Aldrich), 4,7-diphenyl-1,10-phenanthroline, 97%, (Aldrich), mesostructured hexagonal silica, MCM-41 (Aldrich) were used without further purification. 3-(Triethoxysilyl)-propylisocyanate (TESPIC) was provided by Lancaster Synthesis Ltd. The ligand 4,4,5,5,5-pentafluoro-1-(naphthalen-2-yl)pentane-1,3-dione (HPFNP) was synthesized according to the method described in chapter 4. All the other chemicals used were of analytical reagent grade.

Preparation of sodium 4,4,5,5,5-pentafluoro-1-(naphthalen-2-yl)-1-oxo-2-((3-(triethoxysilyl)propyl)carbamoyl)pent-2-en-3-olate (SiPFNP-Na). 1 mmol of HPFNP was first dissolved in anhydrous tetrahydrofuran (THF), and 2.5 mmol of NaH (60%) was added to the solution with stirring. Two hours later, 1 mmol of TESPIC was added dropwise into the refluxing solution. The whole mixture was heated to 65 °C under an argon atmosphere for 8 h. After isolation and purification, the sodium salt of SiPFNP was obtained as a yellow solid, which was used without further purification. ^{1}H NMR: (CDC1$_3$, 300 MHz): δ (ppm) 0.56–0.86 (t, 2H), 1.20–1.24 (t, 9H), 1.54–1.59 (m, 2H), 3.05–3.12 (2H, m), 3.72–3.82 (q, 6H), 6.22 (broad, 1H), 7.27–7.41 (m, 2H), 7.61–7.73 (m, 4H), 8.13 (s, 1H). FT-IR (KBr) ν_{max}: 3400, 2925, 2857, 1692, 1628, 1516, 1323, 1281, 1188, 1133, 1064, 878, 789, 682 cm^{-1}. FT-Raman ν_{max}: 1285, 1385, 1460, 1523, 1626 cm^{-1}.

Synthesis of luminescent hexagonal mesoporous silica, Eu(PFNP-Si)$_3$(bath)/MCM-41 (1). 3.5 mmol of SiPFNP-Na was dissolved in 20 mL ethanol with stirring. Then an appropriate amount of MCM-41 (molar ratio of MCM-41: PFNP-Si = 1 : 3) was added to the solution. Six hours later, the corresponding amount of Eu$(NO_3)_3(6H_2O)$ (1.17 mmol) and bathophenanthroline (bath: 1.17 mmol) was added and stirred vigorously in air atmosphere at room temperature for 48 h (Scheme 5.1). Finally, the solid product was recovered by centrifugation, washed with ethanol, and dried at 80 °C. This covalently bonded hybrid material with mesoporous host containing Eu^{3+} ions was denoted as Eu(PFNP-Si)$_3$(bath)/MCM-41.

FT-IR (KBr) ν_{max}: 3430, 2918, 2851, 1692, 1608, 1521, 1468, 1384, 1194, 1127, 1079, 858, 788, 465 cm^{-1}. FT-Raman ν_{max}: 1283, 1385, 1463, 1510, 1633 cm^{-1}.

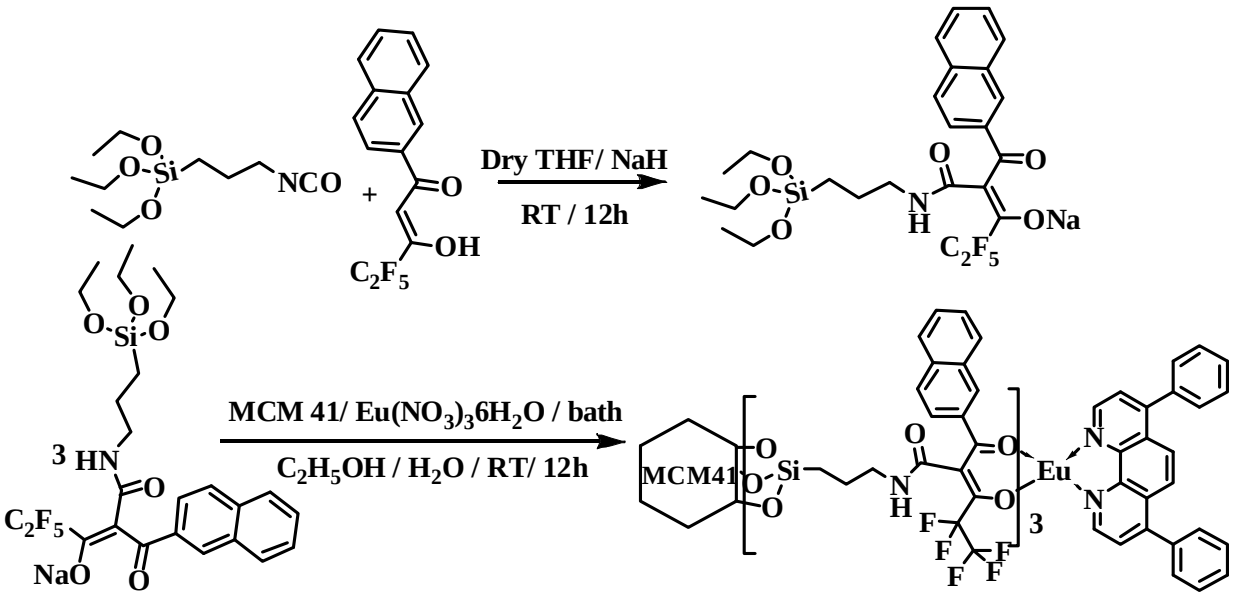

Scheme 5.1. Synthesis procedure for the SiPFNP-Na and Eu(PFNP-Si)$_3$.bath/MCM-41 complex.

Physical measurements. FT-Raman spectra of the solid samples were recorded on a Horiba JY Lab Raman HR800 Micro Raman Spectrometer (with excitation wavelength using an internal HeNe 20 mW 632 nm laser polarized 500 : 1 spectrograph, 800 mm focal length, hole size 400

μm, slit 100 μm, grating 1800, objectives 10× NA 0.25, 50× NA 0.7, 100× NA 0.9). ^{29}Si and ^{13}C NMR spectra of the solid samples were obtained on a Bruker DRX500 spectrometer (the measurements were obtained in natural abundance at frequencies of 75.47 and 59.61 MHz for carbon and silicon, respectively). BET surface area of the hybrid material was measured using a Micromeritics Gemini 2375 V5.01 surface area Analyzer. Pore size distribution was obtained by the Barrett–Joiner–Halenda method from the desorption curve of the isotherm. X-Ray powder diffraction was performed using Ni-filtered Cu Kα radiation with a Philips X'pert Pro diffractometer. Data were collected by step scanning from 2 to 20° 2θ. Dynamic Light Scattering experiments were conducted using a Malvern Instruments zetasizer nano Zis Model no: ZEN3600 to determine the particle size of the hybrid material. TEM and SEM were used to determine the morphology and particle size. TEM analyses were done on a JEOL 2010 (200 kV). A pinch of material was suspended in ethanol. Then, a carbon-coated grid was dipped in the solution and allowed to dry at room temperature. SEM analyses were done on a JEOL JSM-5600LV. Other instrumental techniques employed for the characterization of the ligands and complexes are the same as that described in the chapter 1.

5.4. Results and Discussion

Characterization of SiPFNP-Na and Eu(PFNP-Si)$_3$(bath)/MCM-41 (1). The synthesis procedure for the silylated polyfluorinated β-diketonate ligand (SiPFNP-Na) and the mesoporous hybrid material (Eu(PFNP-Si)$_3$(bath)/MCM-41) is shown in Scheme 5.1. The structure of the modified ligand, SiPFNP-Na has been confirmed by ^{1}H NMR spectroscopy ($CDCl_3$) (Figure 5.1) and solid-state ^{13}C NMR spectroscopy (Figure 5.2). A broad peak at δ = 6.22 ppm in the ^{1}H NMR and at δ = 168 ppm in the ^{13}C NMR spectra indicates the formation of amide –CO–NH– linkages in the SiPFNP-Na ligand. The propyl chain in the ligand gives peaks at 0.56–3.12 ppm in the ^{1}H NMR spectra and 10–44 ppm in the ^{13}C NMR spectra. The purity of

the product was confirmed by the absence of signal at δ = 6.68 ppm characteristic of the free H in between the two carbonyl groups in the ^{1}H NMR spectra.

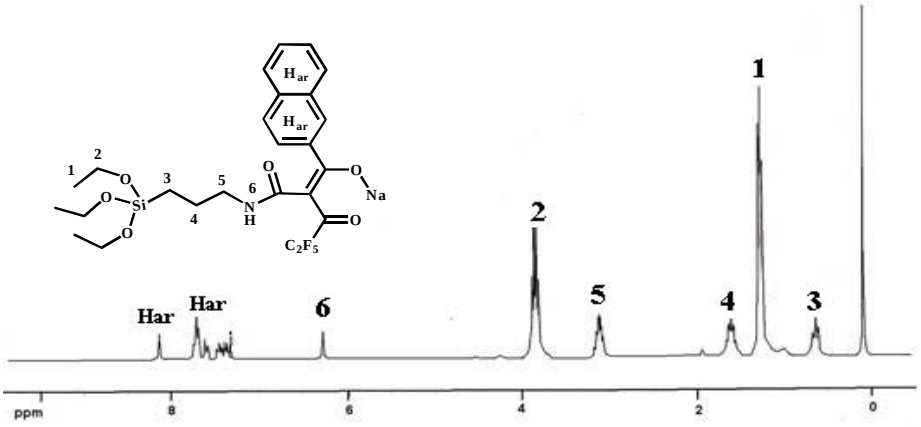

Figure 5.1. ^{1}H NMR spectra of SiPFNP-Na.

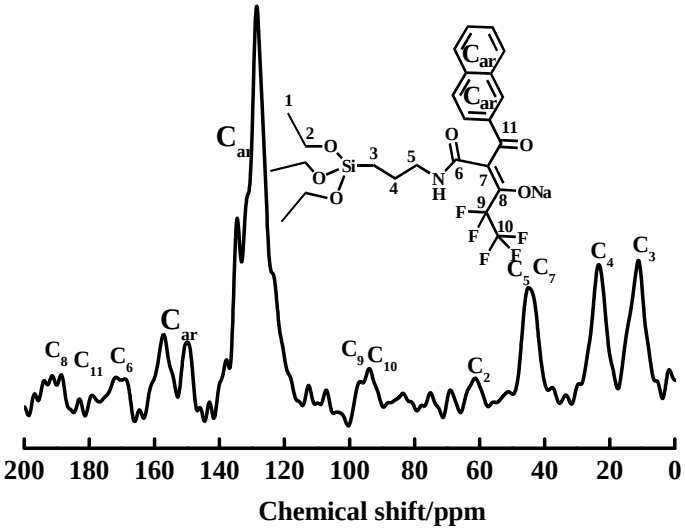

Figure 5.2. Solid-state ^{13}C NMR spectra of SiPFNP-Na.

The ^{29}Si CPMAS NMR spectrum of Eu(PFNP-Si)$_3$(bath)/MCM-41 is shown in Figure 5.3. The ^{29}Si CPMAS NMR spectrum of unmodified MCM-41 displays two broad overlapping resonances at δ = −101.4 and −110.6 ppm, which correspond to Q_3 and Q_4 species of the silica framework [Q*n* = *Si*(OSi)*n*(OH)4–*n*] (Figure 5.4). A weak shoulder is also observed at δ = −91.9 ppm for the Q_2 species. The Q_3 sites are associated with single Si–OH groups that include both free and hydrogen-bonded silanols, and the Q_2 sites correspond to geminal silane diols. For

the modified material Eu(PFNP-Si)$_3$(bath)/MCM-41, two additional signals appear at δ = −58.9 and −66.8 ppm, which can be assigned to T_2 and T_3 organosilica species [T*m* = R*Si*(OSi)*m*(OEt)$_{3-m}$], respectively. In parallel, the relative intensities of the Q_2 and Q_3 resonances decrease with an increase in the intensity of Q_4 at −111.8 ppm. The presence of T_2 and T_3 signals indicates that the organic groups are covalently bonded to the silica matrix.

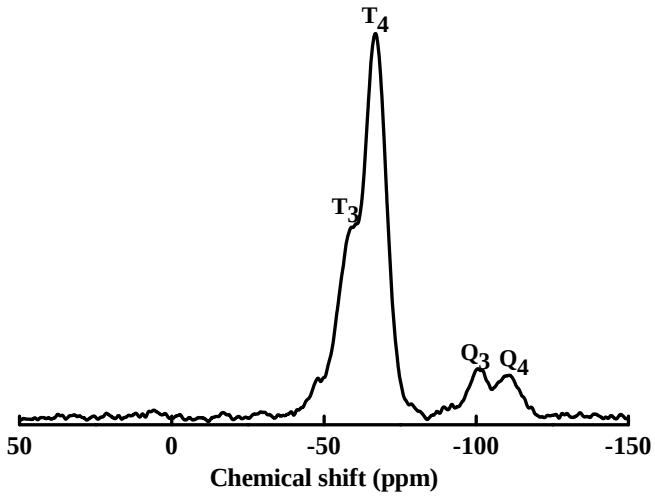

Figure 5.3. Solid-state ^{29}Si CPMAS NMR spectra of Eu(SiPFNP)$_3$(bath)/MCM-41.

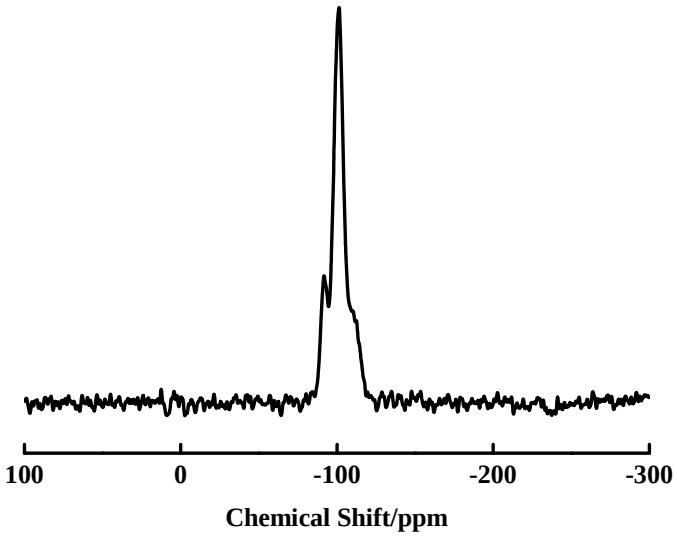

Figure 5.4. Solid-state ^{29}Si CPMAS NMR spectra of MCM-41.

The FT-IR spectra of the grafted ligand SiPFNP-Na and of Eu(PFNP-Si)$_3$(bath)/MCM-41 are shown in Figure 5.5. The presence of the amide group in SiPFNP-Na was confirmed by the appearance of new bands at 3400 (ν NH), 1692 cm^{-1} (ν NHCO) and 1410 cm^{-1} (δ NH). The

strong broad bands located at around 2963, 2925, 2857 cm^{-1} indicates the three methylene groups of 3-(triethoxysilyl)-propylisocyanate. Furthermore, the bands centered at 3386 cm^{-1} correspond to the stretching vibration of grafted NH groups. The spectrum of SiPFNP-Na shows the stretching vibration absorption bands at 1281 cm^{-1} (*ν* C–Si) and at 1064 cm^{-1} (*ν* Si–O), characteristic of the trialkoxylsilyl functional group, derived from the cross-linking reagent 3-(triethoxysilyl)-propylisocyanate (TESPIC) proving that it was successfully grafted onto the *β*-diketone ligand.

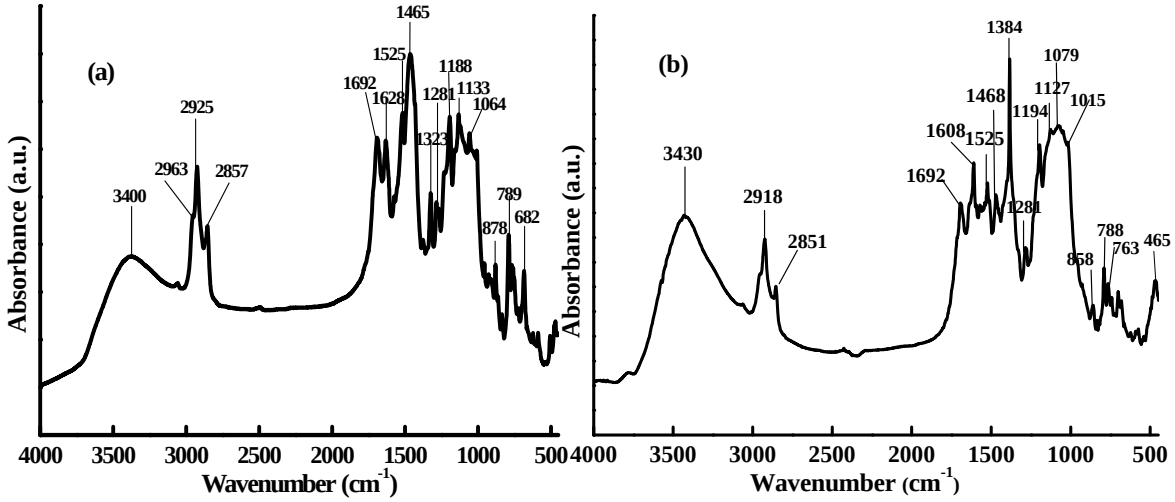

Figure 5.5. FT-IR spectra of SiPFNP-Na (a) and $Eu(SiPFNP)_3$(bath) MCM-41 (b).

The FT-IR spectrum of $Eu(PFNP\text{-}Si)_3$(bath)/MCM-41 consists of a broad band located at around 1015–1127 cm^{-1} (ν_{as}, Si–O), 858 cm^{-1} (ν_s, Si–O), and 465 cm^{-1} (δ, Si–O–Si), which demonstrates the success of the hydrolysis and copolycondensation reactions. (*ν* represents stretching, δ in plane bending, Φ ring deformation, s symmetric, and as asymmetric vibrations). Furthermore, the peak at 1692 originating from the –CONH– group of SiPFNP-Na, can also be observed in Figure 5.5b, which is consistent with the fact that the carbonyl groups of the precursor invariably remain after hydrolysis and condensation reactions, confirming that the two carbonyl groups of the *β*-diketones are coordinated to the Eu^{3+} ions, not the carbonyl groups of the TESPIC [Qiao and Yan 2009; Qiao and Yan 2008]. In addition to the above, a red-shift

noted in the C=N stretching frequency of bath (1615 to 1602 cm^{-1}) in Eu(PFNP-Si)$_3$(bath)/MCM-41 shows the involvement of nitrogen atoms in the complex formation with Eu^{3+} ion [Biju *et al.* 2006].

The FT-Raman spectra of the SiPFNP-Na ligand and that of Eu(PFNP-Si)$_3$(bath)/MCM-41 are shown in Figure 5.6. The peak at 1430 cm^{-1} in the ligand (Figure 5.6a) and that at 1463 cm^{-1} in Eu(PFNP-Si)$_3$(bath)/MCM-41 are due to the symmetric stretching vibrations of the C=O group (ν_s, C=O). The peaks at around 1384 cm^{-1} in both the ligand and in Eu(PFNP-Si)$_3$(bath)/MCM-41 are due to the in-plane bending of CH_2 group (δ, CH_2). The detailed vibrational spectral data are summarized in Table 5.1. In the vibrational spectra, bands arising from the nitrogen donor (bath) were not observed. This is not unexpected since in the spectra of Eu(PFNP-Si)$_3$(bath)/MCM-41 the bands from this ligand are considerably weaker than those from the Eu(PFNP-Si)$_3$ fragment [Bruno *et al.* 2008]. Additionally, the bands due to bath molecule appear in the region dominated by the C=O bands of HPFNP ligand.

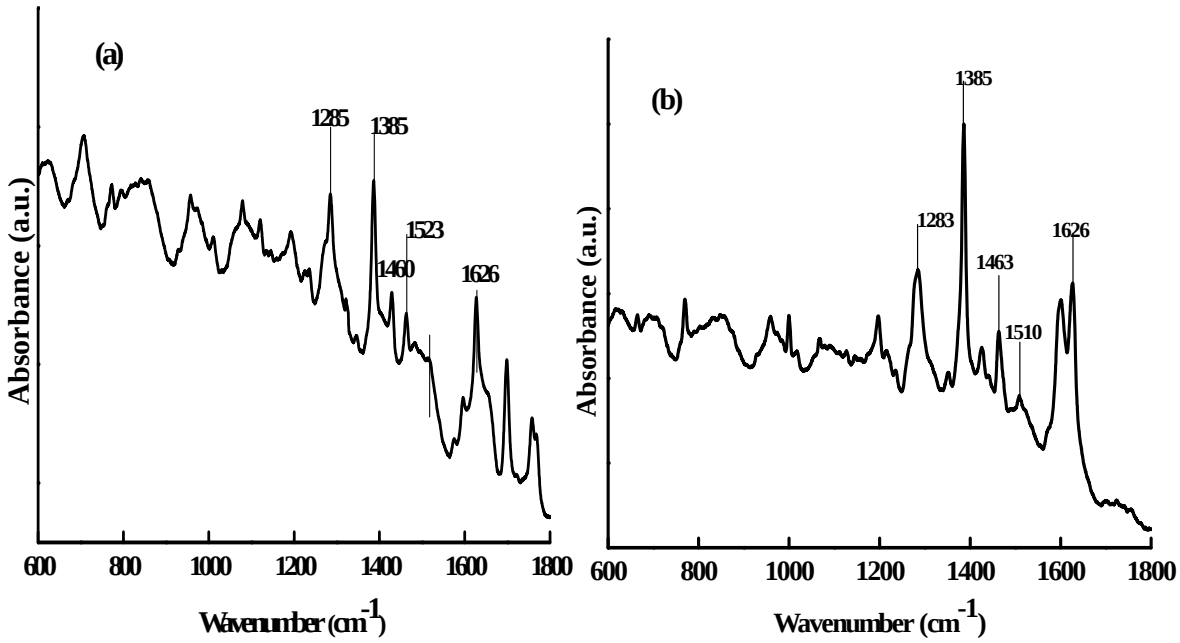

Figure 5.6. FT-Raman spectra of SiPFNP-Na (a) and Eu(SiPFNP)$_3$(bath)/MCM-41 (b).

Table 5.1. Wave numbers observed in FT-IR spectra and FT-Raman spectra of SiPFNP-Na and the Eu(PFNP-Si)$_3$(bath)/MCM-41 and the respective vibrational assignments**.**

PFNP-Si		Eu(PFNP-Si)$_3$(bath)/MCM-41		Description
IR (cm^{-1})	Raman (cm^{-1})	IR (cm^{-1})	Raman (cm^{-1})	
3400		3422		ν (N-H)
2927		2918		ν (C_{sp3}-H)
1692	1626	1692	1626	ν (C=O)
1516	1523	1524	1510	ν (C=C)
	1430		1463	ν_s (C=O)
1383	1385	1383	1385	δ (CH_2)
	1285		1283	$\Phi\,\nu$ (C-C)
1087		1077		ν (Si-O-Si)

Figure 5.7. Shows the powder XRD patterns of MCM-41 and the modified material Eu(PFNP-Si)$_3$(bath)/MCM-41. The XRD pattern for MCM-41 is characteristic of a well-ordered hexagonal mesoporous phase. The Bragg peaks indexed as (100), (110), (200) and (210) are also observed in Figure 5.7a which indicates the long-range hexagonal symmetry. On the other hand, in the grafted complex, a single diffraction peak was noted in the low 2θ region at 3.27, which is a characteristic peak of the formation of periodic hexagonal mesostructures [DeOliveira *et al.* 2007; Ogawa *et al*. 2001].

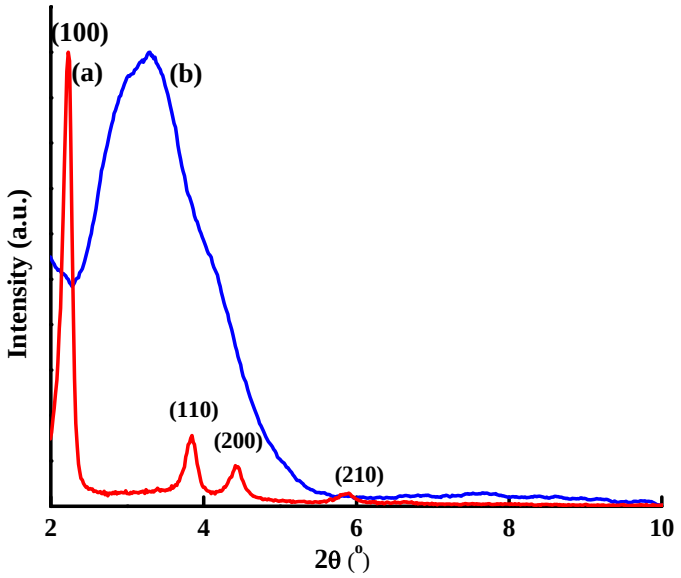

Figure 5.7. X-ray diffraction patterns of MCM-41 (a) and of the Eu(SiPFNP)$_3$(bath)/MCM-41 (b).

Furthermore, a loss of structural order could be observed in the XRD pattern and this can be attributed to the introduction of the bulky Eu(PFNP-Si)$_3$(bath) fragment inside the channels of the support which affects the X-ray scattering contrast between the silica framework and pore-filling material [Bruno *et al.* 2008; Gago *et al.* 2005].

Incorporation of Eu(PFNP-Si)$_3$ into MCM-41 resulted in the reduction of the surface area from 1000 m^2 g^{-1} for MCM-41 to 0.67 m^2 g^{-1} for Eu(PFNP-Si)$_3$(bath)/MCM-41, suggesting that microenvironment of MCM-41 has drastically changed due to the introduction of luminescent centers. Likewise, the pore volume for MCM-41 of 0.980 cm^3 g^{-1} decreased to 0.001 cm^3 g^{-1} for Eu (PFNP-Si)$_3$(bath)/MCM-41. This loss in surface area may be explained by the fact that N_2 molecules are repelled from the silica surface by the grafted organosilanes so no longer adsorb [Cousinié *et al.* 2007].

From the dynamic light scattering (DLS) measurements it is evident that the mesoporous hybrid material has an average particle size of 313 nm (Figure 5.8).

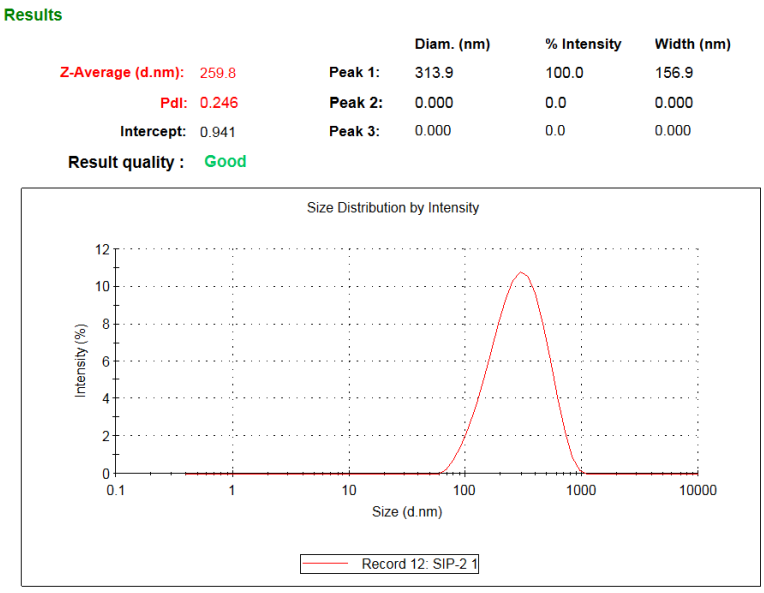

Figure 5.8. DLS particle size distribution curve for Eu(PFNP-Si)$_3$(bath)/MCM-41.

A scanning electron microscopy (SEM) micrograph of the mesoporous hybrid material is given in Figure 5.9. The SEM micrographs of the mesoporous hybrid material is typical for covalently bonded hybrids with a mesoporous host, and show the morphology of spherical

particles of diameter of around 300 nm. The silica host covalently bonded hybrid Eu^{3+} complex seems to be highly homogeneous. The absence of any distinct grain distribution between the emissive Eu^{3+} moiety and the host material MCM-41 indicates that the silylated ligand PFNP-Si acts as a double functional bridge between inorganic matrices and organic components.

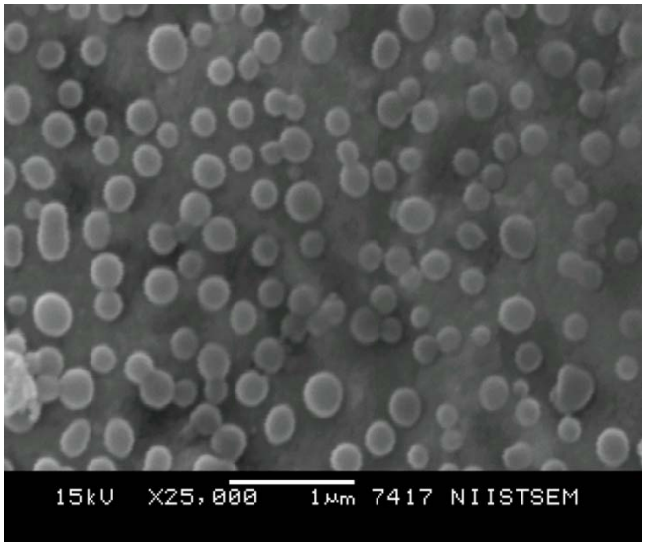

Figure 5.9. SEM picture of $Eu(SiPFNP)_3(bath)$/MCM-41**.**

The morphology and size of the grafted nanoparticles were examined by transmission electron microscopy (TEM). Figure 5.10 shows TEM micrograph of the grafted silica complex. This picture indicates that the monodispersity of the nanosized MCM units was conserved in the mesoporous hybrid material.

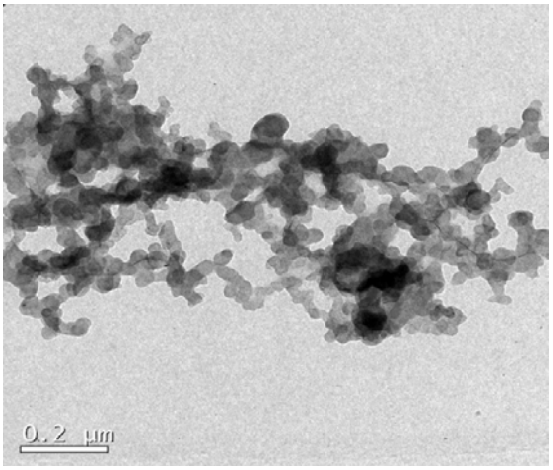

Figure 5.10. TEM picture of $Eu(SiPFNP)_3(bath)$/MCM-41**.**

The thermogravimetric curve (Figure 5.11) showed two distinct stages of decomposition. The one between 40–180 °C was related to absorbed water and the other one, between 180–800 °C, was assigned to the decomposition of organic matter and water from silanol group condensation.

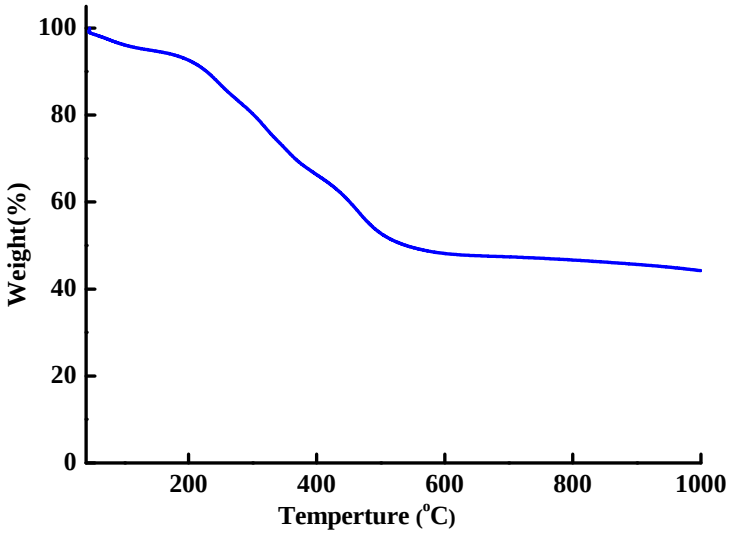

Figure 5.11. Thermo gravimetric curve for Eu(SiPFNP)$_3$(bath)/MCM-41.

Photophysical studies. The UV absorption spectra of the parent ligand HPFNP, grafted ligand SiPFNP-Na and of the mesoporous hybrid material, Eu(PFNP-Si)$_3$(bath)/MCM-41 in acetonitrile solution are shown in Figure 5.12.

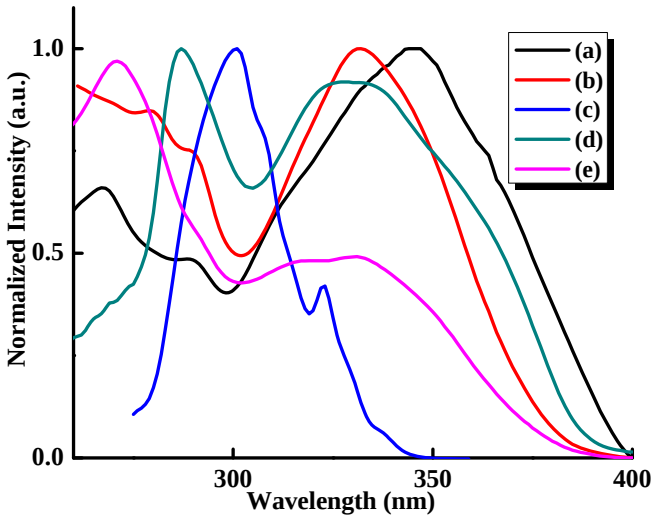

Figure 5.12. UV absorption spectra of the ligands HPFNP (a), SiPFNP-Na (b) and bath (c) and of the complexes Eu(PFNP)$_3$(bath) and Eu(SiPFNP)$_3$(bath)/MCM-41 (e) in acetonitrile solution.

The maximum absorption band at 345 nm for HPFNP, 332 nm for SiPFNP-Na, and the hump observed around 330 nm in the mesoporous hybrid material are attributed to singlet–singlet π–π* enol absorption of the *β*-diketonate [Judd 1962]. Compared with the ligand HPFNP (λ_{max} = 345 nm), the absorption maximum is blue-shifted to 332 nm in SiPFNP-Na and to 330 nm in the mesoporous hybrid material. The noticeable blue-shift in the absorption maximum observed for SiPFNP-Na, when compared to that of HPFNP suggests a change in π–π* electron distribution of the grafted ligand SiPFNP-Na [Qiao and Yan 2009]. In addition, the spectral shapes of the mesoporous hybrid material in CH_3CN are similar to that of the free ligands, suggesting that the coordination of the Eu^{3+} ion does not have a significant influence on the $^1\pi$–π* state energy.

Figure 5.13 shows the room-temperature excitation and emission spectra for the pure $Eu(PFNP)_3(bath)$ complex and the MCM-41 mesoporous material covalently bonded with $Eu(PFNP\text{-}Si)_3(bath)$. The excitation spectra of these materials were all obtained by monitoring the strongest emission wavelength of the Eu^{3+} ions at 613 nm. The excitation spectra of both the Eu^{3+} complexes exhibit a broad excitation band between 250 and 450 nm (λ_{ex} = 385 nm), which can be assigned to the π–π* transition of the ligands [Biju *et al.* 2006; Pavithran *et al.* 2006; Remya *et al.* 2008]. In addition, a sharp line observed at 465 nm in the excitation spectra can be assigned to transition between the $^7F_0 \rightarrow {}^5D_2$ level of the Eu^{3+} ion. This transition is weaker than the absorption of the organic ligands and is overlapped by a broad excitation band, which proves that luminescence sensitization *via* excitation of the ligand is much more efficient than the direct excitation of the Eu^{3+} absorption level.

In the emission spectra of pure $Eu(PFNP)_3(bath)$ and $Eu(PFNP\text{-}Si)_3(bath)$/MCM-41, characteristic Eu^{3+} ion emissions are observed. Bands in the 450–700 nm range can be clearly seen, which are assigned to the $^5D_0 \rightarrow {}^7F_J$ (J = 0–4) transitions at 580, 592, 613, 653, and 705 nm [Biju *et al.* 2006; Pavithran *et al.* 2006; Binnemans 2005]. In addition, a weak green

emission band at 535 nm (inset in Figure 5.13), occurs, corresponding to the high-energy transition of $^5D_1 \rightarrow {}^7F_1$ [Kadjane *et al.* 2008; Dejneka *et al.* 1995].

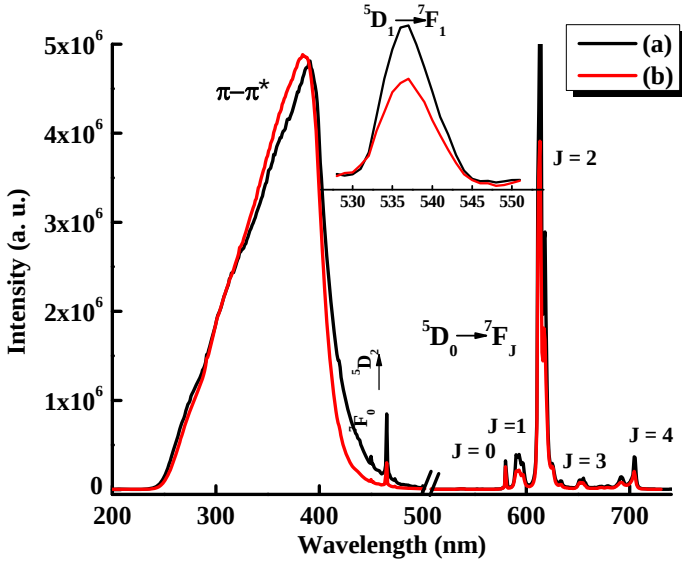

Figure 5.13. Solid state excitation and emission for $Eu(PFNP)_3(bath)$ (a) and hybrid $Eu(SiPFNP)_3(bath)$/MCM-41 (b) at 298 K, emission monitored at around 613 nm(λ_{ex} = 385 nm).

No broad emission band resulting from organic ligand molecules in the blue region can be observed, which indicates that the silica-modified ligand system transfers energy completely to the emitting level of the metal ion. The $^5D_0 \rightarrow {}^7F_2$ transition is a typical electric dipole transition and strongly varies with the local symmetry of Eu^{3+} ions, while the $^5D_0 \rightarrow {}^7F_1$ transition corresponds to a parity-allowed magnetic dipole transition, which is practically independent of the host material. Among these transitions, the $^5D_0 \rightarrow {}^7F_2$ transition shows the strongest emission, suggesting the chemical environment around Eu^{3+} ions is in low symmetry [Kai *et al.* 2008; Liu *et al.* 2008]. The intensity ratio of the electric dipole transition to the magnetic dipole transition in the lanthanide complex measures the symmetry of the coordination sphere [Kirby *et al.*1983] and this ratio increases with the number and mass of the ligand coordinated by the Ln^{3+} ion [Poluektov *et al.* 1975]. The relative luminescent intensities of the $^5D_0 \rightarrow {}^7F_2$ and the $^5D_0 \rightarrow {}^7F_1$ transition, $^5D_0 \rightarrow {}^7F_2/{}^5D_0 \rightarrow {}^7F_1$ intensity ratios (red/orange

ratio) for all materials are listed in Table 5.2. For the pure Eu(PFNP)$_3$(bath), in the absence of mesoporous material, the intensity ratio of the transitions of $^5D_0 \rightarrow {}^7F_2/{}^5D_0 \rightarrow {}^7F_1$ (I_{21}) is 10 (Table 5.2). This intensity ratio increases to 11 in Eu(PFNP-Si)$_3$(bath)/MCM-41. In short, the presence of mesoporous material increases the luminescent intensity of the hypersensitive transitions of the Eu^{3+} ion.

Table 5.2. Radiative (A_{RAD}) and nonradiative (A_{NR}) decay rates, $^5D_0$ lifetime (τ_{obs}), intrinsic quantum yield (Φ_{Ln},%), energy transfer efficiency ($\Phi_{sens,}$%), and overall quantum yield ($\Phi_{overall}$, %) for Eu(PFNP-Si)$_3$(bath)/MCM-41 (**1**) and Eu(PFNP)$_3$(bath) (**2**) at 303 K.

Parameters	**1**	Eu (PFNP)$_3$(bath)
ν_{00} (cm^{-1})[a]	17,241	17,248
ν_{01} (cm^{-1})[a]	16,863	16,863
ν_{02} (cm^{-1})[a]	16,286	16,286
ν_{03} (cm^{-1})[a]	15,290	15,290
ν_{04} (cm^{-1})[a]	14,204	14,204
I_{02}/I_{01} [b]	11.0	10.06
τ_{obs} (ms)	1053	1218
A_{RAD} (s^{-1})	766	661
A_{NR} (s^{-1})	183	145
$\Phi_{overall}$ (%)	43	48
Φ_{Ln} (%)	81	81
Φ_{sens} (%)	53	59

[a] the energies of the $^5D_0 \rightarrow {}^7F_J$ transitions $\nu_{0J,}$ [b] the intensity ratio (red/orange ratio)

The $^5D_0$ lifetime values (τ_{obs}) were determined from the luminescent decay profiles for the pure Eu(PFNP)$_3$(bath) and mesoporous hybrid material at room temperature by fitting with a monoexponential curve and the values are depicted in Table 5.2. Typical decay profiles of mesoporous hybrid material along with the pure Eu(PFNP)$_3$(bath) are shown in Figure 5.14. From Table 5.2 it is clear that longer lifetime values have been observed for these materials due to the absence of non-radiative pathways in the first coordination sphere [Biju *et al.* 2006; Pavithran *et al.* 2006; Binnemans 2005].

The overall quantum yield ($\Phi_{overall}$), radiative (A_{RAD}) and non-radiative (A_{NR}) decay rates, intrinsic quantum yield (Φ_{Ln}) and energy transfer efficiency (Φ_{sens}) of the complexes were presented in Table 5.2. It is evident that the mesoporous hybrid material, Eu(PFNP-

Si)$_3$(bath)/MCM-41 exhibits very high intrinsic quantum yield (Φ_{Ln} = 81%) and energy transfer efficiency (Φ_{sens} = 53%) similar to that of the pure Eu(PFNP)$_3$(bath). Furthermore, the intrinsic quantum yield obtained for the newly designed mesoporous hybrid material is found to be significantly higher than that of the mesoporous hybrid materials containing Eu^{3+}-1-(2-naphthoyl)-3,3,3-trifluoroacetonate-bipyridine complexes covalently bonded to SBA-15 (Φ_{Ln} = 29%) [Li *et al.* 2008] and Eu^{3+}-1-(2-naphthoyl)-3,3,3-trifluoroacetonate-pyridine complexes covalently bonded to MCM-41(Φ_{Ln} = 29.9%) [Bruno *et al.* 2008].

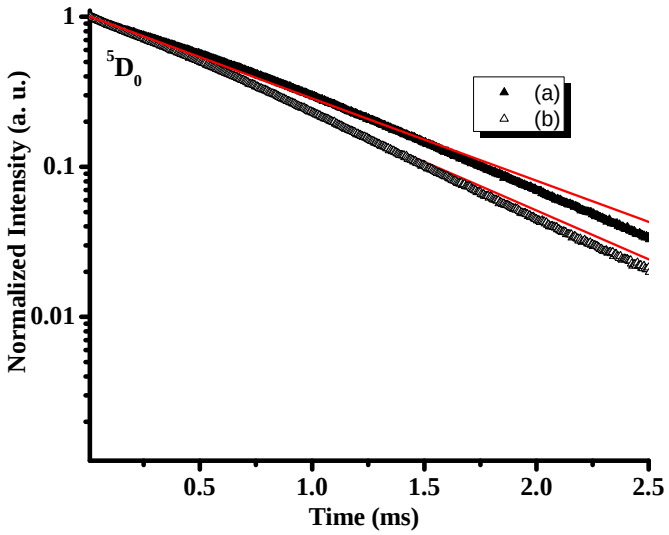

Figure 5.14. Experimental luminescence decay profiles of Eu(PFNP)$_3$(bath) (a) and Eu(SiPFNP)$_3$(bath)/MCM-41 (b) monitored around 612 nm and excited at their maximum emission wave lengths.

It is well demonstrated in many previous luminescence studies of trivalent lanthanide chelates that the general mechanism for the sensitization of Ln^{3+} ion luminescence *via* the "antenna effect" involves the following steps: (i) UV absorption by the organic chromophore which results in excitation to the first excited singlet state; (ii) non-radiative intersystem crossing from the singlet to the triplet state; (iii) intramolecular energy transfer from the ligand-centered triplet state to the excited 4f states of the Ln^{3+} ion; and (iv) radiative transition from the Ln^{3+} ion emissive states to lower energy states which results in the characteristic lanthanide emission. Thus, the intramolecular energy migration efficiency from the organic ligands to the

central Ln^{3+} is the most important factor determining the luminescence efficiency of lanthanide complexes [Lehn 1990; Bekiari and Lianos 1998; Petoud *et al.* 2003]. The singlet energy level ($^1\pi\pi^*$) of PFNP-Si is estimated by referencing its higher absorption edge, which is 26,500 cm^{-1}. The shortest-wavelength phosphorescence band in the phosphorescence spectrum of the $Gd(PFNP\text{-}Si)_3(H_2O)_2$ at 77K (Figure 5.15) was assumed to e the 0–0 transition [Biju *et al.* 2006; Pavithran *et al.* 2006; Binnemans 2005], from which the energy of the lowest triplet state, T_1 ($^3\pi\pi^*$ = 19,800 cm^{-1}) was determined.

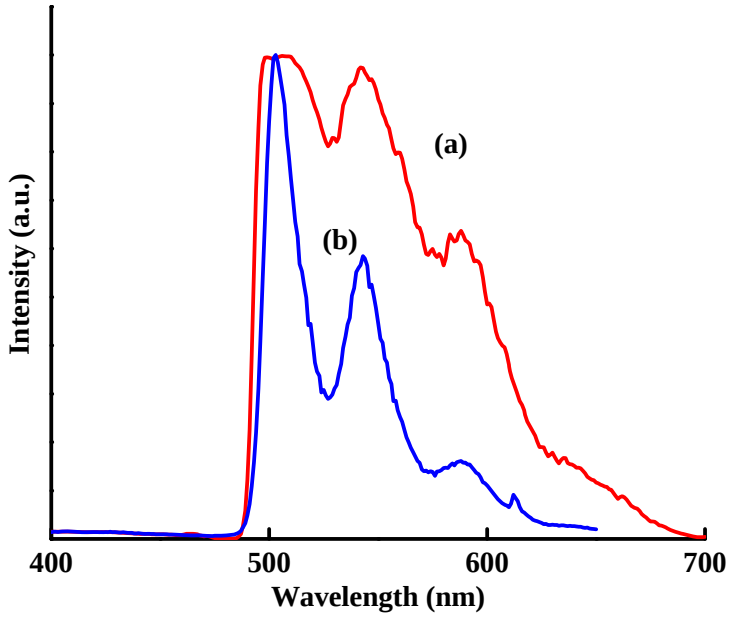

Figure 5.15. Phosphorescence spectra of Gd $(PFNP\text{-}Si)_3(H_2O)_2$ (a) and $Gd(PFNP)_3(H_2O)_2$ (b).

The triplet energy level of PFNP-Si was found to be same as that of HPFNP, indicating that silylation of the *β*-diketone ligand does not change its electronic states significantly. The singlet ($^1\pi\pi^*$ = 29,000 cm^{-1}) and triplet ($^3\pi\pi^*$ =21,000 cm^{-1}) energy levels of 4,7-diphenyl-1,10-phenanthroline were taken from the chapter 4. The triplet levels of PFNP-Si and bath were found to be higher in energy than the $^5D_0$ state of Eu^{3+}. According to the empirical rule proposed by Latva, for an optimal ligand-to-metal energy transfer process $2500 < \Delta E(^3\pi\pi^* - ^5D_0) < 4000$ cm^{-1} for Eu^{3+} [Latva *et al.* 1997]. It is also noted that the energy gaps, ΔE ($^3\pi\pi^* - ^5D_0$) of the PFNP-Si and bath are 2300 and 3500 cm^{-1}, respectively. As a consequence these

ligands can transfer energy effectively to the emitting states of the Eu^{3+} ion. In addition, Reinhoudt's empirical rule [Steemers *et al.* 1995] states that the intersystem crossing process becomes effective when $\Delta E(^1\pi\pi^*-^3\pi\pi^*)$ is at least 5000 cm^{-1}. Thus the $\Delta E(^1\pi\pi^*-^3\pi\pi^*)$ energy gaps for PFNP-Si and bath are 6700 and 8000 cm^{-1}, respectively, and hence the intersystem crossing processes are effective for these ligands.

5.5 Conclusions

In summary, a highly luminescent Eu^{3+} ternary complex has been covalently immobilized in the ordered MCM-41 mesoporous host through modification of a novel polyfluorinated *β*-diketone with 3-(triethoxysilyl)propylisocyanate by a co-condensation route. X-Ray diffraction confirms that this luminescent material has ordered hexagonal mesoporosity. Dynamic light scattering and SEM studies indicate that the newly designed mesoporous luminescent material has particle size in the range 250–300 nm. Investigations of the luminescence properties of the Eu(PFNP-Si)$_3$(bath)/MCM-41 mesoporous material shows that the characteristic luminescence of the corresponding Eu^{3+} occurs through intramolecular energy transfer from the modified ligand (PFNP-Si) to the central Eu^{3+} ions. Further, the photoluminescent properties indicates that the present hybrid material exhibits higher $^5D_0$ quantum efficiency (Φ_{Ln} = 81%) and longer lifetime (1.05 ms) as compared to that of the mesoporous hybrid materials containing Eu^{3+}-1-(2-naphthoyl)-3,3,3-trifluoroacetonate-bipyridine complexes covalently bonded to SBA-15 (Φ_{Ln} = 29%; τ_{obs} = 0.48 ms) [Li *et al.* 2008] and Eu^{3+}-1-(2-naphthoyl)-3,3,3-trifluoroacetonate-pyridine complexes covalently bonded to MCM-41(Φ_{Ln} = 29.9%; τ_{obs} = 0.31 ms) [Bruno *et al.* 2008] reported elsewhere. Moreover, the MCM-based material provides several additional advantages, such as being able to be processed as silica based templates for optical centers (compatible with the silicon devices technology), opening up the possibility of designing new luminescent displays with highly oriented MCM-41 films impregnated with emitting centers showing enhanced antenna effects.

List of Publications

LIST OF PUBLICATIONS

Publications from the thesis

1. **D. B. Ambili Raj**, Biju Francis, M. L. P. Reddy, Rachel R. Butorac, Vincent M. Lynch, Alan H. Cowley, "Highly luminescent poly(methyl methacrylate)-incorporated europium complex supported by a carbazole-based fluorinated *β*-diketonate ligand and a 4,5-bis(diphenylphosphino)-9,9-dimethylxanthene oxide co-ligand," *Inorg. Chem.*, **2010,** *49,* 9055-9063.
2. **D. B. Ambili Raj**, Silvanose Biju, M. L. P. Reddy, "Highly luminescent europium(III) complexes containing organosilyl 4,4,5,5,5-pentafluoro-1-(naphthalen-2-yl)pentane-1,3-dionate ligands grafted on silica nanoparticles," *J. Mater. Chem*., **2009,** *19,* 7976-7983.
3. **D. B. Ambili Raj,** Silvanose Biju, M. L. P. Reddy, "4,4,5,5,5-Pentafluoro-1-(9H-fluoren-2-yl)-1,3-pentanedione complex of Eu^{3+} with 4,5-bis(diphenylphosphino)-9,9-dimethylxanthene oxide as a promising light-conversion molecular device," *Dalton Trans.*, **2009**, 7519-7528.
4. **D. B. Ambili Raj**, S. Biju, M. L. P. Reddy, "One-, two-, and three-dimensional arrays of Eu^{3+}-4,4,5,5,5-pentafluoro- 1-(naphthalen-2-yl)pentane-1,3-dione complexes: synthesis, crystal structure and photophysical properties," *Inorg. Chem.*, **2008**, *47*, 8091-8100.

Publications not related to this thesis

1. Biju Francis, **D. B. Ambili Raj,** M. L. P. Reddy, "Highly efficient luminescent hybrid materials covalently linking with europium(III) complexes via a novel fluorinated *β*-diketonate ligand: Synthesis, characterization and photo physical properties," *Dalton Trans., **2010**, 39,* 8084-8092.
2. Silvanose Biju, **D. B. Ambili Raj**, M. L. P. Reddy, C. K. Jayasankar, Alan H. Cowley, Michael Findlater, "Dual emission from stoichiometrically mixed lanthanide complexes of 3-phenyl-4-benzoyl-5-isoxazolonate and 2,2'-bipyridine," *J. Mater. Chem.*, **2009**, *19*, 1425–1432.
3. S. Biju, **D. B. Ambili Raj**, M. L. P. Reddy, B. M. Kariuki, "Synthesis, crystal structure, and luminescent properties of novel Eu^{3+} heterocyclic β-diketonate complexes with bidentate nitrogen donors," *Inorg. Chem.*, **2006,** *45,* 10651-10660.

Papers presented at National/International Conferences

1. **One-, two-, and three-dimensional arrays of Eu^{3+}-4,4,5,5,5-pentafluoro- 1-(naphthalen-2-yl)pentane-1,3-dione complexes: synthesis, crystal structure and photophysical properties-** Poster presented in *India- Japan Cooperative Science Programme: 'Recent Trends in molecular Materials"*, Thiruvananthapuram, India, January, **2008**.
2. **Highly luminescent europium(III) complexes containing organosilyl 4,4,5,5,5-pentafluoro-1-(naphthalen-2-yl)pentane-1,3-dionate ligands grafted on silica nanoparticles -** Poster presented in *MTIC- XIII*, IISc, Bangalore, India, December **2009**.

References

[a]Alpha, B.; Lehn, J.-M.; Mathis, G. "Energy transfer luminescence of europium(III) and terbium(III) cryptates of macrobicyclic polypyridine ligands," *Angew. Chem., Int. Ed. Engl., 26,* **1987**, 266-267.

[b]Alpha, B.; Balzani, V.; Lehn, J.-M.; Perathoner, S.; Sabbatini, N. "Luminescence probes: The Eu^{3+}- and Tb^{3+}-cryptates of polypyridine macrobicyclic ligands," *Angew. Chem., Int. Ed. Engl., 26*, **1987**, 1266-1267.

Accorsi, G.; Listorti, A.; Yoosaf; K.; Armaroli, N. "1,10-Phenanthrolines: Versatile building blocks for luminescent molecules, materials and metal complexes," *Chem. Soc. Rev*., *38*, **2009**, 1690–1700.

Aebischer, A.; Gumy, F.; Bunzli, J.-C. G. "Intrinsic quantum yields and radiative lifetimes of lanthanide tris(dipicolinates)," *Phys. Chem. Chem. Phys., 11*, **2009**, 1346-1353.

Armaroli, N.; Accorsi, G.; Barigelletti, F.; Couchman, S. M.; Fleming, J. S.; Harden, N. C.; Jeffery, J. C.; Mann, K. L. V.; McCleverty, J. A.; Rees, L. H.; Starling, S. R.; Ward, M. D. "Structural and photophysical properties of mononuclear and dinuclear lanthanide^{3+} complexes of multidentate podand ligands based on poly(pyrazolyl)borates," *Inorg. Chem., 38*, **1999**, 5769–5776.

Armelao, L.; Quici, S.; Barigelletti, F.; Accorsi, G.; Bottaro, G.; Cavazzini, M.; Tondello, E. "Design of luminescent lanthanide complexes: From molecules to highly efficient photo-emitting materials," *Coord. Chem. Rev*., *254*, **2009**, 487-505.

Baek, N. S.; Kim, Y. H.; Eom, Y. K.; Oh, J. H.; Kim, H. K.; Aebischer, A.; Gumy, F.; Chauvin, A.-S.; Bünzli, J. –C. G. "Sensitized near-IR luminescence of lanthanide complexes based on push-pull diketone derivatives," *Dalton Trans., 39*, **2010**, 1532–1538.

Balamurugan, A.; Reddy, M. L. P.; Jayakannan, M. "Single polymer photosensitizer for Tb^{3+} and Eu^{3+} ions: An approach for white light emission based on carboxylic-functionalized poly(*m*-phenylenevinylene)s," *J. Phys. Chem. B, 113*, **2009**, 14128–14138.

Batista, H. J.; de Andrade, A. V. M.; Longo, R. L.; Simas, A. M.; de Sa, G. F.; Ito, N. K.; Thompson, L. C. "Synthesis, X-ray structure, spectroscopic characterization, and theoretical prediction of the structure and electronic spectrum of $Eu(btfa)_3(bipy)$ and an assessment of the effect of fluorine as a *β*-diketone substituent on the ligand-metal energy transfer process," *Inorg. Chem., 37,* **1998,** 3542-3547.

Beeby, A.; Clarkson, I. M.; Dickins, R. S.; Faulkner, S.; Parker, D.; Royle, L.; de Sousa, A. S.; Williams, J. A. G.; Woods, M. "Non-radiative deactivation of the excited states of europium, terbium and ytterbium complexes by proximate energy-matched OH, NH and CH oscillators: An improved luminescence method for establishing solution hydration states," *J. Chem. Soc., Perkin Trans. 2*, **1999**, 493-504.

Bekiari, V.; Lianos, P. "Strongly luminescent poly(ethylene glycol)-2,2′-bipyridine lanthanide ion complexes," *Adv. Mater., 10*, **1998**, 1455-1458.

Bellusci, A.; Barberio, G.; Crispini, A.; Ghedini, M.; La Deda, M.; Pucci, D. "Synthesis and luminescent properties of novel lanthanide(III) *β*-diketone complexes with nitrogen *p,p′*-disubstituted aromatic ligands," *Inorg. Chem., 44*, **2005**, 1818-1825.

Berlman, I. B. "*Energy transfer parameters of aromatic compounds*;" Academic press: New York, **1973**.

Biju, S.; Ambili Raj, D. B.; Reddy, M. L. P.; Kariuki, B. M. "Synthesis, crystal structure, and luminescent properties of novel Eu^{3+} heterocyclic *β*-diketonate complexes with bidentate nitrogen donors," *Inorg. Chem., 45,* **2006**, 10651-10660.

[a]Biju, S.; Reddy, M. L. P.; Cowley A. H.; Vasudevan, K. V. "3-Phenyl-4-acyl-5-isoxazolonate complex of Tb^{3+} doped into poly-*β*-hydroxybutyrate matrix as a promising light-conversion molecular device," *J. Mater. Chem., 19,* **2009**, 5179-5187.

[b]Biju, S.; Reddy, M. L. P.; Cowley A. H.; Vasudevan, K. V. "Molecular ladders of lanthanide-3-phenyl-4-benzoyl-5-isoxazolonate and bis(2-(diphenylphosphino)phenyl)ether

oxide complexes: The role of the ancillary ligand in the sensitization of Eu^{3+} and Tb^{3+} luminescence," *Cryst. Growth Des.*, *8*, **2009**, 3562-3569.

Binnemans, K.; Lenaerts, P.; Driesen, K.; Görller-Walrand, C. "A luminescent tris(2-thenoyltrifluoroacetonato)europium(III) complex covalently linked to a 1,10-phenanthroline-functionalised sol–gel glass," *J. Mater. Chem.*, *14*, **2004,** 191-195.

Binnemans, K. "*Handbook on the physics and chemistry of rare earths*," Elsevier, Amsterdam, **2005**, ch. 225, (vol. 35), p. 107.

Binnemans, K. "Lanthanide-based luminescent hybrid materials," *Chem. Rev., 109,* **2009,** 4283–4374.

Blasse, G. "The influence of charge-transfer and rydberg states on the luminescence properties of lanthanides and actinides," *Struct. Bonding, 26*, **1976**, 43-79.

Boyer, J. C.; Johnson, N. J. J.; van Veggel, F. C. J. M. "Upconverting lanthanide-doped $NaYF_4$−PMMA polymer composites prepared by in situ polymerization," *Chem. Mater., 21*, **2009**, 2010-2012.

Bril, A.; De Jager-Veenis, A. W. "Quantum efficiency standard for ultraviolet and visible excitation," *J. Electrochem. Soc., 123*, **1976**, 396-398.

Brunet, E.; Juanes, O.; Rodriguez-Ubis, J. C. "Supramolecularly organized lanthanide complexes for efficient metal excitation and luminescence as sensors in organic and biological applications," *Curr. Chem. Biol., 1*, **2007**, 11-39.

Bruno, S. M.; Coelho, A. C.; Ferreira, R. A. S.; Carlos, L. D.; Pillinger, M.; Valente, A. A.; Ribeiro-Claro, P.; Gonçalves, I. S. "MCM-41 derivatised with pyridyl groups and its use as a support for luminescent europium(III) complexes," *Eur. J. Inorg. Chem., 2008*, **2008**, 3786-3795.

Bünzli, J.-C. G. "*Luminescent probes. in lanthanide probes in life, chemical and earth sciences, theory and practice*," Bünzli, J.-C. G., Choppin, G. R., Eds.; Elsevier: New York, **1989**; p 219.

Bünzli, J.-C. G.; Froidevaux, P.; Harrowfield, J. M. "Photophysical properties of lanthanide dinuclear complexes with *p*-tert-butylcalix[8]arene," *Inorg. Chem., 32*, **1993**, 3306-3311.

Bünzli, J.-C. G.; Ihringer, F. "Photophysical properties of lanthanide dinuclear complexes with *p*-nitro-calix[8]arene," *Inorg. Chim. Acta, 246*, **1996**, 195-205.

Bünzli, J.-C. G.; Piguet, C. "Taking advantage of luminescent lanthanide ions," *Chem. Soc. Re*v., *34*, **2005**, 1048-1077.

Bünzli, J.-C. G. "Lanthanide luminescence for biomedical analyses and imaging," *Chem. Rev.*, *110*, **2010,** 2729–2755.

Capecchi, S.; Renault, O.; Moon, D.-G.; Halim, M.; Etchells, M.; Dobson, P. J.; Salata O. V.; Christou, V. "High-efficiency organic electroluminescent devices using an organoterbium emitter," *Adv. Mater.*, *12*, **2000**, 1591-1594.

Carlos, L. D.; de Mello Donega, C.; Albuquerque, R. Q.; Alves Jr. S.; Menezes, J. F. S.; Malta, O. L. "Highly luminescent europium(III) complexes with naphtoiltrifluoroacetone and dimethyl sulphoxide," *Mol. Phys.*, *101*, **2003**, 1037-1045.

Carlos, L. D.; Ferreira, R. A. S.; de Zea Bermudez, V.; Ribeiro, S. J. L. "Lanthanide-containing light-emitting organic-inorganic hybrids: A bet on the future," *Adv. Mater.*, *21*, **2009**, 509-534.

Carnall, W. T.; Gruen, D. M.; McBeth, R. L. "Near-infrared transitions of the trivalent lanthanides in solution I. Praseodymium(III), neodymium(III), samarium(III), and europium(III) ions," *J. Phys. Chem.*, *66*, **1962**, 2159-2164.

Carnall, W. T. "The near-infrared transitions of the trivalent lanthanides in solution. II. Tb^{+3}, Dy^{+3}, Ho^{+3}, Er^{+3}, Tm^{+3}, and Yb^{+3}," *J. Phys. Chem.*, *67*, **1963**, 1206-1211.

Carnall, W. T.; Fields, P. R.; Wybourne, B. G. "Spectral intensities of the trivalent lanthanides and actinides in solution. II. Pr^{3+}, Nd^{3+}, Er^{3+}, Tm^{3+}, and Yb^{3+}," *J. Chem. Phys.*, *42*, **1965**, 3797-3806.

Carnall, W. T. " *Handbook on the physics and chemistry of rare-earths*," Gschneidner, K. A., Jr., Eyring, L., Eds.; North Holland Publishing Co.: Amsterdam, 1979; Vol. 3, Chapter 24, p 172.

Charbonniere, L. J.; Balsiger, C.; Schenk, K. J.; Bunzli, J.-C. G. "Complexes of *p-tert*-butylcalix[5]arene with lanthanides: Synthesis, structure and photophysical properties," *J. Chem. Soc., Dalton Trans.*, **1998**, 505-510.

Chauvin, A.-S.; Gumy, F.; Matsubayashi, I.; Yuko Hasegawa, Y.; Bünzli, J.-C. G. "Fluorinated β-Diketones for the extraction of lanthanide ions: Photophysical properties and hydration numbers of their Eu^{3+} complexes," *Eur. J. Inorg. Chem., 2006*, **2006**, 473-480.

Chen, X. Y.; Bretonniere, Y.; Pecaut, J.; Imbert, D.; Bünzli, J.-C. G.; Mazzanti, M. "Selective self-assembly of hexameric homo- and heteropolymetallic lanthanide wheels: Synthesis, structure, and photophysical studies," *Inorg. Chem.*, *46*, **2007**, 625-637.

Chen, X.-Y.; Yang, X.; Holliday, B. J. "Photoluminescent europium-containing inner sphere conducting metallopolymer*" J. Am. Chem. Soc.*, *130*, **2008**, 1546-1547.

Colle, M.; Gmeiner, J.; Milius, W.; Hillebrecht, H.; Brutting, W. "Preparation and characterization of blue-luminescent tris(8-hydroxyquinoline)-aluminum (Alq_3)," *Adv. Funct. Mater., 13*, **2003**, 108-112.

Comby, S.; Imbert, D.; Anne-Sophie, C.; Bünzli, J.-C. G.; Charvonniere, L. J.; Ziessel, R. F. "Influence of anionic functions on the coordination and photophysical properties of lanthanide(III) complexes with tridentate bipyridines," *Inorg. Chem.*, *43*, **2004**, 7369-7379.

Comby, S.; Bünzli, J.-C. G. "*Handbook on the Physics and Chemistry of Rare Earths*;" Gschneidner, K. A., Jr., Bünzli, J.-C. G., Pecharsky, V. K., Eds.; *Elsevier Science BV: Amsterdam*, *37*, **2007**, Chapter 235, 217.

Corriu, R. J. P.; Mehdi, A.; Reye, C.; Thieuleux, C.; Frenkel, A.; Gibaud, A. "Preparation of ordered SBA-15 mesoporous silica containing chelating groups. Study of the complexation of Eu^{3+} inside the pore channels of the materials," *New J. Chem., 28,* **2004**, 156-160.

Cousinié, S.; Gressier, M.; Alphonse, P.; Menu, M.-J. "Silica-based nanohybrids containing dipyridine, urethan, or urea derivatives," *Chem. Mater.*, *19*, **2007**, 6492-6503.

Cousinié, S.; Gressier, M.; Reber, C.; Dexpert-Ghys, J.; Menu, M.-J. "Europium(III) complexes containing organosilyldipyridine ligands grafted on silica nanoparticles," *Langmuir*, *24*, **2008**, 6208-6214.

Day, P. N.; Nguyen, K. A.; Pachter, R. "TDDFT study of one- and two-photon absorption properties: donor-π-acceptor chromophores," *J. Phys. Chem. B, 109,* **2005**, 1803-1814.

de Bettencourt-Dias, A. "Lanthanide-based emitting materials in light-emitting diodes," *Dalton Trans.,* **2007**, 2229-2241.

de Mello, C.; Wittmann, H. F.; Friend, R. H. "An improved experimental determination of external photoluminescence quantum efficiency," *Adv. Mater., 9,* **1997**, 230-232.

de Sa, G. F.; Malta, O. L.; de Mello Donega, C.; Simas, A. M.; Longo, R. L.; Santa-Cruz, P. A.; da Silva Jr, E. F. "Spectroscopic properties and design of highly luminescent lanthanide coordination complexes," *Coord. Chem. Rev., 196,* **2000**, 165-195.

Dejneka, M.; Snitzer, E.; Riman, R. E. "Blue, green and red fluorescence and energy transfer of Eu^{3+} in fluoride glasses," *J. Lumin., 65,* **1995**, 227-245.

Demasa, J. N.; Crosby, G. A. "The measurement of photoluminescence quantum yields. A review," *J. Phys. Chem., 75,* **1971**, 991-1024.

DeOliveira E.; Neri, C. R.; Serra O. A.; Prado, A. G. S. "Antenna effect in highly luminescent Eu^{3+} anchored in hexagonal mesoporous silica," *Chem. Mater.*, *19*, **2007**, 5437-5442.

Deun, R.V.; Fias, P.; Nockemann, P.; Hecke, K. V.; Meervelt, L. V.; Binnemans, K. "Visible-light-sensitized near-infrared luminescence from rare-earth complexes of the 9-hydroxyphenalen-1-one ligand," *Inorg. Chem.*, *45*, **2006**, 10416-10418.

Dieke, G. H. "*Spectra and Energy Levels of Rare Earth Ions in Crystals*;" Wiley-Interscience: New York, **1968**.

Dossing, A. "Luminescence from lanthanide(III) ions in solution," *Eur. J. Inorg. Chem.*, *2005*, **2005**, 1425-1434.

Eaton, D. F. "Reference materials for fluorescence measurement**,**" *Pure Appl. Chem., 60,* **1988**, 1107-1114.

Eliseeva, S. V.; Ryazanov, M.; Gumy, F.; Troyanov, S. I.; Lepnev, L. S.; Bünzli, J.-C. G.; Kuzmina, N. P. "Dimeric complexes of lanthanide(III) hexafluoroacetylacetonates with 4-cyanopyridine *N*-oxide: Synthesis, crystal structure, magnetic and photoluminescent properties," *Eur. J. Inorg. Chem., 2006*, **2006**, 4809-4820.

Eliseeva, S. V.; Kotova, O. V.; Gumy, F.; Semenov, S. N.; Kessler, V. G.; Lepnev, L. S.; Bünzli, J.-C. G.; Kuzmina, N. P. "Role of the ancillary ligand *N,N*-dimethylaminoethanol in the sensitization of Eu^{3+} and Tb^{3+} luminescence in dimeric *β*-diketonates," *J. Phys. Chem. A, 112*, **2008**, 3614-3626.

Eliseeva, S. V.; Bünzli, J.-C. G. "Lanthanide luminescence for functional materials and bio-sciences," *Chem. Soc. Rev.*, *39*, **2010**, 189–227.

Eliseeva, S.V.; Pleshkov, D. N.; Lyssenko,K. A.; Lepnev,L. S.; Bunzli,J-C. G.; Kuzmina, N. P. "Highly luminescent and triboluminescent coordination polymers assembled from lanthanide *β*-diketonates and aromatic bidentate O-donor ligands," Inorg. Chem., *49*, **2010**, 9300–9311.

Fan, W-Q.; Feng, J.; Song, S-Y.; Lei, Y-Q.; Zheng, G-L.; Zhang, H-J. "Synthesis and optical properties of europium-complex-doped inorganic/organic hybrid materials built from oxo–hydroxo organotin nano building blocks," *Chem. Eur. J., 16,* **2010**, 1903-1910.

Faulkner, S.; Natrajan, L. S.; Perry, W. S.; Sykes, D. "Sensitised luminescence in lanthanide containing arrays and d–f hybrids," *Dalton Trans.,* **2009**, 3890-3899.

Fernandes, J. A.; Sa´ Ferreira, R. A.; Pillinger, M.; Carlos, L. D.; Goncalves, I. S.; Ribeiro-Claro, P. J. A. "Spectroscopic studies of europium(III) and gadolinium(III) tris-β-diketonate complexes with diazabutadiene ligands," *Eur. J. Inorg. Chem., 2004*, **2004**, 3913-3919.

Fernandes, J.A.; Sa Ferreira, R.A.; Pillinger, M.; Carlos, L.D.; Jepsen, J.; Hazell, A.; Ribeiro-Claro, P.; Goncalves, I.S. "Investigation of europium(III) and gadolinium(III) complexes with naphthoyltrifluoroacetone and bidentate heterocyclic amines," *J. Lumin., 113*, **2005**, 50- 63.

Filipescu, N.; Sager, W. F.; Serafin, F. A.; "Substituent effects on intramolecular energy transfer. II. Fluorescence spectra of europium and terbium *β*-diketone chelates," *J. Phys. Chem*., 68, **1964,** 3324.

Försberg, J. H. "Complexes of lanthanide (III) ions with nitrogen donor ligands," *Coord. Chem. Rev., 10*, **1973**, 195-226.

Fratini, A.; Richards, G.; Larder, E.; Swavey, S. "Neodymium, gadolinium, and terbium complexes containing hexafluoroacetylacetonate and 2,2′-bipyrimidine: Structural and spectroscopic characterization," *Inorg. Chem., 47*, **2008**, 1030-1036.

Fu, Y. J.; Wong, T. K. S.; Yan, Y. K.; Hu, X. " Synthesis, structures and luminescent properties of Sm(III) and Eu(III) chelates for organic-electoluminescent device applications," *J. Alloys Compd.*, 358, **2003,**235-244.

Fu, L.; Sa Ferreira, R. A.; Silva, N. J. O.; Fernandes, J. A.; Ribeiro-Claro, P.; Goncüalves, I. S.; de Zea Bermudez, V.; Carlos, L. D. "Structure-photoluminescence relationship in Eu(III) *β*-diketonate-based organic-inorganic hybrids: Influence of the synthesis method: Carboxylic acid solvolysis versus conventional hydrolysis," *J. Mater. Chem., 15*, **2005**, 3117-3125.

Fu, L-M.; Ai, X-C.; Li, M-Y.; Wen, X-F.; Hao, R.; Wu, Y-S.; Wang, Y.; Zhang, J-P "Role of ligand-to-metal charge transfer state in nontriplet photosensitization of luminescent europium complex," *J. Phys. Chem. A, 114*, **2010**, 4494–4500.

Fukuda, Y.; Nakao, A.; Hiyashi, K. "Syntheses and specific structures of higher-order mixed chelate lanthanide complexes containing terpyridine, acetylacetonate, and nitrate ligands," *J. Chem. Soc., Dalton Trans.*, **2002**, 527-533.

Gago, S.; Fernandes, J. A.; Rainho, J. P.; Sá Ferreira, R. A.; Pillinger. M.; Valente, A. A.; Santos, T.M.; Carlos, L.D.; Ribeiro-Claro, P.J. A.; Goncüalves, I.S. "Highly luminescent tris(*β*-diketonate)europium(III) complexes immobilized in a functionalized mesoporous silica," *Chem. Mater., 17*, **2005**, 5077-5084.

Gao, X.-C.; Cao, H.; Huang, C.-H.; Umitani, S.; Chen, G.-Q.; Jiang, P. "Photoluminescence and electroluminescence of a series of terbium complexes," *Synth. Met., 99*, **1999**, 127-132.

George, M. R.; Golden, C. A.; Grossel, M. C.; Curry, R. J. "Modified dipicolinic acid ligands for sensitization of europium(III) luminescence," *Inorg. Chem., 45*, **2006**, 1739-1744.

Geusic, J. E.; Marcos, H. M.; van Uitert, L. G. "Laser oscillations in Nd-doped yttrium aluminium, yttrium gallium and gadolinium garnets," *Appl. Phys. Lett., 4*, **1964**, 182-183.

Glover, P. B.; Bassett, A. P.; Nockemann, P.; Kariuki, B. M.; Deun, R. V.; Pikramenou, Z. "Fully fluorinated imidodiphosphinate shells for visible- and NIR-emitting

lanthanides: Hitherto unexpected effects of sensitizer fluorination on lanthanide emission properties," *Chem. Eur. J., 13,* **2007,** 6308-6320.

Grazulevicius, J. V.; Strohriegl, P.; Pielichowski, J.; Pielichowski, K. "Carbazole-containing polymers: Synthesis, properties and applications," *Prog. Polym. Sci. 28,* **2003**, 1297-1353.

Grushin, V. V.; Herron, N.; LeCloux, D. D.; Marshall, W. J.; Petrov, V. A.; Wang, Y. "New efficient electroluminescent materials based on organometallic Ir complexes," *Chem. Commun.*, **2001**, 1494-1495.

Guyot, Y.; Canibano, H.; Goutaudier, C.; Novoselov, A.; Yoshikawa, A.; Fukuda, T.; Boulon, G. "Yb^{3+}-doped $Gd_3Ga_5O_{12}$ garnet single crystals grown by the micro-pulling down technique for laser application. Part 2: Concentration quenching analysis and laser optimization," *Opt. Mater., 27,* **2005**, 1658-1663.

Hao, J.; Studenikin, S. A.; Cocivera, M. "Blue, green and red cathodoluminescence of Y_2O_3 phosphor films prepared by spray pyrolysis," *J. Lumin., 93,* **2001**, 313-319.

Harada, T.; Nakano, Y.; Fujiki, M.; Naito, M.; Kawai, T.; Hasegawa, Y. "Circularly polarized luminescence of Eu(III) complexes with point- and axis-chiral ligands dependent on coordination structures," *Inorg. Chem., 48,* **2009**, 11242-11250.

Hasegawa, Y.; Ohkubo, T.; Sogabe, K.; Kawamura, Y.; Wada, Y.; Nakashima, N.; Yanagida, S. "Luminescence of novel neodymium sulfonylaminate complexes in organic media," *Angew. Chem., Int. Ed., 39,* **2000**, 357-360.

Hasegawa, Y.; Yamamuro, M.; Wada, Y.; Kanehisa, N.; Kai, Y.; Yanagida, S. "Luminescent polymer containing the Eu(III) complex having fast radiation rate and high emission quantum efficiency," *J. Phys. Chem. A, 107,* **2003**, 1697-1702.

Hasegawa, Y.; Wada, Y.; Yanagida, S. "Strategies for the design of luminescent lanthanide(III) complexes and their photonic applications," *J. Photochem. Photobiol., C., 5,* **2004**, 183-202.

Hasegawa, Y.; Kawai, H.; Nakamuraa, K.; Yasuda, N.; Wada, Y.; Yanagida, S. "Molecular design of luminescent Eu^{3+} complexes as lanthanide lasing material and their optical properties," *J. Alloys Compd.*, *408*, **2006**, 669-674.

[a]He, P.; Wang, H. H.; Liu, S. G.; Shi, J. X.; Wang, G.; Gong, M. L. "Visible-light excitable europium(III) complexes with 2,7-positional substituted carbazole group-containing ligands," *Inorg. Chem.*, *48*, **2009**, 11382-11387.

[b]He, P.; Wang, H.; Liu, S.; Shi, J.; Wang, G.; Gong, M. "Effect of different alkyl groups at the N-position on the luminescence of carbazole based *β*–diketonate europium(III) complexes," *J. Phys. Chem. A*, *113*, **2009**, 12885-12890.

[c]He, G.; Guo, D.; He, C.; Zhang, X.; Zhao, X.; Duan. C. "A color-tunable europium complex emitting three primary colors and white light," *Angew. Chem., Int. Ed.,121*, **2009**, 6248-6251.

Huang, C. "*Coordination Chemistry of Rare Earth Complexes*;" Science Press: Beijing, **1997**.

Imbert, D.; Cantuel, M.; Bünzli, J.-C. G.; Bernardinelli, G.; Piguet, C. "Extending lifetimes of lanthanide-based near-infrared emitters (Nd, Yb) in the millisecond range through Cr(III) sensitization in discrete bimetallic edifices," *J. Am. Chem. Soc.*, *125*, **2003**, 15698-15699.

Judd, B. R. "Optical absorption intensities of rare earth ions," *Phys. Rev.*, 127, **1962**, 750-761.

Justel, T.; Nikol, H.; Ronda, C. "New developments in the field of luminescent materials for lighting and displays," *Angew. Chem. Int. Ed.*, *37*, **1998**, 3084-3103.

Kadjane, P.; Charbonniere, L.; Camerel, F.; Laine, P. P.; Ziessel, R. "Improving visible light sensitization of luminescent europium complexes," *J. Fluoresc.*, *18*, **2008**, 119-129.

Kai, J.; Parra, F. D.; Brito, H. F. "Polymer matrix sensitizing effect on photoluminescence properties of Eu^{3+}-*β*-diketonate complex doped into poly-*β*-hydroxybutyrate (PHB) in film form," *J. Mater. Chem.*, *18*, **2008**, 4549-4554.

Kawa, M.; Frechet, J. M. J. "Self-assembled lanthanide-cored dendrimer complexes: Enhancement of the luminescence properties of lanthanide ions through site-isolation and antenna effects," *Chem. Mater., 10,* **1998**, 286-296.

Kido, J.; Okamoto, Y. "Organolanthanide metal complexes for electroluminescent materials," *Chem. Rev., 102,* **2002**, 2357-2368.

Kim, Y. H.; Baek, N. S.; Kim, H. K. "Sensitized emission of luminescent lanthanide complexes based on 4-naphthalen-1-yl-benzoic acid derivatives by a charge-transfer process," *Chem. Phys.Chem., 7,* **2006**, 213-221.

Kirby, A. F.; Foster, D.; Richardson, F. S. "Comparison of $^7F_J \leftarrow {}^5D_0$ emission spectra for Eu(III) in crystalline environments of octahedral, near-octahedral, and trigonal symmetry," *Chem. Phys. Lett., 95,* **1983**, 507-512.

Klink, S. I.; Grave, L. Reinhoudt, D. N.; van Veggel, F. C. J. M., Werts, M. H. V.; Geurts, F. A. G.; Hofstraat, J. W. "A systematic study of the photophysical processes in polydentate triphenylene-functionalized Eu^{3+}, Tb^{3+}, Nd^{3+}, Yb^{3+}, and Er^{3+} Complexes," *J. Phys. Chem. A, 104,* **2000**, 5457-5468.

Koslova, N. I.; Viana, B.; Sanchez, C. "Rare-earth-doped hybrid siloxane–oxide coatings with luminescent properties," *J. Mater. Chem., 3,* **1993**, 111-112.

Kuriki, K.; Koike, Y.; Okamoto, Y. "Plastic optical fiber lasers and amplifiers containing lanthanide complexes," *Chem. Rev., 102,* **2002**, 2347-2356.

Lamture, J. B.; Zhou, Z. H.; Kumar, A. S.; Wensel, T. G. "Luminescence properties of terbium(III) Complexes with 4-substituted dipicolinic acid analogs," *Inorg. Chem., 34*, **1995**, 864-869.

Latva, M.; Takalo, H.; Mukkala, V. M.; Matachescu, C.; Rodriguez-Ubis, J. C.; Kanakare, J. "Correlation between the lowest triplet state energy level of the ligand and lanthanide(III) luminescence quantum yield," *J. Lumin., 75,* **1997,** 149-169.

Law, G-L.; Wong, K-L.; Tam, H-L.; Cheah, K-W.; Won, W-T. "White OLED with a single-component europium complex," *Inorg. Chem.*, *48***, 2009**, 10492–10494.

Lazarides, T.; Davies, G. M.; Adams, H.; Sabatini, C.; Barigelletti, F.; Barbieri, A.; Pope, S. J. A.; Faulkner, S.; Ward, M. D. "Ligand-field excited states of hexacyanochromate and hexacyanocobaltate as sensitisers for near-infrared luminescence from Nd(III) and Yb(III) in cyanide-bridged d–f assemblies," *Photochem. Photobiol. Sci.*, *6*, **2007**, 1152-1157**.**

Lazarides, T.; Sykes, D.; Faulkner, S.; Barbieri, A.; Ward, M. D. "On the mechanism of d–f energy transfer in Ru^{II}/Ln^{III} and Os^{II}/Ln^{III} dyads: Dexter-type energy transfer over a distance of 20 Å," *Chem.-Eur. J.*, *14*, **2008**, 9389-9399.

Lazarides, T.; Tart, N. M.; Sykes, D.; Faulkner, S.; Barbieri, A.; Ward, M. D. "$[Ru(bipy)_3]^{2+}$ and $[Os(bipy)_3]^{2+}$ chromophores as sensitisers for near-infrared luminescence from Yb(III) and Nd(III) in d/f dyads: contributions from Förster, Dexter, and redox-based energy-transfer mechanisms" *Dalton Trans.*, **2009**, 3971-3979.

Lehn, J.-M. "Perspectives in supramolecular chemistry–from molecular recognition towards molecular information processing and self-organization," *Angew. Chem., Int. Ed. 29*, **1990**, 1304-1319.

Lenaerts, P.; Driesen, K.; Van Deun, R.; Binnemans, K. "Covalent coupling of luminescent tris(2-thenoyltrifluoroacetonato)lanthanide(III) complexes on a merrifield resin *Chem. Mater.*, *17*, **2005**, 2148-2154.

[a]Li, H. R.; Lin, J.; Zhang, H. J.; Li, H. C.; Fu, L. S.; Meng, Q. G. "Novel, covalently bonded hybrid materials of europium (terbium) complexes with silica," *Chem. Commun.*, **2001**, 1212-1213.

[b]Li, Q.; Li, T.; Wu, J. "Luminescence of europium(III) and terbium(III) complexes incorporated in poly(vinyl pyrrolidone) matrix," *J. phys. Chem. B, 105*, **2001**, 12293-12296.

Li, H. R.; Lin, J.; Zhang, H. J.; Fu, L. S.; Meng, Q. G.; Wang, S. B. "Preparation and luminescence properties of hybrid materials containing europium(III) complexes covalently bonded to a silica matrix," *Chem. Mater., 14*, **2002**, 3651-3655.

Li, S.; Zhu, W.; Xu, Z.; Pan, J.; Tian, H. **"**Antenna-functionalized dendritic *β*-diketonates and europium complexes: Synthetic approaches to generation growth," *Tetrahedron, 62,* **2006,** 5035–5048.

Li, Y.; Yan B.; Yang, H. "Construction, characterization, and photoluminescence of mesoporous hybrids containing europium(III) complexes covalently bonded to SBA-15 directly functionalized by modified *β*-diketone," *J. Phys. Chem. C*, *112*, **2008**, 3959-3968.

Liang, F.; Zhou, Q.; Cheng, Y.; Wang, L.; Ma, D.; Jing, X.; Wang, F. "Oxadiazole-functionalized europium(III) *β*-diketonate complex for efficient red electroluminescence," *Chem. Mater., 15*, **2003**, 1935-1937.

Liang, H.; Chen, B.; Zhang, Q.; Zheng, Z.; Ming, H.; Guo, F. "Amplified spontaneous emission of $Eu(dbm)_3$ phen doped step-index polymer optical fiber by end-pumping with a YAG," *J.Applied Polymer science*, *98,* **2005**, 912-916.

Liu, H.-G.; Lee, Y.-I.; Qin, W.-P.; Jang, K.; Kim, S.; Feng, X.-S. "Distinct composite structure and properties of $Eu(phen)_2Cl_3(H_2O)_2$ in poly(methyl methacrylate) and polyvinylpyrrolidone," *J. Appl. Polym. Sci., 92,* **2004,** 3524-3530.

Liu, J. L.; Yan, B. "Lanthanide (Eu^{3+}, Tb^{3+}) centered hybrid materials using modified functional bridge bonded with silica: Molecular design, physical characterization, and photophysical properties," *J. Phys. Chem. B*, *112,* **2008,** 10898-10907.

Liu, M.-S.; Yu Q.-Y.; Cai, Y. -P.; Su, C.-Y.; Lin, X.-M.; Zhou, X.-X; Cai, J.-W. "One-, two-, and three-dimensional lanthanide complexes constructed from pyridine-2,6-dicarboxylic acid and oxalic acid ligands" *Cryst. Growth Des.*, *11*, **2008**, 4083-4091.

Lunstroot, K.; Driesen, K., Nockemann, P., Viau, L., Mutin, P. H., Viouxb, A., Binnemans, K. "Ionic liquid as plasticizer for europium(III)-doped luminescent poly(methyl methacrylate) films," *Phys. Chem. Chem. Phys.*, *12*, **2010**, 1879-1885.

Luo**,**Y**.;** Yan**,** Q**.;** Wu**,** S**.;** Wu**,** W**.;** Zhang**,** Q**. , "**Inter- and intra-molecular energy transfer during sensitization of Eu(DBM)$_3$Phen luminescence by Tb(DBM)$_3$Phen in PMMA," *J. Photochem. Photobiol.A-Chem. 191*, **2007**, 91-96.

Malta, O.L.; Brito, H.F.; Menezes, J.F.S.; Goncalves e Silva, F.R.; deMello, C.D.; Alves, Jr.S. "Experimental and theoretical emission quantum yield in the compound Eu(thenoyltrifluoroacetonate)$_3$(dibenzyl sulfoxide)$_2$," *Chemical Physics Lett*., *282*, **1998**, 233-238.

Matsuzawa, T.; Aoki, Y.; Takeuchi, T.; Murayama, Y. "A new long phosphorescent phosphor with high brightness, $SrAl_2O_4$: Eu^{2+}, Dy^{3+}," *J. Electrochem. Soc*., *143*, **1996**, 2670-2673.

McGehee, M. D.; Bergstedt, T.; Zhang, C.; Saab, A. P.; O'Regan, M. B.; Bazan, G. C.; Srdanov, V. I.; Heeger, A. "Narrow bandwidth luminescence from blends with energy transfer from semiconducting conjugated polymers to europium complexes," *Adv. Mater*., *11*, **1999**, 1349-1354.

Mehlstäubl, M.; Kottas, G. S.; Colella, S.; De Cola, L. "Sensitized near-infrared emission from ytterbium(III) *via* direct energy transfer from iridium(III) in a heterometallic neutral complex" *Dalton Trans.*, **2008**, 2385-2388.

Melhuish, W. H. "Measurement of quantum efficiencies of fluorescence and phosphorescence and some suggested luminescence standards," *J. Opt. Soc. Am., 54*, **1964**, 183-186.

Miyata, K.; Hasegawa, Y.; Kuramochi, Y.; Nakagawa, T.; Yokoo, T.; Kawai, T. "Characteristic structures and photophysical properties of nine-coordinate europium(III) complexes with tandem-connected tridentate phosphane oxide ligands," *Eur. J. Inorg. Chem., 2009*, **2009**, 4777–4785.

Molina, C.; Dahmouche, K.; Santilli, C. V.; Craievich, A. F.; Ribeiro, S. J. L. "Structure and Luminescence of Eu^{3+}-Doped Class I Siloxane−Poly(ethylene glycol) Hybrids," *Chem. Mater., 13*, **2001**, 2818-2823.

Morin, J. F.; Leclerc, M.; Ades, D.; Siove, A. "Polycarbazoles: 25 years of progress," *Macromol. Rapid Commun., 26*, **2005**, 761-778.

Moudam, O.; Rowan, B. C.; Alamiry, M.; Richardson, P.; Richards, B. S.; Jones, A. C.; Robertson, N. "Europium complexes with high total photoluminescence quantum yields in solution and in PMMA," *Chem. Commun.*, **2009**, 6649-6651.

Mukkala, V.-M.; Kankare, J. J. "New 2,2′-bipyridine derivatives and their luminescence properties with europium(III) and terbium(III) ions," *Helv. Chim. Acta, 75*, **1992**, 1578-1592.

Nakamura, K.; Hasegawa, Y.; Kawai, H.; Yasuda, N.; Kanehisa, N.; Kai, Y.; Nagamura, T.; Yanagida, S.; Wada, Y. "Enhanced lasing properties of dissymmetric Eu^{3+} complex with bidentate phosphine ligands," *J. Phys. Chem. A, 111*, **2007**, 3029-3037.

Nie, D.; Chen, Z.; Bian, Z.; Zhou, J.; Liu, Z.; Chen, F.; Zhao, Y.; Huang, C. "Energy transfer pathways in the carbazole functionalized *β*-diketonate europium complexes" *New J. Chem., 31*, **2007**, 1639-1646.

Ogawa, M.; Ikeue, K; Anpo M. "Transparent self-standing films of titanium-containing nanoporous silica," *Chem. Mater., 13*, **2001**, 2900-2904.

Omary, M. A.; Rawashdeh-Omary, M. A.; Diyabalanage, H. V. K.; Dias, H. V. R. "Blue phosphors of dinuclear and mononuclear copper(I) and silver(I) complexes of 3,5-bis(trifluoromethyl)pyrazolate and the related bis(pyrazolyl)borate," *Inorg. Chem., 42*, **2003**, 8612-8614.

Ostrowski, J. C.; Robinson, M. R.; Heeger, A. J.; Bazan, G. C. "Amorphous iridium complex for electrophosphorescent light emitting devices," *Chem. Commun.*, **2002**, 784-785.

Palsson, L.-O.; Monkman, A. P. "Measurements of solid-state photoluminescence quantum yields of films using a fluorimeter," *Adv. Mater.*, *14*, **2002**, 757-758.

Parra, D. F.; Muccicolo, A.; Brito, H. F. "Green luminescence system containing a Tb^{3+}-*β*-diketonate complex doped in the epoxy resin as sensitizer," *J. Appl. Polym. Sci.*, *94*, **2004**, 865-870.

Pavithran, R.; Saleesh Kumar, N. S.; Biju, S.; Reddy, M. L. P.; Alves, Jr. S.; Freire, R. O. "3-Phenyl-4-benzoyl-5-isoxazolonate complex of Eu^{3+} with tri-*n*-octylphosphine oxide as a promising light-conversion molecular device," *Inorg. Chem., 45*, **2006**, 2184-2192.

Peng, C.; Zhang, H.; Yu, J.; Meng, Q.; Fu, L.; Li, H.; Sun, L.; Guo, X. "Synthesis, characterization, and luminescence properties of the ternary europium complex covalently bonded to mesoporous SBA-15," *J. Phys. Chem. B*, *109*, **2005**, 15278-15287.

Petoud, S.; Cohen, S. M.; Bünzli, J.-C. G.; Raymond, K. N. "Stable lanthanide luminescence agents highly emissive in aqueous solution: Multidentate 2-hydroxyisophthalamide complexes of Sm^{3+}, Eu^{3+}, Tb^{3+}, Dy^{3+}," *J. Am. Chem. Soc.*, *125*, **2003**, 13324-13325.

Piguet, C.; Bünzli, J.-C. G. "Mono- and polymetallic lanthanide-containing functional assemblies: A field between tradition and novelty," *Chem. Soc. Rev.*, *28*, **1999**, 347-358.

Polman, A.; van Veggel, F. C. J. M. "Broadband sensitizers for erbium-doped planar optical amplifiers: Review," *J. Opt. Soc. Am. B*, *21*, **2004**, 871-892.

Poluektov, N. S.; Drobyazko, V. N.; Meshkova, S. B.; Bel'tyukova, S. L., Kononenko, L. I. *Dokl. Akad. Nauk., SSSR 224*, **1975,** 150.

Pope, S. J. A.; Coe, B. J.; Faulkner, S.; Bichenkova, E. V.; Yu, X.; Douglas, K. T. "Self-assembly of heterobimetallic d-f hybrid complexes: Sensitization of lanthanide

luminescence by d-block metal-to-ligand charge-transfer excited states," *J. Am. Chem. Soc.*,*126*, **2004**, 9490-9491.

Qiao, X.; Yan, B. "Assembly, characterization, and photoluminescence of hybrids containing europium(III) complexes covalently bonded to inorganic Si-O networks/organic polymers by modified *β*-diketone," *J. Phys. Chem. B*, *112*, **2008**, 14742-14750.

Qiao, X.-F.; Yan, B. "Hybrid materials of lanthanide centers/functionalized 2-thenoyltrifluoroacetone/silicon-oxygen network/polymeric chain: coordination bonded assembly, physical characterization, and photoluminescence," *Inorg. Chem.*, *48*, **2009**, 4714-4723.

Quici, S.; Cavazzini, M.; Marzanni, G.; Accorsi, G.; Armaroli, N.; Ventura, B.; Barigelletti, F. "Visible and near-infrared intense luminescence from water-soluble lanthanide [Tb(III), Eu(III), Sm(III), Dy(III), Pr(III), Ho(III), Yb(III), Nd(III), Er(III)] complexes," *Inorg. Chem.*, *44*, **2005**, 529-537.

Ramya, A. R.; Reddy, M. L. P.; Cowley, A. H.; Vasudevan, K. V. "Synthesis, crystal structure, and photoluminescence of homodinuclear lanthanide 4-(dibenzylamino)benzoate complexes," *Inorg. Chem.*, *49*, **2010**, 2407-2415.

Remya, P. N.; Biju, S.; Reddy, M. L. P.; Cowley, A. H.; Findlater, M. "1D molecular ladder of the ionic complex of terbium-4-sebacoylbis(1-phenyl-3-methyl-5-pyrazolonate) and sodium dibenzo-18-crown-6: Synthesis, crystal structure, and photophysical properties," *Inorg. Chem.*, *47*, **2008**, 7396-7404.

Reyes, R.; Hering, E. N.; Cremona, M.; da Silva, C. F. B.; Brito, H. F.; Achete, C. A. "Growth and characterization of OLED with samarium complex as emitting and electron transporting layer," *Thin Solid Films*, *420-421*, **2002**, 23-29.

Righini, G. C.; Arnaud, C.; Berneschi, S.; Bettinelli, M.; Brenci, M.; Chiasera, A.; Feron, P.; Ferrari, M.; Montagna, M.; Nunzi Conti, G.; Pelli, S.; Portales, H.; Siligardi, C.;

Speghini, A.; Zampedri, L.“Integrated optical amplifiers and microspherical lasers based on erbium-doped oxide glasses,” *Opt. Mater.*, *27*, **2005**, 1711-1717.

Riis-Johannessen, T.; Dupont, N.; Canard, G.; Bernardinelli, G.; Hauser, A.; Piguet, C. “Towards inert and preorganized d-block-containing receptors for trivalent lanthanides: The synthesis and characterization of triple-helical monometallic Os^{II} and bimetallic Os^{II}–Ln^{III} complexes,” *Dalton Trans.*, **2008**, 3661-3677.

Robinson, M. R.; O’Regan, M. B.; Bazan G. C. “Synthesis, morphology and optoelectronic properties of tris[(*N*-ethylcarbazolyl) (3′,5′-hexyloxybenzoyl)methane] (phenanthroline) europium,” *Chem. Commun.*, **2000**, 1645-1646.

Sabbatini, N.; Guardigli, M.; Lehn, J.-M. “Luminescent lanthanide complexes as photochemical supramolecular devices,” *Coord. Chem. Rev*., *123*, **1993**, 201-228.

Saleesh Kumar, N. S.; Varghese, S.; Rath, N. P.; Das, S. “Solid state optical properties of 4-alkoxy-pyridine butadiene derivatives: Reversible thermal switching of luminescence,” *J. Phys. Chem. C*, *112*, **2008**, 8429-8437.

Shah, B. K.; Neckers, D. C.; Shi, J.; Forsythe, E. W.; Morton, D. “Anthanthrene derivatives as blue emitting materials for organic light-emitting diode applications,” *Chem. Mater.*, *18*, **2006**, 603-608.

Shavaleev, N. M.; Moorcraft, L. P.; Pope, S. J. A.; Bell, Z. R.; Faulkner, S.; Ward, M. D. “Sensitised near-infrared emission from lanthanides using a covalently-attached Pt(II) fragment as an antenna group,” *Chem. Commun.*, **2003**, 1134-1135.

Shavaleev, N. M.; Scopelliti, R.; Gumy, F.; Bunzli, J.-C. G. “Surprisingly bright near-infrared luminescence and short radiative lifetimes of ytterbium in hetero-binuclear Yb−Na chelates,” *Inorg.Chem.*, *48*, **2009**, 7937-7946.

Shavaleev, N. M.; Eliseeva, S. V.; Scopelliti, R.; Bünzli, J.-C. G. “*N*-Aryl chromophore ligands for bright europium luminescence,” *Inorg. Chem.*, *49*, **2010**, 3927-3936.

Sheldrick, G. M. SHELXL-PC, Version 5; Siemens Analytical X-ray Instruments. Inc.: Madison, WI, U.S.A., **1994**.

Shi, M.; Li, F.; Yi, T.; Zhang, D.; Hu, H.; Huang, C. "Tuning the triplet energy levels of pyrazolone ligands to match the $^5D_0$ level of europium(III)," *Inorg. Chem.*, *44*, **2005**, 8929-8936.

Shunmugam, R.; Tew, G. N. "Unique emission from polymer based lanthanide alloys," *J. Am. Chem. Soc.*, *127*, **2005**, 13567-13572.

Shyni, R.; Biju, S.; Reddy, M. L. P.; Cowley, A. H.; Findlater, M. "Synthesis, crystal structures, and photophysical properties of homodinuclear lanthanide xanthene-9-carboxylates," *Inorg. Chem.*, *46*, **2007**, 11025-11030.

Shyni, R.; Reddy, M. L. P.; Cowley, A. H.; Findlater, M. "2-Thiopheneacetato-based one-dimensional coordination polymer of Tb^{3+}: Enhancement of terbium centered luminescence in the presence of bidentate nitrogen donor ligands," *Eur. J. Inorg. Chem.*, *2008*, **2008,** 4387-4394.

Sluis, P. V.; Spek, A. L. "BYPASS: an effective method for the refinement of crystal structures containing disordered solvent regions," *Acta Crystallogr., Sect. A*, *46*, **1990**, 194-201.

Stanley, J. M.; Zhu, X.; Yang, X.; Holliday, B. J. "Europium complexes of a novel ethylenedioxythiophene-derivatized bis(pyrazolyl)pyridine ligand exhibiting efficient lanthanide sensitization," *Inorg. Chem.*, *49*, **2010**, 2035–2037.

Steemers, F. J.; Verboom, W.; Reinhoudt, D. N.; Vander Tol, E. B.; Verhoeven, J. W. "New sensitizer-modified calix[4]arenes enabling near-uv excitation of complexed luminescent lanthanide ions," *J. Am. Chem. Soc.*, *117*, **1995**, 9408-9414.

Sun, L. N.; Yu, J. B.; Zheng, G. L.; Zhang, H. J.; Meng, Q. G.; Peng, C. Y.; Fu, L. S.; Liu, F. Y.; Yu, Y. N. "Syntheses, structures and near-IR luminescent studies on ternary

lanthanide (Er^{III}, Ho^{III}, Yb^{III}, Nd^{III}) complexes containing 4,4,5,5,6,6,6-heptafluoro-1-(2-thienyl)hexane-1,3-dionate," *Eur. J. Inorg. Chem.*, *2006*, **2006**, 3962-3973.

Suratwala, T.; Gardlund, Z.; Davidson, K.; Uhlmann, D. R. W; Peyghambarian, N. "Silylated Coumarin Dyes in Sol−Gel Hosts. 1. Structure and Environmental Factors on Fluorescent Properties," *Chem. Mater.*, *10*, **1998**, 190-198.

Swavey, S.; Swavey, R. "Dinuclear and polynuclear lanthanide coordination complexes containing polyazine ligands: Synthesis and luminescent properties," *Coord. Chem. Rev*., 253, **2009**, 2627-2638.

Tan, M.; Wang, G.; Hai, X.; Ye, Z.; Yuan, J. "Development of functionalized fluorescent europium nanoparticles for biolabeling and time-resolved fluorometric applications," *J. Mater. Chem.*, *14*, **2004**, 2896-2901.

Taniguchi, H.; Kido, J.; Nishiya, M.; Sasaki, S. "Europium chelate solid laser based on morphology-dependent resonances," *Appl. Phys. Lett.*, *67*, **1995**, 1060-1062.

Tanner, P. A.; Yan, B.; Zhang, H. "Preparation and luminescence properties of sol-gel hybrid materials incorporated with europium complexes," *J. Mater. Sci*., *35*, **2000**, 4325-4328.

Thompson, L. C.; Atchison, F. W.; Young, V. G. "Isomerism in the adduct of tris(4,4,4,-trifluoro-1-(2-naphthyl)-1,3-butanedionato)europium(III) with dipyridyl," *J. Alloys Compds.*, *275−278*, **1998,** 765-768.

Torelli, S.; Delahaye, S.; Hauser, A.; Bernardinelli, G.; Piguet, C. "Ruthenium(II) as a novel "labile" partner in thermodynamic self-assembly of heterobimetallic d–f triple-stranded helicates," *Chem.-Eur. J., 10,* **2004**, 3503-3516.

Velasco, D. S.; de Moura, A. P. ; Medina, A. N.; Baesso, M. L.; Rubira, A. F.; Cremona, M.; Bento, A. C. "Preparation, characterization, and spectroscopic properties of PC/PMMA doped blends: Study of the effect of rare-earth doping on luminescence,

quenching rate, and lifetime enhancement," *J. Phys. Chem. B, 114,* **2010**, 5657–5660.

Viswanathan, S.; de Bettenacourt-Dias, A. "Eu(III) and Tb(III) luminescence sensitized by thiophenyl-derivatized nitrobenzoato antennas," *Inorg. Chem., 45*, **2006**, 10138-10146.

Wada, Y.; Ohkubo, T.; Ryo, M.; Nakarawa, T.; Hasegawa, Y.; Yanagida, S. "High efficiency near-IR emission of Nd(III) based on low-vibrational environment in cages of nanosized zeolites," *J. Am. Chem. Soc.*, *122*, **2000**, 8583-8584.

Wang, S.; Gaylord, B. S.; Bazan, G. C. "Fluorescein provides a resonance gate for FRET from conjugated polymers to DNA intercalated dyes," *J. Am. Chem. Soc.*, *126*, **2004**, 5446-5451.

Watson, W. H.; Williams, R. J.; Stemple, N. R. "Crystal structure of tris(acetylacetonato)(1,10-phenanthroline)europium(III)," *J. Inorg. Chem.*, *34*, **1972,** 501-508.

Weissman, S. I. "Intramolecular energy transfer the fluorescence of complexes of europium," *J. Chem. Phys., 10*, **1942**, 214-217.

Werts, M. H. V.; Jukes, R. T. F.; Verhoeven, J. W. "The emission spectrum and the radiative lifetime of Eu^{3+} in luminescent lanthanide complexes," *Phys. Chem. Chem. Phys., 4*, **2002**, 1542-1548.

Werts, M. H. V.; Gmouh, S., Mongin, O.; Pons, T.; Desce, M. B. "Strong modulation of two-photon excited fluorescence of quadripolar dyes by (de)protonation," *J. Am. Chem. Soc.*, *126*, **2004**, 16294-16295.

Werts, M. H. V. "Making sense of lanthanide luminescence," *Sci. Prog., 88*, **2005**, 101-131.

Wrighton, M. S.; Ginley, D. S.; Morse, D. L." Technique for the determination of absolute emission quantum yields of powdered samples," *J. Phys. Chem.*, *78*, **1974**, 2229-2233.

Xiao, M.; Selvin, P. R. "Quantum yields of luminescent lanthanide chelates and far-red dyes measured by resonance energy transfer," *J. Am. Chem. Soc*., *123*, **2001**, 7067-7073.

Xin, H.; Li, F. Y.; Shi, M.; Bian, Z. Q.; Huang, C. H. "Efficient electroluminescence from a new terbium complex," *J. Am. Chem. Soc.*, *125*, **2003**, 7166-7167.

Xu, H.; Wang, L.-H.; Zhu, X.-H.; Yin, K.; Zhong, G.-Y.; Hou X.-Y.; Huang, W. "Application of chelate phosphine oxide ligand in Eu(III) complex with mezzo triplet energy level, highly efficient photoluminescent, and electroluminescent performances," *J. Phys. Chem. B*, *110*, **2006**, 3023-3029.

Xu, H.; Yin, K.; Huang, W. "Highly improved electroluminescence from a series of novel Eu^{3+} complexes with functional single-coordinate phosphine oxide ligands: Tuning the intramolecular energy transfer, morphology, and carrier injection ability of the complexes," *Chem. Eur. J.*, *13*, **2007**, 10281-10293.

Xu, H.; Yin, K.; Huang, W. "Comparison of the electrochemical and luminescence properties of two carbazole-based phosphine oxide Eu^{3+} complexes: Effect of different bipolar ligand structures," *Chem Phys Chem.*, *9*, **2008**, 1752-1760.

Xu, H. B.; Zhang, L. Y.; Chen, X. M.; Li, X. L.; Chen, Z. N. "Modulation of Pt → Ln energy transfer in $PtLn_2$ (Ln = Nd, Er, Yb) complexes with 2,2′-bipyridyl/2,2′:6′2″-terpyridyl ethynyl ligands," *Cryst. Growth Des.*, *9*, **2009**, 569-576.

Xu, H.; Yin, K.; Huang, W. "Novel light-emitting ternary Eu^{3+} complexes based on multifunctional bidentate aryl phosphine oxide derivatives: Tuning photophysical and electrochemical properties toward bright electroluminescence," *J. Phys. Chem. C.*, *114*, **2010**, 1674-1683.

Xu, Q.; Li, L.; Liu, X.; Xu, R. "Incorporation of rare-earth complex $Eu(TTA)_4C_5H_5NC_{16}H_{33}$ into surface-modified Si-MCM-41 and its photophysical properties," *Chem. Mater.*, *14*, **2002**, 549-555.

Yan, B.; Lu, H.-F. "Lanthanide-centered covalently bonded hybrids through sulfide linkage: Molecular assembly, physical characterization, and photoluminescence," *Inorg. Chem., 47*, **2008**, 5601-5611.

Yan, B.; Wang, Q.-M. "Two luminescent molecular hybrids composed of bridged Eu(III)- β -diketone chelates covalently trapped in silica and titanate gels," *Cryst. Growth Des., 8*, **2008**, 1484-1489.

Yan, B.; Zhou, B. "Two photoactive lanthanide (Eu^{3+}, Tb^{3+}) hybrid materials of modified β -diketone bridge directly covalently bonded mesoporous host (MCM-41),"*J. Photochem. Photobiol., A, 195*, **2008,** 314-322.

Yang, B.; Li, Y. "Luminescent ternary inorganic–organic mesoporous hybrids Eu(TTASi-SBA-15)phen: covalent linkage in TTA directly functionalized SBA-15," *Dalton trans., 39,* **2010**, 1480-1487.

Yang, C.; Fu, L. -M.; Wang, Y.; Zhang, J.-P.; Wong, W.-T.; Ai, X.-C.; Qiao, Y.-F.; Zou, B.-S.; Gui, L.-L. "A highly luminescent europium complex showing visible-light-sensitized red emission: Direct observation of the singlet pathway," *Angew Chem. Int. Ed., 43*, **2004,** 5010-5013.

Yu, J.; Zhang, H.; Fu, L.; Deng, R.; Zhou, L.; Li, H.; Liu, F.; Fu, H. "Synthesis, structure and luminescent properties of a new praseodymium(III) complex with β.-diketone," *Inorg. Chem. Commun., 6*, **2003**, 852-854.

Yu, X.; Su, Q. "Photoacoustic and luminescence properties study on energy transfer and relaxation processes of Tb(III) complexes with benzoic acid," *J. Photochem. Photobiolog. A: Chem., 155*, **2003**, 73-78.

Yu, J.; Zhou, L.; Zhang, H.; Zheng, Y.; Li, H.; Deng, R.; Peng, Z.; Li, Z. "Efficient electroluminescence from new lanthanide (Eu^{3+}, Sm^{3+}) complexes," *Inorg. Chem., 44*, **2005**, 1611-1618.

Yuan, Y-F.; Cardinaels, T.; Lunstroot, K.; Van Hecke, K.; Meervelt, L. V.; Gorller-Walrand, C.; Binnemans, K.; Nockemann, P. "Rare-earth complexes of ferrocene-containing ligands: Visible-light excitable luminescent materials," *Inorg. Chem.*, *46*, **2007**, 5302-5309.

Zhang, H.; Song, H.; Dong, B.; Han, L.; Pan, G.; Bai, X.; Fan, L.; Lu, S.; Zhao, H.; Wang, F. "Electrospinning preparation and luminescence properties of europium complex/polymer composite fibers," *J. Phys. Chem. C.*, *112*, **2008**, 9155-9162.

Zheng, Y.; Cardinali, F.; Armaroli, N.; Accorsi, G. "Synthesis and photoluminescence properties of heteroleptic Europium(III) complexes with appended carbazole units," *Eur. J. Inorg. Chem.*, *2008*, **2008**, 2075-2080.

Ziessel, R.; Diring, S.; Kadjane, P.; Charbonnière, L. J.; Retailleau, P.; Philouze, C. "Highly efficient blue photoexcitation of europium in a bimetallic Pt–Eu complex," *Chem. Asian J.*, *2*, **2007**, 975-982.

Zolin, V. F.; Puntus, L. N.; Tsaryuk, V. I.; Kudryashova, V. A.; Legendziewicz, J.; Gawryszewska, P.; Szostak, R. "Spectroscopy of europium and terbium pyridine-carboxylates," *J. Alloys Compd.*, *380*, **2004**, 279-284.